# Conceptual Design of Fuel Cell Commuter Aircraft

## A study into the performance and viability of CS-23 category transport aircraft utilising hydrogen fuel cell propulsion

### Master Thesis Report

# Miha Zupanič

Delft University of Technology

**TU**Delft

# Conceptual Design of Fuel Cell Commuter Aircraft

## A study into the performance and viability of CS-23 category transport aircraft utilising hydrogen fuel cell propulsion

by

# Miha Zupanič

to obtain the degree of Master of Science in Aerospace Engineering
at the Delft University of Technology,
to be defended publicly on Friday, April 14, 2023.

Student number:     4440560
Thesis committee:   Dr. Ir. F. Oliviero       TU Delft, supervisor
                    Dr. Ir. G. La Rocca,     TU Delft, committee chair
                    Ir. P. C. Roling          TU Delft

An electronic version of this thesis is available at `http://repository.tudelft.nl/`.

# Preface

This thesis project represents the final step in obtaining the master's degree at the faculty of Aerospace Engineering at the Delft University of Technology.

It was my love for flying, and a general fascination with the technology behind it, that made me pursue this career. However, there was another important issue that I could not ignore. In particular, the impact of aviation on climate change and its environmental effects have motivated me to seek education in this field to obtain the knowledge and skills required to try to address this immense challenge. Thus, I hope that my contribution with this thesis and my career beyond it will help achieve positive change for society and the planet.

Like for many of my colleagues, the path to this degree has not always been easy. That is why I am incredibly grateful for the support and encouragement of those who have helped me along the way. I could not have completed this thesis without their assistance.

I would like to thank my supervisor Dr. Fabrizio Oliviero for the guidance and feedback throughout the thesis process. I would also like to extend my gratitude to Daniel Juschus and Tom Hoogerdijk, with whom I was able to discuss the details of my work, as well as Şan Kilkiş to whom I owe a lot of my programming knowledge.

A big thanks also goes to Kilian and Michael for lighting up those dark Dutch winters. My lovely man, Kipras, thank you for all the laughs and I hope to see you in the mountains very soon. And what would I do without the burpee queen Yvonne, who helped me keep my sanity throughout this endeavour. Thank you, everyone.

Finally, I would like to thank my family for their unwavering support. Hvala vam za vso podporo in se opravičujem da je trajalo malenkost dlje kot je bilo predvideno.

*Miha Zupanič*
*Madrid, April 2023*

# Abstract

The demand for air travel has been increasing continuously over the past few decades, resulting in a rise in aviation greenhouse gas emissions. As passenger numbers are expected to keep growing in the coming years, it is crucial to significantly reduce the aviation industry's environmental impact. To contribute to this goal, this research project investigated the potential advantages of using hybrid hydrogen fuel-cell powertrains in new types of aircraft. The study focused on commuter aircraft certified under the EASA CS-23 category since there is a high potential for innovation in this aviation segment. While some existing research has explored the performance of fuel-cell powertrains for transport aircraft in the CS-23 category, these analyses often yielded unclear results regarding the viability of this new solution. Furthermore, despite high uncertainties in the models for fuel cell aircraft, the existing research often failed to provide a sensitivity analysis of the powertrain or mission parameters. To address this research gap, the following overarching research goal was identified: *To evaluate the performance and viability of fuel-cell powertrain integration on board a CS-23 category commuter aircraft compared to conventional powertrain architectures by modelling and comparing results obtained through a single aircraft design synthesis software.*

The aircraft modelling was conducted using an in-house developed aircraft design synthesis software called the Initiator. Before the start of this project, this software already possessed capabilities of modelling conventional and various hybrid powertrains, including the hybrid hydrogen fuel-cell powertrain used in this research. However, the capability to model commuter aircraft had to be developed and validated as a part of this project. Furthermore, the existing fuel-cell models were verified, validated, and adjusted wherever necessary in order to increase their estimation accuracy. Finally, rudimentary flight emissions models and energy cost models were developed to perform a comparison between conventional aircraft and fuel cell aircraft in terms of operational cost and environmental impact.

To compare the fuel cell aircraft against the conventional aircraft the following steps were performed. First, four existing conventional commuter aircraft were selected to serve as a performance benchmark. These were the Dornier Do 228-212, Fairchild Metro 23, BAE Jetstream 31, and Embraer EMB 110P2. Next, these conventional aircraft were modelled in the Initiator software, where they also served to validate the new CS-23 modelling capability. Next, the top-level aircraft requirements or TLARs and general configuration of benchmark aircraft were used to create four equivalent aircraft utilising the new hybrid fuel-cell powertrain. By doing so, the fuel-cell aircraft could be compared to their conventional counterparts. Finally, a sensitivity analysis was performed for the take-off mass and mission energy usage of all four fuel cell aircraft.

In general, it was found that the fuel cell aircraft take-off mass increased between 30 and 60% compared to their conventional counterparts. Despite this increase in mass, the increase in net powertrain efficiency for fuel cell aircraft meant that the mission energy needs were less negatively affected. Concretely, for most aircraft, the energy use increased by only 1.5% to 5%, while the energy use for one of the four aircraft decreased by 30%. When utilising green hydrogen from wind or photovoltaic power the global warming potential (GWP) of the energy used in flight was shown to reduce between 76% to 98% compared to conventional aircraft. The aircraft energy purchase costs for the fuel cell aircraft running on green hydrogen were shown to be between 30% and 95% higher than for conventional aircraft running on Jet-A1. When the emission allowance costs from the European union emissions trading scheme were included in the price, the costs were shown to be equal for the two aircraft solutions in the mid-term future. The sensitivity analysis showed that the cruise Mach number is the most consequential parameter determining the aircraft mass and energy usage.

Looking at the individual aircraft in the study, the fuel cell EMB 110P2 performed considerably better than the other three aircraft. It can be concluded that the short range and low cruising speed of this aircraft proved to be very favourable when utilising the fuel-cell powertrain.

# Contents

# Nomenclature

## List of Abbreviations

| | |
|---|---|
| **AEO** | All Engines Operating |
| **AMC** | Acceptable Means of Compliance |
| **APU** | Auxiliary Power Unit |
| **BoP** | Balance of Plant |
| **CCS** | Carbon Capture & Storage |
| **CCUS** | Carbon Capture, Utilisation & Storage |
| **CCU** | Carbon Capture & Utilisation |
| **CiC** | Contrail-Induced Cloudiness |
| **CS** | Certification Specification |
| **DEP** | Distributed Electric Propulsion |
| **DLR** | Deutsches Zentrum für Luft- und Raumfahrt (German Aerospace Center) |
| **DoH** | Degree of Hybridisation |
| **EASA** | European Union Aviation Safety Agency |
| **EC** | European Commission |
| **EESI** | Environmental and Energy Study Institute |
| **EM** | Electric Motor |
| **EoL** | End of Life |
| **ETS** | Emissions Trading Scheme |
| **EU** | European Union |
| **FCS** | Fuel Cell System |
| **FC** | Fuel Cell |
| **GA** | General Aviation |
| **GT** | Gas Turbine |
| **GWP** | Global Warming Potential |
| **HHV** | Higher Heating Value |

**HSE**        Horizontal Stability Estimation

**HTE**        High Temperature Electrolysis

**ICE**        Internal Combustion Engine

**IEA**        International Energy Agency

**IFR**        Instrumental Flight Rules

**LCA**        Life Cycle Assessment

**LHV**        Lower Heating Value

**MEA**        Membrane Electrode Assembly

**MRO**        Maintenance, Repair, Overhaul

**MTOM**       Maximum Take Off Mass

**NGSR**       Natural Gas Steam Reforming

**OEI**        One Engine Inoperative

**OEM**        Operational Empty Mass

**PEMFC**      Proton Exchange Membrane Full Cell

**PMAD**       Power Management And Distribution

**PRCE**       Payload-Range Cost Efficiency

**PREE**       Payload-Range Energy Efficiency

**PtL**        Power-to-Liquid

**PV**         Photovoltaics

**SAF**        Sustainable Aviation Fuel

**STOL**       Short Take-Off and Landing

**T/O**        Take Off

**TAS**        True Airspeed

**TLAR**       Top-Level Aircraft Requirement

## List of Symbols

| | | |
|---|---|---:|
| $F$ | Faraday's constant | $96485.3321\ C \cdot mol^{-1}$ |
| $g$ | Standard gravitational acceleration | $9.80665\ m \cdot s^{-2}$ |
| $R$ | Universal gas constant | $8.3145\ J \cdot K^{-1} mol^{-1}$ |
| $T_0$ | Reference temperature | $298.15\ K$ |
| $\alpha$ | Electron transfer coefficient | $-$ |

| | | |
|---|---|---:|
| $\eta_{act}$ | Activation overpotential | $V$ |
| $\eta_{cell}$ | Fuel cell efficiency | $-$ |
| $\eta_{conc}$ | Concentration overpotential | $V$ |
| $\eta_{grav}$ | Gravimetric efficiency | $-$ |
| $\eta_i$ | Efficiency of component $i$ | $-$ |
| $\eta_{ohm}$ | Ohmic overpotential | $V$ |
| $\eta_{sys}$ | Fuel cell system efficiency | $-$ |
| $\mu_g$ | Aeroplane mass ratio | $-$ |
| $\mu_{fuel}$ | Fuel utilisation factor | $-$ |
| $\Phi$ | Supplied power ratio | $-$ |
| $\rho$ | Air density | $kg \cdot m^{-3}$ |
| $\rho_0$ | Sea-level air density | $kg \cdot m^{-3}$ |
| $\rho_{A_{MEA}}$ | Area density of the membrane-electrode assembly | $kg \cdot m^{-2}$ |
| $\rho_{bolt}$ | Density of fuel-cell stack bolt material | $m$ |
| $\rho_{mat,BP}$ | Density of the bipolar plate material | $kg \cdot m^{-3}$ |
| $\rho_{mat,EP}$ | Fuel-cell stack endplate material density | $kg \cdot m^{-3}$ |
| $\Delta \hat{s}$ | Entropy of reaction | $J \cdot K^{-1} \cdot mol^{-1}$ |
| $\overline{C}$ | Mean geometric chord | $m$ |
| $a$ | Slope of the aeroplane normal force coefficient curve | $-$ |
| $a_i$ | Activity of reactant species $i$ | $-$ |
| $A_{cell}$ | Fuel cell active area | $cm^2$ |
| $b$ | Tafel slope | $-$ |
| $c$ | Mass transport loss constant | $V$ |
| $C_D$ | Aircraft drag coefficient | $-$ |
| $C_{N_\alpha}$ | Aeroplane normal force coefficient | $-$ |
| $D_{bolt}$ | Diameter of fuel-cell stack bolts | $m$ |
| $E^0$ | Reference potential | $V$ |
| $E_{mission}$ | Required mission energy | $J$ |
| $f_m$ | Unaccounted mass factor | $-$ |
| $f_V$ | Unaccounted volume factor | $-$ |
| $i_\circ$ | Exchange current density | $A \cdot cm^{-2}$ |

| | | |
|---|---|---|
| $I_{cell}$ | Fuel cell/battery cell electric current | $A$ |
| $i_{cell}$ | Fuel cell current density | $A \cdot cm^{-2}$ |
| $i_{leak}$ | Leakage current density | $A \cdot cm^{-2}$ |
| $i_{lim}$ | Limit current density | $A \cdot cm^{-2}$ |
| $k_g$ | Gust alleviation factor | $-$ |
| $l_{bolt}$ | Length of fuel-cell stack bolts | $m$ |
| $m_{fuel}$ | Fuel mass | $kg$ |
| $m_{payload}$ | Payload mass | $kg$ |
| $m_{stack}$ | Fuel-cell stack mass | $kg$ |
| $m_{tank}$ | Tank mass | $kg$ |
| $n$ | Flight load factor | $-$ |
| $n_{bolt}$ | Number of fuel-cell stack bolts | $-$ |
| $n_{cell}$ | Number of individual fuel cells in a stack | $-$ |
| $n_{e^-}$ | Number of electrons | $-$ |
| $n_{stack}$ | Number of fuel-cell stacks | $-$ |
| $p$ | Partial pressure | $Pa$ |
| $P_{bat}$ | Battery power | $W$ |
| $P_{FCS}$ | FCS output power | $W$ |
| $P_{fuel}$ | Power provided by the fuel | $W$ |
| $P_{in}$ | Input power | $W$ |
| $P_{out}$ | Output power | $W$ |
| $P_{prop}$ | Aircraft propulsive power | $W$ |
| $P_{stack}$ | Fuel-cell stack power | $W$ |
| $r$ | Combined resistance | $\Omega$ |
| $R_{mission}$ | Mission trip range | $m$ |
| $S$ | Aircraft wing reference area | $m^2$ |
| $S^\circ$ | Standard entropy value of reaction species (at 25°C) | $J \cdot K^{-1} \cdot mol^{-1}$ |
| $T$ | Absolute (operational) temperature | $K$ |
| $t_{BP}$ | Thickness of bipolar plates | $m$ |
| $t_{EP}$ | Fuel-cell stack endplate thickness | $m$ |
| $t_{mat,BP}$ | Thickness of the bipolar plate material | $m$ |

| | | |
|---|---|---|
| $t_{MEA}$ | Thickness of MEA | $m$ |
| $U_{de}$ | Gust velocity | $m \cdot s^{-1}$ |
| $V$ | Velocity | $m \cdot s^{-1}$ |
| $V_{cell}$ | Fuel cell electric potential | $V$ |
| $V_{FCS}$ | FCS output voltage | $V$ |
| $V_{oc}$ | Open (reversible) circuit potential | $V$ |
| $V_{stack}$ | Fuel cell volume stack | $m^3$ |
| $W$ | Weight | $N$ |

# List of Figures

# List of Tables

# 1

# Introduction

Despite continuous innovation and efficiency improvements throughout the aviation sector, an ever-increasing demand for air travel means that aviation greenhouse gas emissions have been experiencing continuous growth over the past decades. Since the passenger numbers are projected to increase further over the next few years, the need to drastically reduce the industry's environmental impact is paramount. Besides noise and air pollution that the current aircraft fleets are responsible for, their greenhouse gas emissions remain the primary concern. In 2018, commercial aviation emissions were estimated to account for approximately 2.4% of the global carbon dioxide emissions, according to the Environmental and Energy Study Institute (EESI) [1]. However, this is not the entire picture. Combined with the aircraft contrails and other exhaust pollutants, commercial aviation alone was responsible for about 5% of the world's climate warming effect. Furthermore, with the current growth continuing, these emissions could triple by the year 2050.

According to the European Commission (EC), this increasing demand for air travel is already making the aviation sector one of the fastest growing greenhouse gas emitters in the European Union [2]. To fight back against this trend, the EC has laid out ambitious goals of reducing aviation $CO_2$ emissions to reach EU-wide climate neutrality by 2050. Namely, the *Flightpath 2050* [3] report envisions a 75% reduction in $CO_2$ emissions compared to typical new aircraft in the year 2000. Additionally, the report also calls for a 90% reduction in $NO_x$ emission and a perceived noise reduction of 65%.

In part, these goals can be achieved with more efficient aircraft operations, improved aircraft aerodynamics and more efficient conventional turbine engines. However, these incremental improvements in aircraft efficiency have slowed down over the recent years and the future projections indicate they will not be sufficient to reach the necessary goals of reducing aviation carbon emissions, such as the ones laid out by the EC [4]. Thus, aircraft will eventually need to adopt new propulsion technologies which emit much less, or ideally zero, net greenhouse gas emissions.

Increasing the use of sustainable aviation fuel (SAF)[1], battery technology and hydrogen are currently the most promising paths to achieve aviation sustainability goals. Out of the three, SAF would require by far the smallest changes in aircraft design to enable wide-scale adoption [6]. However, the SAF solution would not eliminate local emissions. Thus, it is often seen only as a short- to mid-term solution. Meanwhile, battery technology is gaining a lot of traction in the transportation sector, such as in the automotive or railway industry. However, despite its popularity and high drive-train efficiency, the low energy density of current batteries makes them prohibitively heavy to install in all but the smallest, low-endurance passenger and unmanned aircraft. Unlike battery technology, hydrogen fuel is not suffering from low specific weight or long refuelling times. Therefore, it holds high potential to power larger aircraft over longer distances making them realistic competitors to their conventional counterparts. While hydrogen brings with it a plethora of other engineering challenges which have to be addressed, it is still regarded as one of the most promising clean energy sources for aircraft propulsion.

Generally, hydrogen can be converted into aircraft thrust in two ways [7]. The first is by burning a

---

[1]Although there is no internationally agreed upon definition of SAF, it normally refers to non-fossil based aviation fuel that presents some reduction in life-cycle greenhouse gas emissions [5].

mixture of hydrogen and oxygen in modified piston or turbine engines. A large drawback to this solution is the lower energy conversion efficiency and production of some greenhouse gas emissions. While the burning of hydrogen avoids any carbon and sulphur emissions, it still produces water vapour and $NO_x$. Although water vapour emissions are not a concern at lower altitudes, they are known to have a net warming effect if emitted at cruising altitudes of modern jets. Additionally, aircraft exhaust emissions are responsible for the formation of high-altitude clouds which might increase the Earth's net radiative forcing. $NO_x$ emissions on the other hand are linked to ozone ($O_3$) creation, which, at lower altitudes, is harmful to humans while also causing the formation of acid rain. [8, 9]

Alternatively, hydrogen can be used in fuel cells where it reacts with oxygen in a redox reaction, producing an electrical current in the process. Electricity is then used to propel the aircraft via electric motors. Such a system boasts better energy conversion efficiency with water and oxygen-depleted air as the only byproducts. Moreover, the fuel cells also avoid the noise produced by combustion engines. For these reasons, fuel cell technology is oftentimes seen as the best candidate for sustainable aviation and will be the focal point of this project.

It is also possible to combine the benefits of batteries and fuel cells, by integrating them into a hybrid architecture. One of the major drawbacks of non-hybrid powertrains is the need to size all components for the aircraft's maximum power requirement. However, most aircraft, especially transport aircraft, use only a fraction of the available power for the majority of their flight. Thus, it might be worthwhile to investigate whether the use of battery power to aid the fuel cells in covering peak loads could reduce the overall weight of the powertrain and improve aircraft efficiency.

Currently, the majority of commercial aviation's environmental impact is caused by the aircraft certified under the European Union Aviation Safety Agency (EASA) Certification Specification part 25 (CS-25) [10]. Thus, reducing the impact of CS-25 aircraft should be a high priority in transforming aviation into a more sustainable industry. However, this research project will instead focus on the smaller commuter aircraft with a capacity of up to 19 passengers and certified under the CS-23 regulation set. Although flights up to 500 km where such aircraft are most likely to operate currently present only around 5% of commercial aviation's $CO_2$ emissions [10, 11], the CS-23 commuter aircraft are much better suited for implementing and proving most of the novel propulsion technologies [12]. This is due to a variety of factors, such as their more flexible certification process, lower power requirements and lower development costs. Furthermore, the $CO_2$ emissions report by Graver *et al.* [10] indicates that the commuter aircraft segment is the most carbon-intensive per passenger kilometre flown. Therefore, commuter aircraft have more room for efficiency improvements. Because of this higher innovation potential, the scope of the presented research will be limited to the CS-23 category commuter class aircraft.

This research aims to assess the performance and viability of commuter aircraft powered by a combination of hydrogen fuel cells and batteries, while also comparing the results to those obtained for conventional aircraft. This will be achieved by analysing the current state of the technology, evaluating its potential benefits and drawbacks, and identifying the key challenges and opportunities for further development. With this final report, the author wishes to provide valuable insights and recommendations for the development of future sustainable aircraft, as well as provide possible directions for further research.

The remainder of this report is structured as follows. First, background information on the commuter aircraft, the hydrogen fuel, and the hybrid fuel-cell powertrain will be given in Chapter 2. Next, in Chapter 3 the research gap in the existing literature will be identified, followed by the presentation of the research goal and research questions. Moreover, the aircraft design tool that will be used to obtain the results, as well as select the conventional commuter aircraft that will serve as the benchmark for the fuel-cell-powered aircraft alternatives will be presented. The implementation of the necessary modifications to the aircraft design software and the setup of any models required to obtain the results will be described in Chapter 4. Chapter 5 will include a presentation and commentary on the obtained results before a broader discussion on the significance and quality of the results will follow in Chapter 6. This chapter will also be used to answer the research questions posed at the beginning of this report. Finally, the report will conclude with Chapter 7 where the main findings of this research will be summarised.

# 2

# Background Information

This chapter will outline the most important background knowledge that facilitated the setup and execution of this research. First, the CS-23 commuter aircraft will be defined and presented in Section 2.1. Next, in Section 2.2 the motivations behind using hydrogen as an aviation fuel alternative will be discussed. In the following section, the fuel cell technology that has the ability to turn hydrogen fuel into electricity will be explored. Specific focus will be given to the fuel cell type used in this research. Then, the chosen integration of the fuel cell systems into a fuel-cell powertrain will be presented in Section 2.4. Finally, the existing experimental fuel cell aircraft, as well as the contemporary research into commuter fuel cell aircraft will be given in Section 2.5 and Section 2.6, respectively.

## 2.1. CS-23 Commuter Aircraft

As discussed in the introduction, this research focuses on a very specific segment of aviation. Namely, the commuter aircraft certified under EASA's CS-23 regulation set. Over the next few paragraphs, this section will elaborate on what the terms 'commuter aircraft' and 'CS-23 regulation' stand for, and present some existing conventional commuter aircraft.

### 2.1.1. Certification Regulations and Definitions

EASA established the Certification Specification part 23 (CS-23) to regulate the airworthiness of general aviation and small commercial aircraft with 19 or fewer seats, excluding the pilots. Although the CS-23 was first published in 2003, the document was revised and amended on a few occasions. Most significantly, Amendment number 5 [13] was put in place in 2017, replacing many of the prescriptive design requirements with more performance-based standards. For example, previously, many requirements were written in such a way that their fulfilment was only possible with a conventional powertrain. In the latest amendment, these powertrain and component-specific requirements have largely been removed or rephrased to focus on the final safety result rather than specific means to achieve it. Thus, this change in the formulation of requirements should, at least in principle, enable certification of novel powertrain architectures, such as electric and hybrid propulsion. [14]

The term 'commuter aircraft' is used somewhat inconsistently, both in regular use, as well as within published scientific literature. Sometimes, the term is used to simply describe the aircraft in commercial use that serve on short-haul routes with very low demand. These routes are often specifically designed to bring travellers to a larger airport hub where they can transfer to another flight, facilitating a so-called hub-and-spoke airline model. Besides the low passenger demand, these routes frequently favour small aircraft because they often serve destinations with shorter runways or difficult approach procedures. [15]

However, there is also a much more rigid definition of the term commuter aircraft that stems directly from the aircraft certification regulation. In the EASA's original CS-23 document, commuter aircraft are defined as *'Propeller-driven twin-engined airplanes that have a seating configuration, excluding the pilot seat(s), of nineteen or fewer and a maximum certificated take-off weight of 8618 kg (19 000 lb) or less'* [16]. This specific definition of commuter aircraft will be used throughout this research work. It is

3

worth mentioning, however, that EASA has subsequently dropped the certification term 'commuter' in its 5th amendment to the CS-23 and replaced it with different classifiers. The most equivalent certification classification to the former commuter category would currently be a 'Normal-category level 4 aeroplane, not certified for aerobatics'.

## 2.1.2. Existing Commuter Aircraft

Now that the definition of commuter aircraft has been established, it is also important to discuss the role of these aircraft in the aviation industry, as well as point out some common characteristics and differences between different commuter aircraft. To better facilitate this discussion, a list of existing noteworthy commuter aircraft is presented in Table 2.1.

From a business perspective, the main purpose of commuter aircraft is to serve thin-haul routes. Besides being in low demand, these routes are often very short. Apart from low passenger numbers, an aircraft operator might be constrained to using these more manoeuvrable and slow commuter aircraft to serve airports with short runways or a very difficult approach. Nevertheless, due to the high costs of operating such routes, the demand for commuter aircraft is not as great as for the larger passenger aircraft, which generally offer a lower cost per transported passenger. However, especially in remote places where other means of transportation are inefficient or non-existent, commuter aircraft can provide vital connectivity for the local communities. [12, 17]

**Table 2.1:** List of noteworthy conventional commuter aircraft. Information compiled from: [15, 18]

| Aircraft type | Seats | MTOM [kg] | Range [km] | Cruise Speed [km/h] | Stall Speed [km/h] | T/O Field Length* [m] | Landing Field Length* [m] |
|---|---|---|---|---|---|---|---|
| Cessna Conquest II | 9 | 4468 | 4064 | 480 | 139 | 752 | 572 |
| Beechcraft 350ER | 11 | 7484 | 4986 | 561 | 150 | 1237 | 908 |
| Mitsubishi MU-2L | 12 | 5273 | 2334 | 483 | 142 | 660 | 575 |
| Beechcraft Model 99A | 15 | 4727 | 1686 | 380 | 120 | 975 | 808 |
| GAF Nomad N24A | 16 | 4264 | 1352 | 311 | 87 | 521 | 408 |
| Harbin Y-12 F | 17 | 8400 | 1333 | 390 | N/A | N/A | N/A |
| DHC-6 Twin Otter 400 | 19 | 5670 | 740 | 337 | 108 | 366 | 321 |
| Embraer EMB 110P2 | 19 | 5670 | 520 | 413 | 128 | N/A | N/A |
| Dornier Do 228-212 | 19 | 6400 | 1166 | 428 | 125 | 686 | 512 |
| BAE Jetstream 31 | 19 | 6950 | 1192 | 487 | 160 | 975 | 1165 |
| Let L-410 Turbolet NG | 19 | 7000 | 2570 | 417 | 123 | 590 | 600 |
| Fairchild Metro 23 | 19 | 7484 | 2065 | 543 | 165 | 1342 | N/A |
| Beechcraft 1900D | 19 | 7764 | 1279 | 518 | 167 | 1163 | 851 |

*Required field length is a take-off or landing distance over a 15m obstacle at maximum take-off or landing mass, respectively.

As can be seen from Table 2.1, most of the listed aircraft require a relatively short take-off and landing field length compared to larger commercial transport aircraft. However, there is still a fair amount of variation in the required distances between the presented examples. Besides their weight, the main reason for these discrepancies lies in their mission requirements. Specifically, some aircraft are designed to operate from very short landing strips with difficult approach and departure procedures. These aircraft are often referred to as short take-off and landing (STOL) aircraft.

The typical characteristics of a STOL aircraft include low wing loading and extensive use of high-lift devices allowing to perform a slow, steep approach and a short landing run. Additionally, STOL aircraft often exhibit high thrust-to-weight ratios allowing them to achieve a short take-off run and a steep climb angle. Most of these aircraft are also equipped to serve remote areas and to land on unpaved runways. [19] Some noteworthy examples of STOL aircraft from Table 2.1 include the DHC-6 Twin Otter 400, GAF Nomad N24A, and Let L-410 Turbolet NG.

On the other side of the spectrum, some commuter aircraft are designed for a faster and more comfortable flight experience, rather than STOL. They are not as restricted in the runway length or approach procedures, which makes their design more akin to larger propeller transport aircraft. Good

examples of such aircraft from Table 2.1 are the BAE Jetstream 31, Fairchild Metro 23, and Beechcraft 1900D. Generally, they are designed to fit 19 people. These aircraft also have a pressurised cabin allowing them to fly at higher altitudes, which increases speed and the ability to avoid adverse weather.

## 2.2. Hydrogen as Aviation Fuel

In the interest of ending the over-dependence on fossil fuels, hydrogen has become one of the main contenders for a replacement. However, with many competing options available one might ask themselves why hydrogen is seen by many as the fuel of the future and more specifically, why it is being considered a viable aviation fuel replacement. This section will attempt to answer these questions.

### 2.2.1. Why Hydrogen?

As mentioned in the introduction, there are many alternatives to the current aviation fuel that are being investigated, and some are already in use. The majority of these alternative aviation fuels revolve around producing kerosene-based aviation fuel from alternative feedstock, such as waste oils, biomass, or even direct carbon capture. Instead of using crude oil and the corresponding traditional refining process, these fuels are synthesised using other chemical processes. Since the end product is very similar to conventional jet fuel, there are minimal or even zero modifications necessary for conventional aircraft to use it. [20] This solution is promising, since it can be gradually implemented with the current aircraft fleet by blending the synthetic fuels with regular kerosene. [21] However, promoting these fuels also runs the risk of making the industry complacent. After all, although the net $CO_2$ emissions might be reduced with synthetic fuels, the effects of aviation on global warming extends far beyond just $CO_2$. In fact, as already discussed in Chapter 1, the impact of non-$CO_2$ related emissions, such as $NO_x$, water vapour, and particulate emissions, is just as high as the impact of $CO_2$ emissions. While there are indications that synthetic aviation fuels might be able to reduce some of these effects as well [22], they will not eliminate them. Overall, the SAF solution does present a compelling environmental impact mitigation pathway for aviation. Nevertheless, due to the non-$CO_2$ related effects, it does not appear truly sustainable in the long term.

Alternatively, fully electrified aircraft powered by batteries are being considered. However, the battery energy density is still very low. Even with the net powertrain efficiency of electric aircraft exceeding 70% [23], battery-powered electric aircraft are very limited in range. The low energy density issue is exacerbated by the fact that the batteries are usually not discharged below 20% in order to increase their longevity [24]. Thus, it is not clear when batteries will be able to power transport aircraft over long distances.

Unlike synthetic aviation fuel, hydrogen does not produce carbon emissions when consumed. When combusting hydrogen, the main product is water. Additionally, due to the high temperatures of combustion and the presence of atmospheric nitrogen in the combustion process, some $NO_x$ emissions are being produced. Still, combusting hydrogen eliminates the carbon and particulate emissions, while most likely also reducing the $NO_x$ effects. [25] According to Wehrspohn *et al.* [26], powering single-aisle turbofan aircraft with hydrogen combustion would reduce the global warming potential from in-flight emissions by around 60%. Moreover, when using hydrogen in fuel cells instead of combustion engines, the only reaction product is liquid water. Naturally, this further reduces the environmental impacts of in-flight emissions. Furthermore, unlike batteries, molecular hydrogen stores more energy than traditional jet fuel per unit of mass. These attributes make hydrogen an attractive energy carrier that could at least in part pave the way for a considerably more sustainable aviation industry.

### 2.2.2. Hydrogen Production Methods

One of the main challenges that have to be addressed before hydrogen can be considered a sustainable alternative to jet fuel is hydrogen production. Unfortunately, molecular hydrogen is not readily available to be harvested or extracted. Instead, hydrogen has to be obtained by converting other sources into molecular hydrogen. Nowadays most hydrogen is produced by extracting it from fossil fuels, namely, natural gas (76%) and coal (23%) [27]. The fact that the main goal of using hydrogen as aviation fuel is to move away from fossil fuels makes these methods far from ideal. Fortunately, many other methods of hydrogen production are currently available. The rest of this section will present some of the most prominent hydrogen production methods, using both the fossil fuel pathways, as well as some of its alternatives.

A trend of colour-coding hydrogen according to its production method has become common in the industry and academia. While there are minor inconsistencies among different academic and industry sources concerning the use of specific colour codes, the following codes appear most often: [28, 29]

- **Grey hydrogen** – Produced by using fossil fuels. While there are numerous production methods, the most prominent ones are natural gas steam reforming (NGSR) and coal gasification. In the grey hydrogen category, no carbon capture occurs in the hydrogen production process. However, almost half of the grey hydrogen is obtained by harvesting the by-products of other chemical processes. Some sources split the grey hydrogen into more categories, such as black hydrogen obtained from black coal, brown hydrogen obtained from brown coal, and grey hydrogen obtained from steam-reforming natural gas;

- **Blue hydrogen** – Produced in the same fashion as grey hydrogen, but with the addition of some sort of carbon capture and storage (CCS) or utilisation (CCU). It is worth noting that besides being more technologically complex and expensive, not all carbon is captured in the process. Even more troubling, there are no standards for what percentage of total emissions should be captured and thus, most of the emissions are still released freely into the atmosphere. Furthermore, the often underestimated effect of methane leaks in the process is not mitigated either;

- **Turquoise hydrogen** – Produced via methane pyrolysis, resulting in solid carbon byproducts. These solid carbon byproducts are easier to store or sell off for further processing. While it appears more environmentally promising than blue hydrogen, the process has not been commercialised yet;

- **Purple hydrogen** – Produced using nuclear power in one of two ways. In the first option, hydrogen is extracted from water using high-temperature electrolysis or HTE. In the latter case, the heat of nuclear power generation is used to achieve thermochemical hydrogen production. While the risks of nuclear energy are well-known, the method does not produce any direct carbon emissions. In some sources this type of hydrogen is also labelled as yellow hydrogen;

- **Green hydrogen** – Produced via water electrolysis using electricity from renewable energies. In this category, solar and wind power are most often proposed. Besides 'green', this hydrogen product is also often labelled as 'clean' or 'renewable' hydrogen.

- **Yellow hydrogen** – Produced via electrolysis using grid electricity mix. Unsurprisingly, this production path is similar to the other electrolysis methods. However, the cost and environmental impact of this method depends highly on the suppliers of the local electrical grid.

### 2.2.3. Hydrogen Cost and Environmental Impact

Naturally, every hydrogen production method is associated with a different hydrogen cost and environmental impact. Unfortunately, it would be difficult to include a comprehensive analysis of both of these two issues for all of the methods listed above. Instead, the approximate production $CO_2$ emissions and final cost estimates for some of the processes mentioned will be presented.

Figure 2.1 illustrates the carbon intensity of hydrogen production for 9 different production methods. While there are many other negative environmental effects beyond the direct $CO_2$ emissions associated with every hydrogen production option, Figure 2.1 provides a general impression of the environmental impact differences between various production pathways. As can be seen from the figure, hydrogen extracted from coal releases a large amount of $CO_2$. A better alliterative to coal in terms of direct $CO_2$ emissions is natural gas. Using natural gas, the $CO_2$ emissions are more than halved. Furthermore, with effective carbon capture methods, the $CO_2$ footprints of both methods can be greatly reduced. Nevertheless, powering electrolysis with renewable or nuclear power generation has by far the lowest $CO_2$ intensity of all the listed options.

Interestingly, due to larger losses in the entire process, the electrolysis powered by coal or natural gas electricity generation releases even more $CO_2$ than directly extracting hydrogen from coal or natural gas. Even when electrolysis is powered by the global average grid electricity mix the $CO_2$ emissions are higher than using the other most $CO_2$ intense method, coal gasification.
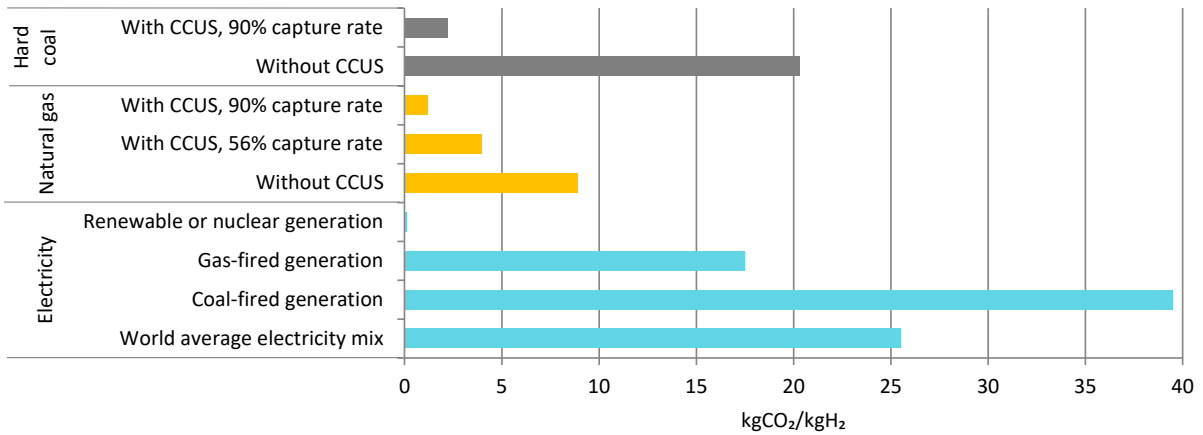
**Figure 2.1:** $CO_2$ intensity of hydrogen production. Adapted from [27].

As can be seen from Figure 2.2, unfortunately, hydrogen obtained using water electrolysis and low-carbon electricity generation is still the most expensive. The NGSR option is currently the cheapest of all the included production pathways. However, with future technology improvements, the low-carbon alternatives, such as electrolysis with renewable electricity generation, will decrease in price. Additionally, the greenhouse gas emission allowances that have recently been introduced into many markets will likely raise the cost of production for $CO_2$-intense methods. These factors are reflected in the 2060 price predictions given by IEA [30].
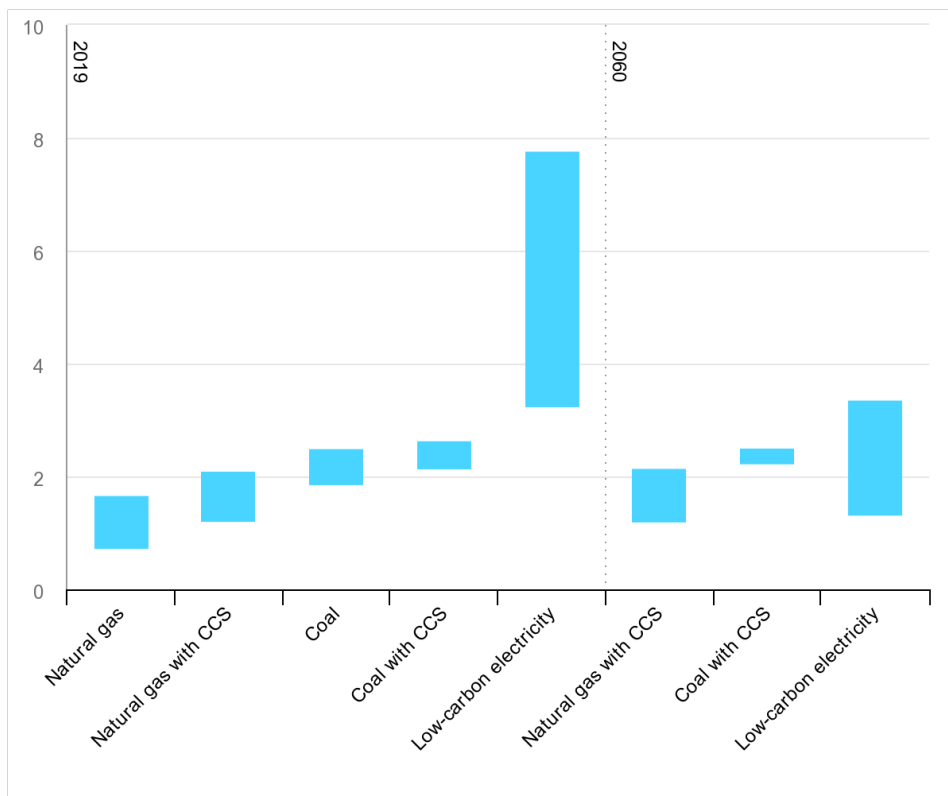


**Figure 2.2:** Hydrogen cost (2019 data and 2060 estimates). Retrieved from [30].

## 2.3. Fuel Cell Power

This section will explore the principles of fuel cell power generation and present the fuel cell type that will be used throughout this research project. Furthermore, this section will introduce the support systems that facilitate fuel cell operation.

### 2.3.1. Fuel Cell Working Principle

Similarly to a battery, a fuel cell relies on electrochemical reactions to provide electrical current. However, unlike a battery, a fuel cell is not an energy storage device, but merely an energy converter that relies on a constant supply of fuel to function. In this regard the fuel cell is more akin to an internal combustion engine (ICE), reacting fuel with oxygen and harnessing the energy released during the chemical reaction. [31]

The principle that makes fuel cells different from the ICE lies in how the reaction energy is harnessed. To understand this difference, however, one has to look into the mechanics of a simple combustion reaction, such as the reaction between hydrogen and oxygen:

$$H_2 + \frac{1}{2}O_2 \rightarrow H_2O \tag{2.1}$$

When a reaction takes place, the bonds in the $H_2$ molecules and the bonds in the $O_2$ molecules are broken up while new hydrogen-oxygen bonds are formed to create water or $H_2O$ [31]. The bonding energy of the reactants is higher than that of the reaction products. Thus, the reaction releases energy. In a combustion engine, this energy is converted directly into heat, causing the combustion gases to expand. The expansion can be converted into mechanical work either by driving pistons or spinning turbines. This process of energy recovery is unfortunately not very efficient. Moreover, internal combustion engines which nowadays still power most of our transportation are mechanically complex due to a large number of moving parts. Additionally, they produce unwanted emissions and vibrations whilst also emitting a fair amount of noise.

Naturally, the question arises, whether there exists a better way to tap into the energy of the reaction while also eliminating some of the downsides of the ICE. Observing the reaction on an atomic level, the breaking and rebuilding of bonds can be seen as a rearrangement of electrons. Thus one could attempt to extract electrical energy by harnessing these electrons when they travel to form the new, lower energy bonds. This is exactly what fuel cells are designed to do. By separating the two reactants and allowing the electrons to only flow over an external circuit they can provide useful work before being allowed to combine with the rest of the reactants on the other side of the fuel cell. [31]
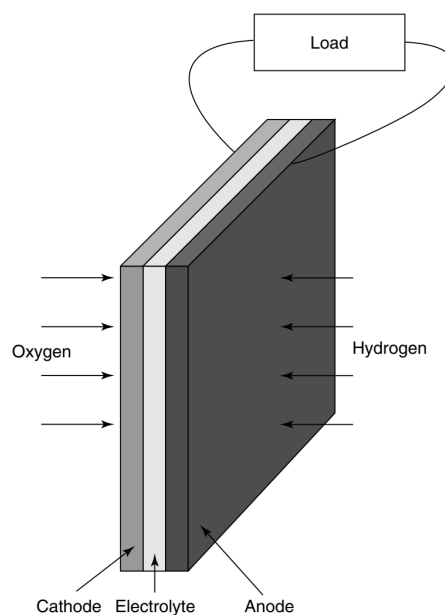


**Figure 2.3:** Schematic representation of a simple hydrogen fuel cell. Retrieved from: [32]

A schematic representation of a simple hydrogen fuel cell is displayed in Figure 2.3. The two electrodes (cathode and anode) are separated by an electrolyte. Depending on the type of electrolyte used, the reactions at the anode and cathode differ, but the overall reaction remains unchanged. For instance, when using an acidic electrolyte, the hydrogen atoms are stripped of their electron at the anode. Now, the hydrogen ions ($H^+$) can move freely through the electrolyte to the cathode. The electrons, meanwhile, travel to the cathode through an external circuit where they can power an electrical load. At the cathode, the free electrons, the hydrogen ions, and the oxygen finally react to form water. The chemical reactions at the anode and cathode are presented in Equation 2.2 and Equation 2.3, respectively. [32]

$$H_2 \rightarrow 2H^+ + 2e^- \tag{2.2}$$

$$\frac{1}{2}O_2 + 2H^+ + 2e^- \rightarrow H_2O \tag{2.3}$$

Since they have no moving parts, fuel cells are mechanically less complex than ICEs and therefore also have a higher potential for reliability. Furthermore, fuel cells in operation are silent and do not produce unwanted pollutant emissions, such as nitrogen oxides ($NO_x$). These qualities make them an attractive option for replacing the ICE in numerous applications.

### 2.3.2. Proton Exchange Membrane Fuel Cell (PEMFC)

The basic fuel cell presented in the previous section is not the only hydrogen fuel cell type available. Moreover, molecular hydrogen is also not the only fuel that can be used to power a fuel cell. In fact, there are numerous different types available on the market and in development utilising various methods to harness the electrical energy released during an oxidation reaction. However, for reasons that will be given in this section, this research will focus on a specific type of fuel cell, namely the Proton Exchange Membrane Fuel Cell or PEMFC.

The PEMFC is low a temperature fuel cell operating between 60 and 100 °C. It utilises a solid proton-conducting polymer electrolyte, usually made from perfluorinated sulfonic acid. The acidic electrolyte allows for free transport of hydrogen ions ($H^+$) between electrodes, while the electrons travel on an outside circuit to generate an electrical current. Once the hydrogen ions and electrons reach the cathode, they react with oxygen to produce water. The reaction equations at the anode and the cathode can thus be written as seen in Equation 2.4 and Equation 2.5, respectively. [31, 33]

$$2H_2 \rightarrow 4H^+ + 4e^- \tag{2.4}$$

$$O_2 + 4H^+ + 4e^- \rightarrow 2H_2O \tag{2.5}$$

The thin and flexible electrolyte membrane is coated on either side with a platinum catalyst and sandwiched between the two opposing electrodes. Together, the electrodes, catalyst, and membrane are simply called Membrane Electrode Assemblies (MEA). To ensure conductivity, the polymer membrane must be hydrated with liquid water at all times. For this reason, the cell temperature cannot raise above 100 °C, since the water would evaporate, drying out the membrane. [31, 33]

The low operating temperature brings a distinct set of advantages and disadvantages. The rapid start-up and stop procedure makes it ideal for transport applications. Furthermore, it provides the highest power density of all the fuel cell types at a relatively high efficiency. On the negative, the PEMFC requires the expensive platinum coating to catalyse the ionising of hydrogen. Furthermore, the efficiency of the cell is proportional to the operating temperature. Hence, the operating temperature cap is limiting the possible efficiency improvements. Another drawback of PEMFC is the susceptibility to carbon monoxide and sulphur contamination (also known as 'poisoning'), of the electrolyte. However, this can be mitigated by assuring high hydrogen fuel purity. [31]

Despite a handful of drawbacks, the listed advantages of the PEMFC make them by far the most promising type of fuel cell for transport applications and the replacement of the ICE. In fact, all manned fuel cell aircraft that have been flown to date were powered by PEMFC. Thus, due to the benefits and relatively high technology maturity, the PEMFC is the fuel cell type selected for this research.

### 2.3.3. Fuel Cell System (FCS)

The Fuel Cell System (FCS) usually includes many individual fuel cells connected to form a fuel-cell stack. While the fuel cell is at the core of an FCS, it is by no means the only important component. Similarly to a conventional internal combustion engine, there are several supporting subsystems necessary to maintain the right operating conditions for the powerplant and ensure that the system can reliably perform useful work. These subsystems can be referred to as the Balance of Plant (BoP) components. This includes, among others, fuel and oxidiser supply, cooling, power management, and fuel cell monitoring. Many of these components require energy to operate and are therefore referred to as parasitic power components or ancillaries. Depending on the fuel cell type and applications, the BoP components will be slightly different. Here, the focus will be on PEMFC used in mobile applications. [31, 32]

**Fuel-cell stack**

Under operational load a single fuel cell produces only between 0.6 and 0.7 V. Therefore, multiple fuel cells are normally interconnected in series to form a so-called fuel cell 'stack' and increase the voltage output. Several distinct stacking architectures have been developed over the years. Here, only the most prevalent arrangement for PEMFC stacks will be presented shortly. This arrangement is called 'bipolar plate stacking'. The name refers to the conductive plate that interconnects two adjacent cells. The plate connects the anode of one cell to the cathode of the next, thus earning its name 'bipolar'. This layering simplifies the electrical connections between cells and provides a large connection area resulting in low ohmic losses. The schematic representation of such a vertical stack can be seen in Figure 2.4 with the 'flow structure' acting as the bipolar plate. A more true-to-life representation of the bipolar plate architecture can be seen in Figure 2.5. This figure also illustrates the groves carved into the bipolar plates that allow the distribution of hydrogen and oxygen throughout the cell. [31, 34]
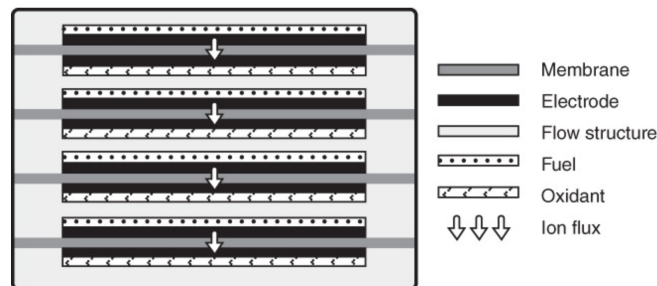


**Figure 2.4:** Schematic representation of a 'bipolar plate' fuel-cell stack. Retrieved from: [31]



**(a)** Single fuel cell assembly

**(b)** Triple-cell stack assembly
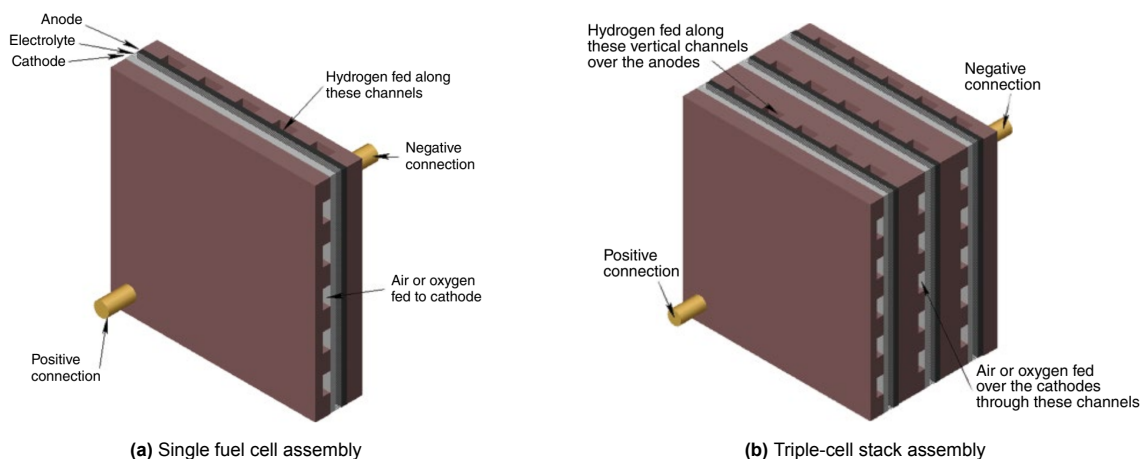
**Figure 2.5:** Simplified bipolar plate fuel cell assembly. Retrieved from: [32]

**Oxygen Supply**

Due to weight and size considerations, the oxygen is rarely stored on board, unless strictly necessary. Thus, the majority of PEMFC systems supply oxygen by simply filtering and sometimes compressing the ambient air. Using ambient air instead of oxygen does come with a significant drawback, however. The presence of gases other than oxygen decreases the oxygen concentration at the cathode, which reduces the maximum power a fuel cell can provide. Furthermore, operating at higher altitudes lowers the ambient pressure which further reduces the oxygen levels. The design choice one has to address is whether to use compressors to increase the air pressure in the fuel cell. While this does provide more oxygen and increase the open circuit voltage of the fuel cell it also incurs a weight and power penalty. The choice of compressing the air is of special interest for aircraft applications. Without compressing the ambient air, the fuel cell performance degrades significantly with increasing altitude. On the other hand, any additional weight as a result of ancillary components will have a detrimental effect on the overall aircraft performance. [32]

**Fuel Storage and Supply**

According to Verstraete *et al.* [35], the on-board storage of hydrogen is one of the major hurdles in hydrogen powertrain adoption. Although hydrogen has a higher weight energy density compared to conventional hydrocarbon fuels, it falls way behind conventional fuels on the volumetric energy density scale. The research community is exploring many different ways of hydrogen storage. However, only a few of these methods have reached the level of maturity, where they can be seen as a serious candidate for aeronautical applications. Currently, the most widely considered forms of pure hydrogen storage in portable applications are compressed gas or cryogenic liquid. There is also a third option that combines the two methods into pressurised cryogenic storage, often referred to as cryo-compression. [15, 36]

Arguably, one of the most important hydrogen tank parameters for aeronautical applications is the gravimetric storage density or $\eta_{grav}$. This metric essentially conveys how mass efficient the tank is at storing hydrogen and can be defined as written in Equation 2.6, with $m_{tank}$ and $m_{fuel}$ being the respective masses of the hydrogen tank and hydrogen fuel. Unsurprisingly, keeping the $\eta_{grav}$ as high as possible is desired for aeronautical applications. [35] With the importance of the gravimetric storage density in mind, the various storage options will be reviewed briefly.

$$\eta_{grav} = \frac{m_{fuel}}{m_{tank} + m_{fuel}} \tag{2.6}$$

The pressurised gas storage tanks are usually designed for either 350 bar or 700 bar. Despite the high pressures, only 4% of the full tank mass is down to hydrogen. Due to the high pressure, the fuel flow toward the fuel cell is usually controlled by a relatively simple system of valves and pressure regulators. Although the high-pressure storage was used in most fuel cell land vehicles and aircraft demonstrators, Verstraete *et al.* [35] believe that cryogenic storage is the only way to truly mitigate the volumetric density penalty and allow for mass adoption of hydrogen in transport aircraft. For cryogenic storage, hydrogen is cooled down and liquefied at around 20.3 K. This allows for smaller tanks but makes the system suffer from hydrogen boil-off caused by heat leaking into the tank. To mitigate that, the cryogenic tanks need to be well insulated. However, a certain amount of boil-off should be permitted to pressurise the fuel lines. The current design of cryogenic fuel tanks is not appropriate for aviation applications. The tanks used in the automotive industry are not as limited by their weight and the tanks used in rocket launch vehicles suffer from high boil-off rates due to their poor insulation.

Cryo-compression attempts to mitigate both of these issues. By compressing the fuel, the boil-off is almost eliminated. Furthermore, cryo-compression uses lower pressures than normal pressurised storage. Hence, the tanks can be designed for lower stress requirements and thus become lighter. Based on the research presented by Verstraete *et al.* [35], for a typical commuter aircraft with a fuselage diameter between 1.3 and 1.9 m, the expected gravimetric efficiency for cryo-compression tanks is between 40 to 60%, depending on the exact tank shape and aircraft performance. However, cryo-compression storage development is fairly limited. Moreover, out of the three methods it suffers from the highest energy footprint due to its high energy requirements for cooling and compression. [15, 35, 36] Nevertheless, it is still deemed to be the most favourable option for designing hydrogen-powered aircraft that can compete with conventional aircraft's mission capabilities.

Further options for storing hydrogen have been proposed. Most notably, these include metal hydrates and various chemical compounds. In metal hydrates, the hydrogen is packed inside a metal

crystal lattice. This option suffers from excessive weight due to the inherent density of metals used. Chemical storage is more attractive for aircraft because the compounds that carry hydrogen remain liquid in atmospheric conditions and provide high storage efficiencies, even above 20%. However, many of these chemicals are toxic and/or corrosive. [36] Kim and Kwon [37] demonstrated a fuel cell UAV with hydrogen stored in sodium borohydrate molecules. Additional weight was incurred due to the need for a hydrogen generator to extract hydrogen from the compound. Moreover, the borate crystals tended to clog the fuel lines, making it an overall unattractive option for commuter aircraft applications.

**Water Management**

As discussed in Section 2.3.2, the PEMFC membrane has to remain hydrated to function. In fact, the proton conductivity of the membrane is directly proportional to its water content. Unfortunately, the excess water can flood the electrodes, clogging the porous structure of the gas diffusion layer. Hence, the water content of the fuel cell has to be carefully managed to balance the needs of the membrane and the electrodes. Ideally, the water that is produced at the cathode would travel across the membrane to the anode, while the excess water at the cathode would be dried out by the incoming oxygen supply. Although not impossible, this self-humidifying process is hard to balance. Especially at high currents, the incoming air can dry out the cathode faster than it can produce water. Moreover, the protons tend to drag the water molecules across the membrane, drying out the anode. The prevalent solution is to pass the reactant gasses through a humidifier before they enter the cell, which can significantly boost the performance of the cell. [32, 38]

**Thermal Management**

Most larger PEMFC systems require active cooling to maintain the correct operating temperature. This is especially true for systems that have to respond quickly to increased power demands, such as aircraft or automotive powertrains. Active cooling can be achieved using either liquid or gas cooling. The former requires a set of fans or blowers while the latter relies on pumps. Naturally, these components consume some of the power produced by the fuel cell, thus the cooling needs should be minimised. However, for the highest power density systems, such as in aircraft, active cooling is normally performed using liquid cooling, since it has a higher heat capacity and thus a higher cooling potential. The coolant is usually circulated in a closed-loop system. The most common coolants are de-ionised water (to prevent it from carrying current) or a water-glycol mixture. [31]

**Power Management**

The electrical or power management subsystem in the FCS acts as an intermediary between the fuel-cell stack and the electrical loads, such as ancillaries and external electrical motors. Besides providing electrical connections it also modifies the electrical energy produced by the fuel cell to match the requirements of the consuming devices. The fuel-cell stack produces DC power at a specific voltage that is, among others, dependent on the stack architecture and current density. Thus, the electrical subsystem has to ensure a constant voltage for the loads. Furthermore, some loads require AC power, hence inverters are usually included. Often, fuel-cell powertrains are combined with batteries to form hybrid architectures. The electronic interface that manages all the power supply, modification, and distribution in more complex systems is then commonly referred to as the Power Management And Distribution (PMAD) system. [36]

## 2.4. Novel Aircraft Powertrain Architectures

A hydrogen fuel-cell powertrain is often associated with the term 'novel powertrain architecture'. Thus, it is worth examining what novel powertrain architectures are, and how and why fuel-cell powertrains fit into this category.

'Novel powertrain architecture' is a fairly broad expression describing any powertrain that does not operate like a conventional powertrain. For this research, a conventional powertrain can be defined as a powertrain that uses fuel in a combustion engine to produce mechanical energy that is then directly used for propulsion. Such a powertrain is used by all of the chosen reference aircraft and is thus a baseline for performance comparisons against the fuel-cell powertrain of a commuter aircraft. A simplified schematic of a conventional powertrain for a propeller-driven aircraft is depicted in Figure 2.6. For the legend of symbols used in these powertrain schematics, the reader can refer to Appendix A
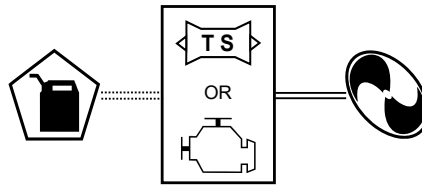
**Figure 2.6:** Conventional powertrain architecture

All novel powertrain architectures revolve around using electrical power transmission somewhere on the propulsion power path. However, this might also be the only universal characteristic of novel powertrain architectures. Hence, the variety of architectures that can be achieved by implementing these electrical power transmissions inside a powertrain is vast. The solutions range from a simple pure battery-electric aircraft, where the electricity is taken from the batteries via a power management unit and routed directly to the electric propulsion motors, to a complicated distributed propulsion architecture where power is drawn from multiple sources, such as batteries and ICEs, with a few power conversions in between. [39–41] Instead of explaining all of these novel architectures, the remainder of this section will focus on the two powertrain architectures that are crucial for the understanding of this research. These are the pure, non-hybrid, fuel-cell powertrain and the fuel-cell & battery serial hybrid powertrain architecture.

### 2.4.1. Pure Fuel-Cell Powertrain

The pure fuel-cell powertrain is the most straightforward powertrain architecture to utilise fuel cell power for propulsion. As depicted in Figure 2.7, this powertrain consists of a single power path, starting at the fuel tank, passing through the fuel-cell system, the power management and distribution unit or PMAD, and finally ending up in the electric propulsion motor that powers the propeller.



**Figure 2.7:** Pure fuel-cell powertrain architecture

However, one of the main issues that fuel cells are facing is their relatively low power density. In fact, this research project failed to create a feasible commuter aircraft by relying solely on fuel-cell for power generation. However, combining fuel cells with another source of energy that has a high specific power can provide a viable hybrid solution.

### 2.4.2. Fuel-Cell-Battery Serial Hybrid Powertrain

While batteries struggle with low energy density, they perform much better in the area of power density. The opposite is true for fuel cells. Therefore, combining the two can create a powertrain that makes fuel-cell-powered aircraft more feasible. The most straightforward way to combine the two power sources is by taking the pure fuel-cell powertrain, seen in Figure 2.7, and connecting a battery to the PMAD subsystem. In this way, a so-called serial hybrid fuel-cell powertrain architecture is obtained. [42] The schematic of such a powertrain is illustrated in Figure 2.8. Unless otherwise stated, this architecture will be used to model fuel cell aircraft throughout this report.
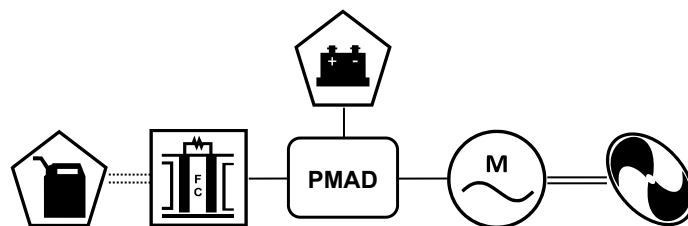


**Figure 2.8:** Series hybrid powertrain architecture with fuel cells and batteries

## 2.5. Existing Fuel-Cell Powered Aircraft

To date, only a handful of small aircraft has achieved flight under the power of fuel cells and none have gone past the experimental phase. This section will present the most notable examples, from the first manned fuel cell aircraft up to the most recent endeavours.

### 2.5.1. Boeing Fuel Cell Demonstrator

In 2008 the first-ever fuel-cell-powered manned flight took off from an airfield in Spain. The aircraft in question was an Austrian-built 2-seat Diamond HK36 Superdimona motor glider that was converted by the European division of Boeing Research & Technology. The original aircraft, certified under EASA's CS-22 regulations, had a MTOM of 770 kg, a wingspan of 16.3 m, and a lift-over-drag ratio of 27. The demonstrator was equipped with a PEMFC stack delivering 20 kW net or 24 kW gross power at around 200 V. This was enough to sustain level flight. During take-off and climb the power was also provided by the onboard Li-ion battery forming a hybrid system. The battery itself could continuously provide around 50–75 kW. The fuel-cell stack ran on hydrogen and compressed ambient air. The hydrogen was stored on board in a high-pressure composite tank at 350 bar. The propeller was driven by an experimental electric brushless permanent magnet DC motor. It was able to produce 75 kW peak power or 30 kW continuous power. [43, 44]



(a) Retrieved from [45]



(b) Retrieved from [46]

**Figure 2.9:** Boeing Fuel Cell Demonstrator (Diamond HK36 Super Dimona EC-003) on display at the 2008 Farnborough Airshow

The conversion increased the weight of the aeroplane by approximately 150 kg. This was partially due to the use of non-aerospace-grade components. Moreover, due to space restrictions, the passenger seat had to be removed to make space for the electronic power management box, as can be seen in Figure 2.9. The final weight of the aircraft exceeded the certified MTOM by 100 kg. The aircraft nevertheless successfully completed 3 test flights lasting between 26 and 28 minutes. [43, 44]

### 2.5.2. ENFICA-FC Rapid 200FC

The ENFICA-FC project, standing for *ENvironmentally Friendly Inter City Aircraft powered by Fuel Cells*, was a project led by the Politecnico di Torino and funded by the European Commission. The main objective of the project was to develop and validate the fuel-cell propulsion system for use in electric aircraft. These efforts culminated in converting an existing light aircraft to run on hydrogen fuel-cell propulsion. In many ways, this was a similar undertaking to the Boeing Fuel Cell Demonstrator, but it achieved its first flight two years after Boeing. [47–49]

The aircraft selected for conversion was the Czech Rapid 200 aircraft manufactured by Jihlavan Airplanes. The 2-seater aircraft with a wing span of 9.9 meters was modified in a similar manner to the Boeing Fuel Cell Demonstrator. The ICE powertrain was replaced by a PEMFC stack that was able to produce 20 kW continuous net power. This was augmented by two separate Li-Po battery packs providing another 20 kW of power for a limited duration of 18 minutes. The base level of power was provided by the fuel cell, while the battery system only interfered when higher levels of power were required.

**Figure 2.10:** ENFICA-FC Rapid 200FC exhibited at Rigenergia fair in May 2012. Retrieved from: [50]

The hydrogen was supplied to the fuel cell from two 26 l tanks designed for pressures of 350 bar. This allowed the aircraft to carry 1.2 kg of compressed hydrogen. The electric motor driving the propeller was rated at 43 kW and was air-cooled, thus providing large weight savings compared to a liquid-cooled system. In Figure 2.10 the air inlet to cool the motor is visible at the base of the propeller. Like done by Boeing, the passenger seat was removed to make space for the powertrain components. [47–49]

The aircraft conversion did increase the weight of the aircraft, but the designers managed to keep the total weight during test flights around 550 kg which was the maximum weight at which the original Rapid 200 was tested. The aircraft completed 6 flight tests. It achieved a maximum endurance of 39 minutes and a level speed of 135 km/h. The average pressure drop in the hydrogen tanks was 5.9 bar/min. [47–49]

### 2.5.3. Antares DLR-H2

The German Aerospace Center (Deutsches Zentrum für Luft- und Raumfahrt or DLR) developed a flying test bed for electric propulsion technologies based on the single-seater Antares 20E motor glider manufactured by Lange Aviation. Unlike the previous two examples, the production version Antares glider already included an electric powertrain, with the battery packs stored in the wings and a retractable electric motor and propeller boom mounted behind the cockpit. DLR converted the aircraft by including two pods below the wings, ass can be seen in Figure 2.11b. One of the two pods houses the PEMFC stack, including all the fuel cell support systems. The other pod contains the high-pressure hydrogen tanks, seen in Figure 2.11a. The batteries originally present were retained in the aircraft but served only as a backup. This means that the DLR-H2 is capable of performing take-off and climb powered solely by fuel cells. This is a major difference from other fuel cell aircraft designed so far. [51–53]
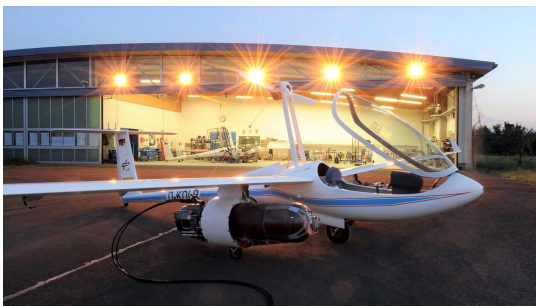


**(a)** On the ground with open hydrogen tank pod. Retrieved from [54]



**(b)** In flight. Retrieved from [55]

**Figure 2.11:** Antares DLR-H2 hydrogen fuel cell powered aircraft

The aircraft has been in service since 2009 and is used to expose the fuel-cell powertrain system to real flight conditions. In 2012 it was fitted with an improved fuel-cell system. The fuel-cell stack itself consists of 3 modules connected in series with a nominal output of 30 kW. The entire nacelle encasing

the fuel cells system is air-cooled through the inlet at the front of the pod. The hydrogen tank in the opposite pod is again rated at 350 bar with a volume of 200 l. This can be translated into a hydrogen capacity of 4.9 kg, which provides the aircraft with a flight time of about 5 hours. The boom-mounted motor is rated at 42 kW, thus being more than capable to handle the power produced by the fuel cells. The entire aircraft, including the pilot, can weigh up to 825 kg. The aircraft successfully demonstrated the reliability of the fuel-cell powertrain and achieved a hydrogen consumption of around 0.96 kg per 100 km at a velocity of 110 km/h. [51–53]

### 2.5.4. Pipistrel/DLR Hy4

The Hy4 made its first flight in 2016, becoming the first four-seater aircraft to be powered by fuel cells. In 2020, the aircraft was upgraded with a new generation fuel-cell powertrain designed as a part of the European MAHEPA (Modular Approach to Hybrid Electric Propulsion Architecture) project. The Hy4 aircraft is based on a Taurus G4 battery-powered motor glider, designed by Pipistrel of Slovenia. Just like the original G4, the Hy4 includes a twin-fuselage with a single motor situated between the two cockpits, as can be observed from Figure 2.12a and Figure 2.12b. The conversion led by DLR included fitting the aircraft with a PEMFC powertrain system, augmented by two Li-Po battery packs. This hybrid configuration was sized to provide half of the maximum power from the fuel-cell stacks and the other half through the battery system. In cruise, the aircraft could be powered solely by fuel cells. The cruise power setting allowed for a 15% power margin in the fuel cells. [42, 56, 57]



**(a)** In level flight during the test campaign. Retrieved from [58]



**(b)** First flight. Retrieved from [59]

**Figure 2.12:** DLR-Hy4 fuel-cell and battery hybrid aircraft

The hydrogen fuel was stored in two high-pressure tanks located in each of the two fuselages. Fully loaded, the aircraft weighed 1500 kg. It could achieve a range between 750 and 1500 km depending on the cruise speed, load, and cruise altitude. The single motor powering the aircraft was rated at 80 kW and propelled the aircraft to a maximum speed of 200 km/h. During a normal cruise, the aircraft travelled at approximately 145 km/h. [60]

### 2.5.5. ZeroAvia Piper M test bed

The British/American start-up ZeroAvia had successfully flown an electrified Piper M series aircraft. Initially, the aircraft was converted to fly using batteries to test the electric powertrain architecture, including the double electric motors that powered a single propeller. After initial test flights, another Piper M class aircraft was equipped with a fuel-cell powertrain. According to ZeroAvia [61], the fuel-cell-powered aircraft completed its first test flight in September 2020. The aircraft can transport 6 people, thus making it the largest flying fuel cell aircraft in the world. It is worth noting, however, that the actual aircraft can no longer house 6 people due to the additional powertrain components occupying the passenger cabin. The powerplant on board the aircraft is capable of generating 250 kW of power. Unfortunately, not many details are known about the powertrain architecture. The company is, however, already testing the powertrain components for its next project. This will be a fuel-cell conversion of the Dornier Do 228, but very little reliable information is available at the time of writing. [62, 63]

### 2.5.6. Discussion on Existing Fuel-Cell Aircraft

A great deal can be learned about the current state of the fuel-cell powertrain technology by looking at the common decisions made by the engineering teams behind the presented aircraft. The majority of projects integrated novel powertrain architectures into existing aircraft instead of designing new aircraft

from the ground up. Using existing aircraft designs not only makes the development cheaper and less risky but also offers a clear performance comparison to the original.

When it comes to fuel-cell propulsion, all presented aircraft took advantage of PEMFC technology for their fuel-cell stack. This is unsurprising since the PEMFCs have demonstrated the best overall performance for transport applications. Secondly, many designs incorporate a Li-ion or Li-Po battery to help alleviate the fuel cell power requirements during peak load conditions and quick changes in power requirements during flight. Finally, all aircraft run on compressed hydrogen stored in high-pressure tanks. Although cryogenic storage offers great potential for increasing the volumetric energy density of hydrogen fuel it is more expensive and the technology appears to be less mature. However, in order to compete with the performance of conventional transport aircraft, commuter aircraft will have to incorporate cryogenic storage. due to the high interest in hydrogen-powered flight, the technology might mature quickly in the near future.

Besides the powertrain architecture commonalities, most fuel cell aircraft flown to date have been light aircraft with high lift-over-drag ratios. This comes as no surprise since fuel-cell powertrains still offer lower specific power density compared to their conventional counterparts. By selecting aircraft with good aerodynamics and low power requirements, the weight penalty encountered by replacing the ICE with a fuel-cell powertrain is somewhat mitigated. Nevertheless, the existing fuel-cell-converted aircraft have struggled to maintain the mass of the aircraft below the certified MTOM even without carrying any useful payload. Besides the incurred weight penalty, the conversion also brought a volume penalty. Engineers had to install powertrain components in the aircraft cabin and thus reduce the passenger space. Nevertheless, by further developing novel powertrain components, specifically for aerospace applications, their weight and size are likely to reduce substantially.

Ultimately, none of the presented aircraft has been certified. Although the EASA's $5^{th}$ Amendment to the CS-23 regulation has been widely regarded as enabling the certification of novel powertrain designs for commuter aircraft [64], no aircraft has so far proven that this is indeed the case.

## 2.6. Existing Research on CS-23 Fuel-Cell Aircraft Design

Over recent years, a few studies on fuel-cell commuter aircraft have been produced. One of the first ones was the ENFICA-FC project. Besides the aircraft conversion described in Section 2.5, the ENFICA-FC project also produced conceptual design studies for a slightly larger fuel-cell-powered transport aircraft. In the paper by Romeo *et al.* [47], some design results for a new all-electric fuel cell powered 10-15 passenger aircraft were presented. The paper notes that compared to a turbine-powered version of the aircraft, the fuel-cell version had an increase in MTOM of 11.5% for a mid-term future technology scenario. Even so, the fuel-cell version had a reduced range of 1500 km, down from 2300 km, and a reduced cruise speed of 320 km/h, down from 550 km/h.

Similarly to ENFICA-FC, the MAHEPA project was also already mentioned in Section 2.5, because of their Hy4 aircraft conversion. However, the scope of the MAHEPA project was again broader than just the aircraft conversion. Generally, the goal of the project was to accelerate and mature hybrid electric propulsion through the collaboration of academia, research centres, and industry. In a similar fashion to ENFICA-FC, the MAHEPA project also produced conceptual studies on fitting larger aircraft with a fuel-cell hybrid powertrain. In their paper, Comincini and Trainelli [56] discuss the methodology for the fuel-cell hybrid powertrain sizing from the MAHEPA project for both, new and retrofitted aircraft designs. They validate their results using the previously converted Hy4 aircraft. With this validated model they produce a conversion study for 4 aircraft of varying sizes, from 4 to 72 seats. The batteries were sized to supply 50% of the total power and 15% of the total energy, while the fuel cell provided the rest. The results indicated that the conversions would result in an MTOM increase of 27 to 36%.

Building on the novel powertrain knowledge obtained through the activities of MAHEPA, a new EU-funded commuter aircraft design project, UNIFIER19, was created. The team behind the project set out to design a novel 19-seat aircraft that could connect small airfields to larger airports in an environmentally friendly way [15]. This was to be achieved with a combination of novel aerodynamic and propulsive technology. 18 different conceptual designs were produced and a trade-off was performed to select the best candidate. The winning design incorporated a traditional tube-and-wing configuration with a high-mounted wing and V-tail stabiliser surfaces. The aircraft was propelled by a distributed electric propulsion (DEP) system along the wing leading edge, as well as a single pusher propeller at the rear of the fuselage. The system drew power from a hydrogen fuel-cell system where hydrogen

was supplied from a cryogenic tank in the rear of the fuselage. Again, the fuel cells were augmented by batteries during peak power requirements. [65]

Another similar undertaking in the design of fuel-cell-powered aircraft was produced by Nicolay *et al.* [66]. They performed a clean-sheet design, analysis, and preliminary optimisation of fuel-cell-powered 4-seat general aviation (GA) aircraft. The aircraft design software used was the open-source SUAVE project from Stanford University. The aircraft requirements were set to typical 4-seat GA aircraft standards. The results show that the hydrogen-powered aircraft was on par with conventional aircraft both in terms of performance and aircraft mass. Compared to the Cessna Skyhawk and Cirrus SR20, the designed aircraft outperformed the reference aircraft in climb rate, range, and cruise speed. It is worth noting that the results appear very optimistic given the current or near-term future technology levels.

Focusing heavily on modelling the powertrain, Strack *et al.* [67] compared the performance and sizing of ICE-battery hybrid, as well as fuel-cell-battery hybrid architectures against the conventional turboprop powertrain. The powertrains were sized for a twin-engine 19-seat CS-23 commuter aircraft with a range of 400 km. Unlike the observations from Nicolay *et al.* [66], the results in this study found that the aircraft incorporating a fuel-cell architecture would weigh approximately twice as much as its conventional counterpart, while also flying at a slightly reduced Mach number. In contrast, the performance and mass of the ICE-battery hybrid designs were in line with the conventional aircraft. However, it appears that the technology-level predictions for the powertrain components are somewhat pessimistic and have been surpassed by the most recent hardware. Thus, the results might no longer be valid if current technological progress is taken into account.

In summary, it seems like there is no clear consensus on the feasibility of fuel-cell propulsion for CS-23 commuter aircraft or its superiority to other novel powertrain solutions. Most sources are unclear on the details of their aircraft design process and the implemented fuel-cell model, presumably due to the inherent complexity of both. Needless to say, this makes it difficult to compare the obtained results and identify where the shortcomings of individual studies may lie. Nevertheless, from the gathered literature it can be concluded that augmenting the fuel cells with a battery system is still necessary for transport aircraft in order to provide the required power levels during the take-off and climb segments. Furthermore, it is clear that fuel cell power is feasible, at least for smaller aeroplanes. This was proven with the presented fuel-cell demonstrator aircraft, especially considering some of them were built over a decade ago with non-aerospace grade components.

<div style="text-align: right; font-size: 3em;">3</div>

# Research Framework and Benchmark

Based on the information presented in the previous chapter, a research framework for this project will be established in the following sections. First, in Section 3.1, the research gap in the field of fuel cell commuter aircraft design will be identified. This section will also formulate the main research goal and set up relevant research questions. Next, a high-level overview of the approach and the necessary steps to fulfil the research goal will be given in Section 3.2. After that, the existing software that will be used to perform aircraft design throughout this project will be presented in Section 3.3. Besides the software description, the justification for selecting this particular tool will be given. Finally, Section 3.4 will explain the reasoning behind selecting four reference aircraft to serve as the benchmark for the fuel cell aircraft study during this research.

## 3.1. Research Goals

As shown in Section 2.6, some quantitative research into the performance benefits of fuel-cell powertrains for transport aircraft in the CS-23 category already exists. Nevertheless, the studies reached different conclusions on the feasibility and sensibility of fuel-cell propulsion. Thus, more research into this topic is needed. Further compounding this need is the fact that the analysis scope of existing studies is sometimes limited, both in the number of mission parameters, as well as in the sensitivity to various technical parameters. Furthermore, many studies refer to multiple different design tools to arrive at the performance metrics. Ideally, the aircraft should be sized using the same design framework to minimise biases introduced with the use of different sizing tools. Thus, the main research objective in this work is:

*To evaluate the performance and viability of fuel-cell powertrain integration on board a CS-23 category commuter aircraft compared to conventional powertrain architectures by modelling and comparing results obtained through a single aircraft design synthesis software.*

To guide this research and achieve the provided research goal the following set of research questions were identified:

**RQ-1** *How does the addition of the hybrid fuel-cell powertrain influence the aircraft conceptual design process?*

   **RQ-1.1** *How do the conventional powertrain sizing procedures have to be modified to permit the sizing of hybrid hydrogen fuel-cell-powered aircraft?*
   **RQ-1.2** *What influence does the addition of hybrid hydrogen fuel-cell powertrain have on the number of conceptual design loops compared to that of aircraft featuring conventional powertrains?*
   **RQ-1.3** *How does the number of iterations required to achieve design convergence for a hydrogen fuel-cell powered aircraft differ from that of aircraft featuring conventional powertrains?*

**RQ-2** *How does the performance of a hybrid hydrogen fuel-cell powered commuter aircraft differ from that of aircraft featuring a conventional powertrain?*

**RQ-2.1** *How does the maximum take-off mass of hybrid hydrogen fuel-cell powered commuter aircraft differ from that of aircraft featuring a conventional powertrain, given the existing CS23 commuter aircraft TLARs?*

**RQ-2.2** *How does the energy efficiency of hybrid hydrogen fuel-cell powered commuter aircraft differ from that of aircraft featuring a conventional powertrain, given the existing CS23 commuter aircraft TLARs?*

**RQ-2.3** *How does the mission cost of hybrid hydrogen fuel-cell powered commuter aircraft differ from that of aircraft featuring a conventional powertrain, given the existing CS23 commuter aircraft TLARs?*

**RQ-2.4** *How does the environmental impact of hybrid hydrogen fuel-cell powered commuter aircraft differ from that of aircraft featuring a conventional powertrain, given the existing CS23 commuter aircraft TLARs?*

**RQ-3** *Which design parameters are the hybrid fuel-cell commuter aircraft designs most sensitive to?*

**RQ-3.1** *Which mission parameters is the take-off mass of the hybrid fuel-cell powered aircraft most sensitive to, given the existing CS23 commuter aircraft TLARs?*

**RQ-3.2** *Which technology parameters is the take-off mass of the hybrid fuel-cell powered aircraft most sensitive to, given the existing CS23 commuter aircraft TLARs?*

**RQ-3.3** *Which mission parameters is the mission energy use of the hybrid fuel-cell powered aircraft most sensitive to, given the existing CS23 commuter aircraft TLARs?*

**RQ-3.4** *Which technology parameters is the mission energy use of the hybrid fuel-cell powered aircraft most sensitive to, given the existing CS23 commuter aircraft TLARs?*

## 3.2. General Approach

As the title suggests, this section will establish the framework to achieve the research goal that was presented in Section 3.1. To set up the framework, it is necessary to identify the required tasks and milestones that will eventually lead to the overall research goal and also help answer the research questions in the process. For this purpose, a road map of the research project summarising all the necessary steps is presented in Figure 3.1. Additionally, the figure also indicates which chapter of this report each of these tasks is presented in.

The first step in fulfilling the overarching research goals is to select an appropriate aircraft conceptual design tool. The selected software should be capable of modelling both the fuel cell and conventional commuter aircraft. However, the selected aircraft design tool may have some limitations that need to be identified and addressed before using it in this study. These limitations may require modifications and expansions to the software to make it suitable for this research project.

As will become clear in the next section, where the selected aircraft design software is discussed, a few shortcomings have indeed been identified and will have to be addressed. First of all, the selected software has initially been created to support the design of larger, CS-25 transport aircraft and thus does not support the design of CS-23 commuter aircraft. Consequently, the necessary modifications will entail identifying, implementing, and enforcing the relevant design constraints stemming directly from the CS-23 regulations. Furthermore, the mass estimation and other sizing methods will have to be updated to better accommodate commute aircraft. The new functionality will also have to be validated by modelling existing conventional CS-23 commuter reference aircraft and comparing the results.

Additionally, while the chosen aircraft design software in its current form already supports various novel powertrain architectures, such as full-electric battery powertrain and various ICE-battery hybrid configurations, fuel-cell powertrain sizing is not yet as advanced or fully validated. Thus, another goal of this research project will be improving and validating the previously developed fuel-cell powertrain sizing model.

In parallel to selecting the design software, reference conventional commuter aircraft need to be selected. These aircraft will be used to validate modifications and functionality expansions of the selected software, establish top-level aircraft requirements for the hybrid hydrogen fuel-cell commuter aircraft, and serve as a performance benchmark for the new fuel cell aircraft.
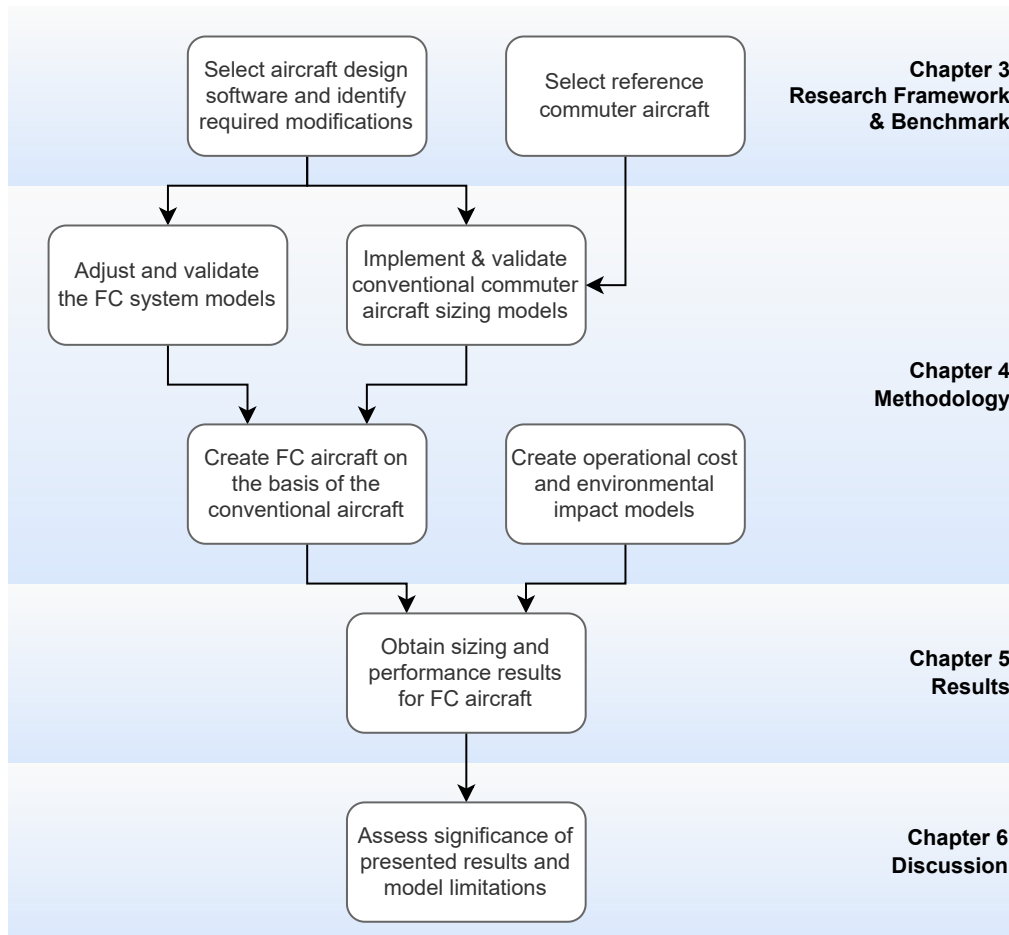
**Figure 3.1:** Research project road-map

In the next steps, which will be discussed in Chapter 4, the modification and validation of the fuel cell models in the selected aircraft design software need to be completed. Concurrently, the commuter aircraft functionality needs to be implemented and validated as well. With these two steps complete, the fuel cell aircraft can be modelled based on the top-level aircraft requirements of existing reference CS-23 commuter aircraft. Additionally, to answer research questions regarding cost and environmental impacts, two new models will need to be developed. These models will estimate mission operational costs and environmental impacts for both conventional and fuel cell aircraft.

After developing and validating the commuter fuel cell aircraft modelling and analysis functionality, the results can finally be obtained in the following step. The results will be compared against the original aircraft using a conventional powertrain in terms of mass, size, mission cost, and environmental impact. A comprehensive sensitivity analysis will also be performed to answer research question 3 on the sensitivity of the fuel cell aircraft's maximum takeoff weight and mission energy use. Ultimately, with all of the above objectives complete, the overall significance of the presented results and any limitations in the methodology, models, or results will be discussed. Completing all of these steps hopefully leads to attaining the research goals for this project.

## 3.3. Aircraft Conceptual Design Software

The aircraft sizing studies were performed with the use of the Initiator, a tool developed by the Faculty of Aerospace Engineering at the Delft University of Technology for rapid design evaluation of larger transport aircraft. While some external modules are written in other programming languages, the core software is written almost exclusively in MATLAB® (MathWorks, Natick, MA, USA). Besides being an in-house developed tool, the software was chosen because of its ability to model conventional, as

well as hybrid powertrain configurations. Moreover, Initiator had recently been expanded to allow the sizing of aircraft with fuel-cell propulsion units and cryogenic hydrogen storage. These capabilities made it almost an ideal software for this research project. However, as mentioned above, the Initiator was developed for large transport aircraft and as such, the implemented design procedures were in accordance with the EASA's CS-25 regulations. This meant that the capability to model CS-23-certified commuter aircraft had to be developed as part of this project. Before this process can be presented, however, it is first necessary to discuss the inner workings of the Initiator software.

On the uppermost level, Initiator is split into two branches, the first one being the 'conventional' branch and the second being the 'hybrid' branch. The 'conventional' branch is solely used for modelling conventional aircraft powertrains. The 'hybrid' branch, however, can model a wide range of electric and hybrid powertrains, as well as conventional powertrains. As the fuel-cell powered aircraft rely on an electric powertrain, the Initiator hybrid branch had to be used to obtain the research results. To ensure consistency, the hybrid branch was also used to obtain results for conventionally powered reference aircraft needed for software validation. For these reasons, the rest of this report will only discuss the hybrid branch.

While this research concerns the *changes* made to the Initiator, the following sections will explain the working principle of the existing software in more detail. This shall provide a basis to better understand the methodology presented in Chapter 4.

### 3.3.1. Hybrid Aircraft Sizing Procedure

The added complexity of a hybrid-electric aircraft powertrain also translates to a more complex aircraft sizing process. The conventional sizing can begin by simply determining the power- and wing-loading design point based on aircraft requirements and constraints. Based on this point, the aircraft powertrain and lifting surfaces can be sized. Conversely, when sizing hybrid-electric powertrains, there are multiple power paths and interacting components that each require their own design point.

The general approach to how this hybrid aircraft sizing was implemented inside Initiator is described in a 2018 paper by Vries *et al.* [39]. According to their methodology, 3 parameters are required to describe a hybrid system power balance. The first parameter is the total power demanded from the powertrain. The other two parameters are the 'supplied power ratio' and the 'shaft power ratio'. They describe the ratio between the shaft power produced by the secondary electrical machinery and the total shaft power produced, respectively. Since none of the powertrains considered in this research produces shaft power for propulsion through electrical machinery this term can be ignored.

Unlike the 'shaft power ratio', the 'supplied power ratio', is very important for a fuel-cell hybrid powertrain. This term describes the ratio of power drawn from an electrical storage device, such as batteries or capacitors, with respect to the total power drawn. In this case, the two power sources are batteries and fuel. The parameter can then be defined as follows:

$$\Phi = \frac{P_{bat}}{P_{bat} + P_{fuel}} \tag{3.1}$$

with $\Phi$ representing the ratio, $P_{bat}$ the power supplied to the propulsor by batteries and $P_f$ the power supplied by the chosen fuel. By specifying the variable $\Phi$ for every phase of the flight, it is possible to determine the peak power and total energy that every power path within the hybrid powertrain has to be able to provide.

Once the required energy and power per power path are determined, the individual components can be addressed. The general equation that needs to be solved when analysing any hybrid powertrain component is:

$$\sum P_{out} = \eta_i \sum P_{in} \tag{3.2}$$

with the left side of the equation representing the power flowing out of the component and the right side the power flowing into the component multiplied by the efficiency of the component in question. Solving a system of equations for the combination of power paths found in the hybrid powertrain being analysed yields the required power and energy requirements for every component.

It is important to note how crucial it is that the components are sized for both total energy and peak power. As an example, a certain battery size is sufficient to supply the required energy throughout the flight, but it might not be able to provide the necessary peak power required during take-off. In such a case the battery pack would have to be sized for peak power requirement instead of total energy.

While the paper does not specifically consider the sizing of fuel-cell powered aircraft, the implemented methods needed only slight modifications to allow for it. Concretely, the fuel-cell-battery powertrain sizing is performed in the same manner as the serial hybrid powertrain, which draws power from a gas turbine and a battery. To arrive at a fuel-cell and battery hybrid powertrain, the gas turbine can simply be replaced by a fuel-cell power unit, while the gearbox and generator can be omitted entirely. Details on how the individual components of the fuel-cell power unit are sized will be discussed later in Section 4.2.

## 3.3.2. Design Loop Structure

The Initiator is composed of individual aircraft sizing and analysis modules that can either be run individually or combined into complex design convergence loops. The design convergence loop that was used to obtain results during this project is depicted in Figure 3.2. The individual blocks represent separate Initiator sizing or analysis modules that connect to form smaller loops within the basic structure. There are two larger nested loops visible, the Class 1 & 2 loop and the Class 2.5 loop. The former loop represents the basis for any aircraft preliminary design. If desired, this loop can be expanded to include the Horizontal Stability Estimation or HSE. Similarly, the Class 2.5 loop provides additional detail and complexity to the design results but can be enabled or disabled depending on the desired fidelity of the results. To better understand the major building blocks of this design convergence loop they will be described in more detail throughout the following subsections.
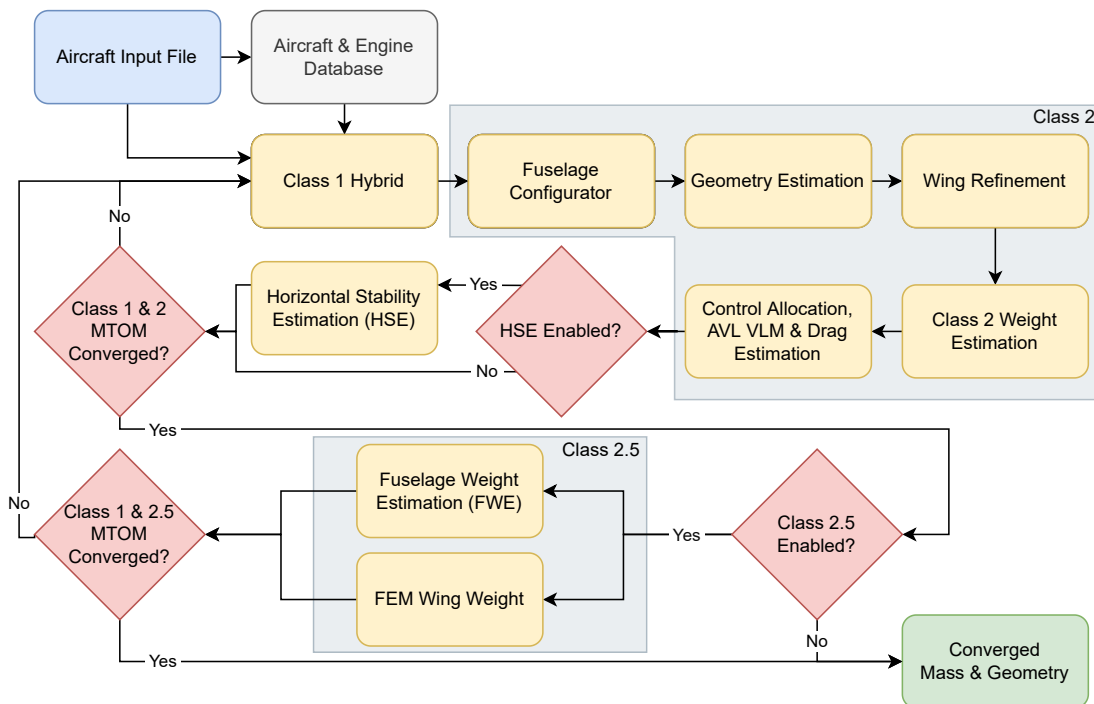


**Figure 3.2:** Initiator top-level convergence loops

### Aircraft Input File & Database

As can be seen from the diagram, the design procedure starts by passing an aircraft input file. This file is written in XML[1] format and contains the aircraft mission requirements, aircraft design parameters, and analysis settings. Many of the parameters and settings are optional and will revert to default values

---

[1]Extensible Markup Language

programmed into the Initiator when omitted from the input file. This ensures the user can freely decide between getting the most accurate result possible by including as many known design parameters as are available or relying mostly on the default values to get a quick aircraft design estimate from the limited information available about the aircraft.

The information in the aircraft input file is then read by the Initiator and the values become available to all the individual modules. This information is also used to construct a sample of reference aircraft and reference aircraft engines from the databases. The database module runs only on the first iteration of the design convergence and provides the starting point estimates for parameters that converge over the subsequent iterations.

**Class 1 Estimations**

In conventional aircraft sizing tools, the class 1 estimations would most likely include the determination of the wing- and power-loading design point, as well as the most top-level mass estimates based on reference aircraft regression values and simple fuel fractions. However, as already indicated in Section 3.3.1, the class 1 estimations of the Initiator hybrid branch require much more complex sizing methods due to various possible power paths.

Besides producing multiple power-loading diagrams to determine the design point of each power-train component, the hybrid class 1 estimation also includes the mission analysis that is integral in the determination of the required fuel and battery mass. However, since some value for the OEM (excluding the battery) is required to perform the mission analysis, the initial OEM value is taken from the conventional aircraft database. In a later iteration, this value is replaced by the OEM determined in the previous iteration.

**Class 2 Estimations**

After class 1 estimates achieve convergence, the *Fuselage Configurator* module is run. For the purposes of this research, the fuselage is sized 'inside-out'. In this way, everything that needs to fit inside the fuselage, such as the passenger cabin and the hydrogen tank, is sized first. Next, the fuselage walls are sized such that they encase all of the necessary components. The nose-cone and tail-cone geometry can be largely controlled by the user. For instance, the user can specify the length of the two 'cones' as a fraction of the fuselage cross-section. Similarly, the user can specify the nose droop and the tail-cone up-sweep as a fraction of the fuselage cross-section.

The next module to run is the *Geometry Estimation* which defines the geometry of the majority of the remaining components, including lifting bodies, stabilisers, pylons, nacelles, fuel tanks, and batteries. The geometrical sizing is then completed with the *Wing Refinement* module, where the wing geometry is further refined. To achieve this the module also incorporates external analysis modules, such as AVL[2].

Following the geometry estimation modules, the *Class 2 Weight Estimation* module is executed. This module consists of various mass estimation methods, combining empirical, semi-empirical, and analytical formulas to provide mass estimates of individual subsystems, operational items, and furnishing. This creates a more detailed mass profile of the aircraft. The vast majority of mass estimating expressions stem from the 1982 aircraft design book of Tornebeek [69]. Unfortunately, these classical aircraft design books have no mass estimation relations for subsystems specific to novel powertrains, such as hydrogen fuel tanks, fuel-cell systems, battery systems, and electrical subsystems for propulsion. Thus, these subsystems are sized by applying analytical and semi-empirical models from various research papers on the topic.

Finally, the class 2 estimations are concluded by a variety of smaller modules such as control allocation and various aerodynamic analyses. In Figure 3.2 these modules were grouped into a single step for simplicity. First, the *Control Allocation* module places control surfaces on the appropriate surfaces on the aircraft. Next, *AVL VLM* module is run, using the AVL software on the updated aircraft to obtain more aerodynamic results. Ultimately, the aptly named *Drag Module* is executed to determine the total drag value of the current aircraft geometry. To achieve this the module retrieves aerodynamic results from the *AVL VLM* module to estimate induced drag. The remainder of the total drag is estimated by calling upon two other modules, named *Parasitic Drag* and *Wave Drag*. Adding all the relevant

---

[2]Athena Vortex Lattice or AVL is an open-source aerodynamic analysis tool developed by Mark Drela and Harold Youngren using an extended vortex lattice model for the lifting surfaces and a slender-body model for fuselages and nacelles. [68]

drag components together, the *Drag Module* outputs the new drag polar maps. With this, the class 2 estimations are completed.

**Horizontal Stability Estimation**

As can be seen from Figure 3.2, if enabled, *Horizontal Stability Estimation* or HSE is executed just after the class 2 modules. As the name suggests, the HSE analyses the horizontal stability of the aircraft for various loading scenarios and various aircraft configurations. These configurations include power-on and power-off scenarios during take-off, landing, and cruise. Based on this analysis, the wing position along the fuselage and the horizontal stabiliser surface area are adjusted to satisfy the stability and manoeuvrability requirements.

**Class 2.5 Estimations**

The class 2.5 estimations refer to two structural estimation modules that can be toggled on or off independently. The first module, the *Fuselage Weight Estimation* or FWE is concerned with the fuselage structural mass, while the *FEM Wing Weight* module is dealing with the main wing structural mass estimate. Both modules rely on a FEM analysis to try to improve the mass estimations from class 2 methods. Both of these methods are very input sensitive and can cause sudden jumps in mass estimates or convergence issues, especially when exploring more unconventional designs.

**Outputs**

Finally, after all the MTOM estimates of class 1, 2, and 2.5 estimations converge within a set of pre-defined convergence tolerance limits, the loop stops. A file containing the results from every module that was included in the design loop is created. This file includes all the information apart from the convergence history. To phrase it differently, the file contains all the results from the last design iteration. Besides this condensed information file, there are numerous plots and figures that the Initiator is able to produce from the results of these modules. These figures range from MTOM convergence history, drag polars, final results on subsystem masses, and a complete aircraft geometry, just to name a few. Two examples, namely the MTOM convergence and the complete aircraft geometry are presented in Figure 3.3 and Figure 3.4, respectively.
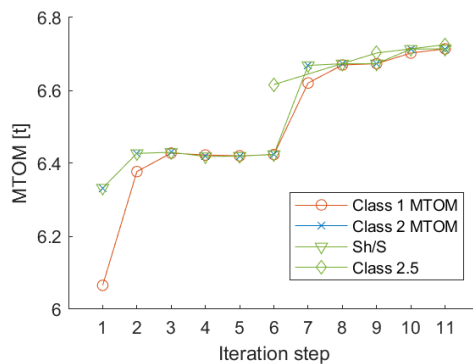


**Figure 3.3:** Example of a MTOM convergence plot from Initiator
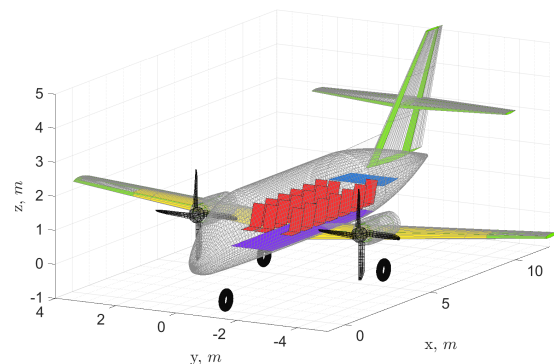


**Figure 3.4:** Example of a complete aircraft geometry plot from Initiator

## 3.4. Selecting Reference Commuter Aircraft

Out of the numerous commuter aircraft presented in Table 2.1, a set of 4 aircraft was selected to serve as reference aircraft. These reference aircraft will serve multiple purposes. Initially, conventional reference aircraft will be modelled in the aircraft design software that will be used throughout this project. Doing so, the existing software and any necessary modifications done for the purposes of this project will have the ability to be validated by comparing the software results to the reference aircraft data. Second, the mission requirements and many design characteristics of these aircraft will be used as a basis for the fuel cell aircraft designs. Finally, once the fuel cell aircraft results are obtained, these reference aircraft will allow for a clear comparison between the two powertrain solutions. The remaining paragraphs will explain the process behind the selection process and present the selected aircraft.

The selection of reference aircraft was done by assigning a suitability score to each aircraft presented in Table 2.1. The scores were given according to how good an aircraft did in the respective category. The scores ranged from very negative '--' to very positive, or '++' The final score was calculated based on three different criteria that will be presented in the following paragraphs. The scoring results can be seen in Table 3.1

**Table 3.1:** Reference aircraft selection scoring

| Aircraft type | Grading criteria | | | Final score |
|---|---|---|---|---|
| | FC powertrain compatibility | Initiator compatibility | Data availability | |
| Cessna Conquest II | 0 | 0 | ++ | 2 |
| Beechcraft 350ER | - | + | + | 1 |
| Mitsubishi MU-2L | 0 | + | + | 2 |
| Beechcraft Model 99A | 0 | + | - - | -1 |
| GAF Nomad N24A | + | - - | 0 | -1 |
| Harbin Y-12 F | + | - | + | 1 |
| DHC-6 Twin Otter 400 | ++ | - - | ++ | 2 |
| Embraer EMB 110P2 | ++ | + | + | 4 |
| Dornier Do 228-212 | + | 0 | ++ | 3 |
| BAE Jetstream 31 | + | ++ | ++ | 5 |
| Let L-410 Turbolet NG | 0 | + | + | 2 |
| Fairchild Metro 23 | 0 | ++ | ++ | 4 |
| Beechcraft 1900D | 0 | 0 | ++ | 2 |

The first criterion could be summarised as the suitability to fulfil the aircraft mission with a fuel-cell powertrain. The first consideration here is the aircraft power-to-weight ratio. Since fuel cells are still trailing behind conventional turbine engines in terms of specific power, fuel-cell-powered aircraft cannot yet compete with aircraft that have been designed to carry out a mission where very high specific power is required. This is often true for aircraft with STOL capabilities. Instead, the fuel-cell powertrain might be a sensible replacement in aircraft with more relaxed field length and climb gradient requirements. Moreover, the classical commuter aircraft without STOL capabilities are more likely to serve predefined scheduled routes to larger airports where the operator can provide the necessary hydrogen refuelling infrastructure for their fleet. Nevertheless, to truly capture the broader commuter aircraft segment it was also important to provide some diversity in terms of aircraft requirements. Thus, aircraft such as Do 228-212 and Let L-410, with some slight STOL characteristics, were not automatically excluded from the reference aircraft candidate list. The second important consideration is the aircraft range. While hydrogen is more competitive with regard to range requirements when compared to pure battery propulsion, it still needs a large and heavy hydrogen tank. Thus, any aircraft with excessive range was scored negatively.

Furthermore, the capabilities of the aircraft design synthesis software had to be considered when selecting reference aircraft. The selected software called the 'Initiator' was originally developed to study larger commercial airliners. Hence, it was not particularly well suited to recreate certain features present on some of the aircraft included in Table 2.1. For instance, features such as non-circular fuselage cross-sections, wing support struts, or non-retractable landing gear required extensive modifications to the core software to be modelled correctly. Thus, aircraft with such features were again scored negatively.

The ultimate consideration for selecting reference aircraft was the availability of aircraft design data. To accurately replicate an aircraft in an aircraft sizing environment such as the Initiator, a great amount of detail concerning mission parameters, flight performance, geometry, and subsystem information is required. Publicly available information on some of the listed aircraft is often too scarce to accurately extract this design data. Thus, the third selection criterion reflects this data availability.

Finally, taking into account all the considerations laid out above and tallying the scores in Table 3.1,

the following four aircraft were selected to serve as reference aircraft: Fairchild Metro 23, Dornier Do 228-212, BAE Jetstream 31, and Embraer EMB 110P2. The general information about these four aircraft is presented in Table 3.2.

**Table 3.2:** Reference commuter aircraft data. Information compiled from Jane's [18].

| Parameter | Unit | Aircraft type | | | |
|---|---|---|---|---|---|
| | | Do 228-212 | Metro 23 | Jetstream 31 | EMB 110P2 |
| **General** | | | | | |
| MTOM | kg | 6400 | 7484 | 6950 | 5670 |
| OEM | kg | 3742 | 4309 | 4488 | 3516 |
| Total length | m | 16.56 | 18.09 | 14.37 | 15.10 |
| Wingspan | m | 16.97 | 17.37 | 15.85 | 15.33 |
| Wing-loading | kg/m$^2$ | 200.0 | 260.7 | 275.8 | 195.5 |
| Power-loading | kg/kW | 5.53 | 4.56 | 4.96 | 5.07 |
| **Performance** | | | | | |
| Max. payload | kg | 1848 | 2268 | 1805 | 1681 |
| Range** | km | 800* | 978 | 780* | 440* |
| Cruise Mach | - | 0.362 | 0.400 | 0.382 | 0.283 |
| Service ceiling | m | 8535 | 7620 | 7620 | 6860 |
| **Passenger cabin** | | | | | |
| Seat number | - | 19 | 19 | 19 | 19 |
| Seat layout | - | 1+1 | 1+1 | 2+1 | 2+1 |
| Pressurisation | - | No | Yes | Yes | No |

*Estimated by the author through analysis and other available data.
**At maximum payload.

<div style="text-align: right; font-size: 4em;">4</div>

# Methodology

This chapter introduces the methodology behind the research presented in this report. First, the changes to the aircraft sizing software will be explained, beginning with the capability to size commuter aircraft in Section 4.1. In the same section, the sizing results for the 4 reference conventional commuter aircraft will be shown and validated. Next, Section 4.2 will describe the existing fuel-cell powertrain model and explain the modifications that were performed for the purpose of this research. Subsequently, the selected fuel-cell powertrain configuration and fuel cell aircraft design missions will be presented in detail in Section 4.3. Finally, the development of models to estimate emissions and mission energy cost will be explained in Section 4.4.

## 4.1. Adding Commuter Aircraft to the Design Software

As mentioned in Section 3.3, the Initiator aircraft sizing software was lacking the ability to size CS-23 certified commuter aircraft. Since such aircraft were never sized with the Initiator before, they inevitably unveiled many shortcomings and bugs within the software. Unfortunately, it would be difficult to mention every modification and fix that had to be implemented to achieve reliable aircraft sizing. Instead, this section will briefly talk about the challenge of modifying the preliminary design software, present some of the more notable modifications to the software, and explain how the results were validated.

Introducing changes to the preliminary sizing software can present a difficult balancing act. To size the reference commuter aircraft more accurately, the software needed more design settings and parameters to be directly controlled by the user, since the existing values did not reflect the characteristics of commuter aircraft. However, adding more settings can lead to design software asking the user to input information that is very specific and perhaps unknown in the preliminary stages of the design process. Thus, the challenge is to satisfy both, the capability to replicate existing aircraft designs in detail, as well as the ability to size completely novel, preliminary designs for which many parameters are still unknown.

Consequently, the changes were made in such a way, that the user is able to input very specific design parameters, but is not obliged to do so if the information is not available. This was made possible by creating a new settings file that contains default values for a typical commuter-type aircraft. Thus, when the user does not have the information available, the software can revert to the default values. Alternatively, when detailed information is available the user can easily override the default values where deemed necessary.

### 4.1.1. CS-23 Requirements

To enable commuter aircraft sizing, the first change to the Initiator software was implementing the relevant CS-23 aircraft certification requirements. All requirements were in accordance with the latest, 5th Amendment to the EASA's CS-23 regulation set. However, naturally, not all requirements in the CS are relevant to the preliminary design process. In fact, only a select few key requirements were identified as critical and ultimately implemented.

Since many of the requirements in the latest amendment have become less prescriptive it was sometimes difficult to quantify required aircraft performance for the purposes of aircraft design. However,

EASA did also specify 'Acceptable Means of Compliance' or AMCs for the majority of requirements for which this could be the case. The AMCs describe non-binding[1] means to comply with the basic regulations[70], usually in a more quantifiable way. Thus, where practical, appropriate AMCs were used as design constraints. As can be seen in the list of the implemented requirements below, all of these AMCs are part of the basic regulations present in the previous, 4th amendment to the CS-23.

**Climb Gradient Requirements**
Arguably, the most important requirements for aircraft preliminary design stem from the restrictions on flight path gradients in various All Engines Operating (AEO) and One Engine Inoperative (OEI) scenarios. These gradients directly restrict the available design space within the aircraft wing- and power-loading diagram. For CS-23 aircraft 7 relevant climb gradient restrictions were implemented. The first 3 come from requirement CS 23.2120 titled 'Climb Requirements':

*The design must comply with the following minimum climb performance out of ground effect:*

- **CS 23.2120.a.2**
  With all engines operating and in the initial climb configuration(s) a climb gradient at take-off of 4%.

- **CS 23.2120.b.3**
  After a critical loss of thrust on multi-engine aeroplanes a 2% climb gradient at 122 m (400 ft) above the take-off surface with the landing gear retracted and flaps in the approach configuration.

- **CS 23.2120.c**
  A climb gradient of 3% during balked landing, without creating undue pilot workload, with the landing gear extended and flaps in the landing configuration(s).

The other 5 climb gradient requirements come from CS 23.2115 titled 'Take-off performance' and CS 23.2125 titled 'Climb Information'. However, these requirements are implemented through their respective AMCs. All 5 climb requirements that will be listed here concern the aircraft with OEI. First, the CS 23.2115 is implemented through the CS 23.57 of amendment 4 where it is stated:

*For each commuter category aeroplane, the take-off path is as follows;*

- **CS 23 Amdt 4; 23.57.c.1**
  During the take-off path determination, in accordance with sub-paragraphs (a) and (b), the slope of the airborne part of the take-off path must not be negative at any point;

Finally, the CS 23.2125 is implemented through the CS 23.67.c of amendment 4 where the following climb restrictions are stipulated:

*For commuter category aeroplanes, the following apply;*

- **CS 23 Amdt 4; 23.67.c.1**
  Take-off: landing gear extended. The steady gradient of climb at the altitude of the takeoff surface must be measurably positive with –
  
  - i. The critical engine inoperative and its propeller in the position it rapidly and automatically assumes;
  - ii. The remaining engine at take-off power;
  - iii. The landing gear extended, all landing gear doors open;
  - iv. The wing flaps in the take-off position(s);
  - v. The wings level; and
  - vi. A climb speed equal to $V_2$[2].

---

[1]It is possible for the aircraft manufacturer to show compliance with the regulation by other means than specified in the AMC. However, the regulatory body must agree that the custom proof of compliance is valid.
[2]The speed at which the aircraft may safely climb with one engine inoperative.

- **CS 23 Amdt 4; 23.67.c.3**

  En-route: the steady gradient of climb at an altitude of 457 m (1 500 ft) above the takeoff or landing surface, as appropriate, must be no less than 1.2% with –

    i. The critical engine inoperative and its propeller in the minimum drag position;

    ii. The remaining engine at not more than maximum continuous power;

    iii. The landing gear retracted;

    iv. The wing flaps retracted;

    v. The wings level; and

    vi. A climb speed not less than 1.2; $V_{S1}$[3].

- **CS 23 Amdt 4; 23.67.c.4**

  Discontinued approach: the steady gradient of climb at an altitude of 122 m (400 ft) above the landing surface must be no less than 2.1% with:

    i. The critical engine inoperative and its propeller in the minimum drag position;

    ii. The remaining engine at takeoff power;

    iii. The landing gear retracted;

    iv. The wing flaps in the approach position(s) in which $V_{S1}$[4] for these positions(s) does not exceed 110% of the $V_{S1}$ for the related all-engines-operating landing position(s)

    v. A climb speed established in connection with normal landing procedures but not exceeding 1.5 $V_{S1}$.

Implementing these constraints in the Initiator reflects in the aircraft power- vs. wing-loading diagrams. To illustrate this, Figure 4.1 presents two different constraint diagrams. While the aircraft TLARs are the same, some of the climb gradient requirements differ between the two diagrams. The diagram presented in Figure 4.1a corresponds to climb requirements in CS-25 regulations, while the diagram in Figure 4.1b corresponds to climb requirements in CS-23 regulations.



**(a)** CS-25

**(b)** CS-23
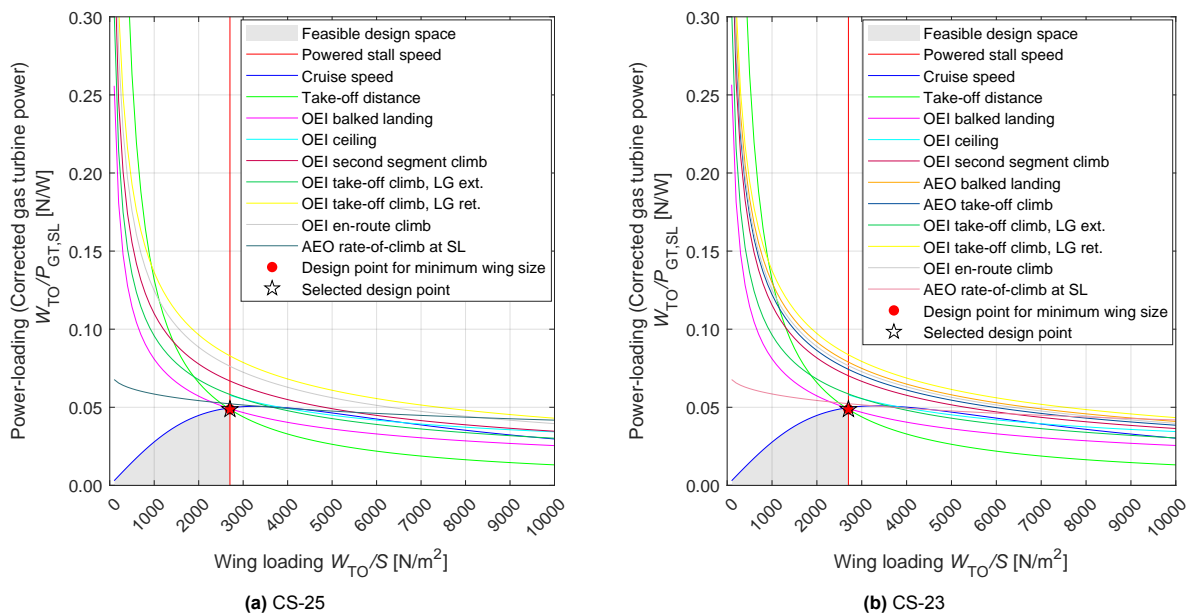
**Figure 4.1:** Examples of aircraft constraint diagrams corresponding to different climb gradient requirements.

Although most of the constraint curves are very similar between the two certification sets, there are a few notable differences. For example, the OEI take-off climb gradient with flaps extended and the

---

[3]Aircraft stall speed in a clean configuration.
[4]See footnote 3

landing gear retracted is less restrictive in CS-23 than in CS-25. Additionally, some constraints were not imposed on the CS-25 aircraft, such as the minimum AEO take-off climb and AEO balked landing constraints.

**Structural Load Factor Requirements**

Another important set of parameters in preliminary aircraft design concerns the structural load factors, more concretely, the maximum positive and negative manoeuvre and gust load, as well as the ultimate load factors. The manoeuvre and gust load values were calculated based on the AMCs corresponding to the requirement CS 23.2200 on the 'Structural design envelope':

- **CS 23 Amdt 4; 23.337.a.1**

  The positive limit manoeuvring load factor n may not be less than $2.1 + 24000/(W + 10000)$ for normal and commuter category aeroplanes (where $W$ = design maximum take-off weight lb), except that $n$ need not be more than 3.8.

- **CS 23 Amdt 4; 23.337.b**

  The negative limit manoeuvring load factor may not be less than 0.4 times the positive load factor for the normal, utility and commuter categories.

- **CS 23 Amdt 4; 23.341.c**

  In the absence of a more rational analysis the gust load factors must be computed as follows: $n = 1 \pm (k_g \cdot \rho_0 \cdot U_{de} \cdot V \cdot a) \, / \, 2(W/S)$, where:

  $k_g$ = $(0.88\mu_g) \, / \, (5.3 + \mu_g)$ = Gust alleviation factor;

  $\mu_g$ = $2\,(W/S) \, / \, (\rho \cdot \overline{C} \cdot a \cdot g)$ = Aeroplane mass ratio;

  $U_{de}$ = Derived gust velocities referred to in CS 23.333(c)[5] $(m/s)$;

  $\rho_0$ = Density of air at sea-level $(kg/m^3)$;

  $\rho$ = Density of air $(kg/m^3)$ at the altitude considered;

  $\frac{W}{S}$ = Wing loading due to the applicable weight of the aeroplane in the particular load case $(N/m^2)$;

  $\overline{C}$ = Mean geometric chord $(m)$;

  $g$ = Acceleration due to gravity $(m/s^2)$;

  $V$ = Aeroplane equivalent speed $(m/s)$; and

  $a$ = Slope of the aeroplane normal force coefficient curve $C_{N_\alpha}$ per radian if the gust loads are applied to the wings and horizontal tail surfaces simultaneously by a rational method. The wing lift curve slope $C_L$ per radian may be used when the gust load is applied to the wings only and the horizontal tail gust loads are treated as a separate condition.

Finally, the ultimate loads were determined through requirements CS 23.2230 on 'Limit and ultimate loads':

- **CS 23.2230.a.2**

  Unless special or other factors of safety are necessary to meet the requirements of this Subpart, the applicant must determine the ultimate loads, which are equal to the limit loads multiplied by a 1.5 factor of safety, unless otherwise provided.

Unlike the climb gradient requirements, the structural loads depend on the mass of the aircraft and its performance. Thus, the specific values of these restrictions had to be computed for every aircraft

---

[5]CS 23 Amdt 4; 23.333.c describes the shape and strength of the gusts that the aircraft has to be designed for, as well as the aircraft speeds at which the compliance must be achieved.

separately. While the manoeuvre limit load and ultimate load calculations were very simple, the gust envelope calculations were slightly more complicated. The gust load envelope determination followed the methods included in the general aviation design book by Gudmundsson [71].

With the help of these calculations, it was determined that the manoeuvre loads were more restrictive than the gust loads for all four selected conventional commuter aircraft, as well as for the four fuel cell aircraft that will be presented later in this study. Additionally, it was found that the default values of the design limit loads in the Initiator did not accurately represent the CS-23 commuter aircraft and had to be updated. Concretely, the positive design limit loads had to be increased to values between 2.8 and 3.1, while the negative limit loads had to be decreased to a value of approximately -1.2, depending on the mass of the aircraft in question.

## 4.1.2. Database Expansion

The Initiator database holds information on existing aircraft and engines. Its role is to provide the design convergence loops with initial statistical estimates for some of the basic aircraft masses and design parameters. There are separate databases for different types of aircraft, such as large jet transport aircraft, business jets, and turboprop transport aircraft. The parameters in the aircraft database range from information on masses, such as aircraft payload and OEM, to aircraft geometric characteristics, such as fuselage dimensions and wing areas. Similarly, the engine database is split into jet engines, turboprop engines, and APUs. The information provided on these engines includes but is not limited to the mass, specific fuel consumption, and geometry.

Unfortunately, the database did not include any aircraft and engines relevant to the commuter class aircraft category. Since the database is responsible for providing the Initiator with initial design estimates, the lack of relevant reference aircraft and engines meant that these estimates were very inaccurate. In summary, while it was possible to run the CS-23 commuter aircraft using the existing database, it prolonged the design convergence. To mitigate this, the database was expanded to include the CS-23 aircraft segment in a separate database sheet, while the existing turboprop engine list was expanded to include a host of smaller turbine engines, used in various CS-23 aircraft.

## 4.1.3. Mass and Geometry Estimation

Many of the existing mass and geometry estimation relations were too focused on the large transport aircraft to provide an accurate description of much smaller, slower, and often less advanced commuter aircraft. Thus, it was necessary to expand or rewrite numerous sizing relations and update various design settings. The following paragraphs will briefly describe a few of the most notable changes made.

**Class 2 Mass Estimates**

As already indicated in Section 3.3.2, the vast majority of class 2 mass estimation equations were taken from the aircraft design book by Tornebeek [69]. Fortunately, while not implemented inside the Initiator, the design methods presented by Torenbeek do in fact include sizing equations for smaller, less complex turboprops, such as commuter aircraft. Hence, in most cases, the adaptation of Initiator class 2 mass estimations for commuter aircraft was possible by simply expanding existing sizing methods to also include these equations. The subsystems for which the mass estimation was updated include:

- Main Wing;
- Fuselage;
- Engine and nacelle;
- Fixed equipment[6];
- Cabin furnishing;
- Operational items.

Among the most impactful changes for commuter mass estimation was the possibility to remove the APU and the corresponding subsystem mass, the possibility to specify manual controls (instead of hydraulically powered), the reduced avionics, furnishing, and operational items mass, and – for some aircraft – the possibility to specify a non-pressurised cabin.

---

[6]Fixed equipment includes the fuel system, aerodynamic controls, hydraulic and pneumatic systems, avionics and instrumentation, electrical system, air conditioning, pressurisation, anti-ice, and the APU

**Geometry Estimation**

The two most visible modifications concern the landing gear and the stabiliser surfaces. In both cases, the preexisting sizing and positioning logic did not represent the configurations encountered on the reference commuter aircraft. To mitigate this the nose landing gear positioning was made such that the user can specify where along the fuselage the wheels should be located. If the position is not specified, the default location at 5% fuselage length is selected instead.

Similarly to the nose gear, the stabiliser surfaces were previously shaped and positioned according to pre-programmed values and flow characteristics. However, the flow conditions in flight are only one of the considerations when designing the stabilisers. The stabiliser surfaces on commuter aircraft are often more swept than necessary to deal with the velocity of the incoming flow. Instead, the sweep is present to increase the moment arm of the surface or to postpone flow separation. To implement these design choices, the user can now specify all of the main shape and location parameters for the stabiliser surfaces, such as their sweep angle, dihedral angle, as well as their vertical and longitudinal location.

### 4.1.4. Mission Data for Aircraft Sizing

Before the aircraft can be sized it is also important to determine the design missions. A representative schematic mission profile is presented in Figure 4.2. The order of the various flight segments visible in the figure corresponds to the order in which the Initiator mission analysis is performed. While some analysis models account for the loiter inside another mission segment, the loiter segment within the Initiator is positioned at the very end of the mission. Thus, it is important to note that the loiter fuel will not be included in the mission (or trip) fuel when presenting the sizing results and throughout the energy efficiency analysis in the next chapter.

The altitudes and distances for each of the three segments can be freely chosen by the user, depending on the mission requirements. Unfortunately, the range data on reference aircraft did not include information on the reserve fuel with which the range was determined. At most, the data indicated that the range is given with 'IFR reserves'. Thus, the values for reserve fuel which covers the diversion and loiter had to be determined by examining the relevant regulations on commercial flight operations. While the exact laws on reserve fuel for commercial IFR flights vary between governing bodies of different governments, they usually require the aircraft to be able to fly to the intended destination airport and divert from there to a designated alternate airport with at least 30-45 minutes of contingency fuel. For this research, the diversion to an alternate airport is set at 200 km and the contingency is satisfied by 45 minutes worth of loiter fuel.
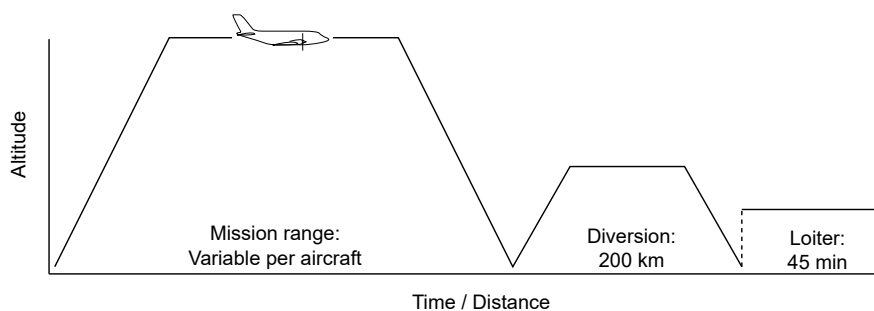


**Figure 4.2:** Typical commuter aircraft mission profile

Another value that had to be set was the mass of an average passenger. According to the latest report on commercial aircraft passengers performed by Lufthansa Consulting for EASA [72] the mean value of adult passengers was determined to be 76.3 kg. Additionally, the average value of carry-on luggage was found to be 7.7 kg. Thus, the typical adult passenger accounts for 84.0 kg. It was decided to increase this value to 85 kg to apply a margin for potential additional luggage.

Furthermore, it was decided that the reference commuter aircraft sizing will be constrained by two missions: a 'harmonic' mission and a 'nominal' mission. A harmonic mission was defined as the maximum range given the maximum permitted aircraft payload, while the nominal mission was defined as the

maximum range with a 19-passenger payload. Setting the average passenger mass to 85 kg, resulted in a nominal mission payload of 1615 kg. The design mission data is summarised in Table 4.1.

**Table 4.1:** Reference commuter aircraft mission data. Information compiled from Jane's [18].

| Parameter | Unit | Aircraft type | | | |
|---|---|---|---|---|---|
| | | **Do 228-212** | **Metro 23** | **Jetstream 31** | **EMB 110P2** |
| **Harmonic mission** | | | | | |
| Payload | kg | 1848 | 2268 | 1805 | 1681 |
| Range | km | 800* | 978 | 780* | 440* |
| Cruise Mach | - | 0.362 | 0.400 | 0.382 | 0.283 |
| Cruise altitude | m | 3048 | 6053 | 7620 | 3048 |
| **Nominal mission** | | | | | |
| Payload | kg | 1615* | 1615* | 1615* | 1615* |
| Range | km | 1166 | 2065 | 1192* | 520* |
| Cruise Mach | - | 0.362 | 0.400 | 0.382 | 0.283 |
| Cruise altitude | m | 3048 | 6053 | 7620 | 3048 |

*Estimated by the author through analysis and any other available data.

### 4.1.5. Validation of CS-23 Commuter Aircraft Implementation

Validation of the previously existing Initiator software in combination with the recent changes introduced to enable the modelling of commuter aircraft was essential to increase confidence in the research and quantify any possible discrepancies. Unfortunately, it was not possible to validate a complete fuel-cell-powered commuter aircraft at once, since none such aircraft has actually been produced to this day. However, it was possible to validate results for conventionally powered commuter aircraft, while performing a separate validation of individual fuel-cell powertrain components. Thus, this section will discuss the validation of the former, while the next section on the fuel-cell powertrain will present the latter.

**Parametric Validation**

The first part of the validation for conventional commuter aircraft was performed by comparing some of the most important parameters in the preliminary aircraft design to the values of reference aircraft. Concretely, the selected validation parameters, are the OEM, MTOM, total fuel fraction, wing loading, and power loading. Table 4.2 presents these Initiator aircraft sizing results for the 4 modelled aircraft and compares them against the reference values.

Generally, the results seem to indicate a high degree of accuracy of the Initiator results. The largest discrepancy that can be observed between the Initiator results and reference takes on a value of 15.6%. In fact, this is the only entry to exceed a 10% discrepancy. Moreover, only one of the MTOM results exceeds a discrepancy of 6%. This level of accuracy is more than satisfying, especially considering the difficulty of accurately estimating these values for commuter aircraft. The selected aircraft have vastly different equipment and technical complexity levels, which makes it hard to produce accurate results for all of them using the same tool.

As can be seen in the table, the results include 3 different 'depths' of Initiator mass and geometry estimations, which have been described in Section 3.3. Looking at the obtained values one can notice some differences between the results from different design convergence 'depths'. Generally speaking, the OEM estimate increased by including the class 2.5 and HSE estimation modules. Especially by adding the HSE analysis module, the OEM estimates grow noticeably. To understand this discrepancy better it is important to investigate the results further, which will be done in the subsequent paragraphs.

**Table 4.2:** Validation of conventional commuter aircraft implementation

| Aircraft | OEM [kg] | | MTOM [kg] | | Fuel Fraction* [%] | | W/S [kg/m2] | | W/P [kg/kW] | |
|---|---|---|---|---|---|---|---|---|---|---|
| **Dornier Do 228-212** | **3742** | **Diff [%]** | **6400** | **Diff [%]** | **12.66** | **Diff [%]** | **200.0** | **Diff [%]** | **5.53** | **Diff [%]** |
| Class 2 | 3781 | +1.0% | 6371 | -0.5% | 11.67 | -7.9% | 200.0 | +0.0% | 5.53 | +0.0% |
| Class 2.5 | 3924 | +4.9% | 6529 | +2.0% | 11.62 | -8.2% | 200.0 | +0.0% | 5.53 | +0.0% |
| Class 2.5 & HSE | 4326 | +15.6% | 6992 | +9.2% | 11.69 | -7.7% | 200.0 | +0.0% | 5.53 | +0.0% |
| | | | | | | | | | | |
| **Fairchild Metro 23** | **4309** | **Diff [%]** | **7484** | **Diff [%]** | **12.12** | **Diff [%]** | **260.7** | **Diff [%]** | **4.56** | **Diff [%]** |
| Class 2 | 4619 | +7.2% | 7800 | +4.2% | 11.67 | -3.7% | 260.8 | +0.0% | 4.53 | -0.7% |
| Class 2.5 | 4467 | +3.7% | 7627 | +1.9% | 11.71 | -3.4% | 260.8 | +0.0% | 4.52 | -0.9% |
| Class 2.5 & HSE | 4638 | +7.6% | 7802 | +4.2% | 11.49 | -5.2% | 260.8 | +0.0% | 4.58 | +0.4% |
| | | | | | | | | | | |
| **BAE Jetstream 31** | **4488** | **Diff [%]** | **6950** | **Diff [%]** | **9.45** | **Diff [%]** | **275.8** | **Diff [%]** | **4.96** | **Diff [%]** |
| Class 2 | 4087 | -8.9% | 6543 | -5.9% | 9.94 | +5.2% | 275.5 | -0.1% | 4.96 | +0.0% |
| Class 2.5 | 4143 | -7.7% | 6606 | -4.9% | 9.97 | +5.5% | 275.5 | -0.1% | 4.96 | +0.0% |
| Class 2.5 & HSE | 4277 | -4.7% | 6758 | -2.8% | 10.00 | +5.8% | 275.5 | -0.1% | 4.96 | +0.0% |
| | | | | | | | | | | |
| **Embraer EMB 110P2** | **3516** | **Diff [%]** | **5670** | **Diff [%]** | **8.34** | **Diff [%]** | **195.5** | **Diff [%]** | **5.07** | **Diff [%]** |
| Class 2 | 3555 | +1.1% | 5706 | +0.6% | 8.27 | -0.8% | 195.1 | -0.2% | 5.31 | +4.7% |
| Class 2.5 | 3664 | +4.2% | 5823 | +2.7% | 8.24 | -1.3% | 195.1 | -0.2% | 5.31 | +4.7% |
| Class 2.5 & HSE | 3662 | +4.2% | 5825 | +2.7% | 8.30 | -0.4% | 195.1 | -0.2% | 5.31 | +4.7% |

*Fuel fraction is calculated as total fuel mass for the harmonic mission, including a diversion and loitering time, divided by the aircraft MTOM. For the reference aircraft fuel fraction value, the total fuel mass value was obtained by subtracting the maximum payload and OEM from the MTOM.

**Geometric Validation**

While the values seen in Table 4.2 appear very promising, they do not offer the entire picture. Although unlikely, the numerical sizing values may match the reference aircraft by chance. To try to disprove that, another, more visual, method of validation can be used. Thus, this second part of the validation compares the aircraft top-view geometry results against the reference aircraft drawings.

First, the Initiator design convergence geometry results with class 2.5 'depth' were analysed. Without the HSE module enabled, it was possible to specify the exact longitudinal location of the main wing and the horizontal stabiliser. Furthermore, it was possible to specify the horizontal stabiliser size by tuning the horizontal tail volume value, as well as all the geometry parameters, such as sweep, aspect ratio, and taper. Thus, the wing and stabiliser location, as well as the horizontal stabiliser shape could be matched perfectly to the reference aircraft. The resulting aircraft top views, reference aircraft drawings, and overlays for all four aircraft can be seen in Figures 4.3–4.6.

Retaining the aircraft order that can be seen in Table 4.2, the Dornier Do 228-212 results displayed in Figure 4.3 are analysed first. While the aircraft geometry produced by the Initiator generally matches that of the reference aircraft, two discrepancies can be pointed out. The more obvious of the two is the difference in the main wing shape. While the reference aircraft has a distinct wing planform with two 'kinks' in the leading edge, the Initiator aircraft does not. This is one of the limitations currently present in the Initiator where the user is only able to specify one change or 'kink' in the wing planform. Furthermore, the reference wing has different sweep angles along the wing length compared to the Initiator version. This is a result of the Initiator determining the sweep automatically to increase the critical Mach number based on the most critical incoming flow conditions encountered by the aircraft. However, the wing sweep on the reference aircraft might have been dictated by other considerations, which the Initiator did not successfully capture.

The second, less visible discrepancy is present in the fuselage shape. Carefully examining Fig-

ure 4.3c, one might notice that the fuselage of the reference aircraft is slightly narrower compared to the Initiator results. Again, this is a result of Initiator limitations. While the reference aircraft has a rectangular fuselage cross-section, the Initiator is unable to capture this. Instead, the fuselage section is more circular. Enclosing a cabin that would otherwise be rectangular using a circular cross-section results in a slightly wider fuselage. The difference in fuselage shape also contributes negatively to the aerodynamic and structural analysis accuracy which might also explain some of the discrepancies in the total fuel fraction seen in Table 4.2.



**(a)** Initiator result (Class 2.5)      **(b)** Reference geometry. Adapted from [18]      **(c)** Result overly
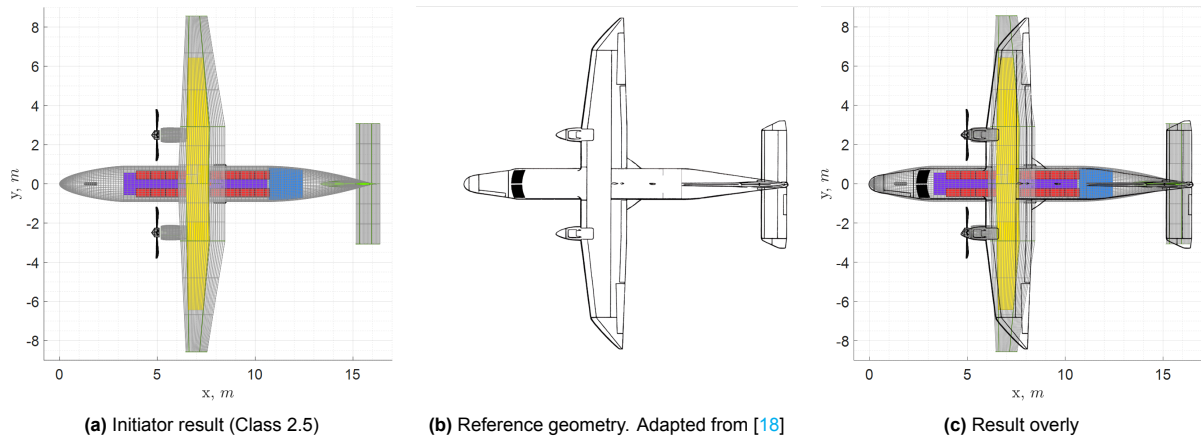
**Figure 4.3:** Dornier Do 228-212 aircraft planform geometry comparison

For the Fairchild Metro 23, depicted in Figure 4.4, the Initiator geometry matches the reference drawings very well with only some minor imperfections. While errors in the fuselage and wing size, shape, and placement are almost invisible, the engines and the horizontal tail are slightly misplaced. The engines are positioned a bit further from the fuselage than those seen on the reference aircraft drawing. Similarly, the horizontal tail is located a small distance too far toward the back of the aeroplane. Unlike the discrepancies seen in the case of Do 228-212 that were due to the Initiator limitations, this slight mismatch was caused by minor errors in the tuning of geometry parameters controlling engine and stabiliser placement. Nevertheless, these minor imperfections are unlikely to cause notable discrepancies in the aircraft sizing results.



**(a)** Initiator result (Class 2.5)      **(b)** Reference geometry. Adapted from [73]      **(c)** Result overly
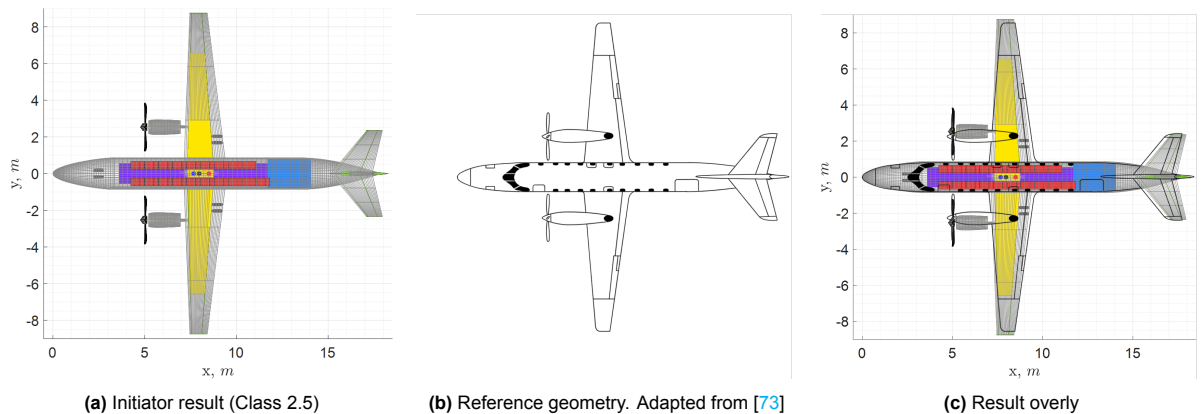
**Figure 4.4:** Fairchild Metro 23 aircraft planform geometry comparison

The last two aircraft that have to be analysed are the BAE Jetstream 31 and the Embraer EMB 110P2, seen in Figure 4.5 and Figure 4.6, respectively. For these two aircraft, the top-view geometrical results and the reference aircraft match almost perfectly. Hence, these results will not be discussed further.

Overall, apart from a few minor imperfections, the presented geometrical results showed an excellent

**(a)** Initiator result (Class 2.5)  **(b)** Reference geometry. Adapted from [18]  **(c)** Result overly
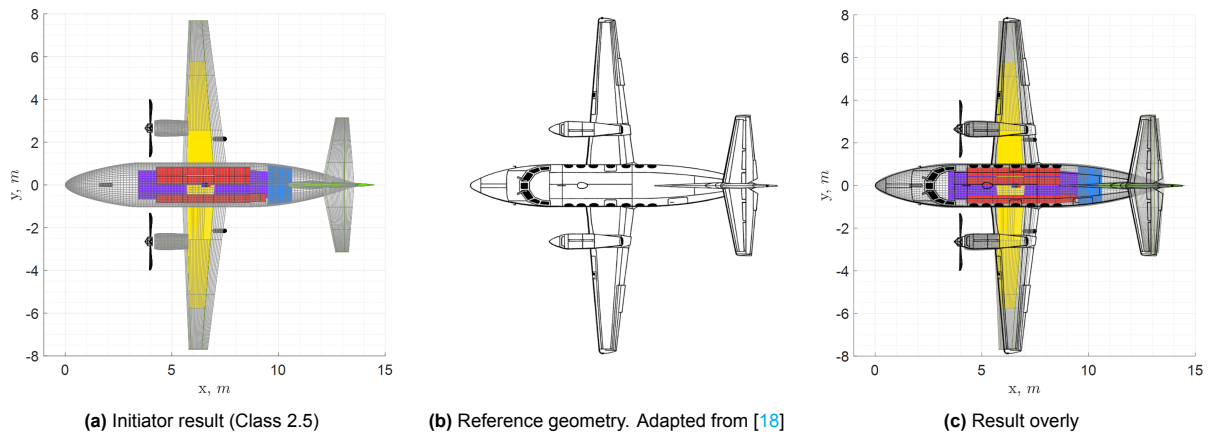
**Figure 4.5:** BAE Jetstream 31 aircraft planform geometry comparison



**(a)** Initiator result (Class 2.5)  **(b)** Reference geometry  **(c)** Result overly
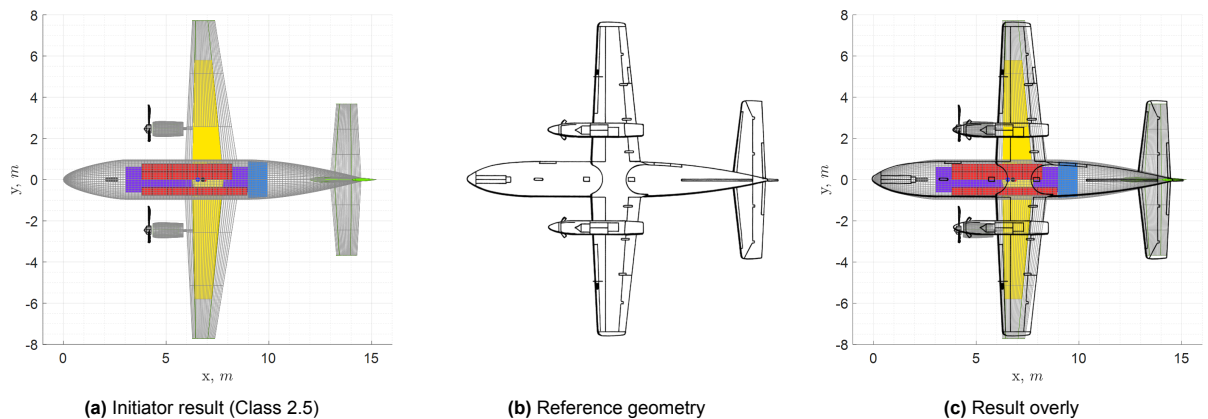
**Figure 4.6:** Embraer EMB 110P2 aircraft planform geometry comparison

match with the reference data. However, it is important to remember that these were only the results produced with Initiator's class 2.5 'depth'. Therefore, it is also necessary to analyse the rest of the results. Since the geometry produced by the class 2 'depth' was almost identical to that of the presented class 2.5 'depth' it will not be discussed separately. Conversely, adding the HSE to the convergence loop gives Initiator the authority to position the main wing and scale the horizontal stabiliser as it sees fit to ensure pitch stability and manoeuvrability of the aircraft. Thus, a brief analysis of the results produced with a full class 2.5 & HSE has to be performed as well.

Figure 4.7 displays the top-view of the aircraft geometry as produced by the Initiator on the class 2.5 & HSE 'depth'. Additionally, the reference aircraft drawings are again overlaid onto the figures for comparison. Note, that the geometry of the Embraer EMB 110P2 is not present in Figure 4.7. This is due to the very high degree of result similarity to the one obtained with class 2.5 'depth' only, seen in Figure 4.6.

In all three presented plots, the main wing can be seen shifted backwards substantially. This could suggest a possible miscalculation inside the HSE module. Additionally, the size of the horizontal stabiliser on the Do 228-212 is greatly increased in size. Furthermore, running the HSE with other high-wing aircraft the same trends can be observed, suggesting the error is affecting high-wing aircraft more than their low-wing counterparts. This horizontal tail size difference can at least partially explain the large discrepancy between different Initiator OEM results for the Do 228-212 seen in Table 4.2.

In summary, the class 2 and class 2.5 Initiator geometry results show a high degree of accuracy when compared against the reference aircraft geometry. Thus, these modules can be considered validated. However, the discrepancies introduced by the HSE module do not offer the same confidence in results. Unfortunately, horizontal stability analysis will be an important component in sizing the fuel cell aircraft due to the high mass of the cryogenic fuel tank which will most likely be placed far away from the

**(a)** Dornier Do 228-212          **(b)** Fairchild Metro 23          **(c)** BAE Jetstream 31
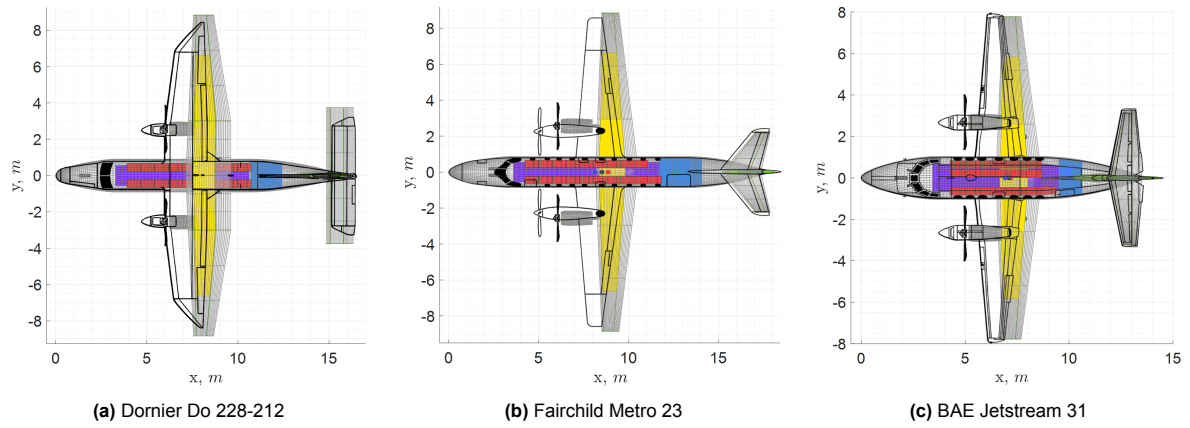
**Figure 4.7:** Overly of Initiator class 2.5 & HSE results with reference geometry

centre of mass. Therefore, while no concrete errors are known to be present in HSE the module, any significant results incorporating this module will have to be assessed with a degree of scepticism.

## 4.2. Fuel-Cell Powertrain Model Modifications

As mentioned in Section 3.3, the fuel-cell powertrain model was already integrated into the Initiator aircraft design synthesis software. The existing models for performance and sizing the entire fuel cell power unit (i.e. single fuel-cell performance, fuel-cell stacks, and BoP components) were implemented by Juschus [74], whereas the cryogenic hydrogen tank model was implemented by Onorato [75]. However, before using these models to obtain any aircraft sizing results it was decided to attempt to better verify and validate the models for which commercially available hardware data was possible to obtain. Thus, this section will describe the existing models, describe the validation process and present any modifications or other changes to these models for the purposes of this research project.

### 4.2.1. Fuel-Cell Performance Model

The performance model of a fuel cell is based on the polarisation curve. This equation is the backbone of any fuel cell performance analysis. It relates the real fuel cell output voltage $V_{cell}$ to the current density loading $i$. The current density loading $i$ is obtained by dividing the cell current $I_{cell}$ with the cell area $A_{cell}$ and is usually given in $A/cm^2$.

Generally, the open circuit voltage $V_{oc}$ (also referred to as the reversible voltage) of an individual fuel cell can be predicted by thermodynamic analysis. However, when the cell is connected to an electrical circuit, the fuel cell voltage decreases. This decrease in potential can be attributed to irreversible loss mechanisms [76]. Thus, to arrive at a realistic voltage output, one has to subtract a range of over-voltage losses that occur in the cell. Namely, these are activation potential ($\eta_{act}$), concentration overpotential ($\eta_{conc}$) and ohmic overpotential ($\eta_{ohm}$). With these losses in mind, the polarisation curve can be written as presented by Equation 4.1 [31, 77–82]. Some authors make a distinction between the losses happening at the anode and cathode, arriving at the slightly more elaborate relation seen in Equation 4.2 [83, 84].

$$V(i) = V_{oc} - \eta_{act}(i_{cell}) - \eta_{conc}(i_{cell}) - \eta_{ohm}(i_{cell}) \tag{4.1}$$

$$V(i) = V_{oc} - (\eta_{act,a}(i_{cell}) + \eta_{act,c}(i_{cell})) - (\eta_{conc,a}(i_{cell}) + \eta_{conc,c}(i_{cell})) - \eta_{ohm}(i_{cell}) \tag{4.2}$$

These three losses affect the voltage output in different parts of the current density range. Looking at Figure 4.8, one can observe how the activation loss is having the greatest effect on the voltage output at low current densities, while the concentration loss is occurring mostly towards the maximum current density. Finally, the ohmic loss dominates in the mid-range. The remainder of this section will examine each term of Equation 4.1 in more detail, starting with the open circuit voltage.
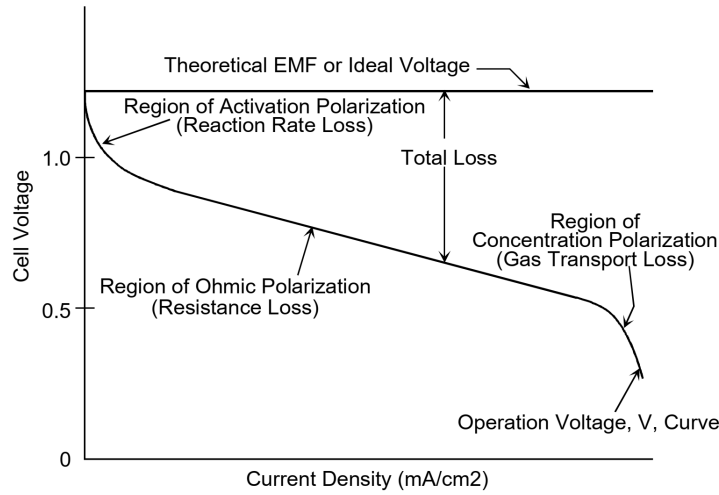
**Figure 4.8:** Example of a typical polarisation curve for a PEMFC, including the regions of main loss mechanisms. Retrieved from: [34]

**Open Circuit Voltage**

The $V_{oc}$ represents the thermodynamic potential of the cell and is based on the law of Nernst. The law stipulates that for the following electrochemical reaction: [78]

$$A + n_{e^-} \rightleftharpoons B \tag{4.3}$$

where A and B are the reactant species, the electrode potential reads as: [78]

$$V_{A/B} = E^0_{A/B} + \frac{RT}{n_{e^-}F} ln\left(\frac{a_A}{a_B}\right) \tag{4.4}$$

with:

- $E^0_{A/B}$ – reference potential $[V]$
- $R$ – universal gas constant $[8.3145\, J \cdot K^{-1} \cdot mol^{-1}]$
- $T$ – absolute (operational) temperature $[K]$
- $n$ – number of electrons
- $F$ – Faraday's constant $[96485.3321\, C \cdot mol^{-1}]$
- $a_A$ & $a_B$ – activities of species A and B

Applying the Nernst equation to a PEMFC running on pure hydrogen yields the following expression for the open circuit voltage of an individual cell: [83]

$$V_{oc} = E^0 + \frac{\Delta\hat{s}}{nF}(T - T_0) + \frac{RT}{nF} ln\left(\frac{a_{H_2} \cdot \sqrt{a_{O_2}}}{a_{H_2O}}\right) \tag{4.5}$$

where $\Delta\hat{s}$ is the entropy of reaction and $T_0$ is the reference temperature, set at 25 °C or 298.15 K.

The reference potential $E^0$ can be derived from Gibbs' free energy of reaction. In reference conditions (i.e. atmospheric pressure ad 25 °C) the maximum potential of reaction is 1.229 V [84]. Next, assuming that the water produced during the reaction is in liquid form, the entropy of reaction $\Delta\hat{s}$ can be computed using the standard entries of the reaction species. This can be seen in Equation 4.6.

$$\Delta\hat{s} = S^\circ(H_2(g)) + \frac{1}{2}S^\circ(O_2(g)) - S^\circ(H_2O(l)) = 131.0 + \frac{1}{2} \cdot 205.0 - 69.9 = 163.6\, \frac{J}{K \cdot mol} \tag{4.6}$$

Furthermore, since the PEMFCs generally operate at relatively low pressures, the activities of reaction species can be expressed in terms of pressure [34]. More accurately, the activity is expressed as the

ratio between the pressure of the individual reactant and the atmospheric pressure [84]. Finally, it can be assumed that water is exiting the cell at ambient pressure and can therefore be omitted from the equation. By inserting all the variables in Equation 4.5 the open circuit voltage can now be written out as presented in Equation 4.7, which is the most common form used in literature. [78–83]

$$V_{oc} = 1.229 - 0.85 \cdot 10^{-3} \left(T - 298.15\right) + 4.31 \cdot 10^{-5} \cdot T \left[ ln\left(p_{H_2}\right) + \frac{1}{2} ln\left(p_{O_2}\right) \right] \quad (4.7)$$

To arrive at the value of $V_{oc}$ that is used in the Initiator cell model the following assumptions are made:

- Constant cell operational temperature of T = 353.15 K (80 °C);
- Constant sea-level pressure of hydrogen fuel at the anode (1 atm or 1013.25 hPa);
- Constant sea-level pressure of ambient air supplied via a compressor at the cathode (1 atm or 1013.25 hPa);
- Partial pressure of oxygen is 21% of total pressure at the cathode (due to the standard composition of ambient air).

With these assumptions the value $V_{oc}$ = 1.170 V is obtained. The existing cell model in the Initiator, however, arrived at a value of 1.468 V. The author argues that this was due to 3 errors in the original model. First, the erroneous assumption that the water produced in the cell is in gaseous instead of liquid form was employed. Second, the partial pressures were given in Pascals instead of atmospheres. Third, an additional error in reference temperature input was found. To resolve this, the model was updated to reflect the calculations performed in this section.

**Activation Loss**
To start the electrochemical reaction processes inside a fuel cell some initial difference in potential is required. This is called activation polarisation and it is the reason for the polarisation losses. Essentially, it is caused by the 'sluggish' electrode kinetics and it diminishes as the rate of reaction increases. These losses occur on both electrodes. Nonetheless, when considering a hydrogen PEMFC, the oxygen reduction reaction demands a much greater overpotential than hydrogen oxidation and is thus a much larger source of losses. To describe the activation losses on either electrode the Butler-Volmer expression can be used. Often, however, a simplification of the expression is used. Namely, the Tafel equation presented in Equation 4.8, with terms $a$ and $b$ obtained using the two expressions in Equation 4.9. [34, 83–85] For the explanation of the term $(RT)/(n_{e^-}F)$ refer back to Equation 4.5.

$$\eta_{act} = a + b \cdot ln(i) \quad (4.8)$$

$$a = -\frac{RT}{\alpha n_{e^-}F} ln(i_\circ) \qquad b = \frac{RT}{\alpha n_{e^-}F} \quad (4.9)$$

The term $b$ is commonly referred to as the 'Tafel slope'. The variable $\alpha$ denotes the electron transfer coefficient of the reaction at an electrode and $i_\circ$ represents the exchange current density. Both, $\alpha$ and $i_\circ$, are constants dependent on the characteristics of the electrode and are often determined empirically. [34, 85] In the existing model, only the losses for oxygen reduction at the cathode are modelled. The empirically determined values are based on the previous work by Swannet [86]. Concretely, the value for $\alpha$ was made equal to 0.3 and the value of the exchange current $i_0$ is assumed constant at $8 \cdot 10^{-4}$ $A/cm^2$.

**Ohmic Loss**
The ohmic loss is caused by the resistance to the flow of charged particles through the fuel cell. Concretely, it is a combined effect of the resistance from the ion flow travelling through the electrolyte and the resistance of the electron flow moving through the electrode or any other conductive fuel cell components. The resistance losses can be expressed by Ohm's law, as seen in Equation 4.10. [34, 82, 84, 85] For this research, the chosen $r$ value of $7.5 \cdot 10^{-6}$ $\Omega m^2$ was again based on the work by Swannet [86].

$$\eta_{ohm} = ir \quad (4.10)$$

**Concentration Loss**

When the electrochemical reaction takes place at the electrode the reactants are consumed and replaced with the reaction products. Since the mass transport rate for the reactants and the products is finite, the reactant concentration at the electrode becomes diluted by the presence of the products. At higher rates of reaction, this problem becomes more apparent, since the reactants at the electrode begin to deplete rapidly while creating more products that have to be evacuated. This results in concentration gradients within the fuel cell, which is the reason for the concentration losses. This loss is also known as transport loss, referring to the underlying cause of the unfavourable concentration gradient. In a limiting case, the surface reactant concentration depletes to zero. In this case, since there is no excess reactant at the catalyst surface, the fuel cell is not able to produce any more current. The current at which this is achieved is commonly referred to as the 'limit current density' or $i_{lim}$. [34, 85]

The expression to estimate this loss in the current model can be seen in Equation 4.11. [31] The parameter $c$ represents the mass transport loss constant. The value of this constant has been set to 0.1 $V$, which is a typical value for PEMFC according to O'Hayre *et al.* [31]. The $i_{lim}$ has been set to 3.8 $A/cm^2$ once again based on the PEMFC study by Swannet [86].

$$\eta_{conc} = c \cdot ln\left(\frac{i_{lim}}{i_{lim} - i}\right) \tag{4.11}$$

**Leakage Loss**

The final loss that was included in the cell model was leakage loss. This loss accounts for all reactant leaks and any unaccounted parasitic losses in the reaction process. The leakage current density $i_{leak}$ was set to 0.1 $A/cm^2$, as recommended by O'Hayre *et al.* [31]. This loss term is simply introduced into the general polarisation model of Equation 4.1 by adding it to the free variable $i$. Thus, at any position where $i$ appears, the term is expanded to $i + i_{leak}$. Consequently, the final polarisation curve equation with all the losses reads as:

$$V(i) = V_{oc} - \frac{RT}{2\alpha F} ln\frac{i + i_{leak}}{i_0} - ir - c \cdot ln\frac{i_{lim}}{i_{lim} - (i + i_{leak})} \tag{4.12}$$

**Inlet Pressure Effects**

The fuel cell performance model includes a simple model for cathode inlet pressure effects on the cell output voltage. In this way, the fuel-cell system sensitivity to changes in operating altitude and compressor performance can be investigated. The model was implemented by Juschus [74] using a polynomial curve fitting on experimental data. The resulting plot is illustrated in Figure 4.9.
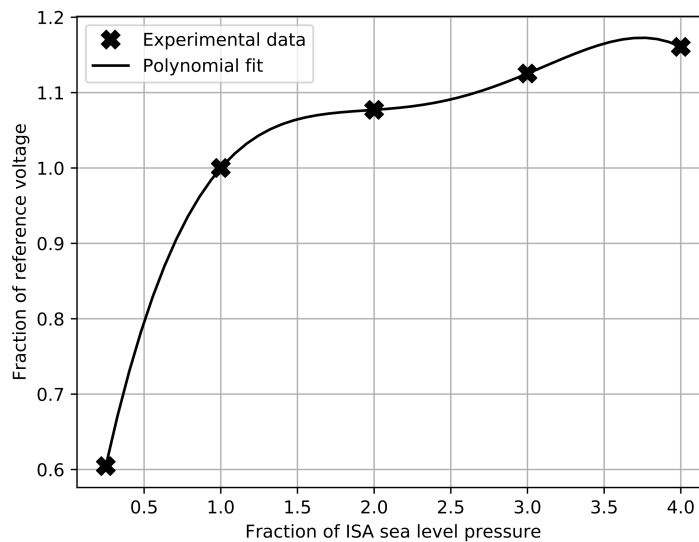


**Figure 4.9:** Individual fuel cell voltage versus the fuel cell cathode inlet pressure. Retrieved from: [74].

**Efficiency**

The fuel-cell system efficiency is crucial for aircraft sizing since it relates the produced fuel-cell energy used to power the aircraft to the chemical energy of hydrogen fuel. Before the efficiency models can be presented, a clarification about the use of the higher heating value (HHV) and lower heating value (LHV) of hydrogen fuel is required. The heating value communicates the energy released by the oxidation reaction of the fuel. The difference between LHV and HHV is in the state of the released water. LHV corresponds to the produced water being in gaseous form, whereas HHV corresponds to the produced water being in liquid form. The difference between the two values is thus in the energy required for the water to transition from a liquid to a gaseous state. [87]

In the majority of the common oxidation reactions, such as kerosene combustion in a turbine engine, the water produced is in gaseous form and thus LHV should be used when obtaining energy extraction efficiency. In the case of PEMFC, the operating temperature is well below the boiling point of water and thus, the reaction produces water in liquid form. Hence, HHV was used to calculate fuel cell efficiency.

The cell efficiency or $\eta_{cell}$ can simply be given as the cell voltage $V_{cell}(i)$ divided by the potential corresponding to the HHV of hydrogen, which is 1.482 V. [87] On the system level, the efficiency of the fuel-cell powertrain also includes losses stemming from imperfect hydrogen fuel utilisation, the parasitic power draw for BoP components, and propulsive motor inefficiencies. By borrowing the notation from Juschus [74], the efficiency can be then written as follows:

$$\eta_{sys} = \eta_c \mu_{fuel} \frac{P_{prop}}{P_{stack}} = \frac{V_{cell}(i)}{1.482} \mu_{fuel} \frac{P_{prop}}{P_{stack}} \tag{4.13}$$

where $\mu_{fuel}$ is the fuel utilisation factor which was set to 95%, as suggested by Larminie and Dicks [32]. The $P_{prop}/P_{stack}$ represents the ratio between the propulsion motor power and stack output power. Unlike the fuel utilisation factor, the value of this factor is not constant but is dependent on the power draw of the BoP components.

**Summary**

To provide a better overview of the cell performance model, Table 4.3 lists the values of all of the constants used to construct the model and the sources for these values.

**Table 4.3:** Fuel cell model parameters

| Parameter | Symbol | Value | Unit | Source |
|---|---|---|---|---|
| Cell operational temperature | $T$ | 353.15 | $K$ | [31] |
| Cathode transfer coefficient | $\alpha$ | 0.3 | $-$ | [86] |
| Cathode exchange current density | $i_0$ | $8 \cdot 10^{-4}$ | $A \cdot cm^2$ | [86] |
| Internal resistance | $r$ | $7.5 \cdot 10^{-6}$ | $\Omega \cdot m^2$ | [86] |
| Limit current density | $i_{lim}$ | 3.8 | $A \cdot cm^2$ | [86] |
| Mass transport loss constant | $c$ | 0.1 | V | [31] |
| Leakage current density | $i_{leak}$ | 0.1 | $A \cdot cm^2$ | [31] |
| Fuel utilisation factor | $\mu_f$ | 0.95 | $-$ | [32] |

## 4.2.2. Fuel-Cell Stacks

With the performance of the individual cells determined it is possible to size the entire fuel-cell stacks using empirical estimates. First, this section will look into the existing sizing model. Next, the existing model results will be compared against the data compiled from commercially available hardware. Finally, the model will be tweaked to better match the validation data.

**Existing Sizing Model**

As already described in Section 2.3.3, an individual stack is made up of multiple cells sandwiched together. These cells themselves are composed of bipolar plates, MEAs, and gaskets. Additionally, each stack is equipped with two endplates, one on each side of the stack. To hold the entire assembly together, the two endplates are connected by several bolts. At higher powers and thus voltages, the stack assembly might get too large to be held together with a single set of endplates and bolts. Thus, the cells might have to be split into multiple smaller stacks. In this model, it was deemed necessary to divide the cells into 2 stacks per FCS. Furthermore, an assumption was made that the mass contribution of gaskets is negligible.

Given the information above, the expression describing the mass of these two stacks or $m_{stack}$ can be constructed as shown in Equation 4.14:

$$m_{stack} = n_{stack} \cdot A_{cell} \left[ n_{cell} \cdot (t_{mat,BP}\rho_{BP} + \rho_{A_{MEA}}) + 2t_{EP}\rho_{EP} \right] + n_{bolt} \cdot \pi \frac{D_{bolt}^2}{4} \cdot l_{bolt}\rho_{bolt} \quad (4.14)$$

with:

- $n_{stack}$ – number of fuel-cell stacks in a FCS [-];
- $A_{cell}$ – individual cell area [$m^2$];
- $n_{cell}$ – number of cells per stack [-];
- $t_{mat,BP}$ – bipolar palate material thickness [$m$];
- $\rho_{BP}$ – bipolar plate material density [$kg/m^3$];
- $\rho_{A_{MEA}}$ – MEA area density [$kg/m^2$];
- $t_{EP}$ – endplate thickness [$m$];
- $\rho_{EP}$ – endplate material density [$kg/m^3$];
- $n_{bolt}$ – number of bolts [-];
- $D_{bolt}$ – bolt diameter [$m$];
- $l_{bolt}$ – bolt length [$m$];
- $\rho_{bolt}$ – bolt material density [$kg/m^3$].

To compute the number of cells required in the FCS, the specified voltage that the FCS has to produce is divided by the individual cell voltage $V_{cell}$ and the number of stacks in a series, as shown in Equation 4.15.

$$n_{cell} = \frac{V_{FCS}}{V_{cell} \cdot n_{stack}} \quad (4.15)$$

With this, the cell area can be obtained by dividing the required FCS power by the number of stacks, the number of cells per stack, and the area power density of an individual fuel cell $i_{cell}$:

$$A_{cell} = \frac{P_{FCS}}{n_{stack} \cdot n_{cell} \cdot i_{cell}} \quad (4.16)$$

The diameter of the bolts is approximated based on the methods presented in the paper by Dey *et al.* [88] and is obtained as shown in Equation 4.17.

$$D_{bolt} = \sqrt{\frac{A_{cell}}{600}} \quad (4.17)$$

Finally, the bolt length or $l_{bolt}$ is simply the length of the stack assembly, which is computed as the thickness of all bipolar plates, MEAs, and two endplates:

$$l_{bolt} = 2 \cdot t_{EP} + n_{cell} \cdot (t_{BP} + t_{MEA}) \quad (4.18)$$

with $t_{BP}$ the thickness of the bipolar plate assembly[7] and $t_{MEA}$ the thickness of MEA.

To estimate the stack volume $V_{stack}$ the cell area can be simply multiplied by the length of the entire assembly. The length of the entire assembly has already been determined when calculating the required length of the bolts. Ultimately, the result has to be multiplied by the number of stacks in the FCS. Thus, the total volume of the fuel-cell stacks can be determined as done in Equation 4.19.

$$V_{stack} = n_{stack} \cdot A_{cell} \cdot l_{bolt} \tag{4.19}$$

**Existing Model Validation**
To attempt to validate the existing model, commercially available fuel-cell stack data was compiled. The entire dataset can be seen in Table B.1. Using the information from this table it was possible to construct a regression curve relating the stack mass to the stack output power. Next, the existing Initiator stack model was used to size fuel-cell stacks with the same power requirements and other operational parameters, as seen in the validation dataset. The results from both, the real-life hardware and the Initiator model are shown in Figure 4.10.
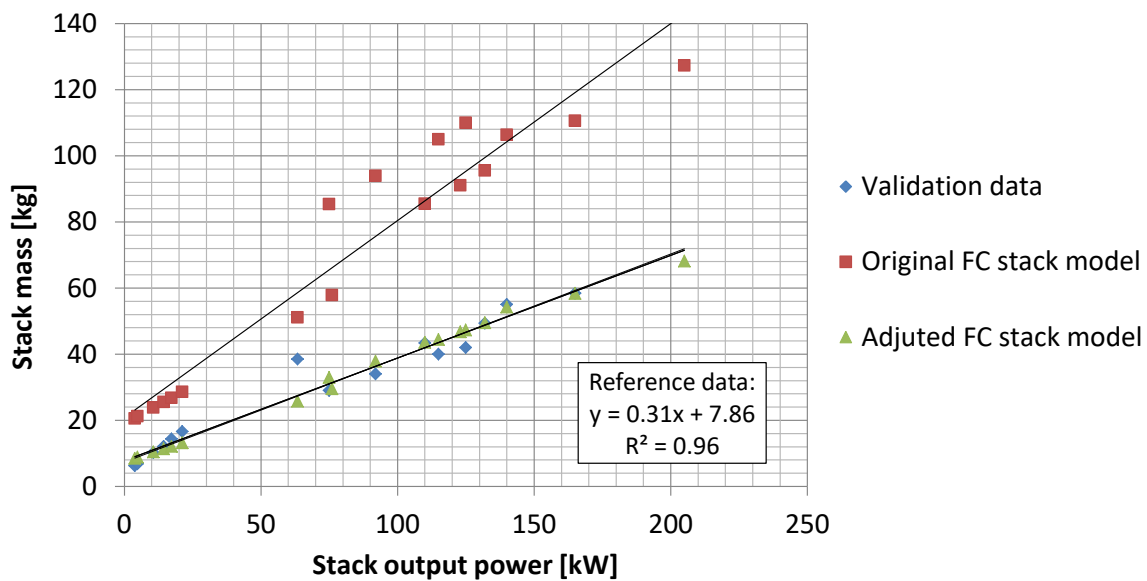


**Figure 4.10:** Fuel-cell stack mass versus stack output power for the Initiator models and validation (reference) data.

It can be seen that the original fuel-cell stack model quite severely overestimated the mass of the fuel-cell stacks. In fact, the stacks were oversized by more than 50%. Interestingly, the exact opposite is true for the volume estimations. As illustrated in Figure 4.11, the original model substantially undersized the fuel-cell stacks. Because of these discrepancies, the existing model had to be adjusted.

**Model Recalibration**
The existing Initiator model, as well as the reference data, showed a strong linear trend for both, the stack mass and volume. Therefore, instead of replacing the estimation expressions completely, it was decided to modify the mass and volume estimation parameters in such a way that they better match the reference data. While some of the parameters could be directly determined using academic and industry sources, some parameters had to be derived by comparing the sizing results to the reference data. Furthermore, to match the reference data as closely as possible, the unaccounted mass factor and packing factor were applied to the final mass and volume values, respectively. The final set of parameters used to estimate the stack mass and volume can be seen in Table 4.4. Using these parameters, it was possible to almost perfectly match the regression curve of the reference data for both mass and volume, as can be seen by looking at the 'Adjusted FC stack model' data points in Figures 4.10 and 4.19, respectively.

---

[7]Plate thickness after pressing in the flow channels (not to be confused with the $t_{mat,BP}$ which is the thickness of the bipolar plate material and is used for stack mass estimations)
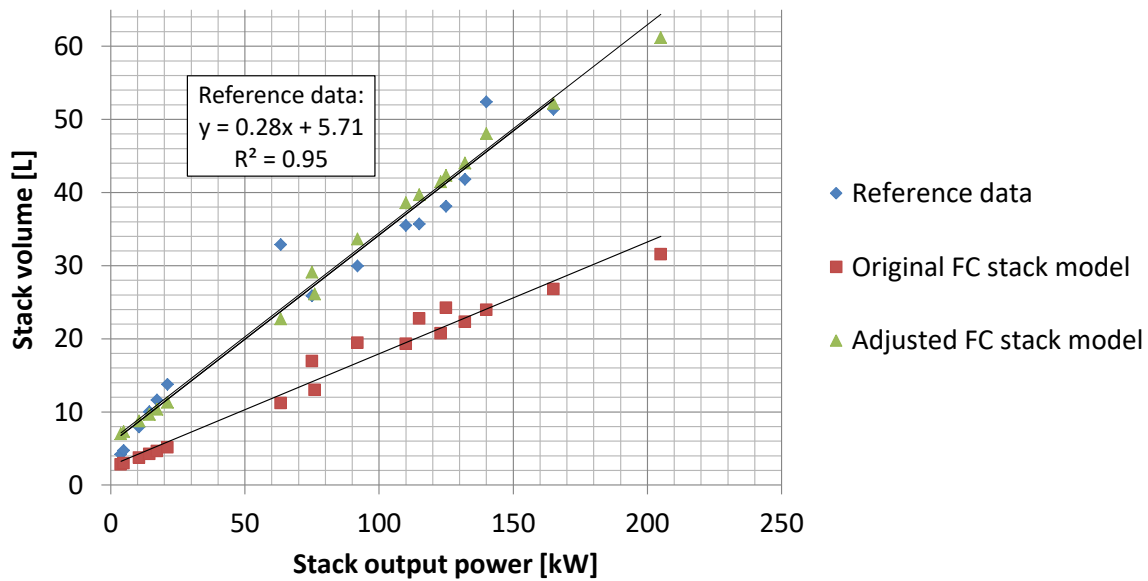
**Figure 4.11:** Fuel-cell stack volume versus stack output power for the Initiator models and validation (reference) data.

**Table 4.4:** Fuel-cell stack mass and volume model parameters

| Parameter | Symbol | Value | Unit | Source |
|---|---|---|---|---|
| FCS voltage | $V_{FCS}$ | 500 | $V$ | - |
| Number of stacks in series | $n_{stack}$ | 2 | — | - |
| Bipolar plate assembly thickness | $t_{bp}$ | 1 | $mm$ | [89] |
| Bipolar plate material thickness | $t_{mat,BP}$ | 0.25 | $mm$ | [4]* |
| Bipolar plate material density | $\rho_{BP}$ | 8600 | $kg/m^3$ | - |
| MEA thickness | $t_{MEA}$ | 285 | $\mu m$ | [4] |
| MEA area density | $\rho_{A_{MEA}}$ | 0.2 | $kg/m^2$ | [4] |
| Endplate thickness | $t_{EP}$ | 35 | $mm$ | - |
| Endplate material density | $\rho_{EP}$ | 2770 | $kg/m^3$ | [88] |
| Number of bolts | $n_{bolt}$ | 10 | — | [88] |
| Bolt material density | $\rho_{bolt}$ | 8600 | $kg/m^3$ | [88] |
| Unaccounted mass factor | $f_m$ | 1.13 | — | - |
| Packing factor | $f_V$ | 2.13 | — | - |

*Kadyk *et al.* [4] speculate 0.1–0.2 mm will be possible using metallic plates in the near future.

### 4.2.3. Balance of Plant

Three balance of plant or BoP components are sized in the existing model: the compressor, the humidifier, and the heat exchanger. Their respective Initiator models will be examined in the following paragraphs.

**Compressor**

The compressor can be separated into two main components: the impeller, which is an aerodynamic component that compresses the air, and the electric motor used to provide rotational power to the impeller. In the existing model implemented by Juschus [74], the impeller was sized through a preliminary aerodynamic analysis adapted from the book by Gambini and Vellini [90]. After the required perform-

ance of the compressor was determined through this analysis, the electric motor was sized empirically, according to the required power.

Since many compressors for fuel cell power units are available on the market, it was decided to use the commercially available hardware data to verify the existing model. Unfortunately, once compared to validation data on existing hardware, it was discovered that the model severely oversized the impeller in both, size and mass. Thus, the model had to either be tweaked, replaced by another analytical model, or replaced by a fully empirical model.

Because of the level of disparity between the validation data and the existing model, simply tweaking the existing model was not seen as a viable option. Thus, the model had to be replaced. While a more elaborate physics-based model can naturally better capture subtle differences in operating requirements, an empirical model offers simplicity and robustness. Considering the scope of this research project, implementing a simple statistical model for a small component, such as the compressor was preferred.

The new model uses a simplified compressor mass flow and power requirement calculations from the original model. The isentropic efficiency of the compressor is kept at 75%. Next, with the use of the commercially available compressor data presented in Table B.2, a regression curve linking the required compressor power to total compressor mass could be established. This regression can be observed in Figure 4.12. A similar regression curve relating the compressor volume to its power rating was used to estimate the size of the compressor.
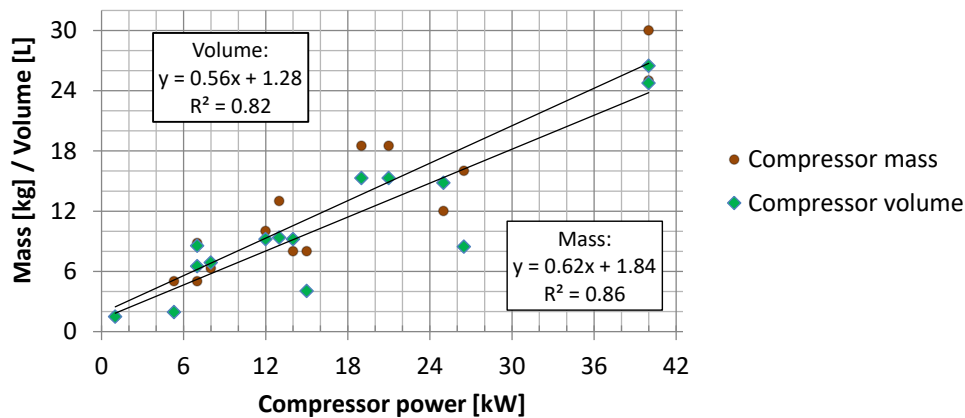


**Figure 4.12:** FCS compressor mass and volume versus compressor power rating.

The new model also accounts for the pressure drop in the humidifier, located downstream from the compressor. By averaging the humidifier pressure drop from the reference data in Table B.3 a value of approximately 12 kPa was achieved. During compressor sizing, this pressure drop is simply added to the difference between the compressor inlet pressure and the required fuel-cell inlet pressure.

**Humidifier**

The existing humidifier model was adapted from the paper by Huizing *et al.* [91]. Similarly to the compressor, however, the results were not in line with the validation data compiled from the commercially available hardware. Thus, just like with the compressors, it was decided to opt for a simpler, but more reliable model. By constructing a regression curve based on the data from Table B.3 a satisfactory fit was achieved. The regression curves for both, the humidifier mass and volume can be seen in Figure 4.13.

It is worth pointing out, that sizing the humidifier purely based on the power rating of the corresponding fuel-cell stack is not seen as ideal. In this way, many possibly important parameters, such as the properties of ambient air are completely disregarded. Nevertheless, based on the available commercial data the mass and volume of the humidifier seem to correspond reasonably well with the fuel cell power rating. Furthermore, the humidifier is not expected to present a large mass and volume contribution to the FCS. Therefore, the possible inaccuracies of such a simple model are less notable. Overall, such a model is deemed sufficient for preliminary FCS sizing.
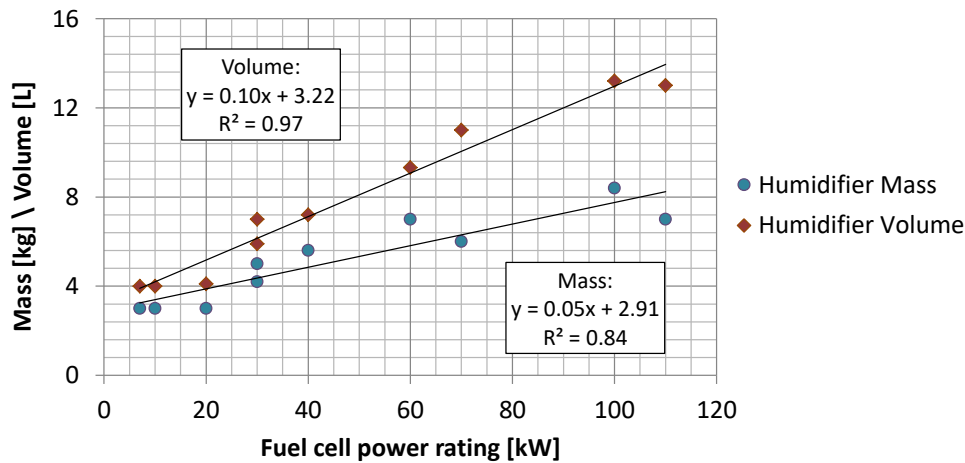
**Figure 4.13:** FCS humidifier mass and volume versus stack output power.

**Heat Exchanger**

The original Initiator fuel-cell heat exchanger model was Implemented by Juschus [74] and was constructed by simplifying the model described in a 2020 paper by Kožulović [92]. The sizing is based on computing the heat that is produced during the FCS operation. Using this value the heat exchanger mass and size are computed through a preliminary fluid dynamics and heat transfer analysis. The existing model is unfortunately hard to validate due to the lack of commercially available hardware data and highly specialised components. Furthermore, the heat exchanger design is very sensitive to varying design conditions and is, therefore, harder to construct a simple statistical linear mass and volume regression, as was done for the compressor and the humidifier.

While it is harder to validate the heat exchanger model, there is ongoing research into the Initiator heat exchanger model. No results have been published to this date, but the interim results suggest the current heat exchanger model overestimates the mass by around 25%. Thus, a correction factor of 0.75 was applied to both the heat exchanger mass and volume. Nevertheless, since the heat exchanger presents one of the largest mass and volume contributions to the fuel-cell unit, a recommendation is made in Chapter 6 to continue directing further research into expanding and validating the heat exchanger model.

### 4.2.4. Electric Propulsion Motors and Batteries

The sizing of electric motors and batteries in the Initiator is fairly rudimentary. For the electric motor, the required power determined in the class 1 estimation is used to compute the motor mass and volume. The required power is simply divided by the motor-specific power, giving the motor mass. Subsequently, the motor volume and dimensions are obtained by simple statistical relationships of commercially available hardware.

**Table 4.5:** Sizing values for electric propulsion motors and battery packs

| Component | Battery pack | | | Propulsion motors |
|---|---|---|---|---|
| **Parameter** | **Energy density** | **Power density** | **Volumetric density** | **Power density** |
| **Unit** | [Wh/kg] | [W/kg] | [kg/m$^3$] | [kW/kg] |
| **Value** | 260 | 1670 | 2615 | 5795* |

*Includes a 30% mass penalty for cooling and inverter compared to original UNIFER19 [65] value;

A similar sizing technique is also used for the battery packs. However, the batteries have to be sized for both, the maximum required power, and the total required energy. This is done by sizing the batteries for the two requirements separately. Using the specified battery-specific power the required battery mass to satisfy the maximum power requirement is obtained. Analogously, the specified battery energy density is used to obtain the battery mass to satisfy the total energy requirement. Here it is also important to note that the battery minimum level of discharge is set to 20%. Once computed, the two

masses are compared and the higher of the two is kept. Finally, the specifier battery volumetric density is used to check whether the battery will fit into the aircraft wing.

The values required for propulsion motor and battery pack sizing were adapted from the 2025 technology estimates in the report of the UNIFIER19 project [65]. To provide a clear overview, the selected sizing values are summarised in Table 4.5.

### 4.2.5. Liquid Hydrogen Tank

The Initiator cryogenic hydrogen tank sizing capability was introduced by Onorato [75]. The tank sizing model assumes a tank structure with an inner aluminium lining, surrounded by insulating polyurethane foam, as depicted by Figure 4.14. As already alluded to in Section 2.3.3, the insulation is crucial to minimise heat ingress into the tank. Since liquid hydrogen will begin to boil at around 20.3 K, even a small heat influx can cause a hydrogen gas buildup in the tank and a consequent pressure rise. To prevent the tank from exploding, the excess pressure has to be vented out, losing valuable aircraft fuel in the process. However, adding insulation to the tank increases its mass and size. Alternatively, one can contain the boil-off by designing the tank to sustain higher pressures. Once again, however, this increases the tank mass. Thus, a compromise has to be found between insulation thickness, maximum tank pressure, and potential hydrogen venting losses.
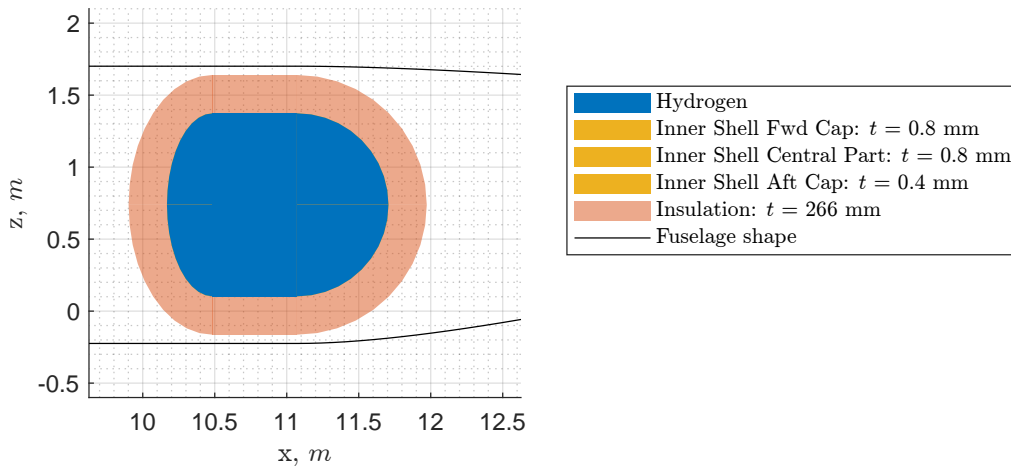


**Figure 4.14:** Cryogenic hydrogen fuel tank side-profile cutaway.
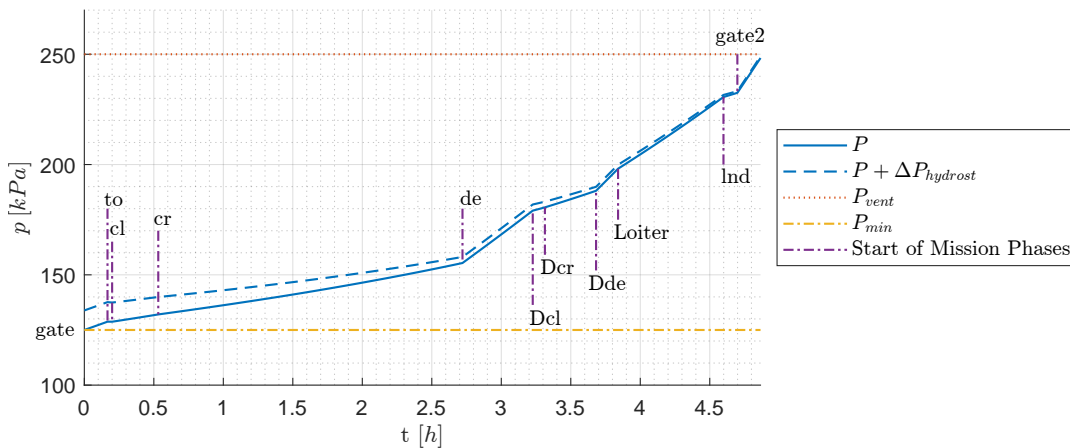


**Figure 4.15:** Cryogenic hydrogen fuel tank pressure rise throughout an aircraft mission.

The implemented design method is based on the principle that no venting would be needed throughout the course of the entire design mission, including the diversion and loiter. More precisely, the design is optimised such that the venting pressure is reached shortly after the point when the aircraft arrives at the gate at the diversion destination. To achieve this, the user specifies the maximum allowed pressure

of the tank (venting pressure), which is used to size the tank structure, while the surrounding insulation thickness is sized to satisfy the 'no-venting' condition.

The starting pressure is set to 125 kPa, slightly above the atmospheric sea level pressure to prevent air from entering the tank. The default venting pressure in this study is set to 250 kPa. This value was found to correspond to the minimum aircraft MTOM, according to the sensitivity studies performed by Onorato [75]. Nevertheless, it is worth analysing the effects of this value on the overall aircraft mass for commuter aircraft, which will be done in the sensitivity analysis of this report.

An example of a typical pressure profile inside a cryogenic hydrogen fuel tank can be seen in Figure 4.15. Besides the pressure rise, the graph also illustrates the transitions between one mission phase to the next.

## 4.3. Fuel Cell Aircraft Model

Now that both, the conventional commuter aircraft model, as well as the fuel-cell powertrain model have been presented, it is time to use them in unison to size fuel-cell-powered commuter aircraft. This section will first present how the different fuel-cell powertrain components were integrated into the aircraft structure, followed by an explanation of the fuel cell aircraft design mission considerations.

### 4.3.1. Fuel-Cell Aircraft Powertrain Configuration

Before discussing the results it is also important to go over the exact fuel-cell powertrain architecture used and establish the layout of powertrain components within the aircraft. Figure 4.16 illustrates the major fuel-cell powertrain components inside the aircraft.

The fuel-cell powertrain architecture considered in this research project is a fuel-cell & battery serial hybrid. This means that the aircraft is primarily powered by fuel cells, with batteries providing an additional power source for the most power-intense segments of the flight. The need for a hybrid configuration arises from the low specific power of the current fuel-cell technology. Connecting these two power sources into a series hybrid configuration provides the most straightforward coupling of the two. Thus, this configuration is preferred. The default power degree of hybridisation (DoH) is set to 50% during take-off and 25% during normal climb segments. During the cruise and other flight segments, the powertrain draws energy solely from the fuel cells. For the purposes of evaluating the various OEI and AEO climb gradient requirements, a 50% power hybridisation is used.

As already mentioned in Section 4.2, the FCS is sized such that the fuel-cell stacks are oversized by 10% to increase their efficiency and reduce the necessary BoP components masses. Furthermore, the FCS compressor is sized such that the aircraft receives air at sea-level pressure.
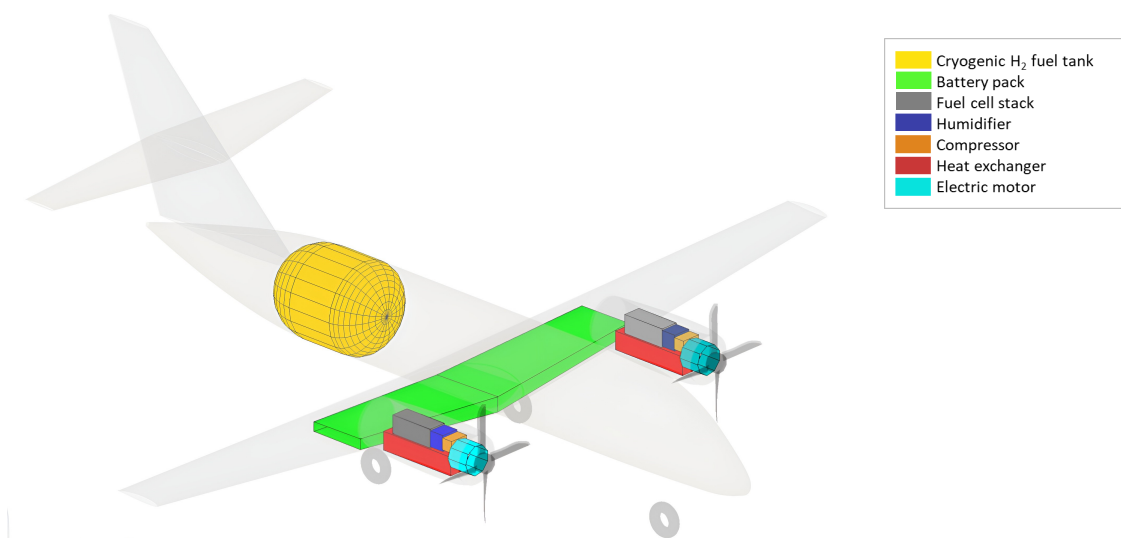


**Figure 4.16:** Layout of a fuel-cell and battery hybrid powertrain with a cryogenic hydrogen tank

To power the fuel cells, hydrogen fuel is stored in a single cryogenic tank located behind the aircraft cabin. Cryogenic storage is chosen over non-cryogenic storage since it allows for better volumetric effi-

ciency and therefore a more competitive range performance. To achieve greater gravimetric efficiency of the hydrogen tank, splitting the required total tank volume over multiple smaller tanks was rejected in favour of a single large tank. By splitting the fuel over multiple smaller tanks, the total tank wall area would increase, causing an increase in weight and potential boil-off.

The single hydrogen tank is positioned behind the cabin. In this configuration, the aircraft tail-cone volume can be partially utilised for hydrogen storage. Conversely, by locating the hydrogen tank between the cabin and the flight deck, which is another popular solution, the aircraft would require separate doors for the passengers and the pilots. Moreover, the pilots would either lose access to the lavatory or require a separate lavatory directly behind the flight deck.

Since the kerosene tank is no longer present in the wing, this space can be used for batteries. Locating the batteries in the wing provides bending relief and occupies the space that would otherwise be left empty. By locating the batteries in the wing the total electrical cable length is also reduced since the electromotor is positioned inside a nacelle on the wing.

Finally, the fuel-cell stacks and the corresponding BoP components are positioned within the nacelle, just behind the electric propulsion motors. While locating the fuel-cell units inside the aircraft fuselage next to the fuel tank would shorten the fuel supply lines drastically, it would put another very large mass in the back of the aircraft. For this research, it was decided to locate the fuel cells inside the nacelles on the wings. Although this placement does increase the nacelle size and the corresponding drag, the fuselage placement would simply increase the weight and drag of the fuselage instead. Moreover, the nacelle placement of the BoP allows for better airflow, which should prove beneficial when sizing the heat exchanger. Positioning the fuel cell right behind the electromotor also reduces the required cable length. Finally, just like the conventionally powered reference aircraft, the fuel cell aircraft designs have two identical independent fuel-cell propulsion units for redundancy, one on each wing.

### 4.3.2. Aircraft Design Mission

The conventional aircraft results obtained in Section 4.1 were computed by specifying two missions: the maximum payload mission and maximum passenger mission, where the maximum passenger load is 19 people with carry-on luggage (85kg total mass per passenger). Naturally, it would have been desirable to design the fuel cell aircraft with the same two-mission requirements. However, this proved challenging, since the payload-range diagram for a hydrogen fuel cell aircraft has a distinctly different shape to that of a kerosene-powered aircraft.

The main difference between the two aircraft types lies in the mass and size of the fuel tank. While kerosene is relatively heavy, the kerosene fuel tank is very light, since it normally uses the existing wing and/or fuselage structure as the fuel tank. Consequently, due to the low mass penalty, the kerosene fuel tanks are usually oversized compared to the fuel requirements for the design mission. This allows a wider mission envelope where the payload can be reduced to increase the fuel load and therefore range. The tank oversizing crates a typical shape with two distinct kinks in the take-off mass, as shown in Figure 4.17a. In the first section of the diagram, the payload is kept at its maximum value and the trip fuel value is increased until MTOM is reached. Then, during the following segment, the take-off mass is held at MTOM while the payload is traded off for increased fuel load and thus more range. At the next kink, the maximum fuel capacity is reached and further reducing the payload does not allow for more fuel. Nevertheless, reducing payload continues to increase the available flight range until the point where no payload is left in the aircraft.

Unlike kerosene, cryogenic hydrogen is extremely light, but the fuel tank to store it is very heavy and bulky due to the large volume of hydrogen required and the insulation required to limit boil-off. Thus, the hydrogen tank has to be as small as possible to reduce aircraft mass and size. This naturally limits the ability to oversize the tank to achieve the same payload-range trade-off that was possible with kerosene aircraft. Thus, a typical payload-range envelope for the fuel cell aircraft skips the flat segment at MTOM where the payload is traded off for more fuel completely. Instead, the envelope has a very sharp corner as soon as MTOM is reached, as displayed in Figure 4.17b. After this point, the only means of increasing the range for a fuel cell aircraft is to reduce the payload. However, because the OEM of fuel cell aircraft is usually much larger, the payload reduction has a smaller effect on the range than is the case with conventional aircraft.

Consequently, sizing fuel cell aircraft that would fulfil both the mission with maximum payload, as well as the mission with nominal 19-passenger payload would in the best case result in a severely oversized aircraft or, in the worst case, fail to even achieve design convergence. Thus, it was decided

**(a)** Conventional aircraft

**(b)** Cryogenic hydrogen aircraft
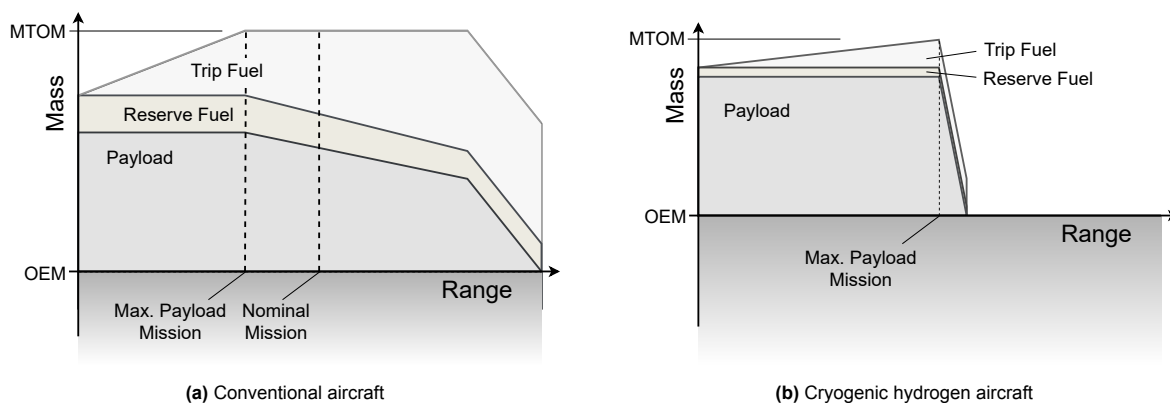
**Figure 4.17:** Typical payload-range diagram for conventional and hydrogen-powered aircraft

to take the nominal 19-passenger mission payload with the corresponding range as the default sizing mission for fuel cell aircraft. Nevertheless, the sizing was also performed for the maximum payload mission for the purpose of comparison. It is important to point out that the reserve fuel provisions have been kept the same as for conventional aircraft. Concretely, the reserve fuel accounts for a diversion of 200 km and an additional loiter time of 45 minutes.

## 4.4. Mission Cost and Emissions Estimations

To better understand the mission environmental impacts and mission cost of fuel cell aircraft a simple economic and emissions analysis was developed. Due to the immense complexity of a holistic approach to both issues, this research focused on the most noteworthy components of mission costs and environmental impacts.

In total, three different power carrier solutions were examined. The first solution was a fuel-cell commuter aircraft powered by a combination of liquid hydrogen and batteries. As a benchmark, the conventional commuter aircraft powered by fossil-based Jet-A1 fuel were included. Finally, as a middle-ground solution, the cost and emissions of a conventional aircraft powered by sustainable aviation fuel (SAF) produced using the power-to-liquid process or PtL[8] were included in the analysis. It is worth stressing that, for the purpose of this analysis, it is assumed that the conventional aircraft require no modification and do not experience any degradation in performance when utilising SAF.

### 4.4.1. Mission Emissions

The environmental impact of aircraft stems from various sources. Thus, a comprehensive framework spanning over the entire lifespan of the aircraft is needed to fully capture the environmental impacts. The environmental impact of a product can be determined using the Life Cycle Assessment (LCA) method. Such an analysis accounts not only for the direct aircraft impact, such as emissions generated during the flight but also for the impact of supporting processes and infrastructure. For example, aircraft manufacturing, fuel extraction, and processing, as well as impacts of airport infrastructure. [94–96] An example of an aviation LCA domain is illustrated in Figure 4.18.

Naturally, when considering such a wide scope, the complexity of the problem becomes immense. Moreover, when including aircraft incorporating unconventional powertrains, the analysis again becomes plagued with high uncertainties due to the lack of available information. Thus, to reduce the complexity of the environmental impact comparison between aircraft designs, the focus of this research was on the emissions produced for the aircraft powertrain operation, specifically, the 'well-to-wake' emission footprint of the energy source. In Figure 4.18 this is represented by the 'Fuel Life Cycle Well to Wake' segment. Besides being the largest source of emissions for commercial aircraft [97–99], the power source environmental impact is also expected to differ greatly between the fuel-cell and conventional powertrains.

---

[8]Power-to-Liquid (PtL) fuel production uses hydrogen via water electrolysis with renewable energy followed by Fischer-Tropsch synthesis process [93]
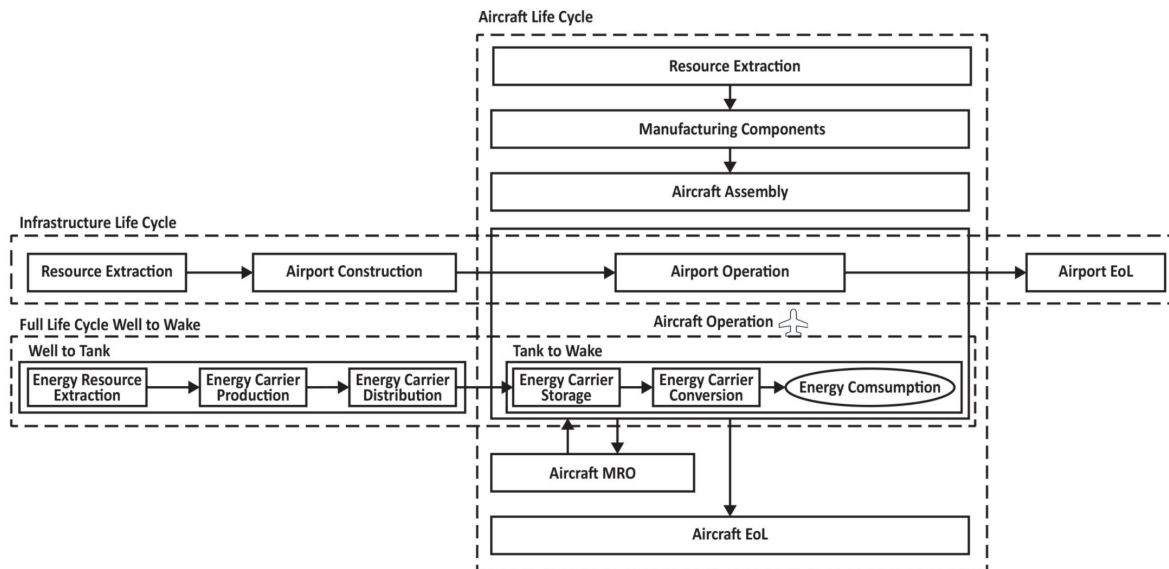
**Figure 4.18:** Life cycle assessment (LCA) of aviation. Retrieved from: [96]

**Emissions Impact Metric**

The basis for the energy source emissions model in this report is the 2022 paper by Wehrspohn *et al.* [26]. Concretely, their model focuses on the contribution of these emissions to global warming. To assess this, the global warming potential or GWP is used given in kilograms of $CO_2$ equivalent emissions per kilogram of fuel or kg$CO_2$eq/kg. This metric can account for the non-$CO_2$ related impacts on the greenhouse effect, such as $NO_x$ emissions and contrail-induced cloudiness or CiC. While it is a strong metric it is nevertheless important to also recognise its shortcomings. According to Jungbluth and Meili [100] the GWP is relatively useful for comparing the effects of long-lived well-mixed atmospheric gases. However, as they put it, many of the emissions and their effects, especially in aviation, cannot be accurately accounted for using GWP due to their transient nature or because their effects are highly dependent on the atmospheric makeup at the emission location. Because of this, the GWP is far from an ideal metric for accurately estimating the total global warming impact of aviation. Nevertheless, when simply comparing the effects of different aircraft powertrains in commuter aircraft, the GWP metric is still deemed adequate. In fact, many preliminary studies focus solely on the effect of $CO_2$ emissions while disregarding others.

The GWP was accounted for in two stages. In the first stage, the GWP of the energy source before the flight was estimated. In the second stage, the GWP of the emissions during the actual flight was determined.

**GWP of Energy Production, Refinement, Transport, and Storage**

In this segment, the GWP of the energy source up to the point of consumption in flight is given. In Figure 4.18 this segment is illustrated under the 'Fuel Life Cycle' from 'Energy Resource Extraction' up to and including the 'Energy Carrier Conversion'.

Table 4.6 presents the GWP of the same four energy sources as in the cost estimation section. This time, however, GWP is given for two different electricity generation scenarios. In the first scenario, electricity is produced in Denmark with the use of wind turbines. In the second scenario, electricity generation is done in Spain with the use of photovoltaic (PV) power plants. While both of these methods make use of renewable energy, the GWP impact of PV is still much greater than using wind turbine farms. Because electricity use is a minor component in oil extraction and refinement, the GWP footprint of Jet-A1 fuel does not depend on the electricity generation scenario. Note, that the GWP of Jet-A1, SAF, and Green LH$_2$ is given per kilogram of fuel, while the GWP of electrical energy is given per kilowatt-hour.

**Table 4.6:** GWP of various energy sources before consumption.

| Energy carrier | GWP [kgCO$_2$eq] | | Per | Information source |
|---|---|---|---|---|
| | Wind (Denmark) | PV (Spain) | | |
| **Jet-A1** | 0.457 | 0.457 | [kg] | Wehrspohn *et al.* [26] |
| **SAF (PtL)** | 0.334 | 1.653 | [kg] | Wehrspohn *et al.* [26] |
| **Green LH$_2$** | 0.852 | 4.216 | [kg] | Wehrspohn *et al.* [26] |
| **Electricity** | 0.013 | 0.039 | [kWh] | Marashli *et al.* [101]* |

*Global averages for wind and PV solar, not country specific

**GWP of Energy Consumption**

The GWP analysis of in-flight emissions was done by looking at the following possible contributions: carbon dioxide emissions ($CO_2$), nitrogen oxide emissions ($NO_x$), water vapour emissions ($H_2O$), and contrail-induced clouding (CiC). While there are other effects that have an impact on radiative forcing, these 4 are the most notable ones [102].

Starting with the $CO_2$ emissions, only Jet-A1 and SAF produce $CO_2$ when consumed in flight. However, it is assumed that PtL fuel is produced using direct carbon capture and thus, in theory, does not produce any net carbon emissions. Hence, only Jet-A1 will have a $CO_2$ contribution in flight.

Next, the $NO_x$ emissions are examined. These emissions are produced during high-temperature combustion where oxidation of atmospheric nitrogen occurs. Thus, $NO_x$ emissions are only relevant in combustion engines. The largest contribution to the warming effect of these emissions comes from accelerating ozone ($O_3$) production, which is a strong greenhouse gas. The impact of $NO_x$ emissions is highly dependent on their location and the existing concentration of $NO_x$ at this location [103]. The same absolute increase in $NO_x$ concentrations has a stronger effect in an atmosphere with a low concentration of $NO_x$ and vice versa. However, accurately estimating the global flight paths of commuter aircraft in this research and the existing $NO_x$ concentration in those locations is beyond the scope of this project. Thus, it will be assumed that the commuter aircraft are predominantly flying within Europe and that the concentration of $NO_x$ in their flight path is similar to that encountered at the cruise altitudes of most jets or around 10 km. Since commuter aircraft operate at lower, less busy altitudes, the $NO_x$ will likely be lower as well. Thus, the $NO_x$ impact might be underestimated due to this assumption.

Similarly to $NO_x$, the radiative forcing of water molecules is highly dependent on their altitude. The effects are notable only if water reaches stratospheric altitudes. While the majority of aircraft cruise below these levels, the water can be lifted into higher layers of the atmosphere with atmospheric currents. Nevertheless, considering the work by Wilcox *et al.* [104] it can be assumed that the radiative forcing effects of water vapour emissions below the altitudes of around 9000 m are negligible. Furthermore, Sherwood *et al.* [105] confirm that water vapour emitted close to the ground does not have a net positive warming effect. Thus, the GWP of $H_2O$ emissions is set to 0.

Finally, the CiC effects are examined. The CiC is again highly dependant on atmospheric conditions, especially temperature, and humidity. Generally speaking, higher altitudes are better suited for CiC effects. [106] Thus, the CiC GWP of lower-flying commuter aircraft will be lower than that of most jets. In fact, it would be safe to assume that the two low-flying aircraft, the Do 228-212, and the EMB 110P2 would not have noteworthy CiC effects at their cruise altitude of approximately 3000 m. Even the higher cruise altitudes of Metro 23 and Jetstream 31 are still well below the normal contrail altitude most of the time. However, as Gierens [107] discusses, when it comes to fuel cells, the contrails are likely to be produced even at low altitudes. In fact, contrails might even appear at ground level when the temperatures drop close to 0. Nevertheless, the paper also suggests that the strength and longevity of the CiC effects will be much smaller than that of conventional aircraft. Overall, the total magnitude, as well as the difference in CiC effects between commuter aircraft using conventional and fuel-cell propulsion is likely small. Thus, the CiC effect was neglected in this analysis.

After reviewing all four effects, Table 4.7 provides a GWP quantification of the relevant effects based on the work by Wehrspohn *et al.* [26].

Table 4.7: GWP of various energy sources in flight. Adapted from: [26]

| Energy source | GWP [kgCO$_2$eq] | | | | Per |
|---|---|---|---|---|---|
| | CO$_2$ | NO$_x$ | H$_2$O | CiC | |
| Jet-A1 | 2.568 | 1.271 | 0 | 0 | [kg] |
| SAF (PtL) | 0 | 1.271 | 0 | 0 | [kg] |
| Green LH$_2$ | 0 | 0 | 0 | 0 | [kg] |
| Electricity | 0 | 0 | 0 | 0 | [GJ] |

## 4.4.2. Mission Cost

To capture some of the economic differences between the proposed aircraft powertrain and fuel solutions, the mission cost analysis will compare the aircraft based on two major cost factors. The first one is the purchase price for the required mission energy, whether it is the liquid hydrogen and electricity for the fuel cell aircraft, or Jet-A1 or SAF for the conventional aircraft. Besides the energy cost, the cost of emissions incurred when operating in a region where aviation emission allowances have to be purchased, such as the EU, was included. The crew costs were not included since they are assumed to be the same regardless of the powertrain used.

**Energy Cost**

To make a good preliminary estimate of the energy cost, the aircraft's total energy for the trip has to be established. This is no issue since the Initiator sizing is based on the energy balance and thus, this information can be easily obtained directly from the Initiator sizing results.

The second step is considerably less straightforward, however. For the estimation of fuel costs the respective prices of hydrogen, electricity, as well as Jet-A1 and SAF have to be established. While predicting future prices of energy is difficult as it is, it becomes even harder when considering the uncertainty of unconventional power sources such as green hydrogen. It would be possible to simply take the present price levels. However, sustainable hydrogen production costs are expected to decrease over the next decades [26]. As the specific energy and power for the battery and propulsion motors were set to reflect technology predictions for the year 2025, it would be sensible to set the energy prices for when the aircraft with such a technology would be performing commercial operations. With an assumption of a 10-year aircraft development phase, the aircraft would start commercial operations in 2035. Thus, the price predictions should be set to the year 2035 or slightly beyond. With this in mind, Table 4.8 presents the purchase cost of energy that is used to power the aircraft in this research. Note, that the prices in Table 4.8 do not include the additional emissions allowance cost.

Table 4.8: Future energy price estimates

| Energy carrier | Unit | Price estimate* | | | Forecast year | Information source |
|---|---|---|---|---|---|---|
| | | Low | Base | High | | |
| Jet-A1 | [€/kg] | 0.43 | 0.76 | 1.25 | 2040 | Wehrspohn *et al.* [26] |
| SAF (PtL) | [€/kg] | 1.03 | 1.62 | 2.77 | 2040 | Wehrspohn *et al.* [26] |
| Green LH$_2$ | [€/kg] | 2.67 | 4.55 | 7.52 | 2040 | Wehrspohn *et al.* [26] |
| Electricity | [€/GJ] | 3.00 | 12.1** | 21.2 | 2050 | Silberhorn *et al.* [108] |

*Converted from US dollar to Euro with the exchange rate at the time of writing: 1$ = 0.91€
**Average value between 'Low' and 'High' estimates.

**Cost of Emission Allowances**

As alluded to above, if one is to assume the flights will be taking place in the European Union or any country that includes aviation in its emission trading scheme, emission-related costs have to be considered as well. European aviation is included in the Emissions Trading Scheme or ETS for short.

Under this scheme, aircraft operators are given $CO_2$ emission allowances. While the majority of the emissions allowances are currently awarded to operators for free, this will not be the case in the future. Indeed, already by 2026, no free emissions allowance will be awarded to airlines. Instead, the airlines will have to purchase allowance for their operational emissions from the ETS market. Thus, aircraft operators will incur additional costs for their operations in proportion to their $CO_2$ emissions. Furthermore, the latest deal between the EU Council and Parliament also stipulates that a report on the non-$CO_2$ related environmental effects of aviation will be created by 2027 for the purposes of including these effects in the trading scheme. [109] Thus, it is safe to assume that the non-$CO_2$ effects will be included in the ETS in the near- to mid-term future.

In the near future, the price difference between the regular fossil-based jet-A1 and alternative fuels at airports will be mostly covered by the EU. However, according to current regulations, this financial help will expire in 2030. Thus, according to regulations passed so far, the price of alternative fuels will not be directly influenced by the EU beyond 2030. [109]

As the energy cost estimations in Table 4.8 correspond to the year 2040, it would be most sensible to set the expected emissions cost in the same year. Unfortunately, the price of emissions is highly uncertain even in the short term. Among other factors, price fluctuations are strongly influenced by economic downturns, the speed of the overall green energy transition, and industries entering the ETS. Moreover, the legislation that created the emissions allowance market is likely to change again over the next years, not unlike how it was amended recently, in 2022 [110]. This makes the mid-term and long-term prediction of the emissions cost in the ETS very difficult.

Nevertheless, there are some studies that attempt to model the ETS price in the near- and mid-term future. According to six different prediction models included in the report by Pahle *et al.* [111], the price per metric ton of $CO_2$ is projected to reach between 56€ and 111€ in 2025 and between 84€ and 160€ in 2030. The average price prediction for the year 2030 between all six models is 135€. Another possible insight into the future of ETS pricing is given in the article by Pietzcker *et al.* [112]. According to the current EU legislation and the prediction scenarios that are given in the article, the ETS price in 2030 should reach approximately 130€/$tCO_2$. This matches well with the studies in the report by Pahle *et al.* [111]. Additionally, Pietzcker *et al.* [112] predict the price of ETS will reach 215€/$tCO_2$ in 2040. This is the price that was used as a baseline for the emissions cost analysis in this report. The range of predictions between the 6 models in the report by Pahle *et al.* [111] were used to construct a confidence interval based on relative deviations from the average price prediction.

Overall, it appears that accurately predicting the price of ETS emission allowances in 2040 is exceptionally complex. Nevertheless, ignoring the effects of ETS on aircraft operational costs is not acceptable either. Thus, to simplify the problem, the following assumptions were made to determine the price of emissions for the aircraft operator in the year 2040:

- All flights take place between two airports in the European Union;
- The aircraft operator is required to purchase the emissions allowances through the ETS;
- The non-$CO_2$ emissions are translated into equivalent $CO_2$ emissions using the GWP metric and also require purchasing of the emissions allowances;
- The power or energy carrier producers and distributors will raise the prices of their products to cover the extra costs incurred by purchasing the emission allowances required to produce and distribute the energy or energy carrier;
- No legislation changes that would affect prices in the ETS will occur until beyond 2040.
- The baseline price of emissions allowances in 2040 will be 215€, with a confidence interval between 134€ and 255€ per metric ton of $CO_2$.

With these assumptions, the price of emissions was computed based on the GWP presented in Table 4.6 and Table 4.7 before being added to the baseline energy prices listed in Table 4.8.

# 5

# Results

This chapter will present the sizing results of four different commuter aircraft that incorporate hybrid fuel-cell powertrain technology. These include the Dornier Do228-212, Fairchild Metro 23, BAE Jetstream 31, and Embraer EMB 110P2, selected in Table 3.1.

Unless stated otherwise, the fuel cell aircraft results were sized for the 19-passenger nominal design mission requirements. Additionally, unless explicitly stated, the preliminary design results of the fuel-cell commuter aircraft were obtained by retaining all of the requirements and design settings from the conventional aircraft. However, the fuel-cell commuter aircraft should not be interpreted as conventional aircraft with a powertrain conversion. Classifying it as such might entail that the general size and most of the structural components of the aircraft remain the same. However, this is not the case. While the design parameters, such as the general aircraft configuration, cabin size, wing airfoils, wing aspect ratio, etc., were preserved, the entire aircraft has been resized. Thus, the presented results can be interpreted as preliminary design studies of fuel cell aircraft with the same mission requirements and general characteristics as their conventional counterparts.

One notable exception in these results is the fuel cell Metro 23 aircraft. While the fuselage diameter and seating configuration of the other three fuel cell aircraft is the same as in their conventional counterparts, the fuel cell Metro 23 fuselage diameter had to be enlarged to limit excessive fuselage lengthening when accommodating the large cryogenic tank.

The results will be structured as follows. First, the design point and convergence results for fuel cell aircraft will be presented in Section 5.1, followed by the MTOM and OEM results in Section 5.2. Next, in Section 5.3, the fuel cell aircraft geometry results will be discussed. In Section 5.4 the fuel cell aircraft energy usage, its costs, and environmental implications will be explored. In Section 5.5 the results obtained by sizing the fuel cell aircraft for the maximum payload mission will be briefly discussed and compared to the results of the aircraft sized by the nominal, maximum passenger mission. The chapter will be concluded with a comprehensive sensitivity analysis in Section 5.6, where the aircraft sizing results will be examined for sensitivity to both, mission parameters, as well as the aircraft powertrain design and technology parameters.

## 5.1. Design Point and Convergence Results

While the rest of this chapter presents the end results of the fuel cell aircraft sizing, this section focuses on the process of how these results were ultimately obtained. The first part of this section discusses the aircraft design point and the power- versus wing-loading diagrams which could be considered the basis of any fixed-wing aircraft design. The second part of this section examines the iterative sizing process and highlights some of the limitations encountered during the convergence process.

### 5.1.1. Design Point

As was already mentioned in Section 3.3, there is no single definitive aircraft design point for hybrid aircraft. Instead, different components in the power chain have to be sized according to the most restrictive requirements for that specific component. This is done by constructing power- versus wing-loading plots for each of the components and selecting a design point within the feasible design space.

The design space and restrictions stem from various mission and certification requirements. In the specific case of commuter aircraft, there are 12 constraints limiting the available design space. Those requirements include powered stall speed, specified aircraft cruise speed, take-off distance, AEO sea level rate of climb gradient, as well as various OEI and AEO gradient requirements based on CS-23 regulations, as described in Section 4.1.1. The aircraft design point is selected such that the required wing size is minimised.

The best way to illustrate this process is to present the actual power- versus wing-loading diagrams and corresponding design points for the fuel cell aircraft. However, to limit the length of this section, the BAE Jetstream 31 fuel cell aircraft power- vs. wing-loading diagrams seen in Figure 5.1 will be used as a representative example, while the plots for the other 3 aircraft can be seen in Appendix C.
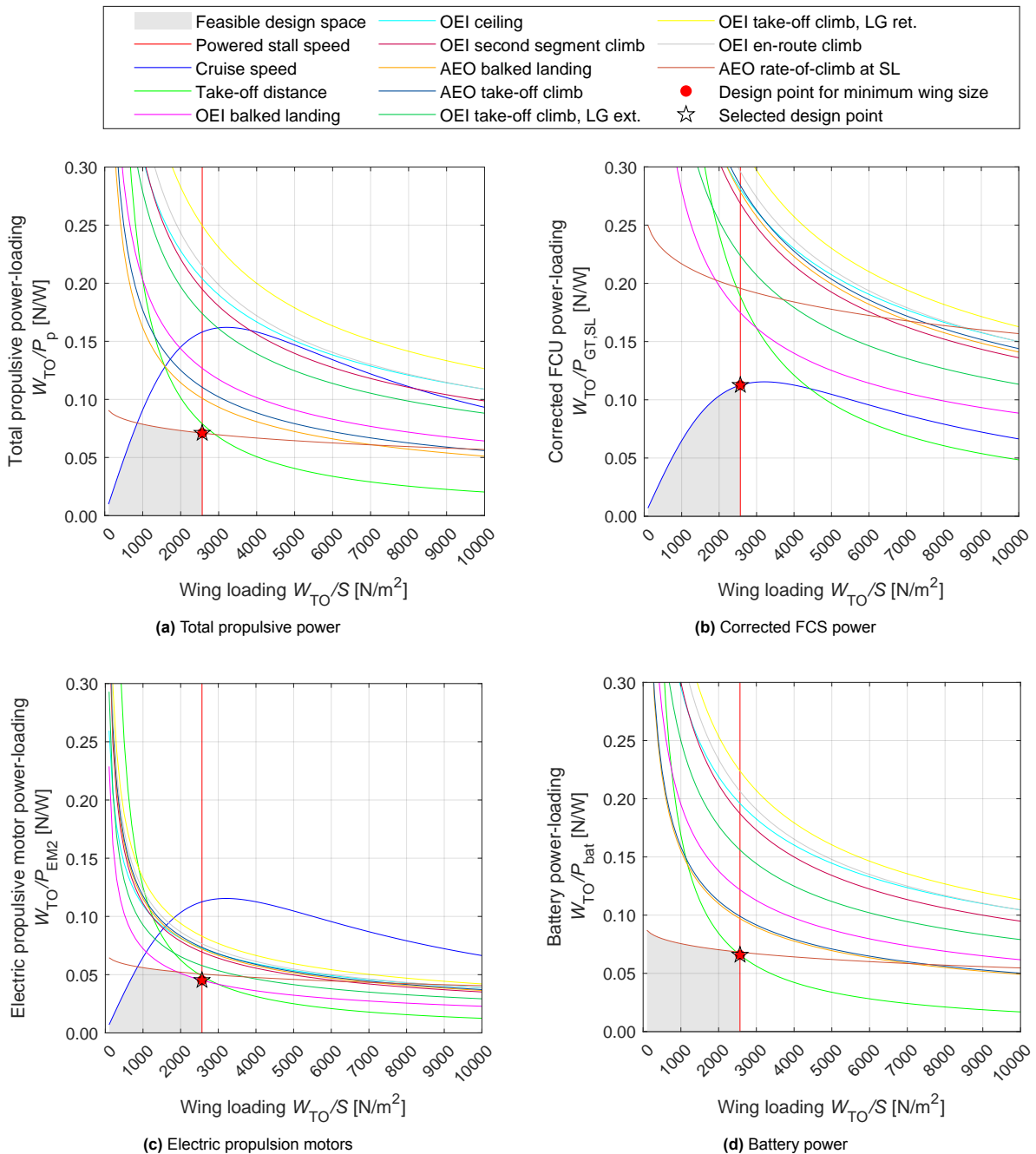


**Figure 5.1:** Power- versus wing-loading diagrams and design points for the BAE Jetstream 31 FC and its various powertrain components

Figure 5.1 displays four different power- versus wing-loading diagrams for the Jetstream 31 fuel cell aircraft. Figure 5.1a plots the total aircraft propulsive power-loading against the wing-loading. This plot is not used for sizing of any specific component but serves as a good illustration of the aircraft's performance. Next, Figure 5.1b displays the corrected power-loading of the FCS. Normally, for conventional propulsion, this plot would be corrected for the engine power lapse with altitude, as well as the engine throttle setting. However, since the FCS compressor is sized to be able to supply sea-level pressure to the fuel cells throughout the flight, the altitude power lapse correction is omitted for the FCS sizing. The last two plots, seen in Figure 5.1c and Figure 5.1d, are used to determine the design point of the electric propulsion motors and the battery pack, respectively.

In each of the 4 presented plots, 12 different requirements constrain the available design space, as mentioned above. The light grey area on all plots indicates the available design space. The red dot and the star symbol indicate the design point for minimum wing size and the selected design point, respectively. Since the Initiator sizing is set such that the minimum wing size is the desired outcome, the selected design point always corresponds to the minimum wing size point.

Now that the determination of the design points has been discussed the selected values of the wing-loading and power-loading for the main powertrain components in all 4 fuel cell aircraft can be reviewed. Table 5.1 lists the design points for the fuel-cell (FC) aircraft and their conventional (Conv.) aircraft counterparts. While there is only a single wing-loading value per aircraft, the power-loading is slightly more complex. Starting from the left, the columns of the power-loading diagram correspond to total propulsive power (Tot. Prop.), corrected FCS power (FCS (Corr.)), propulsive electric motor power (EM), and the battery of the fuel cell aircraft. Finally, the last column represents the corrected gas turbine engine (GT (Corr.)) power-loading of the corresponding conventional aircraft.

**Table 5.1:** Wing- and power-loading design points for conventional and fuel cell aircraft and their powertrain components

| | Wing-loading [kg/m$^2$] | | Power-loading [kg/kW] | | | | |
| | FC | Conv. | FC | | | | Conv. |
| | – | – | Tot. Prop. | FCS (Corr.) | EM | Battery | GT (Corr.) |
| **Dornier Do 228-212 FC** | | | | | | | |
| Class 2 | 190.6 | 200.0 | 8.26 | 8.24 | 4.36 | 7.59 | 5.53 |
| **Fairchild Metro 23 FC (2+1cab mod)\*** | | | | | | | |
| Class 2 | 247.8 | 260.8 | 6.60 | 10.09 | 4.18 | 6.39 | 4.51 |
| **BAE Jetstream 31 FC** | | | | | | | |
| Class 2 | 261.6 | 275.5 | 7.23 | 11.44 | 4.60 | 6.71 | 4.96 |
| **Embraer EMB 110P2 FC** | | | | | | | |
| Class 2 | 195.1 | 195.1 | 7.87 | 12.73 | 5.05 | 6.93 | 5.31 |

\*Cabin widening to 2+1 seating configuration was required to limit overall fuselage length and allow for sizing convergence.

The design wing-loading for fuel cell aircraft lies between 195 and 275 kg/m$^2$. Compared to the conventional aircraft the wing-loading decreased by around 5% for the first three aircraft, while the EMB 110 experienced no change. As expected, the component with the highest power-loading in the considered fuel-cell-hybrid powertrain is the electric propulsion motor. The electric motor has to handle almost 100% of the power produced by the FCS and the battery and thus has to be sized accordingly.

Generally, the design point results appear as expected. Perhaps the most unexpected results came from the Do 228. The conventional Do 228 aircraft has the most relaxed corrected power-loading requirement out of the four aircraft. However, when equipped with the fuel-cell powertrain, its FCS power loading is the most restrictive out of the four fuel cell aircraft. Accordingly, the fuel-cell Do 228 aircraft has the most relaxed battery power-loading requirements. The unusually strict power-loading requirement can at least in part be explained by the relatively high cruise speed at a very low cruise altitude. Since the cruise speed requirement is the most restrictive FCS sizing requirement for all four fuel cell aircraft included in this study, this relatively high speed leads to a very high FCS power requirement.

## 5.1.2. Convergence

As described in Section 3.3, the Initiator software converges towards the final results by iterating over the various sizing modules. In the process, each module produces results based on the results of the other modules from the current or previous iteration step. The goal of the process is to converge the class 1 aircraft MTOM estimate within a specified margin of error. For this project, these margins were set to 0.05% for class 2, and mission analysis estimates, 0.3% for class 2.5 estimates and 0.5% for the HSE module.

As can be seen in Figure 5.2, the average convergence of fuel cell aircraft took considerably more iterations than for their conventional aircraft equivalent. This is especially true for the Initiator runs with the 'class 2.5' or 'class2.5 & HSE' enabled. In most of those cases, more than twice the number of iterations were needed for conventional aircraft convergence. In an attempt to explain this discrepancy, three contributing reasons were identified. These are the limitations of the initial MTOM estimates, oscillations around the final solution between class 1 and 2 modules, and non-convergent behaviour of class 2.5 modules. The remainder of this section will elaborate on these issues.
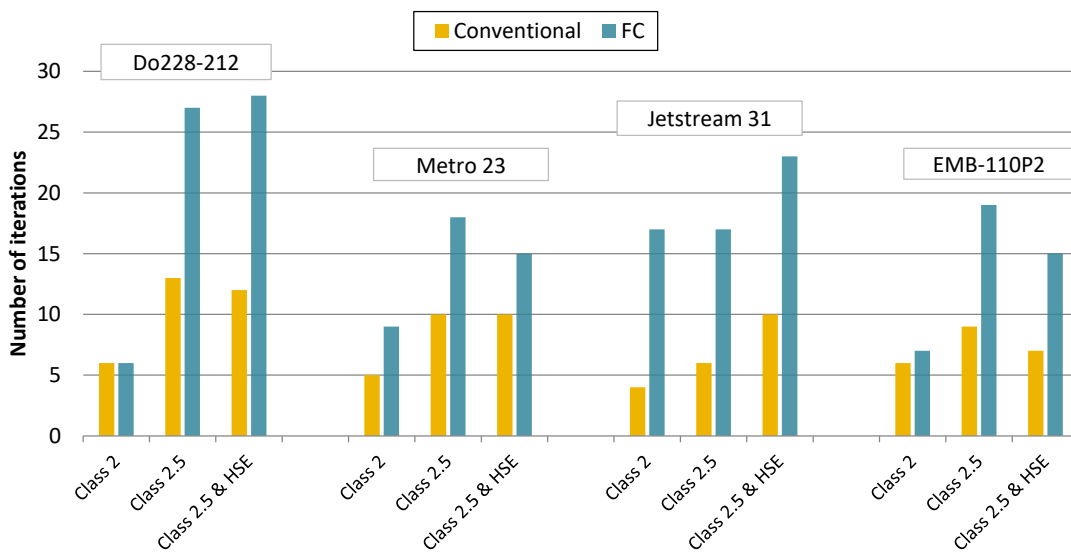


**Figure 5.2:** Number of iterations required to achieve convergence of conventional and fuel cell aircraft

### Limitations in the Initial MTOM Estimate

The first difficulty for fuel cell aircraft occurs at the very beginning of the sizing process. Since the very first class 1 mass guess is based on statistical regression of conventional aircraft, it usually provides a reasonably accurate estimate of the MTOM during conventional aircraft sizing. However, since there is no statistical regression specific to fuel cell aircraft, the same conventional aircraft database is used to provide an initial estimation for the fuel cell aircraft as well. In most cases, this severely underestimates the final converged fuel cell aircraft mass. Compounding the limitations in the initial estimations, the first class 2 iteration has to provide results based on an very rudimentary guess for the mass and size of the powertrain components. Thus, the initial class 1 and class 2 mass estimations are often extremely far from each other, which naturally prolongs the convergence process. For illustrative purposes Figures 5.3a, 5.3c, and 5.3e display examples of the convergence process where the large mismatch between the initial estimates and the final results can be seen.

### MTOM Estimation Oscillations

A slightly less common occurrence is the tendency for class 1 and class 2 MTOM estimates to oscillate around an apparent solution. To illustrate this behaviour, Figure 5.3b provides an example from the convergence process of one of the earlier versions of the fuel-cell Jetstream 31 aircraft. It can be seen that the MTOM estimations of the two sizing loops converge towards a solution, but after converging within a certain margin, the two modules interchangeably over- or underestimate the MTOM value around which they are appearing to converge.
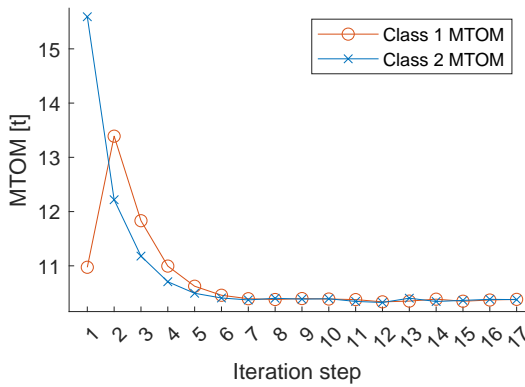
**(a)** Inaccurate initial MTOM estimate for BAE Jetstream 31 FC 'Class 2'
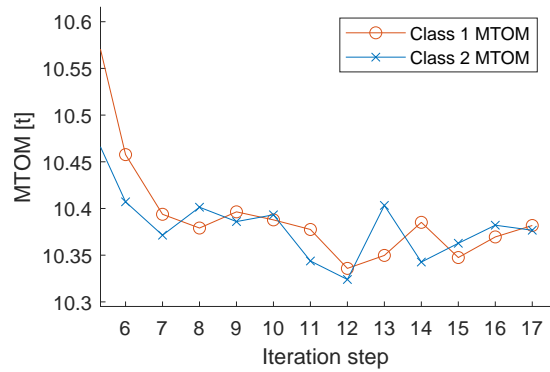
**(b)** MTOM estimate oscillations for BAE Jetstream 31 FC 'Class 2' detail
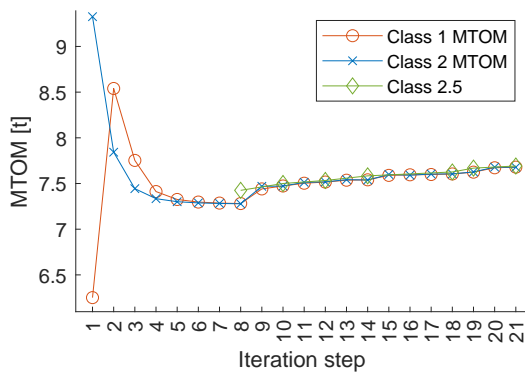
**(c)** Inaccurate initial MTOM estimate for Embraer EMB 110P2 FC 'Class 2.5'
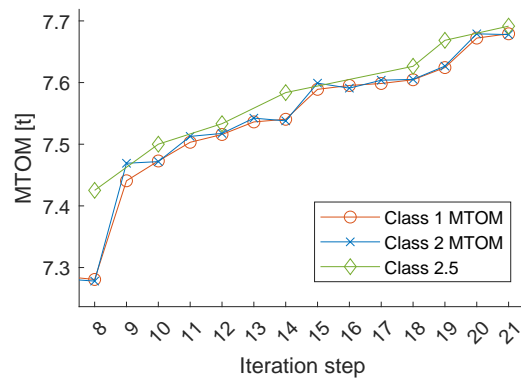
**(d)** Class 2.5 MTOM estimation jump for Embraer EMB 110P2 FC 'Class 2.5'
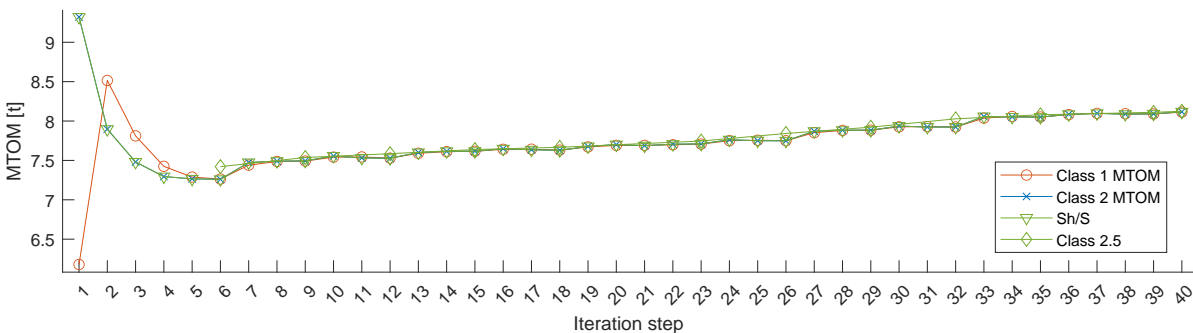
**(e)** Class 2.5 MTOM estimation non-convergence for Embraer EMB 110P2 FC 'Class 2.5 & HSE'

**Figure 5.3:** Example of Initiator convergence issues for fuel cell aircraft

Luckily, this behaviour did not affect the accuracy of the end result greatly. Moreover, slightly increasing the convergence margins can provide a simple workaround for the illustrated issue without a great sacrifice to the accuracy of the results. It is nevertheless important to note that this phenomenon is much more common in fuel cell aircraft and should be investigated further.

**Limitations in Class 2.5 Convergence**
The final limitation in the fuel cell aircraft design process is the non-convergent behaviour of the class 2.5 modules. This behaviour can be observed when class 2.5 modules appear to be converging towards a solution, but after some iterations, their estimates suddenly increase or decrease in value. This is the case with the convergence illustrated in Figure 5.3d, where a comparatively large jump in class 2.5 estimates can be seen between iterations 18 and 19. Alternatively, class 2.5 sometimes appears to continuously increase or decrease the aircraft mass in an almost linear fashion, as is the case in

Figure 5.3e. Either of these behaviours can in rare cases lead to an unbounded increase or decrease in the estimated aircraft mass. Therefore, when this behaviour is present, the final result are unduly influenced by the convergence margin set by the user. While it was made sure that this behaviour did not affect the results presented in this chapter, it is nonetheless an issue worth addressing in the future.

## 5.2. Aircraft Mass Results

This section will present the mass results of fuel cell aircraft sized or the 19-passenger nominal mission and compare them to the conventional aircraft where appropriate. The exact parameters of this mission can be found in Table 3.2. The results will be discussed in 2 parts. First, the basic aircraft mass results, the OEM and MTOM, will be presented. In the second part, the results specific to the powertrain and the FCS will be discussed.

### 5.2.1. OEM and MTOM Results

The MTOM and OEM are presented in Table 5.2. It can be seen that the aircraft OEM has generally increased by 110 to 130%, for the first three aircraft. A definite outlier in this is the EMB 110 fuel cell aircraft, whose mass increase appears to be only around half of those of the other fuel cell aircraft. While these values indicate a severe increase in the aircraft mass, a direct comparison to conventional aircraft would not be evenhanded. The OEM of the fuel cell aircraft already includes one of the energy carriers, that is the batteries. Furthermore, the cryogenic fuel tank has a very high mass compared to the required hydrogen fuel for the mission. Thus, MTOM comparison should provide a more unbiased comparison. The MTOM increase of fuel cell aircraft appears to be around 60% for the first three aircraft and around 30% for the EMB 110. Thus, across all four aircraft, the increase in MTOM is about half as severe as the increase in OEM.

The differences in the relative MTOM increase found using different Initiator sizing 'depths' is within a few percentage points. The noteworthy outlier here is the Metro 23 whose results obtained using the 'class 2' mass estimations differ by 15 percentage points compared to 'class 2.5' estimates. Apart from this specific case, the general consensus on the mass increase by different Initiator 'depths' provides confidence in the results. This is especially important since a notable discrepancy in the results between that of the HSE module and the rest was observed during the conventional commuter aircraft sizing validation in Table 4.2. While the absolute differences in mass and geometry estimates obtained when using the HSE module still exist, the agreement between different Initiator sizing 'depths' on the relative mass increase, is promising.

While no two fuel cell aircraft experienced exactly the same increase in mass, the EMB 110 definitely stands out. The relative mass increase for this aircraft was only about 50% of that of the other aircraft. The most likely cause of this discrepancy is its low range. While all of the other reference aircraft can reach destinations over 1000 km away, the EMB 110 range with 19 passengers is only around 500 km. This is more than a 50% decrease in range requirement, which translates to a much smaller and thus lighter hydrogen tank. Additionally, the aircraft flies lower and slower than other reference aircraft. This relaxes the power requirements. As already alluded to when selecting reference aircraft in Section 3.4, the lower aircraft power requirements were presumed beneficial for the feasibility of fuel cell aircraft. While these results seem to agree with this, further investigation it is nevertheless necessary to fully understand this phenomenon.

Looking at the individual results from the rest of the aircraft, the mass of the Metro 23 did not increase as much as expected. While the Metro 23 is the heaviest conventional aircraft out of the four with by far the longest range of over 2000 km, its mass did not increase more than that of the Jetstream or the Dornier. However, there is a possible explanation for this. The cabin of the Metro 23 aircraft had to be redesigned from a 1+1 seating layout to a 2+1 seating layout to allow for convergence of the fuel cell aircraft. This was necessary since the length of the already slender Metro 23 fuselage became too long after also adding the cryogenic fuel tank. The widening of the fuselage increased the gravimetric efficiency of the cryogenic fuel tank. This reduced the mass penalty that would have been incurred otherwise.

Equally unforeseen, the mass increase of the Do 228 aircraft is higher than expected. The simple, non-pressurised cabin, low cruise speed and altitude and generally low OEM value should give the Do 228 an edge over the mass of the higher-performing Jetstream 31 and Metro 23. With a wing-

**Table 5.2:** Preliminary sizing results for fuel-cell commuter aircraft with nominal mission requirements

| | OEM | | MTOM | |
|---|---|---|---|---|
| | $[kg]$ | $\Delta_{conv.}$* | $[kg]$ | $\Delta_{conv.}$* |
| **Dornier Do 228-212 FC** | | | | |
| Class 2 | 8250 | +118.2% | 10153 | +59.4% |
| Class 2.5 | 8322 | +112.1% | 10229 | +56.7% |
| Class 2.5 & HSE | 9269 | +114.3% | 11198 | +60.2% |
| **Fairchild Metro 23 FC (2+1cab mod)**\*\* | | | | |
| Class 2 | 10926 | +136.5% | 13031 | +67.1% |
| Class 2.5 | 9536 | +113.5% | 11599 | +52.1% |
| Class 2.5 & HSE | 10369 | +123.6% | 12452 | +59.6% |
| **BAE Jetstream 31 FC** | | | | |
| Class 2 | 8756 | +114.2% | 10613 | +62.2% |
| Class 2.5 | 8626 | +108.2% | 10478 | +58.6% |
| Class 2.5 & HSE | 8867 | +107.3% | 10726 | +58.7% |
| **Embraer EMB 110P2 FC** | | | | |
| Class 2 | 5802 | +63.2% | 7521 | +31.8% |
| Class 2.5 | 5882 | +60.5% | 7593 | +30.4% |
| Class 2.5 & HSE | 5896 | +61.0% | 7615 | +30.7% |

*Difference w.r.t. the Initiator results for conventional commuter aircraft sizing with equal design 'depth'.
\*\*Cabin widening to 2+1 seating configuration was required to limit overall fuselage length and allow for sizing convergence.

and power-loading similar to that of the EMB 110, a likewise smaller increase in mass was expected. However, this is not the case. The Do 228 mass rose by an approximately equal amount compared to the Jetstream 31 and Metro 23. One of the reasons for this again lies in the slenderness of the fuselage. Similarly to the Metro 23, the conventional Do 228 also features a 1+1 seating layout, making the fuselage relatively slender. By adding the cryogenic fuel tank, this slenderness is exaggerated further to the point where it becomes strongly disadvantageous, both aerodynamically and structurally. While the Metro 23 encountered convergence problems because of this and was subsequently modified, the Do 228 was not. Therefore, the fuselage length is largely responsible for the large mass increase of the fuel cell aircraft. To investigate this further, the fuel cell aircraft mass sensitivity to fuselage width will be further explored in Section 5.6.3.

Finally, the Jetstream 31 produced expected sizing results. The original aircraft is very heavy for its payload and range capabilities. This is largely due to a relatively large and comfortable pressurised passenger cabin with a toilet and a small galley. Additionally, the cruise speed and altitude of this aircraft are very high. Nevertheless, the wide fuselage increases the mass efficiency of the cryogenic tank, mitigating other detrimental factors.

## 5.2.2. Powertrain Mass Results
This section will examine the fuel-cell powertrain mass. The analysis will be divided into two parts. First, a breakdown of the powertrain mass into its main components will be presented. Next, the focus will shift specifically to the FCS mass composition.

**Overall Powertrain Mass Breakdown**
Table 5.3 lays out the mass sizing results of the major hybrid fuel-cell powertrain components. Similarly to the MTOM and OEM results in Table 5.2, there are some discrepancies between the results of different Initiator sizing 'depths'. However, the discrepancy between these 'depths' are consistent with those encountered in the MTOM and OEM mass estimations.

Looking at the individual components, the FCS mass varies greatly between different aircraft. Given

**Table 5.3:** Absolute mass results from powertrain sizing for fuel-cell commuter aircraft with nominal mission requirements

| | FCS (single) [kg] | FCS specific power [kW/kg] | Motor (single) [kg] | Battery pack [kg] | Fuel supply subsystem [kg] | Cryogenic tank [kg] | Tank mass efficiency* [%] |
|---|---|---|---|---|---|---|---|
| **Dornier Do 228-212 FC** | | | | | | | |
| Class 2 | 391.0 | 1.5653 | 199.8 | 1194.1 | 413.8 | 364.7 | 44.0% |
| Class 2.5 | 393.4 | 1.5654 | 201.1 | 1202.1 | 414.2 | 374.6 | 43.5% |
| Class 2.5 & HSE | 428.6 | 1.5670 | 219.3 | 1314.9 | 420.0 | 397.3 | 44.2% |
| **Fairchild Metro 23 FC (2+1cab mod)\*\*** | | | | | | | |
| Class 2 | 428.7 | 1.4967 | 268.3 | 2684.5 | 451.4 | 434.3 | 52.7% |
| Class 2.5 | 391.3 | 1.4951 | 240.8 | 2406.2 | 444.4 | 408.6 | 52.0% |
| Class 2.5 & HSE | 416.0 | 1.4962 | 258.1 | 2581.0 | 449.1 | 424.9 | 52.5% |
| **BAE Jetstream 31 FC** | | | | | | | |
| Class 2 | 516.3 | 0.8957 | 198.8 | 2253.5 | 402.4 | 181.3 | 56.9% |
| Class 2.5 | 509.3 | 0.8956 | 196.2 | 2224.4 | 401.6 | 180.1 | 56.7% |
| Class 2.5 & HSE | 526.3 | 0.8958 | 201.8 | 2280.6 | 403.7 | 183.0 | 57.2% |
| **Embraer EMB 110P2 FC** | | | | | | | |
| Class 2 | 362.9 | 0.8157 | 128.4 | 775.3 | 356.9 | 101.3 | 50.3% |
| Class 2.5 | 358.1 | 0.8155 | 129.6 | 770.8 | 355.7 | 101.1 | 50.4% |
| Class 2.5 & HSE | 363.9 | 0.8157 | 130.0 | 781.1 | 356.9 | 101.5 | 50.2% |

*Gravimetric tank efficiency; the ratio between the contained fuel mass and the total mass of the tank and contained fuel.
**Cabin widening to 2+1 seating configuration was required to limit overall fuselage length and allow for sizing convergence.

the differences in MTOM and power-loading requirements, this is fairly unsurprising. However, what is surprising are the large differences between aircraft in terms of FCS specific power. The Do 228 and Metro 23 aircraft achieved a FCS specific power of around 1.57 and 1.50 kW/kg, respectively. Conversely, for the Jetstream 31 and EMB 110 this value was only around 0.90 and 0.82 kW/kg, respectively. These phenomena cannot simply be explained through the obvious differences in mission requirements. In fact, the aircraft division between the high and fast-flying Metro 23 and Jetstream 31, and the lower and slower Do 228 and EMB 110 break down completely in this particular case. Thus, there is a need to examine these phenomena further. This will be done later in this section by deconstructing the FCS mass into its individual components.

Although only used for take-off and climb segments, the battery pack mass is still the largest single contribution to the powertrain mass. This is especially notable for the two pressurised aircraft that cruise at an altitude of around 7 km. Indeed, their battery accounts for over 25% of their OEM, as can be seen in Figure 5.4. For the low-flying EMB 110 and Do 228 this value is only around 14%. It is worth noting that during a normal trip with no loiter or diversion the battery provides only between 2.4 and 5.2% of the total energy required for the trip. Naturally, with such a large mass penalty, but a relatively low energy contribution, an obvious question arises: would it be sensible to reduce the aircraft's dependence on the battery power and thus lower the battery pack mass? After all, the current power hybridisation of 50% during take-off and 25% during climb is simply an educated guess. This question will be further explored in the sensitivity analysis present in Section 5.6, where power hybridisation will be varied to explore its effects on aircraft mass and energy consumption.

While not as heavy as the FCS or the battery pack, the cryogenic hydrogen tank still presents a sizeable contribution to the OEM, as was expected. In the rightmost column of Table 5.3, the tank mass efficiency or the gravimetric efficiency is presented. This value is defined as the total fuel mass divided by the combined mass of the fuel and the tank structure. For the fuel cell aircraft in this study, this value ranges from 43% to 57%. With the cabin widths between 1.34 m and 1.85 m, these gravimetric efficiency results are completely in line with the results presented by Verstraete *et al.* [35]. As expected, the worst tank mass efficiency is found in the Do 228. This can be easily explained by the fact that after the fuselage modification on the Metro 23, the Do 228 is left with the by far most narrow fuselage. This
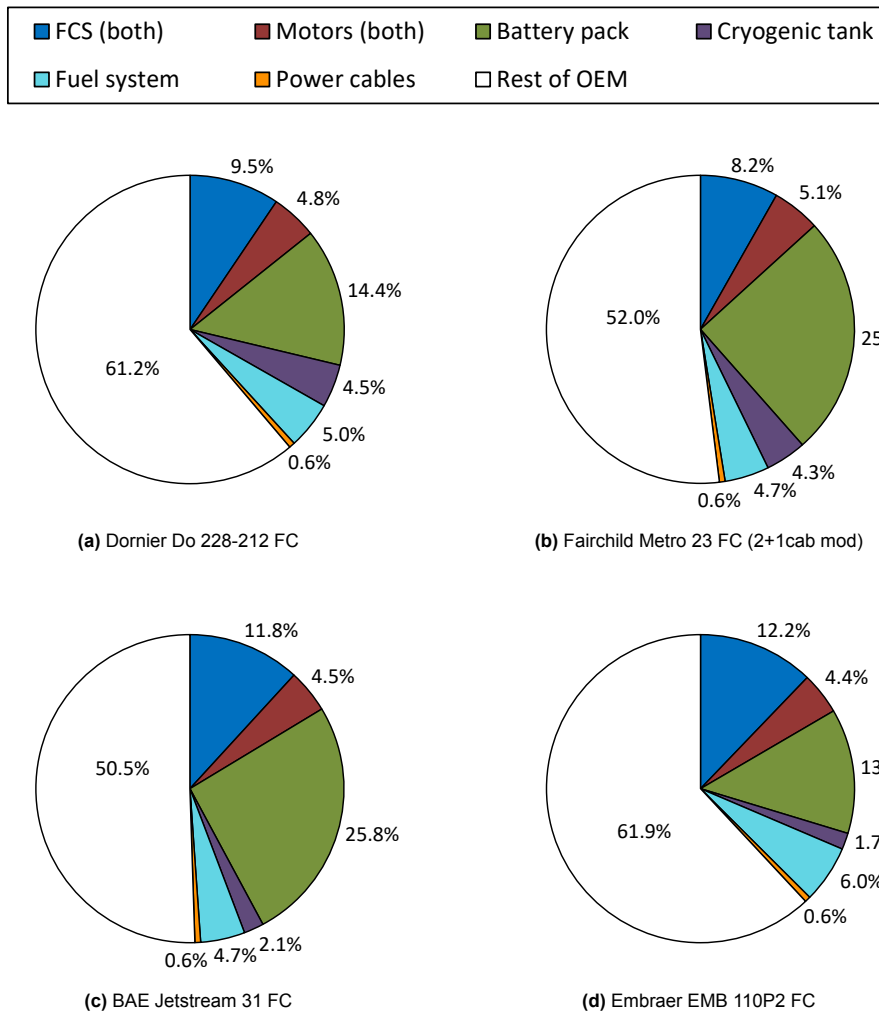
**Figure 5.4:** Relative mass results from powertrain sizing for fuel-cell commuter aircraft with nominal mission requirements (Initiator class 2.5 'depth').

resulted in a very slender and inefficient tank design. Conversely, the Jetstream 31 with a similar range achieves the best tank gravimetric efficiency, in large part because of the widest fuselage diameter.

Finally, it is necessary to also focus on the fuel subsystem needed to supply and regulate the flow of hydrogen to the fuel cells. This sometimes overlooked subsystem in a hydrogen fuel-cell powertrain presents an important mass contribution to the overall powertrain system. In fact, the results shown here consistently indicate the fuel supply and regulation system presents a larger mass than the hydrogen tank itself. Furthermore, the mass of this subsystem depends very little on the amount of hydrogen stored onboard. Thus, for lower-range aircraft, the fuel supply system presents a disproportionately large amount of mass compared to the hydrogen fuel tank. Looking at Figure 5.4, it can be seen that the fuel subsystem accounts for 6% of total aircraft OEM for the EMB 110 and between 4.7 and 5.0% for the other three aircraft.

**FCS Mass Breakdown**

The mass of the four major components of a single FCS for all four aircraft is laid out in Table 5.4. Besides the absolute mass value, Figure 5.5 also displays the relative mass contribution of each component to the total FCS mass.

As expected, it can be seen that the mass of the fuel-cell stacks is fairly consistent with the net power produced by the FCS. Since the humidifier is sized based on the power produced by the fuel-cell stacks, its mass is also proportional to the fuel-cell stacks. This cannot be said for the compressor, however. Since the compressor is sized to provide sea-level pressure to the fuel-cell stacks, the compressor mass presents a higher fraction of the total FCS mass for aircraft that cruise at higher altitudes, as can

**Table 5.4:** Mass breakdown of a single FCS

|  | FCS | | FC Stacks | Compressor | Humidifier | Heat Exchanger |
|---|---|---|---|---|---|---|
|  | $[kW]$* | $[kg]$ | $[kg]$ | $[kg]$ | $[kg]$ | $[kg]$ |
| **Dornier Do 228-212 FC** | | | | | | |
| Class 2.5 | 616 | 393 | 205 | 20 | 31 | 134 |
| **Fairchild Metro 23 FC (2+1cab mod)\*\*** | | | | | | |
| Class 2.5 | 575 | 391 | 192 | 4 | 31 | 129 |
| **BAE Jetstream 31 FC** | | | | | | |
| Class 2.5 | 454 | 509 | 153 | 36 | 25 | 295 |
| **Embraer EMB 110P2 FC** | | | | | | |
| Class 2.5 | 298 | 358 | 97 | 11 | 18 | 233 |

\*Net power of the FC stack, accounting for the parasitic power draw of the BoP components
\*\*Cabin widening to 2+1 seating configuration was required to limit overall fuselage length and allow for sizing convergence.
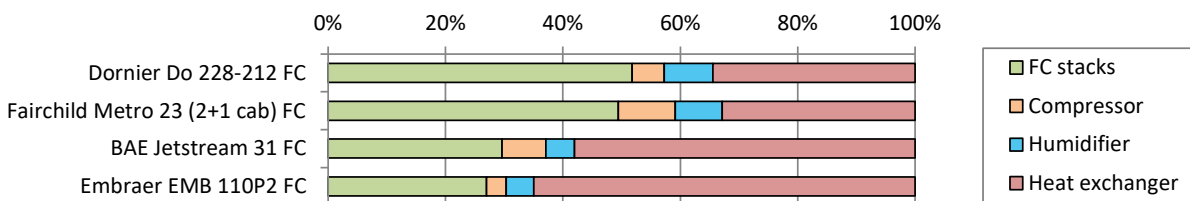


**Figure 5.5:** Relative FCS mass composition

be seen in Figure 5.5. The mass of the humidifier with the current sizing model is independent of the flight altitude and thus, the mass is directly proportional to the power of the fuel-cell stacks.

Unlike the rest of the FCS components, the mass of the heat exchanger appears to vary greatly, irrespective of the FCS power output or fuel-cell stack mass. Recalling the FCS specific power discrepancies discovered in Table 5.3, the heat exchanger results from Figure 5.5 offer some more insights into the issue. As it turns out, a sudden jump in specific power is caused by a particular combination of Mach number and air density which control the efficiency of the FCS heat exchanger through the Reynolds number. However, this section will not go into more detail on this phenomenon. For more information, the reader should refer to Section 5.6 and Chapter 6 where these discrepancies will be addressed in more detail.

## 5.3. Geometrical Sizing Results

Now that the mass estimates for fuel cell aircraft have been discussed, it is also worth briefly examining the results in terms of aircraft geometric sizing. While the increased mass of the fuel cell aircraft naturally translates into an increased aircraft size, it is still worth quantifying the difference and visualising the aircraft.

The overall dimensions of the fuel cell aircraft obtained with the Initiator class 2.5 'depth', as well as their relative changes with respect to the conventional aircraft are listed in Table 5.5. The changes in the wingspan relate clearly with the increase in MTOM and the corresponding increases in wing area. However, The overall length and height changes are slightly less straightforward to explain.

The main parameter controlling the aircraft length increase is the addition of the cryogenic fuel tank. Accordingly, the aircraft with lesser range and wider fuselages experienced lower length growth. The largest increase in length is 43% seen on the Do 228 due to its large slender cryogenic fuel tank. While a much lesser increase is shown for the Metro 23 it is worth remembering that the fuel-cell version of this aircraft has a different seating layout and would be notably shorter than the reference version if not for the large cryogenic fuel tank.

The height growth is a combination of two factors. The first reason is the vertical tail size increase

**Table 5.5:** Overall dimensions of the fuel-cell commuter aircraft with nominal mission requirements

|  | Length | | Wingspan | | Height | |
|---|---|---|---|---|---|---|
|  | [$m$] | [$\Delta_{conv.}$]* | [$m$] | [$\Delta_{conv.}$]* | [$m$] | [$\Delta_{conv.}$]* |
| **Dornier Do 228-212 FC** | | | | | | |
| Class 2.5 | 23.58 | 43% | 22.26 | 28% | 6.17 | 27% |
| **Fairchild Metro 23 FC (2+1cab mod)\*\*** | | | | | | |
| Class 2.5 | 21.75 | 19% | 22.02 | 26% | 6.76 | 29% |
| **BAE Jetstream 31 FC** | | | | | | |
| Class 2.5 | 18.15 | 26% | 19.86 | 32% | 6.85 | 20% |
| **Embraer EMB 110P2 FC** | | | | | | |
| Class 2.5 | 17.11 | 12% | 17.76 | 15% | 6.21 | 14% |

*Difference w.r.t. the Initiator results for conventional commuter aircraft sizing with equal design 'depth'.
**Cabin widening to 2+1 seating configuration was required to limit overall fuselage length and allow for sizing convergence.

which corresponds to the increase in overall aircraft size. The second factor is the tail scrape angle or the angle to which the aircraft can rotate on the ground before the tail cone strikes the ground. As with most aircraft configuration parameters, this angle has been preserved with respect to the conventional aircraft model. Thus, with an elongated fuselage, the fuel cell aircraft require longer main landing gear struts to achieve the same scrape angle. Inadvertently, this also increases the overall aircraft height, as well as mass.

Figure 5.6 illustrates the size differences between the conventional and fuel cell aircraft by superimposing the top-view results. The aircraft displayed above the aircraft centerline are fuel cell aircraft, while the aircraft below the centerline are conventional aircraft. All results in the figure were obtained using the Initiator class 2.5 sizing 'depth' and a nominal mission as the design mission for fuel cell aircraft.

An observation that was not possible to make by simply looking at the Table 5.5, but is visible in Figure 5.6 is the disproportional increase in the size of nacelles on the fuel cell aircraft. While a considerable part of the size difference can be attributed to the overall larger size of the aircraft, the nacelle appears to grow even more than the rest of the aircraft, especially for the Jetstream 31. Thus it could be said that the FCS and the electric motor require more volume than the equivalent conventional turbine engine. Nevertheless, since not much information is available on the packing efficiency of real-world fuel-cell systems, any conclusions based on the presented geometry results should be used with caution. Furthermore, the large nacelle size on the Jetstream 31 is almost entirely due to the large heat exchanger. As one might recall, the heat exchanger model and its results have already received some attention and criticism due to the unexpected deviations between the four presented aircraft. Thus, the accuracy of FCS volume results might have some limitations.

## 5.4. Mission Energy Use and Emissions Analysis

While the previous sections concluded that the mass of the aircraft greatly increases due to the fuel-cell powertrain, it says nothing about the changes in the required energy to perform the mission. While it is clear that heavier aircraft generally consume more energy over the same mission, it is also likely that the increased efficiency that is expected of the hydrogen hybrid fuel-cell powertrain could bring measurable energy savings and at least partially offset the mass penalty. To determine the energy performance of fuel-cell commuter aircraft, including powertrain efficiency, energy costs and environmental aspects, this section will quantify and analyse the aircraft energy use and its impacts.

### 5.4.1. Total Energy Use and Energy Efficiency

First, the total energy required to fly the fuel cell aircraft to the intended destination during a nominal mission is examined. This information can be seen in the first column of Table 5.6. Note, that these

**(a)** Dornier Do 228-212

**(b)** Fairchild Metro 23
(fuel cell aircraft with a modified 2+1 cabin seating)

**(c)** BAE Jetstream 31

**(d)** Embraer EMB 110P2
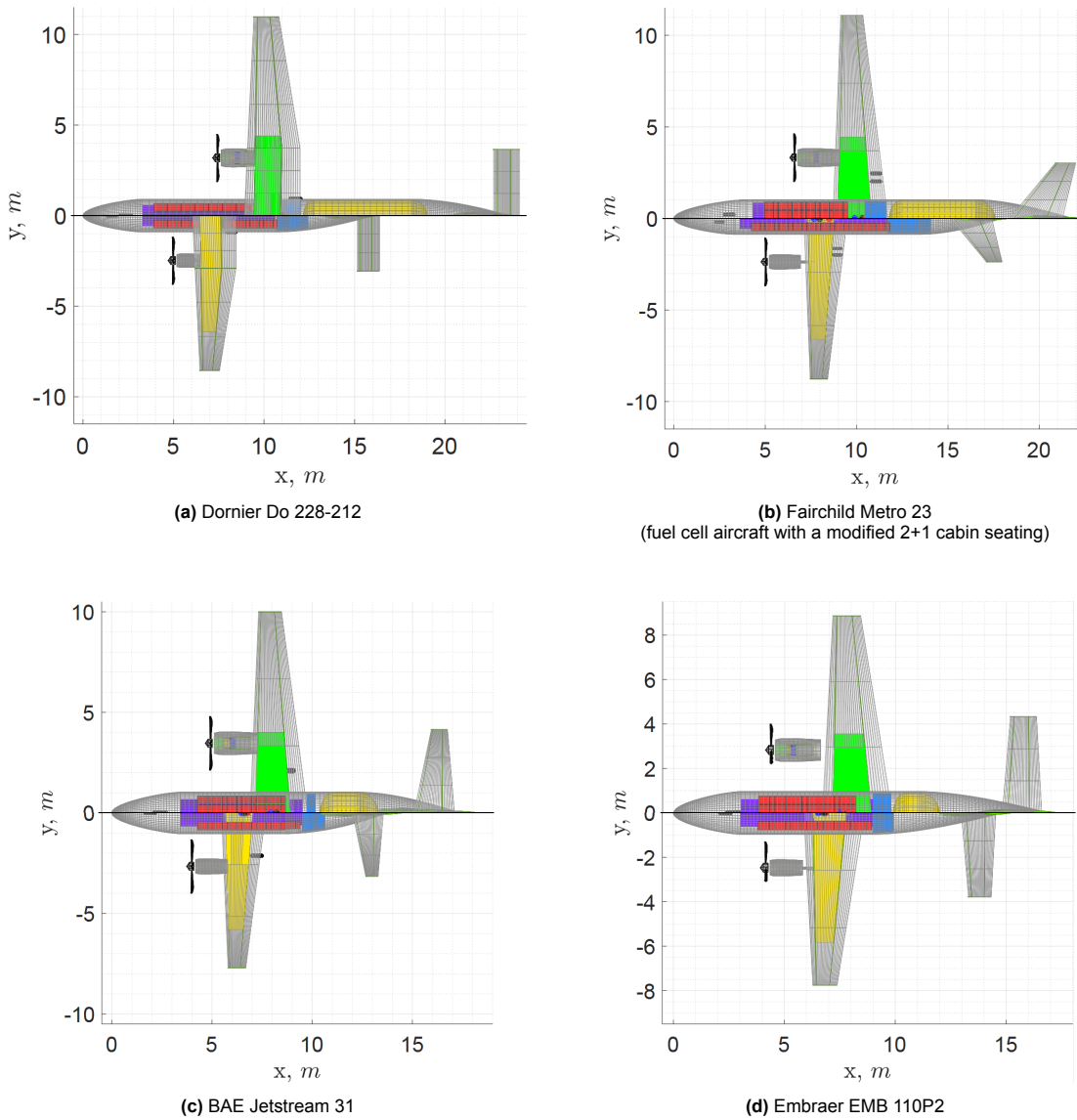
**Figure 5.6:** Size comparison between the fuel cell aircraft sized for a nominal mission and conventional aircraft with Initiator class 2.5 'depth' results (top half: fuel cell aircraft; bottom half: conventional aircraft).

energy figures do *not* include the reserve energy required to fly to the alternate airport, nor the 45-minute loiter period. As can be seen from the table, the total mission energy values range from around 9.5 to 60 GJ. This is a large range of values, but it correlates well with the differences in range, speed, and OEM of the aircraft. Since all 4 aircraft carry equal payload during a nominal mission, no discrepancy in total energy values between aircraft can be attributed to the payload mass.

The second metric that is included in Table 5.6 is the payload-range energy efficiency or PREE. This metric is obtained by multiplying the weight of the payload by the distance flown and dividing the product by the total energy required to reach the destination airport, as demonstrated in Equation 5.1. As can be seen from the equation, the value is dimensionless. In essence, PREE indicates the payload transportation energy efficiency of the aircraft system.

$$PREE = \frac{m_{payload} \cdot g \cdot R_{mission}}{E_{mission}} \tag{5.1}$$

Despite the much higher MTOM and OEM of fuel cell aircraft, their total energy use and payload-range efficiency or PREE values have not suffered greatly. The most negatively affected aircraft is the Metro 23 whose PREE estimates dropped by 4.5%. More notably, however, the EMB 110 actually

**Table 5.6:** Mission energy and efficiency results from fuel-cell commuter aircraft with nominal mission requirements

| | Total mission energy | | Payload-range energy efficiency (PREE) | | FCS net efficiency | Battery mission energy fraction |
|---|---|---|---|---|---|---|
| | $[GJ]$ | $[\Delta_{conv.}]$* | $[-]$ | $[\Delta_{conv.}]$* | $[\%_{HHV}]$ | $[\%]$ |
| **Dornier Do 228-212 FC;** Range: 1166 km | | | | | | |
| Class 2.5 | 34.1 | +3.1% | 0.57 | -3.0% | 37.4% | 2.34% |
| **Fairchild Metro 23 FC (2+1cab mod)**\*\*; Range: 2065 km | | | | | | |
| Class 2.5 | 59.7 | +4.7% | 0.61 | -4.5% | 35.7% | 2.74% |
| **BAE Jetstream 31 FC;** Range: 1192 km | | | | | | |
| Class 2.5 | 26.9 | +1.9% | 0.71 | -1.4% | 34.9% | 5.22% |
| **Embraer EMB 110P2 FC;** Range: 520 km | | | | | | |
| Class 2.5 | 9.5 | -38.3% | 0.63 | +41.2% | 37.2% | 4.91% |

*Difference w.r.t. the Initiator results for conventional commuter aircraft sizing with equal design 'depth'.
**Cabin widening to 2+1 seating configuration was required to limit overall fuselage length and allow for sizing convergence.

improved its PREE by over 40%. Overall, these results show that the increased efficiency of the fuel-cell powertrain indeed largely offsets the aircraft mass penalty. The net FCS efficiency is around 35% for the aircraft with a higher cruise altitude and around 37% for the lower flying aircraft. Since the presented net FCS efficiency includes the parasitic power draw of the compressor, the higher-flying aircraft naturally lose more energy to the compressor. Nevertheless, the compressor power draw seems to have only a small effect on the overall FCS efficiency.

Before moving on, it is also important to point out that the energy efficiency used to calculate the PREE values for conventional aircraft has been obtained using the LHV of Jet-A1 fuel. Conversely, since the fuel cells produce water in liquid form, the consumed hydrogen fuel energy has been calculated using the hydrogen HHV value. By extension, the fuel cell aircraft PREE is then also obtained using the hydrogen HHV value. The HHV value has also been used to compute the FCS net efficiency. While this approach is technically more correct, it skews the perspective on how good the system is in converting fuel into useful energy. For example, if one is to take this approach and consider a FCS and a hydrogen combustion engine that have identical efficiencies, the FCS would still extract more useful energy than the combustion engine. This is because the hydrogen reaction in the fuel cell simply produces more free energy that can be directly extracted, compared to the combustion engine which discards a lot of the reaction energy into the atmosphere in the form of steam. If LHV was to be used for fuel cell aircraft efficiencies, the PREE and FCS net efficiency values would improve by 16.3%. This value is the difference between hydrogen HHV and LHV values.

The last column of Table 5.6 displays the fraction of total mission energy that is provided by the battery. The range of these values is between 2.4 and 5.2%. This is a fairly small amount of energy, especially if one recalls the results presented in Table 5.3, where it was shown that the battery pack contributes 13.3-25.8% to the aircraft OEM. This nicely illustrates the low specific energy of battery packs compared to hydrogen.

### 5.4.2. Environmental Impact Analysis
While the energy use analysis in the previous section did largely not favour the fuel cell aircraft solution, the same cannot be said for the emissions analysis. To support this claim, Figure 5.7 presents the total GWP of the aircraft energy carriers using the 'well-to-wake' analysis. Using the energy analysis shown in Table 5.6 and combining it with the GWP predictions for each energy source in Tables 4.6 and 4.7, the GWP for 5 scenarios was obtained. These include conventional aircraft powered by regular Jet-A1 fuel, conventional aircraft powered by SAF (PtL SAF), and fuel cell aircraft powered by liquid hydrogen and electricity ($LH_2$ + $e^-$). Additionally, the SAF and fuel-cell solutions were further split based on two electricity source scenarios. These two electricity sources are Danish wind farms (DK Wind) and Spanish photovoltaic plants (ES PV).

While it can be seen that the SAF solution presents a sizeable improvement in terms of GWP, the fuel cell aircraft still outclass the competition. This is especially true when wind energy is used to generate
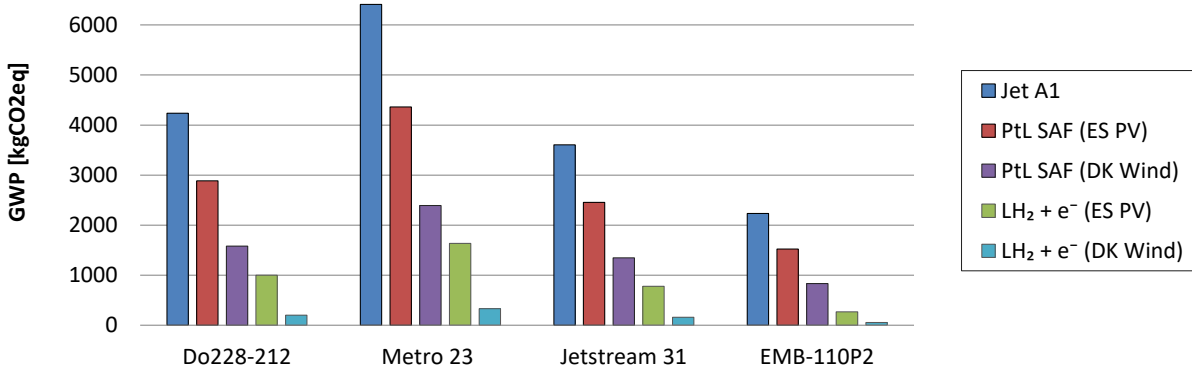
**Figure 5.7:** Nominal mission energy GWP estimation using conventional and fuel-cell commuter aircraft

the required electricity for electrolysis. Nevertheless, according to this analysis, the difference in GWP between utilising SAF obtained using wind energy and liquid hydrogen obtained using solar power is smaller than the difference between the two liquid hydrogen options in most cases. Thus, it can be concluded that the choice of electrical power generation is a major factor in the total GWP even when both sources are renewable. Still, even when using less favourable PV energy generation, the fuel cell aircraft perform better than any presented SAF solution.

In concrete terms, when using PV electrical power, the fuel cell aircraft produce between 73% and 88% less GWP than aircraft using Jet-A1 and between 61% and 82% less GWP than aircraft using SAF. When switching to wind-generated power, these numbers become 95% to 98% when compared to Jet-A1 and 86% to 93% when compared to SAF. For more detailed information the reader is advised to consult Table C.2 under the supplementary material in Appendix C for the complete set of energy GWP estimates for all aircraft.

### 5.4.3. Cost Analysis

Although aircraft energy use and efficiency are great metrics to compare the performance of aircraft, aircraft operators are likely to be more preoccupied with the potential cost implications of powering novel aircraft. Thus, the following paragraphs will examine the total trip energy cost and the aircraft cost efficiency, including the cost for emissions allowances.

**Trip Energy Cost**

By combining the energy figures presented in Table 5.6 and the cost estimates for different energy carriers presented in Table 4.8, the trip energy costs can now be obtained. Figure 5.8 illustrates the nominal mission trip energy cost estimates for all four aircraft.

The solid bars on the figure represent the cost estimate using the 'base' price for energy carriers from Table 4.8. The 'Low' and 'High' estimates from that table are used to construct the confidence intervals, seen represented in Figure 5.8 with dark vertical lines on top of the bars. The cost estimates for the conventional aircraft include both, the regular Jet-A1 aircraft fuel, as well as the SAF alternative obtained using the PtL method. For fuel cell aircraft, the energy cost estimate includes both the liquid hydrogen, as well as the electricity to charge the batteries.

For the complete set of cost estimates for all aircraft, the reader is advised to consult Table C.1 under the supplementary material in Appendix C.

Looking at the figure it becomes clear that in all likelihood neither the fuel cell aircraft nor the SAF solution can outperform the conventional jet fuel in terms of trip energy cost. Nevertheless, it does appear that the fuel cell aircraft solution might have a slight edge over the SAF solution, despite the increased energy consumption of the larger fuel cell aircraft.

Neglecting the confidence intervals and only looking at the 'Base' price predictions, the trip energy cost for fuel cell aircraft is approximately 30% to 95% higher than that of conventional aircraft running on Jet-A1. Specifically, it is approximately 95% higher for the Metro 23, 90% higher for the Do 228, 80% higher for the Jetstream 31, and 30% higher for the EMB 110. The cost of conventional aircraft running on SAF appears even higher than that of fuel cell aircraft running on liquid hydrogen and electricity. Concretely, using a SAF aircraft appears to be 10%–40% more expensive than using fuel
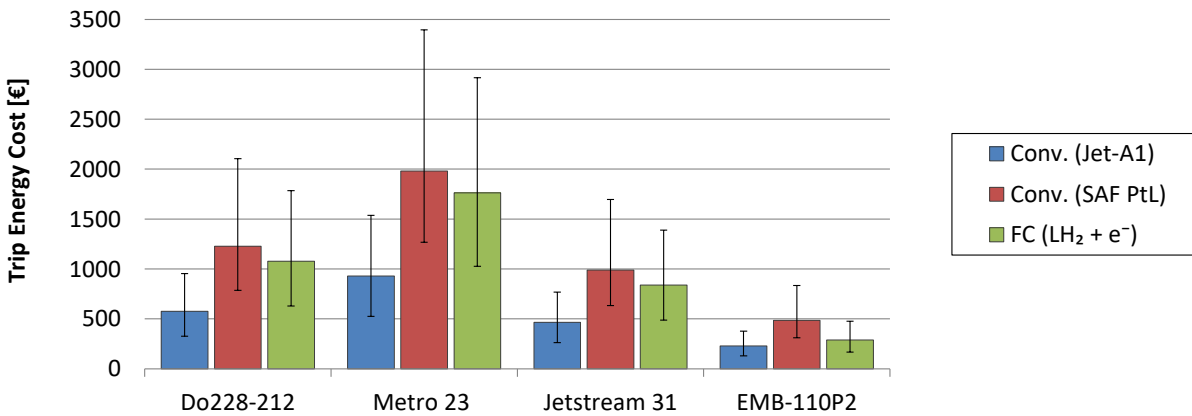
**Figure 5.8:** Mission energy cost estimation for the nominal mission in the year 2040 using conventional and fuel-cell commuter aircraft

cell aircraft. Ultimately, however, it has to be acknowledged that the confidence intervals for all three energy carrier solutions are large and making any concrete predictions about the financial viability of any of the presented options is difficult.

**Accounting for Emission Allowance Costs**

As mentioned in Section 4.4.2, the aircraft operator might incur additional costs when operating in countries or regions with an active emissions trading scheme. Since it is assumed that the aircraft operate within the EU, the costs of the emissions allowances had to be added on top of the baseline energy costs. Based on the costs presented in Figure 5.8, the GWP presented in Figure 5.7, and the assumptions made in Section 4.4.2, the combined energy costs and emissions allowance costs are presented in Figure 5.9
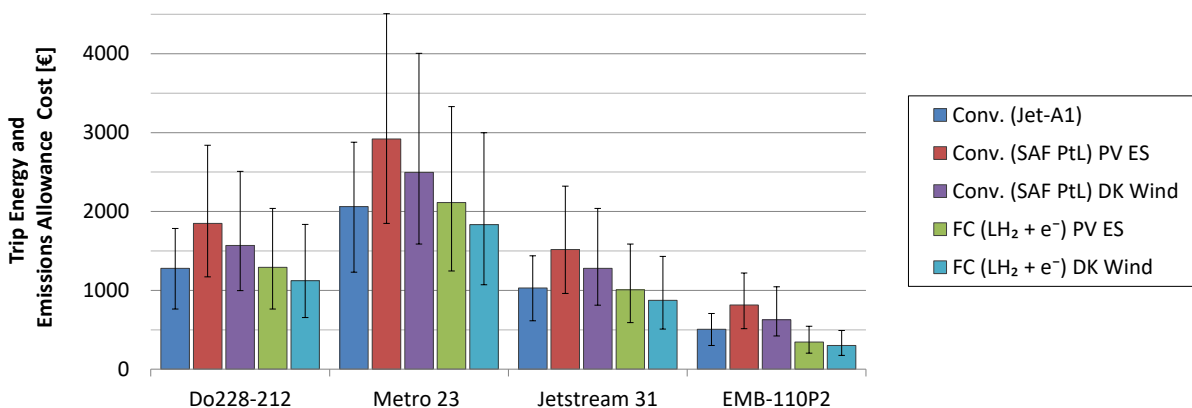


**Figure 5.9:** Combined mission energy cost and emissions allowance cost (purchased from ETS) estimation for the nominal mission in the year 2040 using conventional and fuel-cell commuter aircraft

As can be seen from the figure, applying the emission allowance costs to the default price presented in Section 4.4.2 changes the results substantially. While SAF is still the most expensive option, hydrogen has been made much more competitive. In fact, hydrogen appears to be financially as competitive as the Jet-A1. This is a very promising result for the overall viability of fuel cell aircraft.

**Payload-Range Cost Efficiency (PRCE)**

While the trip cost estimate presented above is an important metric to compare the fuel cell aircraft against their equivalent conventional counterpart, it is not well suited to compare different aircraft designs. Thus, similar to PREE, which is used to compare aircraft energy efficiencies, the payload-range cost efficiency or PRCE has been used to achieve a similar comparison with costs. Figure 5.10 illustrates the PRCE for all four aircraft types in kg·km/€. Note that the price estimates include the
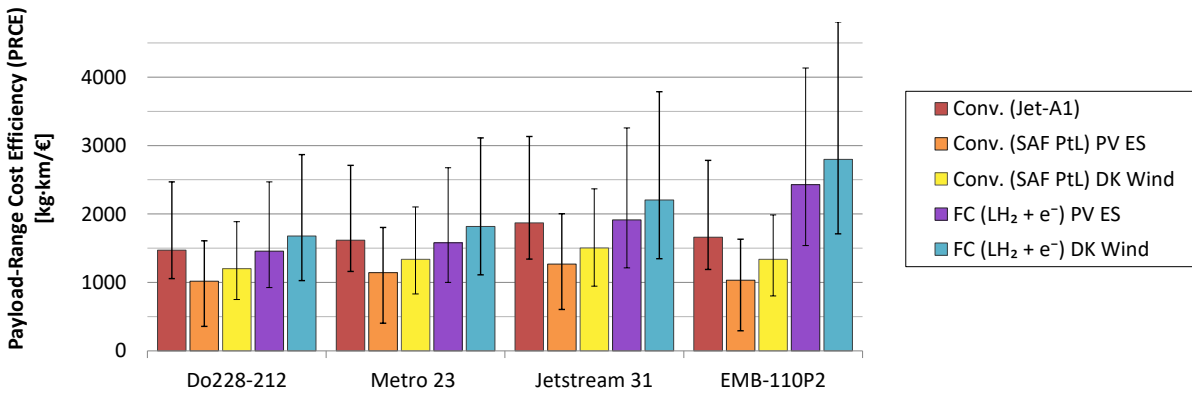
**Figure 5.10:** Mission payload-range cost efficiency for the nominal mission using conventional and fuel-cell commuter aircraft

emission allowances from the previous section. The confidence intervals have been computed in the same fashion as with the cost estimates in Figure 5.9.

Looking at the base price PRCE estimates, the conventional Jet-A1 option shows fairly consistent values of PRCE between 1500 and 1900 for all 4 aircraft. Similarly, the two hydrogen options perform just as well or even slightly better than the conventional Jet-A1 aircraft. Once again, however, the EMB 110 is somewhat of an outlier. The PRCE of hydrogen-powered EMB 110 is much higher than the conventional EMB 110. Nevertheless, this was to be expected, since the fuel-cell EMB 110 outperformed the conventional aircraft in terms of PREE by 40%.

# 5.5. Comparison with Maximum Payload Mission Sizing Results

A similar analysis to that of the fuel cell aircraft sized for the nominal mission will also be performed for the aircraft sized by the maximum payload mission. Nevertheless, since the maximum payload mission sizing was not the primary objective of this study, the results presented in this section will not be as detailed as for the nominal mission. Instead, they will mainly focus on the differences with respect to the fuel cell aircraft sized for the nominal mission, presented above.

## 5.5.1. Overall Aircraft Mass Results

Table 5.7 presents the OEM and MTOM results of the fuel cell aircraft sized by the maximum-payload mission. Besides the absolute mass values, the table also lists the relative mass increase with respect to the conventional aircraft and the relative mass difference compared to the fuel cell aircraft sized using the nominal mission requirements. These results can be found in columns $\Delta_{conv.}$ and $\Delta_{nom.\_fc}$, respectively.

Despite the increased payload requirements, the fuel cell aircraft sized for the maximum payload missions are lighter than their maximum passenger mission counterparts. The largest mass difference between the aircraft sized for the maximum payload and the aircraft sized for the nominal mission can be observed for the Dornier Do 228-212 and Fairchild Metro 23. These two aircraft also had much heavier cryogenic fuel tanks compared to the other two aircraft. Thus, it is unsurprising that lowering the mission range requirement had a very positive effect on lowering the aircraft mass by reducing the tank size and fuselage length.

In general, these results suggest that fuel cell aircraft experience increased sensitivity to the range requirements in comparison to conventional aircraft. When considering the conventional versions of the aircraft, both the nominal mission and the maximum payload mission requirements resulted in the same aircraft MTOM. When looking at the fuel cell aircraft, however, the MTOM for the maximum payload mission is lower than for the nominal mission. Therefore, while this payload-range trade-off between the two design missions is evenhanded for conventional aircraft, it appears that the range is more influential for fuel-cell commuter aircraft MTOM.

## 5.5.2. Mission Energy Use Results

The total mission energy and the payload range energy efficiency (PREE) for the fuel cell aircraft sized by the maximum-payload mission are listed in Table 5.8. Similarly to the mass results in Section 5.5.1,

**Table 5.7:** Preliminary sizing results for fuel cell commuter aircraft with maximum payload mission requirements

| | OEM | | | MTOM | | |
|---|---|---|---|---|---|---|
| | $[kg]$ | $\Delta_{conv.}$* | $\Delta_{nom.\_fc}$** | $[kg]$ | $\Delta_{conv.}$* | $\Delta_{nom.\_fc}$** |
| **Dornier Do 228-212 FC** | | | | | | |
| Class 2.5 | 7226 | +84.1% | -13.2% | 9264 | +41.9% | -9.4% |
| **Fairchild Metro 23 FC (2+1cab mod)*** | | | | | | |
| Class 2.5 | 8054 | +80.3% | -15.5% | 10540 | +38.2% | -9.1% |
| **BAE Jetstream 31 FC** | | | | | | |
| Class 2.5 | 8251 | +99.2% | -4.3% | 10221 | +54.7% | -2.5% |
| **Embraer EMB 110P2 FC** | | | | | | |
| Class 2.5 | 5874 | +60.3% | 0.0% | 7475 | +31.3% | -1.6% |

*Difference w.r.t. the Initiator results for conventional commuter aircraft sizing with equal design 'depth'.
**Difference w.r.t. the Initiator results for nominal mission fuel-cell commuter aircraft sizing with equal design 'depth'.
***Cabin widening to 2+1 seating configuration was required to limit overall fuselage length and allow for sizing convergence.

the table in this section also lists the relative change compared to the conventional aircraft, as well as the relative difference compared to the fuel cell aircraft sized using the nominal mission. Again, these results can be found in columns $\Delta_{conv.}$ and $\Delta_{nom.\_fc}$, respectively.

**Table 5.8:** Mission energy and efficiency results from fuel-cell commuter aircraft with maximum payload mission requirements

| | Total mission energy | | | Payload-range energy efficiency (PREE) | | |
|---|---|---|---|---|---|---|
| | $[GJ]$ | $\Delta_{conv.}$* | $\Delta_{nom.\_fc}$** | $[-]$ | $\Delta_{conv.}$* | $\Delta_{nom.\_fc}$** |
| **Dornier Do 228-212 FC**; Range: 800 km | | | | | | |
| Class 2.5 | 21.2 | -7.8% | -37.7% | 0.68 | +22.2% | +25.2% |
| **Fairchild Metro 23 FC (2+1cab mod)****; Range: 978 km | | | | | | |
| Class 2.5 | 23.7 | -11.8% | -57.5% | 1.38 | +49.4% | +71.5% |
| **BAE Jetstream 31 FC**; Range: 780 km | | | | | | |
| Class 2.5 | 17.1 | -8.4% | -36.8% | 1.11 | +14.1% | +17.3% |
| **Embraer EMB 110P2 FC**; Range: 440 km | | | | | | |
| Class 2.5 | 8.0 | -28.9% | -13.5% | 0.91 | +43.8% | +3.6% |

*Difference w.r.t. the Initiator results for conventional commuter aircraft sizing with equal design 'depth'.
**Difference w.r.t. the Initiator results for nominal mission fuel-cell commuter aircraft sizing with equal design 'depth'.
***Cabin widening to 2+1 seating configuration was required to limit overall fuselage length and allow for sizing convergence.

With a higher payload, but a shorter mission range, all 4 fuel cell aircraft outperformed conventional aircraft in terms of energy use. In fact, as can be seen from the table, the energy savings are considerable. While the EMB 110 aircraft already outperformed the conventional aircraft energy use in the nominal mission, the same was not true for the other three examples. When considering the PREE, the results for the Metro 23 are especially noteworthy. The fuel cell version of the aircraft shows an almost 50% increase in PREE compared to the conventional aircraft flying a maximum payload mission.

## 5.6. Sensitivity Analysis

Most of the presented results for the fuel cell aircraft so far indicated a noteworthy rise in aircraft mass and an increase in energy use compared to conventional aircraft. Thus, it becomes almost imperative to look for potential improvements in those metrics. While a full-fledged optimisation scheme would be a good way to pursue this goal, it falls outside of the scope of this project. However, a sensitivity analysis

can still give a good first impression of the potential mass and energy savings that future optimisation could bring.

Another important aspect of sensitivity analysis is to quantify the uncertainties in the models used to arrive at the results. Unfortunately, many of the sizing models used to obtain the results for fuel cell aircraft designs rely heavily on preliminary technology estimates and educated guesses. Furthermore, there are currently no flying commercial passenger fuel cell aircraft available to validate the complete sizing method. Therefore, a sensitivity analysis, such as the one presented in this section, is crucial in quantifying some of these uncertainties.

This section will present a sensitivity analysis of the fuel cell aircraft MTOM and the mission energy usage. These two indicators were chosen, as they can act as analogues for many other metrics. For instance, the aircraft purchase price, maintenance, and airport fees are strongly linked to the aircraft MTOM. Similarly, the energy use per mission correlates well with the per-hour flying cost and the environmental impact of aircraft operations.

The sensitivity analysis will be done by varying 12 different aircraft mission, powertrain, and airframe geometry parameters. The first 4 parameters are related to mission requirements and include the aircraft payload, cruise Mach number, mission range and cruise altitude. Additionally, the sensitivity to altitude was performed in two ways. Once by keeping a constant cruise true airspeed (TAS) and once by keeping a constant cruise Mach number. This brings the total number of varied mission parameters to 5.

The next 6 parameters relate to powertrain design. Specifically, the power degree of hybridisation (DoH), FC over-sizing parameter, FC inlet compression ratio, cryogenic tank venting pressure, battery-specific energy, and specific power of the electric propulsion motors. The battery-specific energy and propulsion motor-specific power parameters were selected for this sensitivity analysis because of the uncertainty in the current and near-future technology levels. The other 4 powertrain parameters were selected due to another uncertainty. Their initial or default values were based on existing research into this topic. However, it was unclear whether the initially selected values were optimal. Thus, the intention of including them in this sensitivity analysis was to find out whether more optimal values existed and to indicate what potential improvements to the aircraft design could be achieved by altering them.

The final parameter that will be investigated is the fuselage diameter. As one might recall, it was hypothesised that keeping the fuselage diameter equal to the one of the corresponding conventional aircraft resulted in a very large mass increase for the narrow Do 228-212 aircraft when equipped with a hydrogen tank. Thus, this sensitivity analysis will attempt to confirm and quantify this phenomenon.

Finally, it is important to note that all of the results in this section have been obtained using the Initiator aircraft sizing on the lowest, 'class 2' depth.

The sensitivity analysis results will be presented in 3 parts. First, the sensitivity to mission parameters will be outlined. Next, the sensitivity to powertrain design parameters will be discussed. Finally, the influence of the fuselage diameter on the aircraft sizing will be briefly explained. For the sake of brevity, not all 4 fuel cell aircraft will be included in every part. Instead, a single representative aircraft will be used to discuss the major trends that largely hold true for all 4 designs.

## 5.6.1. Sensitivity to Mission Parameters
The aircraft sizing sensitivity to mission parameters will use the BAE Jetstream 31 FC as a representative aircraft. The results for the other four aircraft are available in Appendix C. The mission parameters were varied in the range of $\pm 30\%$, with the input parameters and results obtained using the 19-passenger nominal design mission as the reference point.

**MTOM Sensitivity to Varying Mission Parameters**
The MTOM sensitivity to 5 mission parameters can be seen in Figure 5.11. Before discussing the rest of the results, the obvious anomalies should be addressed first. By observing the trends in the figure it appears that there is an abnormally large reduction in the MTOM when reducing the cruise Mach number beyond 15% and when reducing the cruise altitude beyond 20%. This anomaly is the result of the FCS heat exchanger model, which appears to be extremely sensitive to the Reynolds number of the airflow through the heat exchanger pipes. As discussed in Section 5.2.2, the jump in heat exchanger effectiveness and consequently also in heat exchanger mass happens due to the transition of the airflow through the pipes from turbulent to laminar or vice-versa. When varying the cruise Mach number or

cruise altitude for the Jetstream 31 FC, this flow transition threshold is crossed. Crossing the threshold results in a single, discrete jump in the aircraft MTOM. The Metro 23 and EMB 110 aircraft experience a similar MTOM discontinuity, as can be seen in Figure C.5 and Figure C.6, respectively. Since there is strong doubt about the validity of this model behaviour, the rest of the sensitivity analysis will not address its effects any further.
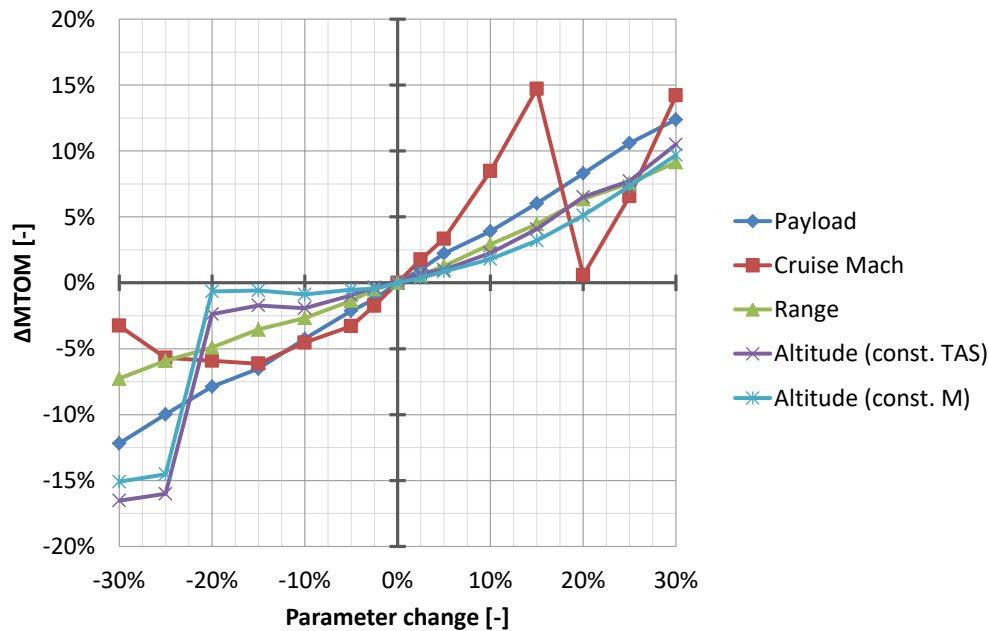


**Figure 5.11:** BAE Jetstream 31 FC MTOM sensitivity to mission parameters

Disregarding the sudden MTOM steps, the Jetstream 31 FC MTOM appears especially sensitive to the changes in cruise Mach number. According to the analysis, a 10% increase in cruise Mach would result in an 8.5% increase in MTOM. On the other hand, a 10% reduction in cruise Mach would result in a 4.5% reduction in MTOM. The very high dependency on cruise Mach number is shared with the rest of the aircraft in this study.

Another observation that can be made is that the Mach number displays a very clear minimum at around 15% requirement reduction. This minimum is created by opposing trends. One of the main culprits is the total aircraft drag. Since the FCS is sized by the cruise condition, lowering the cruise Mach number should lead to a reduced power requirement and consequently, reduced FCS mass. However, the aircraft drag is not only a function of velocity. An important factor determining the overall drag is also the aircraft drag coefficient. When reducing the cruise Mach number, the drag coefficient is actually increasing, since the wing is not as efficient at producing lift in those higher angle-of-attack regimes. In fact, the $C_D$ in the reference point is 0.0143, whereas, around the minimum MTOM point, the $C_D$ is already at 0.0275. Reducing the cruise M further, the $C_D$ reaches 0.0597 when the cruise Mach is reduced by 30%. Thus, the two opposing factors create a minimum point somewhere between the two extremes. For the Jetstream 31 FC, this point corresponds to the Mach number which is around 15% lower than the default value of 0.382.

The remainder of the mission parameters displays a slightly shallower trend than the Mach number, with the payload appearing to have the second-highest gradient around the centre of the plot. Somewhat interestingly, the changes in aircraft mission range do not seem to influence the aircraft MTOM as severely as expected. Reducing the range by 20%, e.g., results in a 5% reduction in MTOM, while increasing the range by 20% results in a 6.3% MTOM growth. In more concrete figures, the 20% range for the Jetstream 31 FC is just shy of 240 km and a 5% mass change is equivalent to approximately 520 kg. Nevertheless, for the Metro 23 and Do 228 aircraft, the two aircraft with heavier tanks, the opposite is true.

Finally, lowering the cruise altitude with either constant Mach or TAS would reduce the total MTOM, but the effects are much smaller than from the rest of the parameters. Increasing the altitude further, especially at constant TAS, would have a similar effect to increasing the aircraft range. While the effect

of altering the cruising altitude for the Jetstream 31 appear to be the least consequential out of all mission parameters analysed, the altitude change effects are even less pronounced for the other three aircraft in this study.

Overall, it appears that by slightly reducing the aircraft range, cruise Mach, and adjusting cruising altitude, a notable reduction in MTOM could likely be achieved without a large compromise in aircraft performance.

**Required Mission Energy Sensitivity to Varying Mission Parameters**
The mission (trip) energy sensitivity of the Jetstream 31 aircraft to 5 mission parameters can be seen in Figure 5.12. Since the aircraft MTOM is very strongly linked to aircraft energy use, similar characteristics to the ones observed in the MTOM sensitivity analysis were expected. Thus, the discussion of aircraft energy use sensitivity will mostly revolve around illuminating any differences in trends with respect to the previously discussed MTOM sensitivity. Note, however, that the y-axis on the Figure 5.12 plot is twice as large as it was in Figure 5.11.
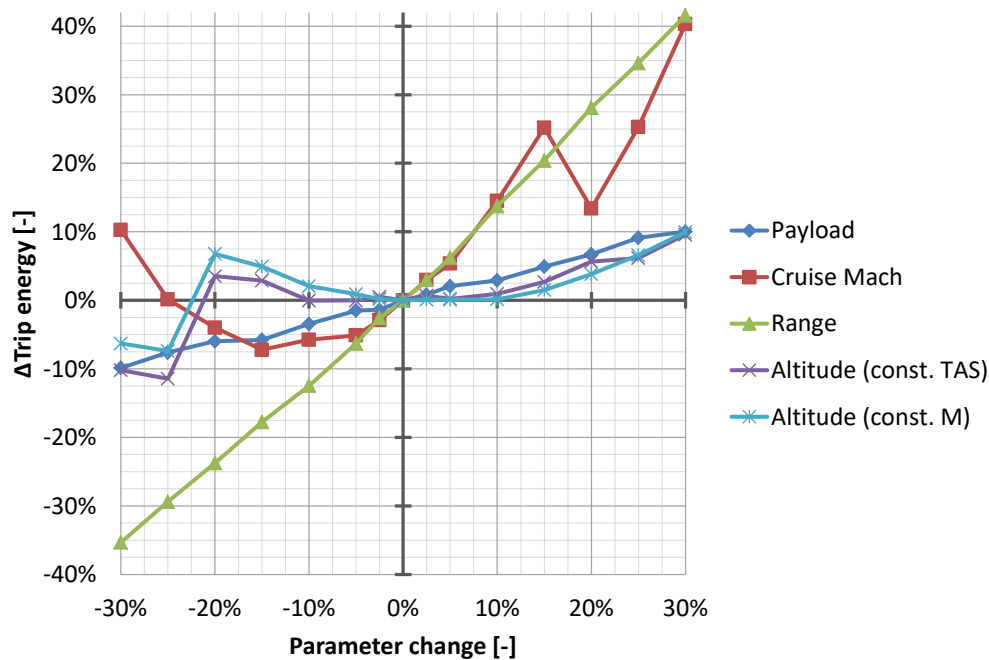


**Figure 5.12:** BAE Jetstream 31 FC mission energy sensitivity to mission parameters

The Mach number appears very influential on the aircraft energy use, just as it was for the aircraft MTOM. Predictably, however, varying the range exhibits a much stronger influence on the sensitivity than it did for MTOM. To illustrate, a 20% reduction in range resulted in approximately a 5% decrease in MTOM and a 24% decrease in energy use. In fact, the influence of range now matches that of the Mach number around the reference point. This is not only true for the Jetstream 31, but for all four aircraft in this study. Observing the payload influence, one can notice that its impact on energy use is somewhat smaller than it was on the aircraft MTOM. Finally, while it was previously seen that reducing the cruise altitude would reduce the aircraft's MTOM, the same cannot be said for the aircraft's energy usage. It appears that the reference altitude is already close to the optimum in terms of aircraft energy usage for the Jetstream 31. For the rest of the aircraft, however, a reduction of altitude would actually increase energy usage. Conversely, increasing the altitude would improve energy consumption.

## 5.6.2. Sensitivity to Powertrain Parameters
Just as the sensitivity analysis to mission parameters, the aircraft sizing sensitivity analysis to powertrain parameters will use the BAE Jetstream 31 FC as a representative aircraft. Similarly to the mission parameters, the 19-passenger nominal design mission will serve as the reference point. Unlike the mission parameters, however, varying the powertrain parameters was slightly less straightforward.

Generally speaking, the powertrain parameters were also varied in the range of $\pm30\%$. However, as will become clear from the figures, it was not possible to obtain the results in that range for all 5 parameters. This was either due to convergence issues or due to the very nature of the varied parameters. To clarify, the following paragraphs will explain the particularities of all 6 powertrain parameters.

Starting with the power hybridisation, the reference point was set to 50% power hybridisation for take-off, maximum climb gradient and all OEI requirements. For the remaining climb segments, the hybridisation was 25%. The cruise and descent segments were set to 0% hybridisation. This is in accordance with the powertrain configuration described in Section 4.3.1. When the hybridisation parameter was varied in the sensitivity analysis, the 'Parameter change' percentage was added or subtracted from the original hybridisation value. In the case of the 25% hybridisation for the regular climb segments, the 'Parameter change' value would be halved. For example, a -10% change to hybridisation would translate into 40% hybridisation (down from 50%) for take-off, maximum climb gradient and all OEI requirements. For other climb segments, the change would be halved and thus, -10% would lead to 20% hybridisation (down from 25%). No results could be obtained beyond +20% hybridisation due to convergence issues. Importantly, while reducing the hybridisation beyond -10% would not cause convergence issues, it could violate some of the FCS model assumptions. Most notably, the assumption that FCS is sized for cruise conditions is no longer true. Thus, more analysis is required to determine whether these results are valid.

Next, the default fuel-cell (FC) over-sizing factor was set to 10%, as in the rest of the results. To vary this parameter, the change in percentage was simply added or subtracted from the default value. Since it is impossible to satisfy the power requirements by under-sizing the FC, no results could be obtained below -10% change to this parameter.

The remainder of the parameters, namely the FC inlet compression ratio, hydrogen tank venting pressure, battery-specific energy, and propulsive electric motor-specific power could be varied without any special considerations. As a reminder, the default sizing was done with the FC inlet compression ratio set to provide sea level pressure at cruise altitude, a tank venting pressure of 250 kPa, a battery pack energy density of 260 Wh/kg, and an electric motor power density of 5795 W/kg.

### MTOM Sensitivity to Varying Powertrain Parameters

The MTOM sensitivity to the 6 powertrain design parameters for the Jetstream 31 is illustrated in Figure 5.13. It can be seen that increasing any of the examined powertrain parameters, apart from the hybridisation, results in a reduction of the aircraft MTOM. The two most influential parameters appear to be battery-specific energy and hybridisation. Both of these parameters are directly connected to the mass of the battery pack. Given the large battery mass that was presented in Section 5.2.2, the large sensitivity of the MTOM to battery mass parameters is not surprising. On the other hand, the electric propulsion motor-specific power, venting pressure, and the FC inlet compression ratio appear to have a smaller influence on the aircraft MTOM. Still, their importance is far from negligible.

The rest of the aircraft included in this study exhibit similar trends with one notable exception. The two aircraft with the heaviest tanks, the Do 228 and Metro 23, are most sensitive to the tank venting pressure. In fact, for both aircraft, increasing the tank venting pressure by 30% would reduce the MTOM by more than 10%, as displayed in Figure C.7 and Figure C.8.

Importantly, while battery and electric motor specific power are constrained by the available technology, the rest of the parameters are not. In fact, the MTOM benefits that could be brought about by increasing the compressor compression ratio, increasing the FC stack over-sizing, or reducing the hybridisation would not impact the aircraft mission capabilities. Thus, this indicates that there are potentially sizeable mass savings in simply updating some powertrain design variables.

### Required Mission Energy Sensitivity to Varying Powertrain Parameters

As was already mentioned in the mission energy sensitivity with respect to mission parameters, the aircraft MTOM has a large influence on the aircraft energy usage. Thus, the focus of this energy sensitivity analysis will be to identify the parameters that also influence energy consumption more directly than through the aircraft mass. The required mission energy versus the powertrain parameter change for the Jetstream 31 can be seen in Figure 5.14.

As anticipated, increasing FC over-sizing has additional benefits to energy usage, beyond just the reduction in aircraft mass. By lowering the required cell power density, the fuel-cell efficiency can be increased. This in turn reduces the energy consumption of the FCS. The opposite is true for hybridisation. While the analysis has shown that reducing the hybridisation has the potential of notably reducing
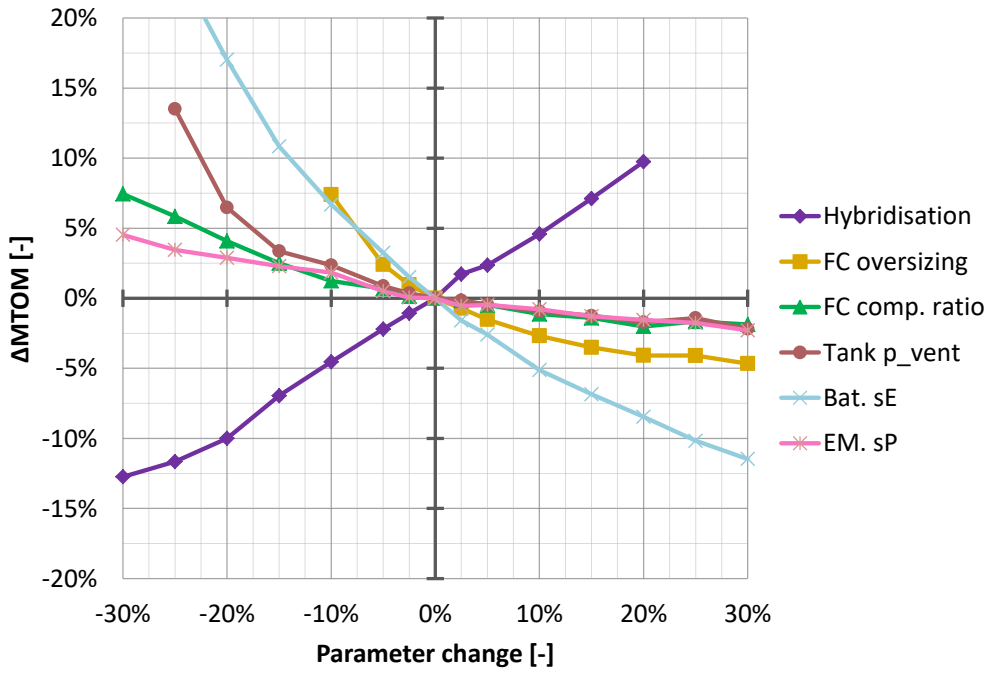
**Figure 5.13:** BAE Jetstream 31 FC MTOM sensitivity to powertrain parameters
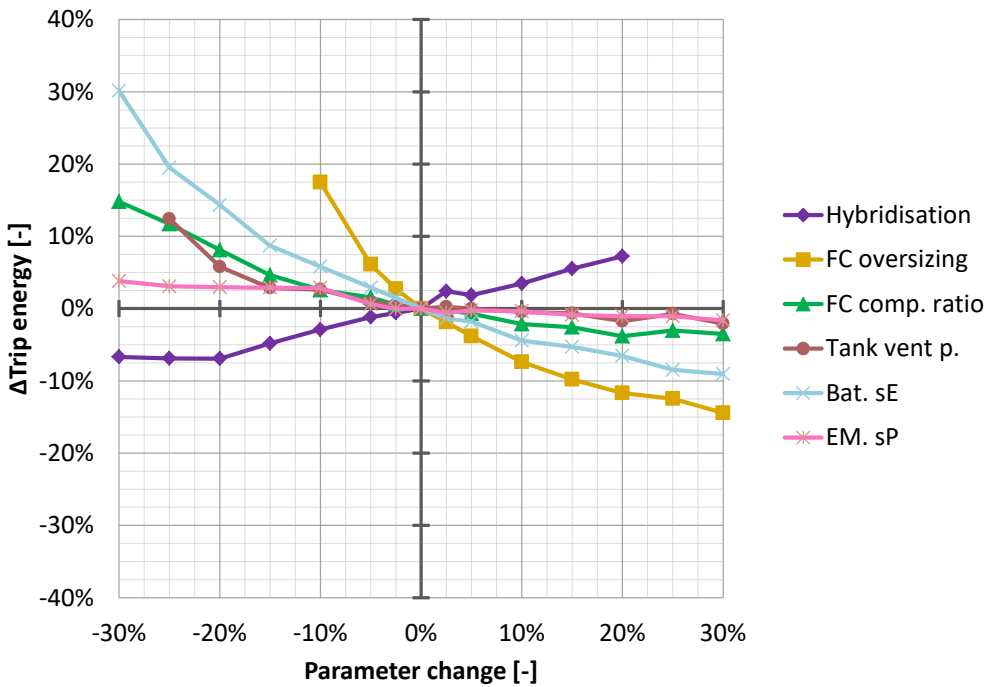


**Figure 5.14:** BAE Jetstream 31 FC mission energy sensitivity to powertrain parameters

the aircraft MTOM, the energy use would not decrease as much. This can be explained by the simple fact that the electric power path from the battery pack to the propulsion motor is more efficient than the FCS path. Thus, reducing the total energy contribution of the battery has the unintended effect of slightly reducing the overall powertrain efficiency.

### 5.6.3. Sensitivity to Fuselage Diameter
In this final part of the sensitivity analysis, the influence of the fuselage diameter on the fuel cell aircraft results will be examined. The fuel cell aircraft selected for this analysis was the Dornier Do 228-212.

As one might recall, this is the only fuel cell aircraft that retained its 1+1 seating layout, after the Metro 23 had to be modified to 2+1 seating to allow for aircraft convergence. Throughout the analysis of the results, it was hinted that the narrow fuselage of the fuel-cell Do 228 was causing a disproportional mass and size increase due to the inefficient shape of the cryogenic tank. Thus, to investigate this hypothesis, this section will redesign the Do 228 by increasing the fuselage diameter and modifying the cabin seating layout.

Two modified versions of the fuel-cell Do 228 were examined. In the first version, the seating layout was raised to 2+1 seats per row, increasing the fuselage diameter from 1.82 to 2.05 m. In the second conversion, the number of seats per row was increased further to 2+2, resulting in a fuselage diameter of 2.47 m. No other design parameters were modified. It is worth mentioning, however, that many of the design parameters are directly proportional to the fuselage length or diameter. For instance, the nose-ad tail-cone lengths are sized relative o the fuselage diameter. Thus, by not changing the cone-length parameter, the length of both cones will nevertheless increase due to the increased fuselage diameter.

The sizing results for the original aircraft and the two redesigned aircraft can be seen in Table 5.9. Additionally, a graphical size comparison between the original aircraft and the resigned aircraft can be seen in Figure 5.15.

**Table 5.9:** Sensitivity of sizing results to changes in fuselage diameter for the Do 228-212 FC aircraft

| Seating | Fuselage diameter | Aircraft length | MTOM | OEM | Trip energy | Cryo. tank mass | Total fuel mass | Tank mass efficiency |
|---|---|---|---|---|---|---|---|---|
| [-] | [m] | [m] | [kg] | [kg] | [GJ] | [kg] | [kg] | [-] |
| **1+1 (original)** | 1.82 | 23.98 | 10153 | 8250 | 33.87 | 364.7 | 286.4 | 44.0% |
| **2+1** | 2.05 | 19.73 | 9115 | 7237 | 31.15 | 230.1 | 263.0 | 53.3% |
| **Diff.** | +12.6% | -17.7% | -10.2% | -12.3% | -8.0% | -36.9% | -8.2% | +21.1% |
| **2+2** | 2.47 | 19.51 | 9315 | 7422 | 32.60 | 195.4 | 274.9 | 58.5% |
| **Diff.** | +35.7% | -18.6% | -8.3% | -10.0% | -3.7% | -46.4% | -5.6% | +33.0% |



**(a)** Above: 2+1; Below: 1+1                                    **(b)** Above: 2+2; Below: 1+1
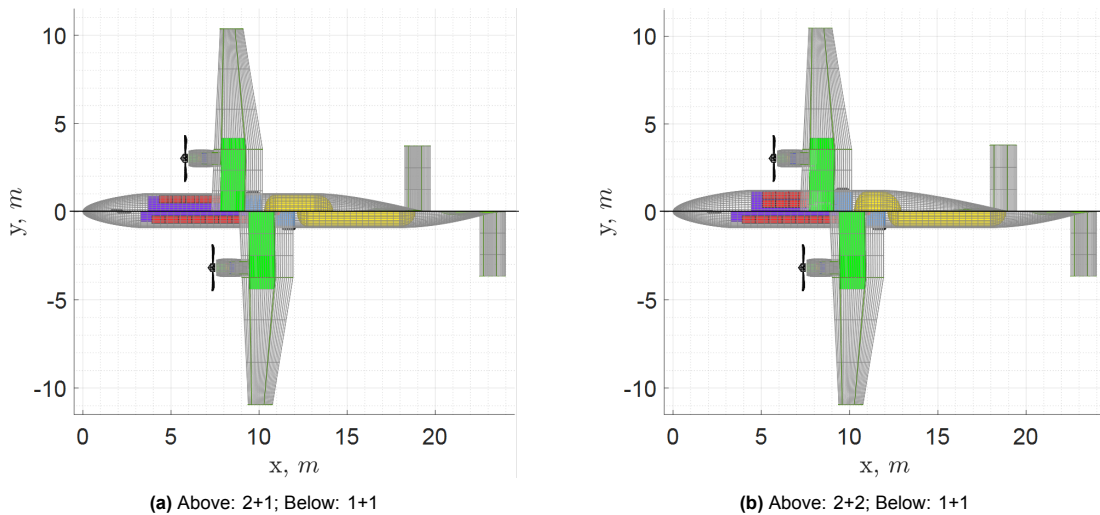
**Figure 5.15:** Size comparison between different cabin seating configurations in the Do 228-212 FC aircraft sized for a nominal mission. All sizing was performed with Initiator class 2 'depth'.

What is immediately obvious is that the redesigned aircraft are much shorter than the original, as was expected. Furthermore, the OEM and MTOM of the modified aircraft are substantially lower than for the original. Additionally, the aircraft energy use and all the metrics connected to hydrogen storage have been improved. However, the results obtained with the 2+1 seating arrangement are notably better than the ones obtained with the 2+2 arrangement. This indicates that the 2+1 seating is the optimum configuration for this particular aircraft.

As hypothesised, the slender and heavy cryogenic tank was indeed very detrimental to the aircraft's mass and performance. By increasing the fuselage diameter from 1.82 m to 2.05 m, the gravimetric tank efficiency increased from 44.0 to 53.3%. Widening the fuselage further, to 2.47 m, resulted in an even better tank gravimetric efficiency of 58.5%. This improvement is illustrated in Figure 5.16, where it can be seen how the increased fuselage diameter allows for a reduced total tank wall area. Not only did the fuselage diameter improve the tank mass and efficiency, but it also drastically reduced the required length of the aircraft. In both cases, the aircraft length decreased by over 4 m, reducing the mass of the aircraft structure in the process.



**(a)** 1+1 seating, diameter: 1.82 m



**(b)** 2+1 seating, diameter: 2.05 m



**(c)** 2+2 seating, diameter: 2.47 m
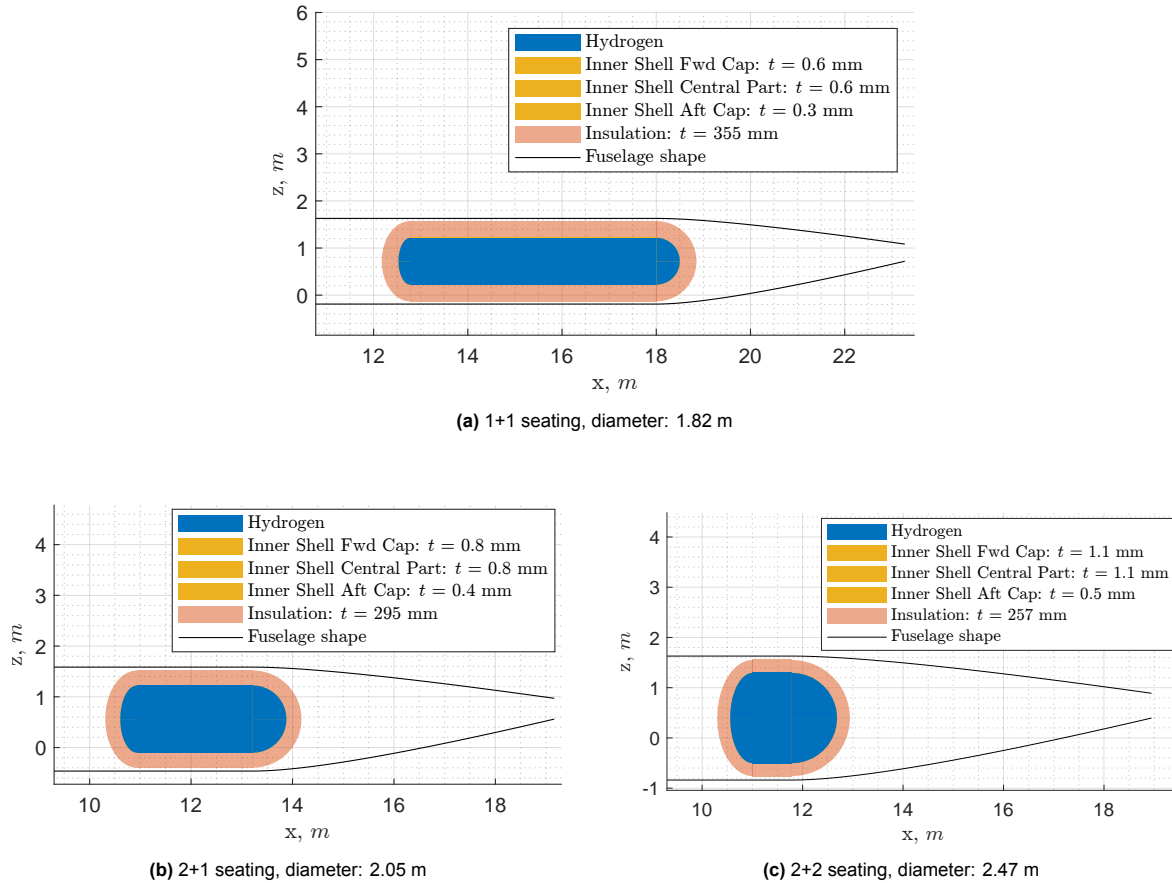
**Figure 5.16:** Cryogenic tank side view comparison for different cabin seating configurations in the Do 228-212 FC aircraft sized for a nominal mission. All sizing was performed with Initiator class 2 'depth'.

Overall, these individual improvement snowball to create a much lighter and more efficient aircraft. The MTOMs of the redesigned fuel-cell Do 228 aircraft are only between 43.1% and 46.2% higher than that of the conventional Do 228 aircraft. In contrast, the original fuel-cell Do 228 aircraft has a 59.4% higher MTOM than the conventional aircraft. Furthermore, the 2+1 seating reduced the energy consumption of the original fuel-cell Do 228 by 8%, which translates into roughly the same reduction in trip energy cost and the trip energy GWP.

<div style="text-align: right; font-size: 4em;">6</div>

# Discussion and Recommendations for Future Work

After reviewing the methodology and results in the previous two chapters, this chapter will be used to provide a critical reflection on the significance of the presented results and the quality of employed methods. First, the research questions set at the beginning of this report will be answered in Section 6.1. Next, the general observations concerning the viability of fuel-cell commuter aircraft will be explored in Section 6.2. After that, in Section 6.3, the limitations in the methodology used for this study will be listed. Finally, the chapter will conclude with Section 6.4 where a few recommendations for future work on this topic will be given.

## 6.1. Answering the Research Questions

When setting up the research objectives at the beginning of this report, three main research questions were posed. Additionally, each question contained sub-questions. This section will attempt to provide answers to all the questions and sub-questions.

**RQ-1** *How does the addition of the hybrid fuel-cell powertrain influence the aircraft conceptual design process?*

**[RQ-1.1]** Overall, the conceptual design of hybrid fuel cell aircraft was notably more complex than the conceptual design of conventional aircraft. As discussed in Section 3.3, the hybrid fuel-cell powertrain needed a separate design point for every major component in the powertrain due to the multiple power paths present in the system. Furthermore, unlike for conventional aircraft, the mission analysis had to be interwoven directly into the initial class 1 aircraft sizing loop. Thus, instead of simply constructing a statistical regression curve to determine the aircraft OEM, the mission energy analysis was required to determine the masses of certain components in the OEM, such as the battery. Moreover, the precise power split between the battery and FCS had to be specified for every phase of the flight. This information was crucial to perform a mission analysis that could be used to size the battery and the FCS.

**[RQ-1.2]** As already alluded to above, there are some additional conceptual design loops required when sizing hybrid hydrogen fuel cell aircraft. However, these additional loops are mostly smaller and buried inside other, larger iteration loops. In fact, the most top-level schematic of the entire design process, as the one that was shown in Figure 3.2, would hardly be any different if it was depicting a design process for a conventional aircraft. Instead, the additional design loops are nested inside the individual module blocks.

The iterative mission energy analysis is a good example of one such nested loop. It is located inside the hybrid class 1 design module and is required to iteratively determine the aircraft battery mass and the aircraft OEM. Another good example of a nested conceptual design loop not present in the conceptual sizing of conventional aircraft is in the iterative FCS sizing. The fuel-cell stack has to produce enough power to propel the aircraft, as well as drive its own

BoP systems. However, the power drawn from the BoP systems is proportional to the power of the fuel-cell stack and thus, the sizing of the FCS has to be done iteratively.

**[RQ-1.3]** The conceptual design process of hybrid fuel cell aircraft also required more iterations to achieve convergence. This was best illustrated in Figure 5.2, where the discrepancy between the number of iterations required for convergence of the conventional aircraft was compared against the iterations required for the fuel cell aircraft. Although the sample size of 4 aircraft was relatively small to answer the question definitively, it nevertheless suggested that the fuel cell aircraft on average require more iterations to achieve convergence than their conventional counterparts.

On average, using the class 2 level Initiator 'depth', the number of iterations approximately doubled from 5 to 10 when running the design convergence for hybrid fuel-cell commuter aircraft. However, this increase was largely caused by only one of the four aircraft – the BAE Jetstream 31. Nevertheless, when considering more detailed aircraft mass estimations of class 2.5 and class 2.5 & HSE Initiator 'depths', the number of iterations for hybrid fuel cell aircraft was notably larger across all 4 aircraft. The average number of iterations required when using either the class 2.5 or class 2.5 & HSE 'depth' rose from 10 to 20 iterations.

In summary, introducing a hybrid fuel-cell powertrain makes the conceptual design process notably more complex, with some additional design loops, and a longer convergence time.

**RQ-2** *How does the performance of a hybrid hydrogen fuel cell powered commuter aircraft differ from that of aircraft featuring a conventional powertrain?*

**[RQ-2.1]** The MTOM of all 4 different hybrid fuel-cell commuter aircraft considered in this study has increased greatly compared to the conventional aircraft with identical TLARs. In concrete terms, when sizing the hybrid fuel cell aircraft for the nominal 19-passenger mission, the MTOM increased by approximately 60% for the first three aircraft and by 30% for the remaining one. When sizing the aircraft for the harmonic mission, the fuel-cell commuter aircraft MTOM was between 30% and 55% higher than for a conventional aircraft with the same TLARs.

**[RQ-2.2]** The increase in MTOM translated into a slight total energy penalty when flying a nominal 19-passenger mission with a fuel cell aircraft. The aircraft energy use in this case was defined as the amount of energy stored in the fuel and/or batteries, that the aircraft consumes when performing the flight from the origin airport to the destination airport, without diverting or loitering. When the fuel cell aircraft considered in this research were sized for the nominal 19-passenger missions, the total energy required to perform a flight to their destination was between 1.4% and 4.5% worse than for their conventional aircraft counterparts. An exception to this was the fourth aircraft, the Embraer EMB 110P2 whose energy efficiency improved by 41.2% compared to the conventional aircraft. When sized for the harmonic mission, all fuel cell aircraft experienced a drastic increase in energy efficiency compared to conventional commuter aircraft. This efficiency advantage ranged from 38.1% to 70.5%.

To provide a more rounded answer to the question of energy usage performance it might also be worth looking at the efficiency of the main power generators in the powertrain. Using the HHV of hydrogen the net efficiency of the FCS in the fuel cell aircraft ranged from 35% to 37%, regardless of the design mission. In comparison, the conventional turbine engines that power the original aircraft exhibited a net efficiency of approximately 23% (using the LHV of Jet-A1).

**[RQ-2.3]** When it comes to mission cost performance it was assumed that the main difference in mission cost between the conventional aircraft and the hybrid fuel cell aircraft would come from the cost of the required energy and any emission-related costs. Thus, the first part of this answer considers solely the purchase cost of the energy used by the aircraft to fly to the destination. The second part of this answer adds the emission costs based on projections for the EU's ETS allowance costs on top of the energy purchase costs. The energy cost comparison in this answer was done assuming green liquefied hydrogen and electricity for the hybrid fuel cell aircraft. For conventional aircraft, two fuel options were considered. These were the regular

Jet-A1 fuel and the SAF produced with the PtL method using renewable solar or wind electricity. All projections were for the year 2040.

When sizing the fuel cell aircraft for the nominal mission, the cost of energy for the first three aircraft was between 80% and 90% higher than for conventional aircraft. The EMB 110P2, however, experienced a price increase of only around 30%. When the emission allowances were factored in, it was shown that the hydrogen and electricity solution was on par with the conventional fuel. Finally, SAF PtL fuel was the most expensive approach, regardless of whether emission allowances were factored in.

**[RQ-2.4]** Similarly to the cost estimates, it was assumed that the majority of the environmental impact difference between the fuel-cell solution and conventional aircraft came from the LCA of the energy or energy carrier. The difference was quantified using the GWP metric. Similarly to energy cost, the GWP comparison in this answer was done assuming green liquefied hydrogen and renewable electricity for the hybrid fuel cell aircraft. For conventional aircraft, two fuel options were considered again. These were the regular Jet-A1 fuel and the SAF produced with the PtL method using renewable solar or wind electricity. Additionally, the same distinction between renewable solar or wind electricity was also applied to green hydrogen production in this case.

Compared to conventional aircraft powered by Jet-A1, the fuel cell aircraft with solar power hydrogen performed between 76% and 88% better in terms of energy LCA. When hydrogen was produced using wind power, the fuel cell aircraft perform between 94% and 98% better in terms of energy LCA. In contrast, conventional aircraft using PtI SAF obtained from solar and wind power performed only 32% and 63% better than Jet-A1, respectively.

Overall, fuel cell aircraft have a higher MTOM than their conventional counterparts. Nevertheless, they exhibit a higher net powertrain efficiency and thus require a similar amount of energy for the mission as conventional aircraft. Additionally, the fuel cell aircraft energy costs are higher than for conventional aircraft. However, future EU emission allowance prices were projected to make up for the cost difference. Finally, the fuel cell aircraft running on green hydrogen cut energy emissions by 76% or more.

Some important notes have to be added to the provided answers. The first important consideration here is that the hybrid fuel cell aircraft designs have not been optimised. Therefore, their MTOM, energy use, environmental impact, and mission energy cost could be reduced considerably, even with a relatively non-sophisticated optimisation. The evidence for this can be seen in the sensitivity analysis presented in Section 5.6.

The second note to the answers above concerns the mission payload-range envelope. Unfortunately, to perform a truly unbiased aircraft performance comparison of the two powertrain solutions and the corresponding aircraft designs, the mission capabilities of the two aircraft across the entire payload-range envelope should be identical. However, as discussed in Section 4.3.2, because of the inherent differences in the typical payload-range envelope between the two powertrain solutions, such a comparison was impossible. If a hydrogen-powered aircraft was sized such that its payload-range envelope fully enclosed that of a conventional aircraft, then there would be regions in the envelope of the hydrogen aircraft that were out of reach for the conventional aircraft. This would make the comparison biased again but in the other direction.

**RQ-3** *Which design parameters are the hybrid fuel-cell commuter aircraft designs most sensitive to?*

The sensitivity studies upon which the answers to this question were based examined the effect of 4 different mission parameters and 6 different powertrain technology parameters. The mission parameters were the aircraft payload, range, cruise Mach number, and altitude, whereas the powertrain parameters were the aircraft degree of power hybridisation, the fuel-cell stack oversizing, fuel-cell inlet compression ratio, venting pressure of the cryogenic hydrogen tank, battery pack specific energy, and electric propulsion motor specific power. Thus, any conclusions should be prefaced with the note that other parameters were not considered. An avid reader might remember that there was one more parameter included in the sensitivity study. Concretely, the effects of changing the fuselage diameter were shown for one aircraft. However, while the fuselage diameter is a very important consideration in designing an efficient fuel cell aircraft, the

observations made when varying the fuselage diameter were harder to compare to the rest of the parameters in the sensitivity analysis. This was mainly because the diameter of the fuselage changed the seating configuration in a discrete manner. Thus, the results of the diameter change were discontinuous and very sparse. Hence, the sensitivity to fuselage diameter is omitted here.

**[RQ-3.1]** Starting with the MTOM sensitivity, out of the 4 considered mission parameters, the MTOM was shown to be the most sensitive to the cruise Mach number for all 4 fuel cell aircraft sized for the nominal 19-passenger mission. The second most crucial parameter differed between the 4 fuel cell aircraft. For the Do 228 and Metro 23, it was the range, and for the Jetstream 31 and EMB 110, it was the payload. While not inconsequential, the cruising altitude was still the least critical parameter determining the MTOM for all four aircraft in this study.

**[RQ-3.2]** When considering the MTOM sensitivity to powertrain parameters there was no consensus for the most influential parameter between all four aircraft. Instead, for the Do 228 and Metro 23, the tank venting pressure was the most important, just ahead of hybridisation. For the EMB 110, the power degree of hybridisation took the top spot, whereas, for the Jetstream 31 aircraft, the influence of hybridisation was overtaken slightly by the battery-specific energy. Overall, the hybridisation percentage and battery specific power consistently presented a high influence over MTOM for all four aircraft. Besides these parameters, it was also found that changing the fuel-cell over-sizing appeared to have a very strong effect on the aircraft MTOM for all aircraft. This was especially notable when the over-sizing parameter was lowered from the default 10% to 0, producing a strong MTOM spike between 3.4% and 8.9%. Finally, the fuel-cell inlet compression ratio and the electromotor-specific power had a similarly small, but not insignificant effect on the aircraft MTOM.

**[RQ-3.3]** Similarly to the aircraft MTOM, the most critical mission parameter for the aircraft energy use was again the cruise Mach number. However, unlike for the MTOM, the changes in the range were equally consequential when considering energy use. Other mission parameters had a notably smaller impact than the first two. The impact of cruising altitude was very different between the four aircraft, both in magnitude, as well as in the shape of the trend. For example, increasing the altitude reduced the energy use for the Do 228 and Metro 23. The trend for these two aircraft appeared to be very linear. In both cases, a 30% change in altitude (constant TAS) would result in about a 10% change in energy usage. When considering the EMB 110, however, increasing the altitude only had a marginal effect on the energy use reduction. Finally, for the Jetstream 31, the minimum energy use seemed to be exactly at the original cruise altitude of 7620 m.

**[RQ-3.4]** When observing the sensitivity of aircraft energy consumption to powertrain parameters there was a clear consensus among all four aircraft. The fuel-cell over-sizing percentage was the most influential parameter. There was a notable trend indicating that increasing FC over-sizing reduces the aircraft energy usage while lowering the over-sizing resulted in the opposite. The rest of the parameters generally exhibited a much weaker influence on the total energy usage than the fuel-cell over-sizing, with the hybridisation, tank venting pressure, and battery specific energy parameters trailing the fuel-cell over-sizing most closely.

In summary, the aircraft MTOM was in general most affected by the cruise Mach number, hybridisation percentage, and battery specific energy. The hybrid tank venting pressure was very important for MTOM of the Do 228 and Metro 23, while fairly insignificant to the other two aircraft. Similarly to MTOM, the aircraft energy consumption generally exhibited the largest sensitivity to the aircraft cruise Mach number. However, the aircraft range became equally important when considering energy consumption.

## 6.2. Viability of Hydrogen Fuel-Cell Aircraft

As already discussed when posing the research goals at the beginning of this report, the term *viability* represents more than just the ability of humans to create airworthy hybrid-fuel cell aircraft. Instead, the goal of this study was to examine the viability of these hydrogen commuter aircraft in both, the engineering sense, as well as in the financial and environmental sense.

Naturally, with such broad criteria for viability, it would be hard to declare hybrid fuel-cell-powered

commuter aircraft either viable or non-viable with a high degree of certainty. The complexity of this question ensures that it can only be definitively answered once these aircraft actually attempt to make their way into the commercial aviation sphere. However, there are some promising and some less promising indicators regarding the eventual adoption of this technology that can be derived from this study and give some pointers to what the final answer may be. First, the generalised observations from all 4 aircraft platforms examined will be given. Next, this section will attempt to comment on the differences between different aircraft in this study, especially why the EMB 110P2 performed so much better as a fuel cell aircraft than the rest.

### 6.2.1. General Observations

Beginning with the negative aspects of the fuel-cell commuter aircraft technology, one can immediately point to the increased aircraft MTOM and OEM that were shown for all four aircraft. This mass increase is definitely not favourable, since aircraft mass and size are usually closely related to the aircraft purchase cost, airport fees, and maintenance costs. The high MTOM might also pose challenges in certification since the current CS-23 regulation limits the aircraft weight to 8618 kg. Similarly, it was shown that the baseline cost of fuel cell aircraft energy is higher than for conventional aircraft when green hydrogen is used. However, it was also shown that when emission allowances are factored in, the fuel-cell solution performs equally in terms of mission energy cost for the operator. Another drawback of flying using hydrogen is the reduced payload-range envelope which translates into lower mission flexibility, as was described in Section 4.3.2. Nevertheless, as Stoll and Mikic [113] point out, most commuter aircraft are over-designed compared to the range they are mostly found operating in. In fact, they claim that the largest commuter aircraft operator in the United States does not operate flights beyond 420 km. Thus, while not ideal, the lower mission flexibility might not be as crucial for the potential operators as one might be led to believe.

Despite the aforementioned drawbacks of the fuel-cell commuter aircraft, there are some important benefits that should not be overlooked. By far the most promising are the results concerning the reduction in environmental impacts of hydrogen fuel cell aircraft operations. In fact, based on this study, when green hydrogen is used, the reduction in GWP compared to conventional aircraft running on Jet-A1 is between 76% and 98%! Furthermore, the sensitivity analysis in this study indicates that there is ample room for optimisation of both, aircraft mass and energy usage. By tuning some of the powertrain parameters, considerable optimisation can even be achieved without impacting the aircraft's mission capabilities. Moreover, by slightly reducing some of the mission capabilities, such as the cruise Mach number, further optimisation can be achieved.

In summary, while this study has highlighted some of the challenges that have to be overcome, they are likely not insurmountable. With aircraft design optimisation and further technological improvements which are likely to happen in the near future due to the ongoing efforts in the industry and academia, the hybrid hydrogen-fuel-cell-powered commuter aircraft appear to be a viable solution for more sustainable aviation.

### 6.2.2. Individual Aircraft

While many observations on the viability of fuel cell commuter aircraft apply to all four aircraft examined in this study, it is hard to overlook some of the differences between them. As expected, fuel cell aircraft with more stringent performance requirements in terms of speed and range incur heftier mass penalties when compared to conventional aircraft. However, there are other factors that negatively influenced the overall fuel cell aircraft mass and energy usage. One of the most important among them is the fuselage diameter. When the diameter is small, the cryogenic tank exhibits a lower mass efficiency, increasing the total mass of the aircraft. Worse still, the required tank volume causes the fuselage to elongate disproportionately and causes an excessive mass and drag penalty. This was clearly shown with the Do 228 and Metro 23 aircraft. In fact, the Metro 23 aircraft fuselage had to be modified to even permit design convergence.

This brings us to the EMB 110. It is hard to ignore the extent to which the EMB 110 performed better as a fuel cell aircraft than the remaining aircraft in this study. The mass of this aircraft increased by only half as much as for the other three aircraft. This also meant that it was the only aircraft whose energy use over the mission actually reduced compared to the conventional aircraft. Hence, one might ask themselves why this is the case.

It is no surprise that the EMB 110 aircraft requirements and configuration worked very well with the

fuel-cell powertrain integration. The low cruising speed requirement of 0.283 M ensured that the aircraft had the by far least restrictive power-loading for its FCS, as could be seen in Table 5.1. This translated directly into a lighter FCS. Moreover, as could be seen in Table 5.3, the EMB 110 battery is by far the lightest. Since the FCS alone cannot sustain a sufficient climb rate, the battery is utilised during the climb. Thus, the two low-flying aircraft, including the EMB 110 required less battery-supplied energy, resulting in a lighter battery. Finally, the EMB 110 has by far the lightest cryogenic fuel tank. The first and most obvious reason for this is the low range of this aircraft, reducing the amount of fuel required. In comparison to other aircraft analysed in this study, the EMB 110 is capable of flying only half the range of the Do 228 or the Jetstream 31. Even more stark is the comparison to Metro 23, since the EMB 110 can only achieve about a quarter of the former aircraft's range. Finally, unlike in the Do 228 where the seating layout is 1+1, the seating layout in the EMB 110 is 2+1. This increase in fuselage diameter ensures a higher gravimetric efficiency of the cryogenic tank. As could be seen from Table 5.3, the tank mass efficiency of EMB 110 is around 50%. While not as high as for the Metro 23 (52%) or Jetstream 31 (57%), it is still much better than the Do 228 (44%). Thus, the EMB does not suffer from a very inefficient tank design. In summary, the EMB 110 requirements and geometry are well-suited for fuel-cell powertrain integration.

## 6.3. Limitations of Presented Fuel-Cell Aircraft Results

While the study presented in this report has several strengths, it is also important to acknowledge its limitations. These limitations will be classified based on whether their effects are known or unknown. Specifically, the direction of the effects (i.e., whether they make the results too optimistic or too pessimistic) will be considered. First, the report will list the limitations of the models and methods for which the direction of the effect is known. Then, the report will discuss the limitations for which the direction of the effects is unknown.

The limitations for which the direction of effect is known can be seen in Table 6.1. As shown in the table, the limitations that make the final results too optimistic generally revolve around the unaccounted mass and drag from the FCS components. For instance, while the drag of the nacelle fairing is included in the analysis, the drag caused by the internal FCS components, such as the heat exchanger, is not. Additionally, the masses of plumbing for air, coolants, and hydrogen fuel that connect different components of the FCS are not fully modelled. Similarly, the mass of power management and distribution units or PMADs are not modelled fully either. Finally, the EMB 110 and the Do 228 aircraft do not have a circular fuselage cross-section. Instead, the cross-section of the EMB 110 is slightly flattened on all four sides, while the Do 228 cross-section is almost rectangular. Because of this, the circular cryogenic tank diameter that would fit inside each of these aircraft, in reality, is slightly smaller than what this study suggests. This would make the aircraft slightly longer and heavier.

**Table 6.1:** Limitations of the models used and the qualitative impact on the final results.

| Too optimistic | Too pessimistic |
|---|---|
| Unaccounted internal drag from the FCS | Non-aerospace-grade FCS component models |
| Unaccounted mass of FCS plumbing | Lack of powertrain and mission optimisation |
| Unaccounted PMAD mass | Ageing reference aircraft designs |
| Inaccurate aircraft cross-section shape | |

Conversely, the fact that the models for various FCS components are based on commercially available hardware is likely making the model predictions too pessimistic. Since this commercially available hardware is currently focused on maritime, construction, and other heavy transportation industries, the components are likely to have some room for mass and/or volume optimisation. The lack of optimisation is not limited to the FSC components, however. As mentioned multiple times throughout this report, the optimisation is also not performed on the aircraft system as a whole. The sensitivity analysis in this report has shown the potential for mass and energy use improvements that could likely be achieved with aircraft design and mission optimisation. Finally, it is also worth mentioning that most of the commuter aircraft that are operating today are fairly old aircraft designs with some improvements added over the years. Hence, the fuel cell aircraft designs in this study are also based on these older airframe

designs. Thus with newer materials, as well as structural and aerodynamic improvements, the all-new fuel-cell commuter aircraft would likely perform better than the aircraft that are presented in this study.

The remainder of this section will list the model and methodology limitations for which the direction of the effect is unknown. For consistency, these effects are also presented in a table format, concretely, in Table 6.2.

**Table 6.2:** Unclassified limitations of the models used.

| Inconsistent or unknown effect |
| --- |
| Constant vertical stabiliser volume |
| HSE model validation |
| Heat exchanger model discontinuity |
| Class 2.5 convergence issues |

Four notable limitations were observed during this study. First, the vertical stabiliser size for fuel cell aircraft is solely determined through the tail volume coefficient, which is kept constant based on the value from the reference conventional aircraft. The horizontal stabiliser, on the other hand, was either determined through the same method of constant tail volume coefficient or by the HSE module. However, as was observed in the conventional aircraft validation in Section 4.1.5, the HSE module did not perform as desired. The third model limitation is the discontinuity in the FCS heat exchanger model, where the change in flow Reynolds number causes the effectiveness of the heat exchanger to change suddenly and drastically. This behaviour is unlikely to accurately reflect real-world phenomena. Finally, it is observed that the class 2.5 mass estimation modules in the Initiator aircraft design synthesis software exhibit convergence issues that can lead to the final converged result being too dependent on the convergence margin set by the user.

# 6.4. Recommendations for Future Work

The results gathered in this research shed light on many interesting characteristics of the fuel-cell commuter aircraft. Nevertheless, based on the observed results, as well as model and methodology limitations, there are several aircraft design software developments and research directions which would be compelling to explore in the future.

Beginning with the FCS model, the following improvements would be very beneficial for the overall fuel cell aircraft estimation accuracy. The models for the individual FCS BoP components should be expanded to estimate the mass and volume of components based on multiple input parameters, as opposed to just one, as is the case now. Alternatively, it would also be beneficial to revert to physics-based models, but with increased estimation accuracy. Additionally, the drag caused by the individual components in the FCS should be modelled as well, such that increases in FCS size can be penalised with increased FCS drag.

The results of this study would also benefit greatly from an aircraft powertrain and mission optimisation scheme. In particular, optimising the levels of hybridisation for each phase of the flight to achieve lighter and more efficient aircraft would be a very interesting research direction. Furthermore, this study shows that there is potential for mass and energy savings by optimising fuel cell over-sizing, fuel cell inlet pressure, and cryogenic tank venting pressure. Such optimisation schemes would allow better quantification and a more detailed assessment of the potential advantages and drawbacks of the fuel cell aircraft. Besides advancing the aircraft design and optimisation capabilities, expanding the aircraft environmental impact and cost models would also present a good opportunity to analyse the viability of fuel-cell commuter aircraft in a more holistic way. These models could include aircraft purchase and maintenance costs, as well as the environmental effects of aircraft production and end-of-life costs.

# 7

# Conclusion

The purpose of this study was to assess the performance of hybrid hydrogen fuel-cell commuter aircraft and compare the results to conventional turboprop commuter aircraft. Furthermore, this study also aimed to assess the viability of the hydrogen fuel-cell powertrain for commuter-type aircraft.

The results presented in this report showed that the fuel cell aircraft mass increases with the introduction of the fuel-cell powertrain. However, it was also shown that the fuel-cell powertrain is more efficient than the conventional one. Thus, it could be seen that energy use is unlikely to increase dramatically. With some minor optimisation, the energy use is likely to be brought well below the conventional aircraft levels, even at higher aircraft mass.

When the fuel cell aircraft are utilising green hydrogen it was shown that the flight GWP reduces by anywhere between 76% and 98% compared to conventional commuter aircraft. If the EU emission allowances are factored in, the price of energy to perform the mission in the mid-term future appeared to be approximately the same as for the conventional aircraft, even without aircraft energy use optimisation.

Despite these promising observations, the viability of hybrid fuel-cell-powered commuter aircraft remains a complex issue that cannot be decisively determined without empirical evidence of their performance in the commercial aviation domain. Any definitive conclusion can only be drawn after thorough experimentation and evaluation of the aircraft's capabilities. Nevertheless, this study offers some valuable insights into the adoption potential of this technology, highlighting both favourable and unfavourable factors that could impact its eventual acceptance in the industry. As such, it hopefully provides a valuable foundation for future research and exploration of this innovative aviation technology.

# Bibliography

[1]   Environmental and Energy Study Institute, *Fact Sheet; The Growth in Greenhouse Gas Emissions from Commercial Aviation; Part 1 of a Series on Airlines and Climate Change*, Oct. 2019. [Online]. Available: `https://www.eesi.org/files/FactSheet_Climate_Impacts_Aviation_1019.pdf` (visited on 30/08/2021).

[2]   European Commission. "Reducing emissions from aviation". (2021), [Online]. Available: `https://ec.europa.eu/clima/policies/transport/aviation_en#tab-0-0` (visited on 30/08/2021).

[3]   M. Darecki, C. Edelstenne, T. Enders, E. Fernandez, P. Hartman, J.-P. Herteman, M. Kerkloh, I. King, P. Ky, M. Mathieu, G. Orsi, G. Schotman, C. Smith and J.-D. Wörne, "Flightpath 2050, Europe's vision for aviation", Report of the High Level Group on Aviation Research, European Commission, 2011, ISBN 978-92-79-19724-6. DOI: `10.2777/50266`. [Online]. Available: `https://ec.europa.eu/transport/sites/default/files/modes/air/doc/flightpath2050.pdf` (visited on 30/08/2021).

[4]   T. Kadyk, C. Winnefeld, R. Hanke-Rauschenbach and U. Krewer, "Analysis and design of fuel cell systems for aviation", *Energies*, vol. 11, no. 2, 2018, ISSN: 1996-1073. DOI: `10.3390/en11020375`. [Online]. Available: `https://www.mdpi.com/1996-1073/11/2/375` (visited on 27/09/2021).

[5]   J. Soone, "Sustainable aviation fuel", European Parliamentary Research Service (EPRS), Tech. Rep., 2020. [Online]. Available: `https://www.europarl.europa.eu/RegData/etudes/BRIE/2020/659361/EPRS_BRI(2020)659361_EN.pdf` (visited on 08/11/2021).

[6]   J. Scheelhaase, S. Maertens and W. Grimme, "Synthetic fuels in aviation – current barriers and potential political measures", *Transportation Research Procedia*, vol. 43, pp. 21–30, 2019, INAIR 2019 - Global Trends in Aviation, ISSN: 2352-1465. DOI: `https://doi.org/10.1016/j.trpro.2019.12.015`. [Online]. Available: `https://www.sciencedirect.com/science/article/pii/S2352146519305824` (visited on 08/11/2021).

[7]   I. Dincer and C. Acar, "A review on potential use of hydrogen in aviation applications", *International Journal of Sustainable Aviation*, vol. 2, no. 1, pp. 74–100, 2016. DOI: `10.1504/IJSA.2016.076077`.

[8]   M. A. Hasan, A. A. Mamun, S. M. Rahman, K. Malik, M. I. U. Al Amran, A. N. Khondaker, O. Reshi, S. P. Tiwari and F. S. Alismail, "Climate change mitigation pathways for the aviation sector", *Sustainability*, vol. 13, no. 7, 2021, ISSN: 2071-1050. DOI: `10.3390/su13073656`. [Online]. Available: `https://www.mdpi.com/2071-1050/13/7/3656` (visited on 21/10/2021).

[9]   B. Khandelwal, A. Karakurt, P. R. Sekaran, V. Sethi and R. Singh, "Hydrogen powered aircraft : The future of air transport", *Progress in Aerospace Sciences*, vol. 60, pp. 45–59, 2013, ISSN: 0376-0421. DOI: `https://doi.org/10.1016/j.paerosci.2012.12.002`. [Online]. Available: `https://www.sciencedirect.com/science/article/pii/S0376042112000887` (visited on 21/10/2021).

[10]  B. Graver, D. Rutherford and S. Zhneg, "$CO_2$ Emissions from Commercial Aviation, 2013, 2018, and 2019", The International Council on Clean Transportation (ICCT), Tech. Rep., 2020. [Online]. Available: `https://theicct.org/sites/default/files/publications/CO2-commercial-aviation-oct2020.pdf` (visited on 08/11/2021).

[11]  A. Filippone and B. Parkes, "Evaluation of commuter airplane emissions: A european case study", *Transportation Research Part D: Transport and Environment*, vol. 98, p. 102 979, 2021, ISSN: 1361-9209. DOI: `https://doi.org/10.1016/j.trd.2021.102979`. [Online]. Available: `https://www.sciencedirect.com/science/article/pii/S1361920921002777` (visited on 08/11/2021).

[12] D. Ciliberti, P. Della Vecchia, V. Memmolo, F. Nicolosi, G. Wortmann and F. Ricci, "The enabling technologies for a quasi-zero emissions commuter aircraft", *Aerospace*, vol. 9, no. 6, 2022, ISSN: 2226-4310. DOI: `10.3390/aerospace9060319`. [Online]. Available: `https://www.mdpi.com/2226-4310/9/6/319` (visited on 02/03/2023).

[13] European Aviation Safety Agency (EASA), *Certification Specifications for Normal, Utility, Aerobatic, and Commuter Category Aeroplanes; CS-23 Amendment 5*, European Aviation Safety Agency (EASA), Cologne, Germany, Mar. 2017. [Online]. Available: `https://www.easa.europa.eu/en/document-library/certification-specifications/cs-23-amendment-5` (visited on 22/12/2022).

[14] T. Tomazic and J. Tomazic, "D2.2: certification basis composition report", Modular Approach to Hybrid Electric Propulsion Architecture project (MAHEPA), Tech. Rep., 2018. [Online]. Available: `https://mahepa.eu/wp-content/uploads/2019/05/D13_MAHEPA_D2.2_Certification-basis-composition-report_final.pdf` (visited on 13/10/2021).

[15] L. Trainelli, C. E. D. Riboldi, A. Rolandoa, F. Salucci, F. Oliviero, J. Pirnar, T. Koopman and A. Znidar, "D1.2: the design framework for an NZE 19-seater", Communty Friendly Miniliner 2019 (UNIFIER19), Tech. Rep., 2020. [Online]. Available: `https://www.unifier19.eu/wp-content/uploads/2021/07/D1.2_The_design_framework_for_an_NZE-19-seater_Open.pdf` (visited on 06/10/2021).

[16] European Aviation Safety Agency (EASA), *Certification Specifications for Normal, Utility, Aerobatic, and Commuter Category Aeroplanes; CS-23*, 1st ed., European Aviation Safety Agency (EASA), Brussels, Belgium, Nov. 2003. [Online]. Available: `https://www.easa.europa.eu/en/document-library/certification-specifications/cs-23-initial-issue` (visited on 22/12/2022).

[17] Rolls-Royce. "A next step in electrification – commuter aircraft". (2021), [Online]. Available: `https://www.rolls-royce.com/media/our-stories/discover/2021/a-next-step-in-electrification-commuter-aircraft.aspx` (visited on 04/03/2023).

[18] Jane's. "All the world's aircraft". (2021), [Online]. Available: `https://customer.janes.com` (visited on 09/11/2021).

[19] R. D. Hiscocks, "STOL Aircraft—A Perspective", *The Aeronautical Journal (1968)*, vol. 72, no. 685, pp. 11–33, 1968. DOI: `10.1017/S0001924000083433`.

[20] D. Chiaramonti, "Sustainable aviation fuels: The challenge of decarbonization", *Energy Procedia*, vol. 158, pp. 1202–1207, 2019, Innovative Solutions for Energy Transitions, ISSN: 1876-6102. DOI: `https://doi.org/10.1016/j.egypro.2019.01.308`. [Online]. Available: `https://www.sciencedirect.com/science/article/pii/S1876610219303285` (visited on 05/02/2023).

[21] T. Kandaramath Hari, Z. Yaakob and N. N. Binitha, "Aviation biofuel from renewable resources: Routes, opportunities and challenges", *Renewable and Sustainable Energy Reviews*, vol. 42, pp. 1234–1244, 2015, ISSN: 1364-0321. DOI: `https://doi.org/10.1016/j.rser.2014.10.095`. [Online]. Available: `https://www.sciencedirect.com/science/article/pii/S1364032114009204` (visited on 15/01/2023).

[22] J. Faber, J. Király, D. Lee, B. Owen and A. O'Leary, *Potential for reducing aviation non-CO2 emissions through cleaner jet fuel*, 2022. [Online]. Available: `https://ce.nl/wp-content/uploads/2022/04/CE_Delft_210410_Potential_reducing_aviation_non-CO2_emissions_cleaner_jet_fuel_FINAL.pdf` (visited on 04/03/2023).

[23] R. C. Bolam, Y. Vagapov and A. Anuchin, "Review of electrically powered propulsion for aircraft", in *2018 53rd International Universities Power Engineering Conference (UPEC)*, 2018, pp. 1–6. DOI: `10.1109/UPEC.2018.8541945`.

[24] N. K. Borer, C. L. Nickol, F. Jones, R. Yasky, K. Woodham, J. Fell, B. Litherland, P. Loyselle, A. Provenza, L. Kohlman and A. Samuel, "Overcoming the adoption barrier to electric flight", in *54th AIAA Aerospace Sciences Meeting*. DOI: `10.2514/6.2016-1022`. eprint: `https://arc.aiaa.org/doi/pdf/10.2514/6.2016-1022`. [Online]. Available: `https://arc.aiaa.org/doi/abs/10.2514/6.2016-1022` (visited on 10/12/2022).

[25] A. Baroutaji, T. Wilberforce, M. Ramadan and A. G. Olabi, "Comprehensive investigation on hydrogen and fuel cell technology in the aviation and aerospace sectors", *Renewable and Sustainable Energy Reviews*, vol. 106, pp. 31–40, 2019, ISSN: 1364-0321. DOI: `https://doi.org/10.1016/j.rser.2019.02.022`. [Online]. Available: `https://www.sciencedirect.com/science/article/pii/S1364032119301157`.

[26] J. Wehrspohn, A. Rahn, V. Papantoni, D. Silberhorn, T. Burschyk, M. Schröder, F. Linke, K. Dahlmann, M. Kühlen, K. Wicke and G. Wende, "A detailed and comparative economic analysis of hybrid-electric aircraft concepts considering environmental assessment factors", in *AIAA AVIATION 2022 Forum*. DOI: `10.2514/6.2022-3882`. eprint: `https://arc.aiaa.org/doi/pdf/10.2514/6.2022-3882`. [Online]. Available: `https://arc.aiaa.org/doi/abs/10.2514/6.2022-3882`.

[27] IEA, *The Future of Hydrogen, Seizing today's opportunities*, 2019. [Online]. Available: `https://www.iea.org/reports/the-future-of-hydrogen` (visited on 04/03/2023).

[28] A. Ajanovic, M. Sayer and R. Haas, "The economics and the environmental benignity of different colors of hydrogen", *International Journal of Hydrogen Energy*, vol. 47, no. 57, pp. 24 136–24 154, 2022, Hydrogen Society, ISSN: 0360-3199. DOI: `https://doi.org/10.1016/j.ijhydene.2022.02.094`. [Online]. Available: `https://www.sciencedirect.com/science/article/pii/S0360319922007066` (visited on 21/01/2023).

[29] E. Cetinkaya, I. Dincer and G. Naterer, "Life cycle assessment of various hydrogen production methods", *International Journal of Hydrogen Energy*, vol. 37, no. 3, pp. 2071–2080, 2012, 2010 AIChE Annual Meeting Topical Conference on Hydrogen Production and Storage Special Issue, ISSN: 0360-3199. DOI: `https://doi.org/10.1016/j.ijhydene.2011.10.064`. [Online]. Available: `https://www.sciencedirect.com/science/article/pii/S036031991102430X` (visited on 20/01/2023).

[30] IEA, *CCUS in Clean Energy Transitions, Special report on carbon capture utilisation and storage*, 2020. [Online]. Available: `https://www.iea.org/reports/ccus-in-clean-energy-transitions` (visited on 04/03/2023).

[31] R. O'Hayre, S.-W. Cha, W. Colella and F. B. Prinz, *Fuel Cell Fundamentals*, 3rd ed. John Wiley & Sons, Incorporated, May 2016, ISBN 9781119114208.

[32] J. Larminie and A. Dicks, *Fuel Cell Systems Explained*, 2nd ed. John Wiley & Sons, Incorporated, 2003, ISBN 978-0-470-84857-9. [Online]. Available: `https://app.knovel.com/hotlink/toc/id:kpFCSEE002/fuel-cell-systems-explained/fuel-cell-systems-explained` (visited on 09/09/2021).

[33] S. Mekhilef, R. Saidur and A. Safari, "Comparative study of different fuel cell technologies", *Renewable and Sustainable Energy Reviews*, vol. 16, no. 1, pp. 981–989, 2012, ISSN: 1364-0321. DOI: `https://doi.org/10.1016/j.rser.2011.09.020`. [Online]. Available: `https://www.sciencedirect.com/science/article/pii/S1364032111004709` (visited on 14/09/2021).

[34] EG&G Technical Services, Inc., *Fuel cell handbook*, 7th ed., U.S. Department of Energy; Office of Fossil Energy; National Energy Technology Laboratory, Morgantown, West Virginia, USA, Nov. 2004. DOI: `10.2172/834188`. [Online]. Available: `https://www.netl.doe.gov/sites/default/files/netl-file/FCHandbook7.pdf` (visited on 29/09/2021).

[35] D. Verstraete, P. Hendrick, P. Pilidis and K. Ramsden, "Hydrogen fuel tanks for subsonic transport aircraft", *International Journal of Hydrogen Energy*, vol. 35, no. 20, pp. 11 085–11 098, 2010, Hyceltec 2009 Conference, ISSN: 0360-3199. DOI: `https://doi.org/10.1016/j.ijhydene.2010.06.060`. [Online]. Available: `https://www.sciencedirect.com/science/article/pii/S036031991001236X` (visited on 04/10/2021).

[36] F. Barbir, "Chapter nine - fuel cell system design", in *PEM Fuel Cells (Second Edition)*, F. Barbir, Ed., Second Edition, Boston: Academic Press, 2013, pp. 305–372, ISBN: 978-0-12-387710-9. DOI: `https://doi.org/10.1016/B978-0-12-387710-9.00009-6`. [Online]. Available: `https://www.sciencedirect.com/science/article/pii/B9780123877109000096` (visited on 04/10/2021).

[37] T. Kim and S. Kwon, "Design and development of a fuel cell-powered small unmanned aircraft", *International Journal of Hydrogen Energy*, vol. 37, no. 1, pp. 615–622, 2012, 11th China Hydrogen Energy Conference, ISSN: 0360-3199. DOI: `https://doi.org/10.1016/j.ijhydene.2011.09.051`. [Online]. Available: `https://www.sciencedirect.com/science/article/pii/S0360319911021641` (visited on 05/10/2021).

[38] W. H. J. Hogarth and J. B. Benziger, "Dynamics of autohumidifed PEM fuel cell operation", *Journal of The Electrochemical Society*, vol. 153, no. 11, A2139–A2146, 2006. DOI: `10.1149/1.2344841`. [Online]. Available: `https://doi.org/10.1149/1.2344841` (visited on 05/10/2021).

[39] R. de Vries, M. T. Brown and R. Vos, "A preliminary sizing method for hybrid-electric aircraft including aero-propulsive interaction effects", in *2018 Aviation Technology, Integration, and Operations Conference*. American Institute of Aeronautics and Astronautics (AIAA), 2018. DOI: `10.2514/6.2018-4228`. eprint: `https://arc.aiaa.org/doi/pdf/10.2514/6.2018-4228`. [Online]. Available: `https://arc.aiaa.org/doi/abs/10.2514/6.2018-4228` (visited on 06/10/2021).

[40] S. Sahoo, X. Zhao and K. Kyprianidis, "A review of concepts, benefits, and challenges for future electrical propulsion-based aircraft", *Aerospace*, vol. 7, no. 4, 2020, ISSN: 2226-4310. [Online]. Available: `https://www.mdpi.com/2226-4310/7/4/44` (visited on 11/10/2021).

[41] B. Aigner, E. Stumpf, A. Hinz and R. W. D. Doncker, "An integrated design framework for aircraft with hybrid electric propulsion", in *AIAA Scitech 2020 Forum*. 2020. DOI: `10.2514/6.2020-1501`. eprint: `https://arc.aiaa.org/doi/pdf/10.2514/6.2020-1501`. [Online]. Available: `https://arc.aiaa.org/doi/abs/10.2514/6.2020-1501` (visited on 06/10/2021).

[42] L. Trainelli, F. Salucci, D. Comincini, C. E. Riboldi and A. Rolando, "Sizing and performance of hydrogen-driven airplanes", Sep. 2019.

[43] N. Lapeña-Rey, J. Mosquera, E. Bataller and F. Ortí, "First fuel-cell manned aircraft", *Journal of Aircraft*, vol. 47, no. 6, pp. 1825–1835, 2010. DOI: `10.2514/1.42234`. eprint: `https://doi.org/10.2514/1.42234`. [Online]. Available: `https://doi.org/10.2514/1.42234` (visited on 16/09/2021).

[44] N. Lapeña-Rey, J. Mosquera, E. Bataller, F. Ortí, C. Dudfield and A. Orsillo, "Environmentally friendly power sources for aerospace applications", *Journal of Power Sources*, vol. 181, no. 2, pp. 353–362, 2008, Fuel cells in a changing world Selected papers from the tenth Grove fuel cell symposium, ISSN: 0378-7753. DOI: `https://doi.org/10.1016/j.jpowsour.2007.11.045`. [Online]. Available: `https://www.sciencedirect.com/science/article/pii/S0378775307024615` (visited on 16/09/2021).

[45] Wikimedia Commons. "Boeing fuel cell demonstrator ab1". (2008), [Online]. Available: `https://commons.wikimedia.org/wiki/File:Boeing_Fuel_Cell_Demonstrator_AB1.JPG` (visited on 16/09/2021).

[46] Wikimedia Commons. "Boeing fuel cell demonstrator ab2". (2008), [Online]. Available: `https://commons.wikimedia.org/wiki/File:Boeing_Fuel_Cell_Demonstrator_AB2.JPG` (visited on 17/09/2021).

[47] G. Romeo, F. Borello, G. Correa and E. Cestino, "ENFICA-FC: Design of transport aircraft powered by fuel cell & flight test of zero emission 2-seater aircraft powered by fuel cells fueled by hydrogen", *International Journal of Hydrogen Energy*, vol. 38, no. 1, pp. 469–479, 2013, European Fuel Cell 2011, ISSN: 0360-3199. DOI: `https://doi.org/10.1016/j.ijhydene.2012.09.064`. [Online]. Available: `https://www.sciencedirect.com/science/article/pii/S0360319912021027` (visited on 16/09/2021).

[48] G. Romeo, E. Cestino, F. Borello and G. Correa, "Engineering method for air-cooling design of two-seat propeller-driven aircraft powered by fuel cells", *Journal of Aerospace Engineering*, vol. 24, no. 1, pp. 79–88, 2011. DOI: `10.1061/(ASCE)AS.1943-5525.0000055`. eprint: `https://ascelibrary.org/doi/pdf/10.1061/\%28ASCE\%29AS.1943-5525.0000055`. [Online]. Available: `https://ascelibrary.org/doi/abs/10.1061/%5C%28ASCE%5C%29AS.1943-5525.0000055` (visited on 16/09/2021).

[49] G. Romeo and F. Borello, "Design and realization of a 2-seater aircraft powered by fuel cell electric propulsion", *The Aeronautical Journal*, vol. 114, pp. 281–297, May 2010. DOI: `10.1017/S0001924000003730`.

[50] Wikimedia Commons. "Prototipo aereo elettrico rigenergia 2". (2012), [Online]. Available: `https://commons.wikimedia.org/wiki/File:Prototipo_aereo_elettrico_Rigenergia_2.JPG` (visited on 17/09/2021).

[51] J. Kallo, P. Rathke, T. Stephan, O. Thalau, J. Schirmer and F. Mayer, "Fuel cell systems for aircraft application & antares DLR-H2 all-electric flying testbed", in *51st AIAA Aerospace Sciences Meeting including the New Horizons Forum and Aerospace Exposition*. DOI: `10.2514/6.2013-936`. eprint: `https://arc.aiaa.org/doi/pdf/10.2514/6.2013-936`. [Online]. Available: `https://arc.aiaa.org/doi/abs/10.2514/6.2013-936` (visited on 17/09/2021).

[52] P. Rathke, O. Thalau, J. Kallo, J. Schirmer and T. Stephan, "Long distance flight testing with the fuel cell powered aircraft ANTARES DLR-H2", in *62. Deutscher Luft- und Raumfahrtkongress*, Sep. 2014. [Online]. Available: `https://elib.dlr.de/90438/` (visited on 17/09/2021).

[53] P. Rathke, J. Kallo, J. Schirmer, T. Stephan, W. Waiblinger and J. Weiss-Ungethum, "Antares DLR-H2 flying test bed for development of aircraft fuel cell systems", *ECS Transactions*, vol. 51, no. 1, pp. 229–241, Jun. 2013. DOI: `10.1149/05101.0229ecst`. [Online]. Available: `https://doi.org/10.1149/05101.0229ecst` (visited on 17/09/2021).

[54] DLR. "Antares DLR-H2". (2013), [Online]. Available: `https://www.dlr.de/content/en/images/2013/3/antares-dlr-h2_12336.jpg?__blob=normal&v=10__ifc1920w` (visited on 17/09/2021).

[55] DLR. "Carbon dioxide free". (2019), [Online]. Available: `https://www.dlr.de/content/en/images/aeronautics/antares-in-flight.jpg?__blob=normal&v=12__ifc1920w` (visited on 17/09/2021).

[56] D. Comincini and L. Trainelli, "A powertrain sizing method for hydrogen-driven aircraft", in *15th Pegasus-AIAA Student Conference*, Glasgow, UK, Apr. 2019, pp. 1–8.

[57] L. Trainelli and I. Perkon, "MAHEPA – a milestone-setting project in hybrid-electric aircraft technology development", in *MEA2019 - More Electric Aircraft*, Toulouse, France, Feb. 2019.

[58] J.-M. Urlacher. "Hy4: Electric flight powered by fuel cell". (2017), [Online]. Available: `https://www.dlr.de/content/en/images/2017/4/hy4-electric-flight-powered-by-fuel-cell_28722.html` (visited on 20/09/2021).

[59] DLR. "Hy4 flying with a fuel cell". (2016), [Online]. Available: `https://www.dlr.de/content/en/images/2016/3/first-flight-hy4-airport-stuttgart_24504.html` (visited on 20/09/2021).

[60] J. Kallo, "DLR leads HY4 project for four-seater fuel cell aircraft", *Fuel Cells Bulletin*, vol. 2015, no. 11, p. 13, 2015, ISSN: 1464-2859. DOI: `https://doi.org/10.1016/S1464-2859(15)30362-X`. [Online]. Available: `https://www.sciencedirect.com/science/article/pii/S146428591530362X` (visited on 20/09/2021).

[61] ZeroAvia. "Zeroavia completes world first hydrogen-electric passenger plane flight". (Sep. 2020), [Online]. Available: `https://www.zeroavia.com/press-release-25-09-2020` (visited on 20/09/2021).

[62] T. Osborne. "Startup sees fuel cell future for regional aviation", Aviation Week. (Aug. 2019), [Online]. Available: `https://aviationweek.com/aerospace/startup-sees-fuel-cell-future-regional-aviation` (visited on 20/09/2021).

[63] D. Kaminski-Morrow. "Zeroavia conducts pioneering flight with hydrogen-electric M350", Flight Global. (Sep. 2020), [Online]. Available: `https://www.flightglobal.com/air-transport/zeroavia-conducts-pioneering-flight-with-hydrogen-electric-m350/140317.article` (visited on 20/09/2021).

[64] Y. Yoma. "EASA's re-written CS-23 certification rules for small aircraft", AeroTime Hub. (Apr. 2017), [Online]. Available: `https://www.aerotime.aero/18177-easa-s-re-written-cs-23-certification-rules-for-small-aircraft` (visited on 15/11/2021).

[65] D. Erzen, L. Trainelli, C. E. D. Riboldi, A. Rolando, F. Salucci, F. Oliviero, J. Pirnar, T. Koopman, A. Znidar, M. Andrejasic, R. Lapuh, J. Soikkeli and G. Cretnik, "D2.2: Final concurrent design report", Community Friendly Miniliner 2019 (UNIFIER19), Tech. Rep., 2021. [Online]. Available: `https://www.unifier19.eu/wp-content/uploads/2021/07/D2.2_Final_concurrent_design_report_Open.pdf` (visited on 06/10/2021).

[66] S. Nicolay, S. Karpuk, Y. Liu and A. Elham, "Conceptual design and optimization of a general aviation aircraft with fuel cells and hydrogen", *International Journal of Hydrogen Energy*, vol. 46, no. 64, pp. 32 676–32 694, 2021, ISSN: 0360-3199. DOI: `https://doi.org/10.1016/j.ijhydene.2021.07.127`. [Online]. Available: `https://www.sciencedirect.com/science/article/pii/S0360319921027920` (visited on 02/06/2022).

[67] M. Strack, T. Zill and B. Nagel, "Integration of Hybrid Propulsion System in a CS23 Commuter Design", in *30th Congress of the International Council of the Aeronautical Sciences*, Sep. 2016.

[68] M. Drela and H. Youngren. "Athena Vortex Lattice (AVL)", Massachusetts Institute of Technology (MIT). (2022), [Online]. Available: `http://web.mit.edu/drela/Public/web/avl/` (visited on 03/01/2023).

[69] E. Tornebeek, *Synthesis of Subsonic Airplane Design*. Delft, The Netherlands: Kluwer Academic Publishers & Delft University Press, 1982, ISBN 90-247-2724-3.

[70] European Aviation Safety Agency (EASA). "Acceptable Means of Compliance (AMC) and Alternative Means of Compliance (AltMoC)". (), [Online]. Available: `https://www.easa.europa.eu/en/document-library/acceptable-means-compliance-amcs-and-alternative-means-compliance-altmocs` (visited on 03/01/2023).

[71] S. Gudmundsson, "Chapter 16 - performance – introduction", in *General Aviation Aircraft Design*, S. Gudmundsson, Ed., Boston: Butterworth-Heinemann, 2014, pp. 761–789, ISBN: 978-0-12-397308-5. DOI: `https://doi.org/10.1016/B978-0-12-397308-5.00016-7`. [Online]. Available: `https://www.sciencedirect.com/science/article/pii/B9780123973085000167` (visited on 21/01/2023).

[72] Lufthansa Consulting GmbH, *Final Report - Review of Standard Passenger Weights*, European Aviation Safety Agency (EASA), Apr. 2022. [Online]. Available: `https://www.easa.europa.eu/en/downloads/137230/en` (visited on 09/01/2023).

[73] Fairchild Aircraft, *Fairchild Aircraft Model SA227-AC – Metro III – ICAO Annex 8; 16,000 Pounds, FAA Approved Airplane Flight Manual*, San Antonio, Texas, United States, May 1989.

[74] D. Juschus, "Preliminary Propulsion System Sizing Methods for PEM Fuel Cell Aircraft", Delft University of Technology, Delft, The Netherlands, Oct. 2021. [Online]. Available: `http://resolver.tudelft.nl/uuid:fdc14875-175e-4a4b-8cde-f2f4b6028194` (visited on 11/01/2023).

[75] G. Onorato, "Fuel Tank Integration for Hydrogen Airliners", Delft University of Technology, Delft, The Netherlands, Aug. 2021. [Online]. Available: `http://resolver.tudelft.nl/uuid:5700b748-82c6-49c9-b94a-ad97c798e119` (visited on 11/01/2023).

[76] C. Spiegel, *PEM Fuel Cell Modeling and Simulation Using Matlab*, 1st ed. Elsevier, May 2008, ISBN: 978-0-12-374259-9. DOI: `10.1016/B978-0-12-374259-9.X5001-0`.

[77] A. Kirubakaran, S. Jain and R. Nema, "A review on fuel cell technologies and power electronic interface", *Renewable and Sustainable Energy Reviews*, vol. 13, no. 9, pp. 2430–2440, 2009, ISSN: 1364-0321. DOI: `https://doi.org/10.1016/j.rser.2009.04.004`. [Online]. Available: `https://www.sciencedirect.com/science/article/pii/S1364032109000872` (visited on 14/09/2021).

[78] R. Tirnovan, A. Miraoui, R. Munteanu, I. Vadan and H. Balan, "Polymer electrolyte fuel cell system (pefc) performance analysis", in *2006 IEEE International Conference on Automation, Quality and Testing, Robotics*, vol. 1, 2006, pp. 457–462. DOI: `10.1109/AQTR.2006.254580`.

[79] M. A. S. Al-Baghdadi, "Modelling of proton exchange membrane fuel cell performance based on semi-empirical equations", *Renewable Energy*, vol. 30, no. 10, pp. 1587–1599, 2005, ISSN: 0960-1481. DOI: `https://doi.org/10.1016/j.renene.2004.11.015`. [Online]. Available: `https://www.sciencedirect.com/science/article/pii/S0960148104004604` (visited on 27/09/2021).

[80] K. Priya, K. Sathishkumar and N. Rajasekar, "A comprehensive review on parameter estimation techniques for proton exchange membrane fuel cell modelling", *Renewable and Sustainable Energy Reviews*, vol. 93, pp. 121–144, 2018, ISSN: 1364-0321. DOI: `https://doi.org/10.1016/j.rser.2018.05.017`. [Online]. Available: `https://www.sciencedirect.com/science/article/pii/S1364032118303642` (visited on 27/09/2021).

[81] S. Sharifi Asl, S. Rowshanzamir and M. Eikani, "Modelling and simulation of the steady-state and dynamic behaviour of a pem fuel cell", *Energy*, vol. 35, no. 4, pp. 1633–1646, 2010, Demand Response Resources: the US and International Experience, ISSN: 0360-5442. DOI: `https://doi.org/10.1016/j.energy.2009.12.010`. [Online]. Available: `https://www.sciencedirect.com/science/article/pii/S0360544209005301` (visited on 01/10/2021).

[82] S. Mert, I. Dincer and Z. Ozcelik, "Performance investigation of a transportation pem fuel cell system", *International Journal of Hydrogen Energy*, vol. 37, no. 1, pp. 623–633, 2012, 11th China Hydrogen Energy Conference, ISSN: 0360-3199. DOI: `https://doi.org/10.1016/j.ijhydene.2011.09.021`. [Online]. Available: `https://www.sciencedirect.com/science/article/pii/S0360319911021008` (visited on 05/10/2021).

[83] S. Haji, "Analytical modeling of pem fuel cell i–v curve", *Renewable Energy*, vol. 36, no. 2, pp. 451–458, 2011, ISSN: 0960-1481. DOI: `https://doi.org/10.1016/j.renene.2010.07.007`. [Online]. Available: `https://www.sciencedirect.com/science/article/pii/S0960148110003319` (visited on 28/09/2021).

[84] F. Barbir and T. Gómez, "Efficiency and economics of proton exchange membrane (pem) fuel cells", *International Journal of Hydrogen Energy*, vol. 22, no. 10, pp. 1027–1037, 1997, ISSN: 0360-3199. DOI: `https://doi.org/10.1016/S0360-3199(96)00175-9`. [Online]. Available: `https://www.sciencedirect.com/science/article/pii/S0360319996001759` (visited on 28/09/2021).

[85] F. Barbir, "Chapter three - fuel cell electrochemistry", in *PEM Fuel Cells (Second Edition)*, F. Barbir, Ed., Second Edition, Boston: Academic Press, 2013, pp. 33–72, ISBN: 978-0-12-387710-9. DOI: `https://doi.org/10.1016/B978-0-12-387710-9.00003-5`. [Online]. Available: `https://www.sciencedirect.com/science/article/pii/B9780123877109000035` (visited on 27/09/2021).

[86] K. Swannet, "Optimal Control And Energy Management For Hybrid Aircraft", Delft University of Technology, Delft, The Netherlands, May 2022. [Online]. Available: `http://resolver.tudelft.nl/uuid:511989dc-0e95-414c-839b-7af0ff5ad7a0` (visited on 20/01/2023).

[87] F. Barbir, "Fuel cell basic chemistry and thermodynamics", in *PEM Fuel Cells (Second Edition)*, F. Barbir, Ed., Second Edition, Boston: Academic Press, 2013, pp. 33–72, ISBN: 978-0-12-387710-9. DOI: `https://doi.org/10.1016/B978-0-12-387710-9.00002-3`. [Online]. Available: `https://www.sciencedirect.com/science/article/pii/B9780123877109000023` (visited on 27/09/2021).

[88] T. Dey, J. Deshpande, D. Singdeo and P. C. Ghosh, "Study of pem fuel cell end plate design by structural analysis based on contact pressure", *Journal of Energy*, vol. 2019, 2019. DOI: `https://doi.org/10.1155/2019/3821082`. [Online]. Available: `https://www.hindawi.com/journals/jen/2019/3821082/` (visited on 10/01/2023).

[89] Ballard. "Fuel Cell Stacks", Ballard Power Systems. (2022), [Online]. Available: `https://www.ballard.com/fuel-cell-solutions/fuel-cell-power-products/fuel-cell-stacks` (visited on 03/01/2023).

[90] M. Gambini and M. Vellini, *Turbomachinery; Fundamentals, Selection and Preliminary Design*, 1st ed. Cham, Switzerland: Springer Publishing, Sep. 2021, ISBN:978-3-030-51299-6. DOI: `https://doi.org/10.1007/978-3-030-51299-6`.

[91] R. Huizing, M. Fowler, W. Mérida and J. Dean, "Design methodology for membrane-based plate-and-frame fuel cell humidifiers", *Journal of Power Sources*, vol. 180, no. 1, pp. 265–275, 2008, ISSN: 0378-7753. DOI: `https://doi.org/10.1016/j.jpowsour.2008.01.046`. [Online]. Available: `https://www.sciencedirect.com/science/article/pii/S037877530800195X` (visited on 10/01/2023).

[92]   D. Kožulović, "Heat Release of Fuel Cell Powered Aircraft", in *Proceedings of Global Power and Propulsion Society; GPPS Chania20*, Sep. 2020.

[93]   Papantoni, Veatriki, Linke, Florian, Dahlmann, Katrin, Kühlen, Markus, Silberhorn, Daniel, Brand, Urte and Vogt, Thomas, "Life cycle assessment of power-to-liquid for aviation: A case study of a passenger aircraft", *E3S Web Conf.*, vol. 349, p. 02 003, 2022. DOI: `10.1051/e3sconf/202234902003`. [Online]. Available: `https://doi.org/10.1051/e3sconf/202234902003` (visited on 06/02/2023).

[94]   G. Parolin, A. T. Borges, L. C. Santos and A. V. Borille, "A tool for aircraft eco-design based on streamlined life cycle assessment and uncertainty analysis", *Procedia CIRP*, vol. 98, pp. 565–570, 2021, The 28th CIRP Conference on Life Cycle Engineering, March 10 – 12, 2021, Jaipur, India, ISSN: 2212-8271. DOI: `https://doi.org/10.1016/j.procir.2021.01.152`. [Online]. Available: `https://www.sciencedirect.com/science/article/pii/S2212827121001827` (visited on 30/10/2021).

[95]   A. Johanning and D. Scholz, "Comparison of the potential environmental impact improvements of future aircraft concepts using life cycle assessment", in *5th CEAS Air & Space Conference*, 2015. [Online]. Available: `https://aerospace-europe.eu/media/books/CEAS2015_080.pdf` (visited on 30/10/2021).

[96]   S. Pinheiro Melo, A. Barke, F. Cerdas, C. Thies, M. Mennenga, T. S. Spengler and C. Herrmann, "Sustainability assessment and engineering of emerging aircraft technologies—challenges, methods and tools", *Sustainability*, vol. 12, no. 14, 2020, ISSN: 2071-1050. DOI: `10.3390/su1214566 3`. [Online]. Available: `https://www.mdpi.com/2071-1050/12/14/5663` (visited on 01/11/2021).

[97]   B. Cox, W. Jemiolo and C. Mutel, "Life cycle assessment of air transportation and the swiss commercial air transport fleet", *Transportation Research Part D: Transport and Environment*, vol. 58, pp. 1–13, 2018, ISSN: 1361-9209. DOI: `https://doi.org/10.1016/j.trd.2017.10.017`. [Online]. Available: `https://www.sciencedirect.com/science/article/pii/S1361920917300482` (visited on 02/11/2021).

[98]   J. Ribeiro, F. Afonso, I. Ribeiro, B. T. Ferreira, H. Policarpo, P. Peças and F. J. P. Lau, "Environmental assessment of hybrid-electric propulsion in conceptual aircraft design", *Journal of Cleaner Production*, vol. 247, p. 119 477, 2020.

[99]   S. Howe, A. Kolios and F. Brennan, "Environmental life cycle assessment of commercial passenger jet airliners", *Transportation Research Part D: Transport and Environment*, vol. 19, pp. 34–41, 2013, ISSN: 1361-9209. DOI: `https://doi.org/10.1016/j.trd.2012.12.004`. [Online]. Available: `https://www.sciencedirect.com/science/article/pii/S1361920913000047` (visited on 03/11/2021).

[100]  N. Jungbluth and C. Meili, "Recommendations for calculation of the global warming potential of aviation including the radiative forcing index", *The International Journal of Life Cycle Assessment*, vol. 24, pp. 404–411, 2019. DOI: `https://doi.org/10.1007/s11367-018-1556-3`. [Online]. Available: `https://link-springer-com.tudelft.idm.oclc.org/article/10.1007/s11367-018-1556-3` (visited on 10/01/2023).

[101]  A. Marashli, A.-M. Gasaymeh and M. Shalby, "Comparing the global warming impact from wind, solar energy, and other electricity generating systems through life cycle assessment methods (a survey)", *International Journal of Renewable Energy Research*, vol. 12, no. 2, pp. 899–920, 2022. DOI: `10.20508/ijrer.v12i2.13010.g8474`. [Online]. Available: `https://www.ijrer.org/ijrer/index.php/ijrer/article/view/13010/pdf` (visited on 06/02/2023).

[102]  D. Lee, D. Fahey, A. Skowron, M. Allen, U. Burkhardt, Q. Chen, S. Doherty, S. Freeman, P. Forster, J. Fuglestvedt, A. Gettelman, R. De León, L. Lim, M. Lund, R. Millar, B. Owen, J. Penner, G. Pitari, M. Prather, R. Sausen and L. Wilcox, "The contribution of global aviation to anthropogenic climate forcing for 2000 to 2018", *Atmospheric Environment*, vol. 244, p. 117 834, 2021, ISSN: 1352-2310. DOI: `https://doi.org/10.1016/j.atmosenv.2020.117834`. [Online]. Available: `https://www.sciencedirect.com/science/article/pii/S1352231020305689` (visited on 06/02/2023).

[103] M. A. H. Khan, J. Brierley, K. N. Tait, S. Bullock, D. E. Shallcross and M. H. Lowenberg, "The Emissions of Water Vapour and NOx from Modelled Hydrogen-Fuelled Aircraft and the Impact of NOx Reduction on Climate Compared with Kerosene-Fuelled Aircraft", *Atmosphere*, vol. 13, no. 10, 2022, ISSN: 2073-4433. DOI: `10.3390/atmos13101660`. [Online]. Available: `https://www.mdpi.com/2073-4433/13/10/1660` (visited on 06/02/2023).

[104] L. Wilcox, K. Shine and B. Hoskins, "Radiative forcing due to aviation water vapour emissions", *Atmospheric Environment*, vol. 63, pp. 1–13, 2012, ISSN: 1352-2310. DOI: `https://doi.org/10.1016/j.atmosenv.2012.08.072`. [Online]. Available: `https://www.sciencedirect.com/science/article/pii/S135223101200859X` (visited on 06/02/2023).

[105] S. C. Sherwood, V. Dixit and C. Salomez, "The global warming potential of near-surface emitted water vapour", *Environmental Research Letters*, vol. 13, no. 10, p. 104 006, Sep. 2018. DOI: `10.1088/1748-9326/aae018`. [Online]. Available: `https://dx.doi.org/10.1088/1748-9326/aae018` (visited on 06/02/2023).

[106] V. Williams, R. B. Noland and R. Toumi, "Air transport cruise altitude restrictions to minimize contrail formation", *Climate Policy*, vol. 3, no. 3, pp. 207–219, 2003. DOI: `10.3763/cpol.2003.0328`. eprint: `https://www.tandfonline.com/doi/pdf/10.3763/cpol.2003.0328`. [Online]. Available: `https://www.tandfonline.com/doi/abs/10.3763/cpol.2003.0328` (visited on 06/02/2023).

[107] K. Gierens, "Theory of contrail formation for fuel cells", *Aerospace*, vol. 8, no. 6, 2021, ISSN: 2226-4310. DOI: `10.3390/aerospace8060164`. [Online]. Available: `https://www.mdpi.com/2226-4310/8/6/164` (visited on 06/02/2023).

[108] D. Silberhorn, J. Hartmann, N. M. Dzikus, G. Atanasov, T. Zill, U. Brand, J. C. G. Trillos, M. Oswald, T. Vogt, D. Wilken and W. Grimme, "The air-vehicle as a complex system of air transport energy systems", in *AIAA Aviation 2020 Forum*. DOI: `10.2514/6.2020-2622`. eprint: `https://arc.aiaa.org/doi/pdf/10.2514/6.2020-2622`. [Online]. Available: `https://arc.aiaa.org/doi/abs/10.2514/6.2020-2622`.

[109] Council of the EU. "ETS aviation: Council and Parliament strike provisional deal to reduce flight emissions". (Feb. 2023), [Online]. Available: `https://www.consilium.europa.eu/en/press/press-releases/2022/12/07/ets-aviation-council-and-parliament-strike-provisional-deal-to-reduce-flight-emissions/` (visited on 04/03/2023).

[110] Council of the EU. "Fit for 55". (Jan. 2023), [Online]. Available: `https://www.consilium.europa.eu/en/policies/green-deal/fit-for-55-the-eu-plan-for-a-green-transition/#what` (visited on 04/03/2023).

[111] M. Pahle, J. Sitarz, S. Osorio and B. Görlach, "The EU-ETS price through 2030 and beyond: A closer look at drivers, models and assumptions, Input material and takeaways from a workshop in brussels", Potsdam-Institut für Klimafolgenforschung (PIK), Tech. Rep., 2022. [Online]. Available: `https://www.ecologic.eu/sites/default/files/publication/2023/30003-Ariadne-Documentation_ETSWorkshopBruessel_December2022.pdf` (visited on 04/03/2023).

[112] R. C. Pietzcker, S. Osorio and R. Rodrigues, "Tightening eu ets targets in line with the european green deal: Impacts on the decarbonization of the eu power sector", *Applied Energy*, vol. 293, p. 116 914, 2021, ISSN: 0306-2619. DOI: `https://doi.org/10.1016/j.apenergy.2021.116914`. [Online]. Available: `https://www.sciencedirect.com/science/article/pii/S0306261921003962` (visited on 04/03/2023).

[113] A. M. Stoll and G. V. Mikic, "Design studies of thin-haul commuter aircraft with distributed electric propulsion", in *16th AIAA Aviation Technology, Integration, and Operations Conference*. Jun. 2016. DOI: `10.2514/6.2016-3765`. eprint: `https://arc.aiaa.org/doi/pdf/10.2514/6.2016-3765`. [Online]. Available: `https://arc.aiaa.org/doi/abs/10.2514/6.2016-3765` (visited on 28/02/2023).

[114] American Institute of Aeronautics and Astronautics (AIAA), *Guidelines for analysis of hybrid electric aircraft system studies, Nomenclature, pictographic representations, standalone and combined properties and attributes, metrics, and figures of merit*, American Institute of Aeronautics and Astronautics (AIAA), Inc., 2019. [Online]. Available: `https://www.aiaa.org/docs/default-source/uploadedfiles/publications/standards/hybrid-electric_properties_attributes.pdf?sfvrsn=c8eb8f11_0` (visited on 06/10/2021).

[115] PowerCell. "P Stack", PowerCell Sweden AB. (2022), [Online]. Available: `https://powercellgroup.com/wp-content/uploads/2022/05/p-stack-v-221.pdf` (visited on 03/01/2023).

[116] EKPO. "Fuel Cell Stack Modules", EKPO Fuel Cell Technologies GmbH. (2022), [Online]. Available: `https://www.ekpo-fuelcell.com/en/products-technology/fuel-cell-stacks` (visited on 03/01/2023).

[117] Horizon. "Fuel cell stacks", TW Horizon Fuel Cell Technologies. (2021), [Online]. Available: `https://www.horizonfuelcell.com/fuelcellstacks` (visited on 03/01/2023).

[118] Rotex. "Fuel Cell Compressors", Rotex A/S. (2022), [Online]. Available: `https://rotrex-fuel-cell-compressor.com/fuel-cell-compressors/` (visited on 03/01/2023).

[119] Fischer. "Compressors – Our Portfolio", Fischer Spindle Group AG. (2023), [Online]. Available: `https://www.fischer-fuelcell-compressor.com/en/products` (visited on 23/01/2023).

[120] Celeroton. "Turbo Compressors", Celeroton AG. (2022), [Online]. Available: `https://www.celeroton.com/en/products/compressors/` (visited on 03/01/2023).

[121] Enogia. "Air Intake Compressor for Fuel Cell", Enogia. (2022), [Online]. Available: `https://enogia.com/wp-content/uploads/2022/05/datasheet-compressor.pdf` (visited on 03/01/2023).

[122] Fumatech BWT GmbH. "Humidifier Modules Ecomate", BWT Holding GmbH. (2022), [Online]. Available: `https://www.fumatech.com/en/products/humidifier-modules-ecomate/` (visited on 03/01/2023).

[123] Dpoint Humidifiers. "Ax Series Fuel Cell Humidifiers", CORE Energy Recovery Solutions. (2022), [Online]. Available: `https://dpoint.ca/?ddownload=129` (visited on 03/01/2023).

[124] Freudenberg. "MicronAir Fuel Cell Humidifier", Freudenberg Filtration Technologies GmbH & Co. KG. (2022), [Online]. Available: `https://www.freudenberg-filter.com/en/world-of-automotive/products/fuel-cell-solutions/#c3143` (visited on 03/01/2023).
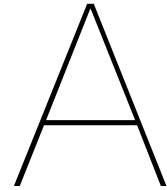
# Legend of Symbols for Novel Powertrain Architecture Representation

**Table A.1:** Symbols used to represent the novel powertrain architecture components (in accordance with the AIAA's Guidelines for Analysis of Hybrid Electric Aircraft System Studies; see [114])

| | | | |
|---|---|---|---|
| Turboshaft Engine | | Motor | |
| Piston engine | | Battery | |
| Fuel cell | | Fuel tank | |
| Forward-Facing Clockwise Rotating Propeller[1] | | | |

**Table A.2:** Symbols used to represent the connections between components in novel powertrain architectures (Adopted from Aigner *et al.* [41])

| | |
|---|---|
| Electrical connection | |
| Mechanical connection | |
| Chemical / Thermodynamic Connection | |

---

[1]Used to represent a generic propulsor device for the purposes of the powertrain schematics in Section 2.4

# B

# Fuel-Cell Powertrain Model Supplementary Material

## B.1. Fuel-Cell Stack Model Data

**Table B.1:** Commercially available fuel-cell stack data

| Company | Model | Max. Power | Mass (dry) | Current | Voltage | Cell count | Length | Width | Height | Volume | Operational Pressure |
|---|---|---|---|---|---|---|---|---|---|---|---|
| | | [kW] | [kg] | [A] | [V] | [-] | [mm] | [mm] | [mm] | [L] | [kPa] |
| Ballard | FCvelocity-9SSL | 3.8 | 6.2 | 300 | 12.9 | N/A | 92 | 760 | 60 | 4 | N/A |
| Ballard | FCvelocity-9SSL | 4.8 | 6.8 | 300 | 16.1 | N/A | 104 | 760 | 60 | 5 | N/A |
| Ballard | FCvelocity-9SSL | 10.6 | 10.2 | 300 | 35.4 | N/A | 174 | 760 | 60 | 8 | N/A |
| Ballard | FCvelocity-9SSL | 14.4 | 12.1 | 300 | 48.2 | N/A | 220 | 760 | 60 | 10 | N/A |
| Ballard | FCvelocity-9SSL | 17.3 | 14.3 | 300 | 57.9 | N/A | 255 | 760 | 60 | 12 | N/A |
| Ballard | FCvelocity-9SSL | 21.2 | 16.6 | 300 | 70.7 | N/A | 302 | 760 | 60 | 14 | N/A |
| Ballard | FCgen-LCS | 63.4 | 38.5 | 360 | 176 | N/A | 675 | 443 | 110 | 33 | 250 |
| Ballard | Fcgen-HPS | 140 | 55 | 645 | 202 | 309 | 484 | 555 | 195 | 52 | 250 |
| PowerCellution | P Stack | 75 | 29 | 450 | 167 | 275 | 420 | 395 | 156 | 26 | N/A |
| PowerCellution | P Stack | 92 | 34 | 450 | 204 | 335 | 420 | 457 | 156 | 30 | N/A |
| PowerCellution | P Stack | 115 | 40 | 450 | 256 | 419 | 420 | 545 | 156 | 36 | N/A |
| PowerCellution | P Stack | 125 | 42 | 450 | 278 | 455 | 420 | 582 | 156 | 38 | N/A |
| EKPO | NMS-EVO | 76 | N/A | 380 | 201 | 335 | 329 | 255 | 687 | 58 | 250 |
| EKPO | NM12 Single | 123 | N/A | 570 | 215 | 359 | 402 | 287 | 700 | 81 | 250 |
| EKPO | NM12 Twin | 205 | N/A | 570 | 359 | 598 | 472 | 437 | 640 | 132 | 250 |
| Horizon | VLS II Pro-110 | 110 | 43.32 | 217 | 200 | 334 | 557 | 425 | 150 | 36 | 150 |
| Horizon | VLS II Pro-132 | 132 | 49.36 | 206 | 240 | 400 | 656 | 425 | 150 | 42 | 150 |
| Horizon | VLS II Pro-165 | 165 | 58.36 | 195 | 300 | 500 | 806 | 425 | 150 | 51 | 150 |

Data compiled from: Ballard [89], PowerCellution [115], EKPO [116], and Horizon [117].

## B.2. Compressor Model Data

**Table B.2:** Commercially available fuel-cell compressor data

| Company | Model | FC power range | Pressure ratio | Mass flow | Motor power | Mass | Length | Width | Height |
|---|---|---|---|---|---|---|---|---|---|
| | | [kW] | [-] | [g/s] | [kW] | [kg] | [mm] | [mm] | [mm] |
| Rotex | EK10 | 20-100 | 2.2 | 80 | 13 | 13 | 321 | 155 | 188 |
| Rotex | EK40 | 100-400 | 2.8 | 300 | 40 | 30 | 450 | 250 | 220 |
| Fischer | EMTC-150K Air | 70 | 2.05 | 77 | 5.3 | 5 | 262 | 86 | 86 |
| Fischer | EMTC-120K Air | 60-100 | 2.5 | 165 | 15 | 8 | 280 | 120 | 120 |
| Fischer | EMTC-90K Air | 120-160 | 2.4 | 200 | 26.5 | 16 | 352 | 155 | 155 |
| Celeroton | CT-17-1000.GB | N/A | 1.65 | 24 | 1 | 1.5 | 183.4 | 90 | 90 |
| Celeroton | CT-25-10000.GB | N/A | 2.1 | 90 | 7 | 8.8 | 303 | 154 | 183 |
| Celeroton | CT-22-12000.GB | N/A | 2.1 | 140 | 12 | 10 | 311 | 154.4 | 191.5 |
| Celeroton | CT-2000 | N/A | 2.2 | 90 | 8 | 6.3 | 244 | 189 | 149 |
| Celeroton | CT-3000 | N/A | 2.6 | 155 | 19 | 18.5 | 370 | 192 | 215 |
| Celeroton | CT-3001 | N/A | 2.7 | 210 | 21 | 18.5 | 370 | 192 | 215 |
| Enogia | EFCC-90 | 30-55 | 2.8 | 90 | 7 | 5 | 190 | 185 | 185 |
| Enogia | EFCC-160 | 55-105 | 2.9 | 160 | 14 | 8 | 230 | 200 | 200 |
| Enogia | EFCC-220 | 105-190 | 3.6 | 220 | 25 | 12 | 280 | 230 | 230 |
| Enogia | EFCC-280 | 190-330 | 4.2 | 280 | 40 | 25 | 350 | 275 | 275 |

Data compiled from: Rotex [118], Fischer [119], Celeroton [120], and Enogia [121].

## B.3. Humidifier Model Data

**Table B.3:** Commercially available fuel-cell humidifier data

| Company | Model | Fuel-cell power (max.) | Air mass flow | Mass | Volume | Pressure drop |
|---|---|---|---|---|---|---|
| | | [kW] | [sLPM] | [kg] | [l] | [kPa] |
| Fumatech | H05 | 7 | 400 | 3 | 4 | 11 |
| Fumatech | H10 | 10 | 600 | 3 | 4 | 26 |
| Fumatech | H20 | 30 | 2500 | 5 | 7 | 7.5 |
| Fumatech | H50 | 70 | 4000 | 6 | 11 | 16 |
| Fumatech | H100 | 110 | 6000 | 7 | 13 | 16 |
| Dpoint | Ax100-65 | 20 | 1200 | 3 | 4.1 | 8.5 |
| Dpoint | Ax100-135 | 30 | 2000 | 4.2 | 5.9 | 7.7 |
| Dpoint | Ax100-187 | 40 | 3000 | 5.6 | 7.2 | 7 |
| Dpoint | Ax150-135 | 100 | 5000 | 8.4 | 13.2 | 17.4 |
| Freudenberg | FC HU-MG2-X | 60 | 3000 | 7 | 9.32 | 11 |

Data compiled from: Fumatech [122], Dpoint [123], Freudenberg [124].
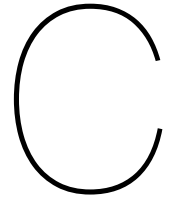
# C.1. Fuel Cell Aircraft Constraint Diagrams
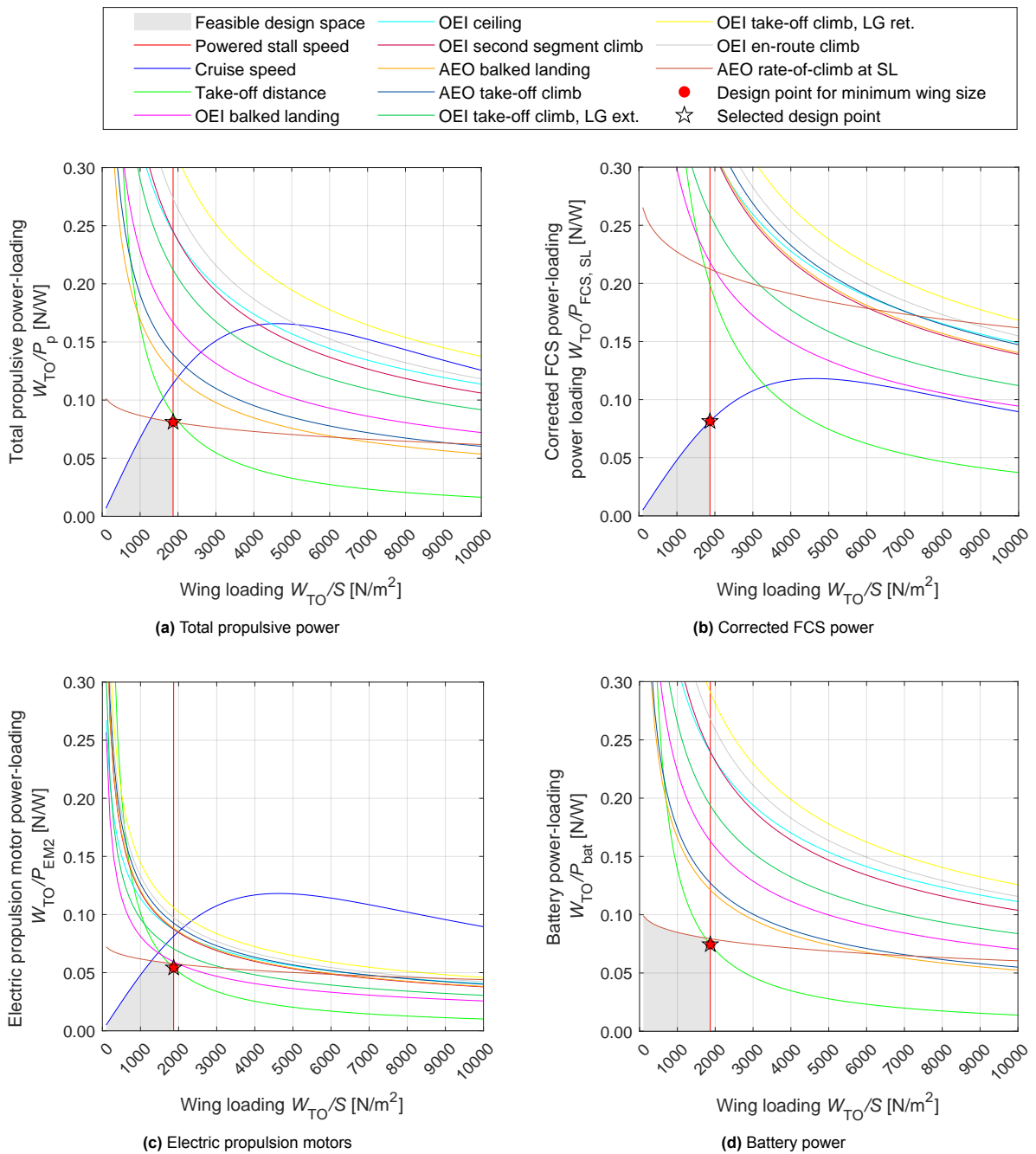


**Figure C.1:** Power- versus wing-loading diagrams and design points for the Dornier Do 228-212 FC and its various powertrain components
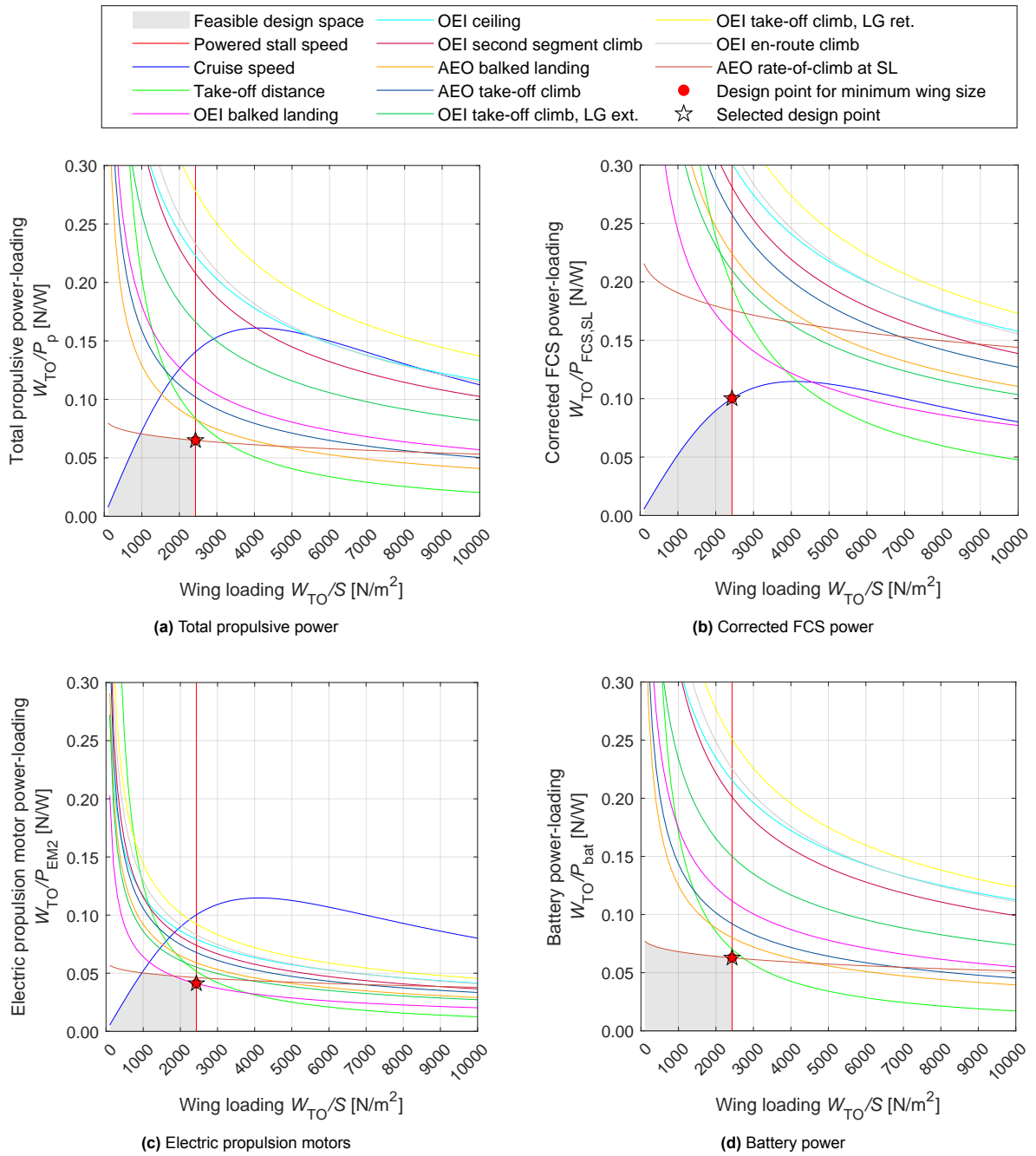
**Figure C.2:** Power- versus wing-loading diagrams and design points for a widened cabin Fairchild Metro 23 FC (2+1 seating) and its various powertrain components
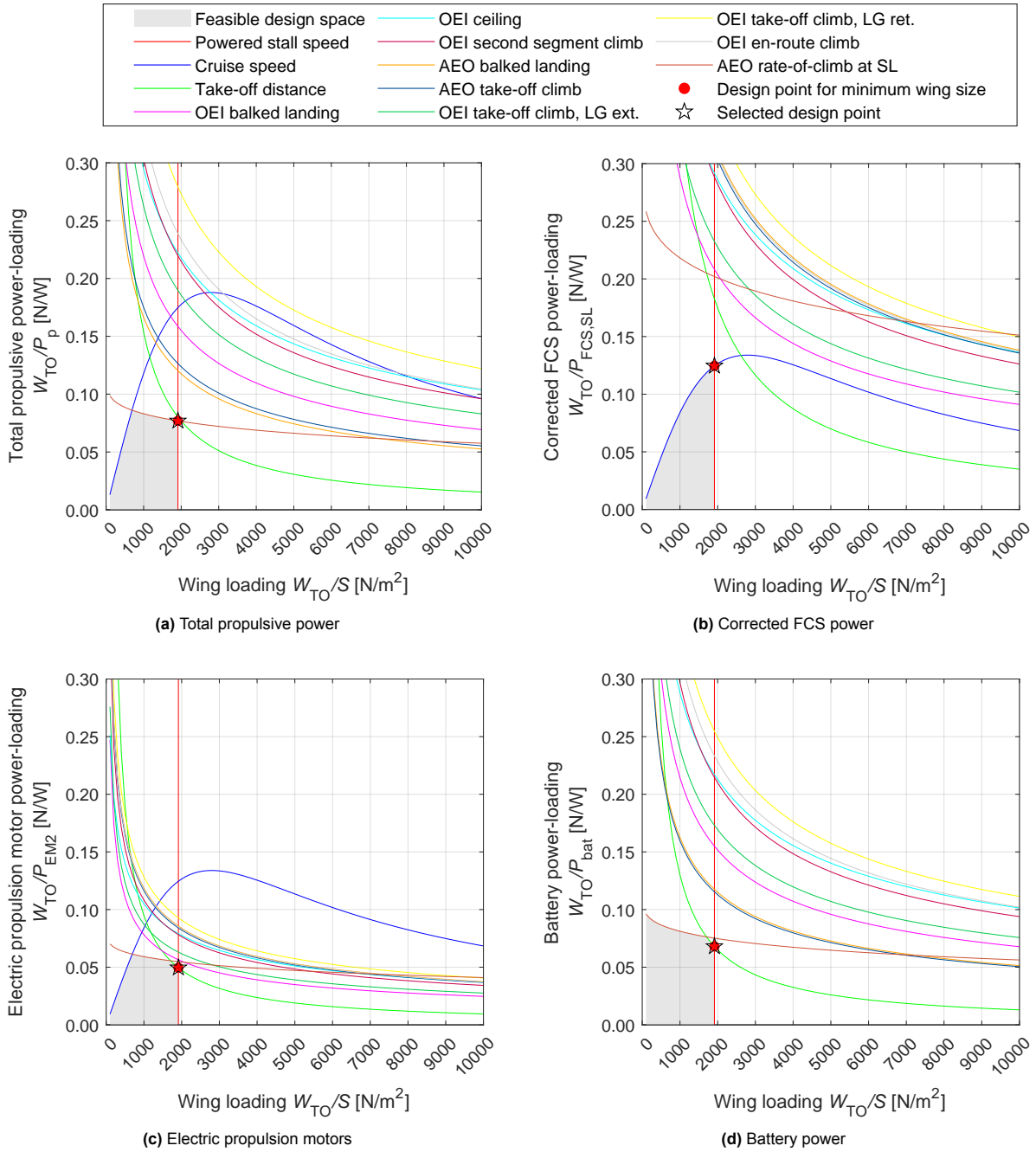
**Figure C.3:** Power- versus wing-loading diagrams and design points for the Embraer EMB 110P2 FC and its various powertrain components

## C.2. Fuel Cell Aircraft Design Mission Trip Energy Cost

**Table C.1:** Mission energy cost estimation for nominal mission using conventional and fuel cell commuter aircraft

| | Low | $\Delta_{conv.}$ | $\Delta_{SAF}$ | Base | $\Delta_{conv.}$ | $\Delta_{SAF}$ | High | $\Delta_{conv.}$ | $\Delta_{SAF}$ |
|---|---|---|---|---|---|---|---|---|---|
| | | | | | Mission (Trip) Energy Cost [€] | | | | |
| **Dornier Do 228-212 FC** | | | | | | | | | |
| Class 2 | 626 | +92% | -20% | 1040 | +86% | -13% | 1720 | +86% | -16% |
| Class 2.5 | 629 | +96% | -19% | 1095 | +90% | -11% | 1811 | +90% | -14% |
| Class 2.5 & HSE | 686 | +93% | -20% | 1172 | +87% | -12% | 1939 | +88% | -15% |
| **Fairchild Metro 23 FC (2+1cab mod)*** | | | | | | | | | |
| Class 2 | 1290 | +104% | -15% | 1867 | +98% | -7% | 3090 | +98% | -10% |
| Class 2.5 | 1267 | +92% | -20% | 1732 | +86% | -12% | 2865 | +87% | -16% |
| Class 2.5 & HSE | 1273 | +100% | -17% | 1811 | +94% | -9% | 2997 | +94% | -12% |
| **BAE Jetstream 31 FC** | | | | | | | | | |
| Class 2 | 624 | +88% | -22% | 836 | +83% | -14% | 1383 | +84% | -17% |
| Class 2.5 | 633 | +86% | -23% | 836 | +82% | -15% | 1383 | +82% | -18% |
| Class 2.5 & HSE | 497 | +84% | -24% | 856 | +79% | -16% | 1418 | +80% | -19% |
| **Embraer EMB 110P2 FC** | | | | | | | | | |
| Class 2 | 164 | +30% | -46% | 283 | +27% | -40% | 469 | +27% | -43% |
| Class 2.5 | 171 | +33% | -45% | 295 | +29% | -39% | 488 | +29% | -41% |
| Class 2.5 & HSE | 171 | +33% | -45% | 294 | +30% | -39% | 487 | +30% | -41% |

*Cabin widening to 2+1 seating configuration was required to limit overall fuselage length allow for sizing convergence.

## C.3. Fuel Cell Aircraft Design Mission Energy GWP

**Table C.2:** Nominal mission energy GWP estimation using conventional and fuel-cell commuter aircraft

| | **Mission Energy LCA GWP [kgCO$_2$eq]** | | | | | | | | |
| | - | DK Wind | | | | ES PV | | | |
| | Jet-A1 | FC | $\Delta_{J.-A1}$ | PtL SAF | $\Delta_{J.-A1}$ | FC | $\Delta_{J.-A1}$ | PtL SAF | $\Delta_{J.-A1}$ |
| **Dornier Do 228-212** | | | | | | | | | |
| Class 2 | 4152 | 202 | -95% | 1551 | -63% | 994 | -76% | 2884 | -32% |
| Class 2.5 | 4238 | 203 | -95% | 1583 | -63% | 1000 | -76% | 2884 | -32% |
| Class 2.5 & HSE | 4599 | 222 | -95% | 1718 | -63% | 1091 | -76% | 3130 | -32% |
| **Fairchild Metro 23\*** | | | | | | | | | |
| Class 2 | 6531 | 365 | -95% | 2440 | -63% | 1792 | -73% | 4445 | -32% |
| Class 2.5 | 6410 | 333 | -95% | 2395 | -63% | 1635 | -74% | 4363 | -32% |
| Class 2.5 & HSE | 6444 | 354 | -95% | 2407 | -63% | 1739 | -73% | 4386 | -32% |
| **BAE Jetstream 31** | | | | | | | | | |
| Class 2 | 3561 | 162 | -96% | 1330 | -63% | 791 | -78% | 2455 | -32% |
| Class 2.5 | 3607 | 160 | -96% | 1348 | -63% | 780 | -78% | 2395 | -32% |
| Class 2.5 & HSE | 3701 | 166 | -96% | 1383 | -63% | 807 | -78% | 2519 | -32% |
| **Embraer EMB 110P2** | | | | | | | | | |
| Class 2 | 2203 | 56 | -97% | 823 | -63% | 273 | -88% | 1499 | -32% |
| Class 2.5 | 2236 | 55 | -98% | 835 | -63% | 268 | -88% | 1522 | -32% |
| Class 2.5 & HSE | 2256 | 56 | -98% | 843 | -63% | 273 | -88% | 1535 | -32% |

\*Cabin widening to 2+1 seating configuration was required for the FC aircraft to limit overall fuselage length allow for sizing convergence.

## C.4. Sensitivity Analysis
### C.4.1. MTOM Sensitivity to Mission Parameters
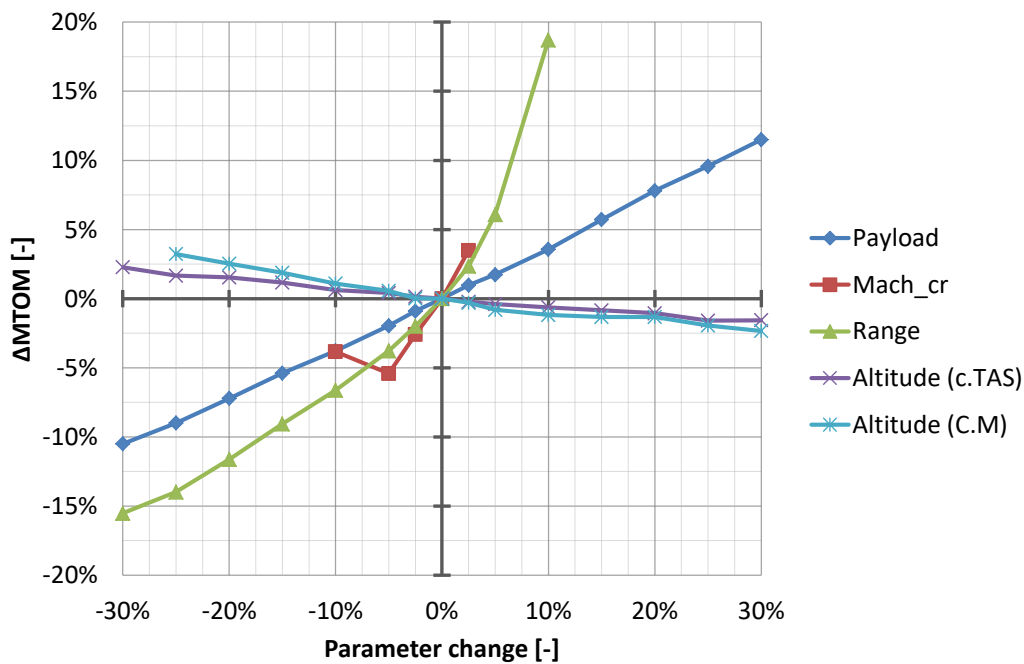


**Figure C.4:** Do 228-212 FC MTOM sensitivity to mission parameters
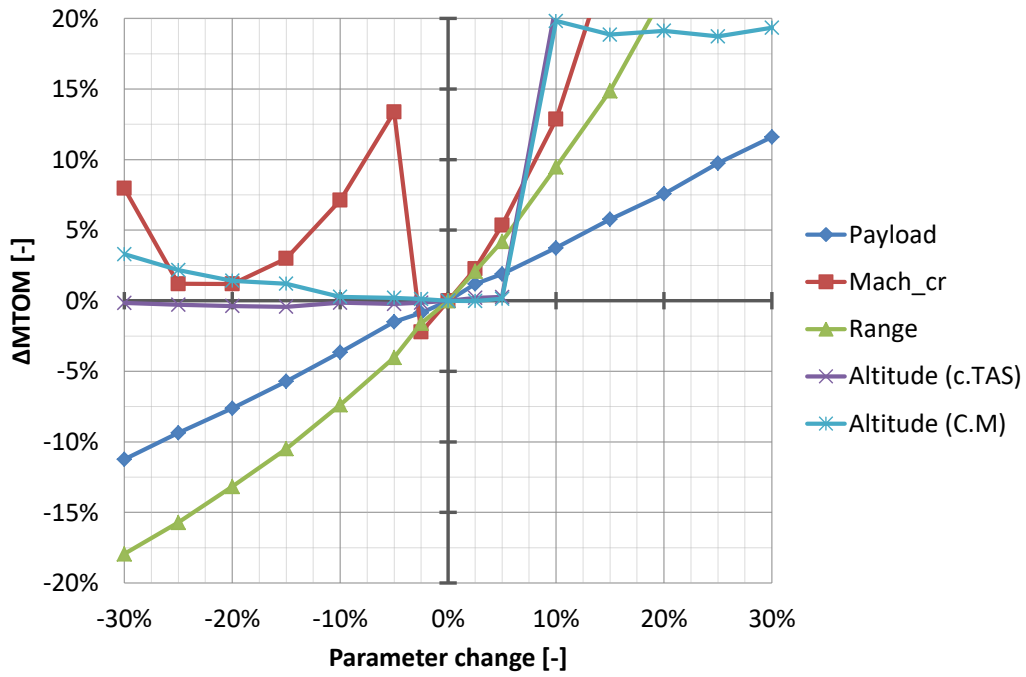
**Figure C.5:** Metro 23 FC MTOM sensitivity to mission parameters
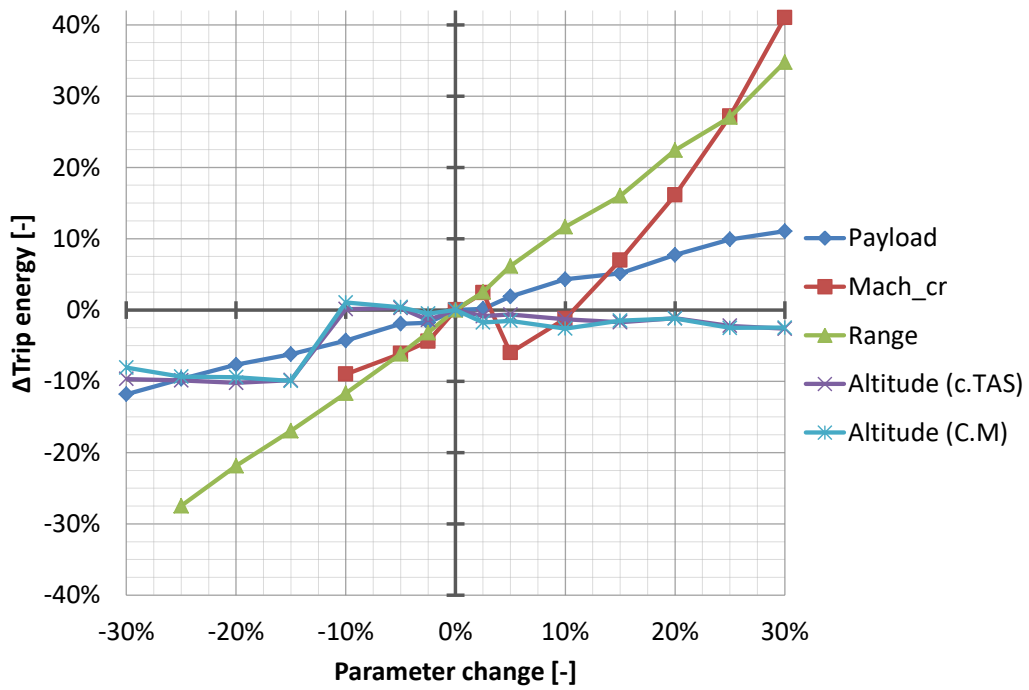


**Figure C.6:** EMB 110P2 FC MTOM sensitivity to mission parameters

## C.4.2. MTOM Sensitivity to Powertrain Parameters
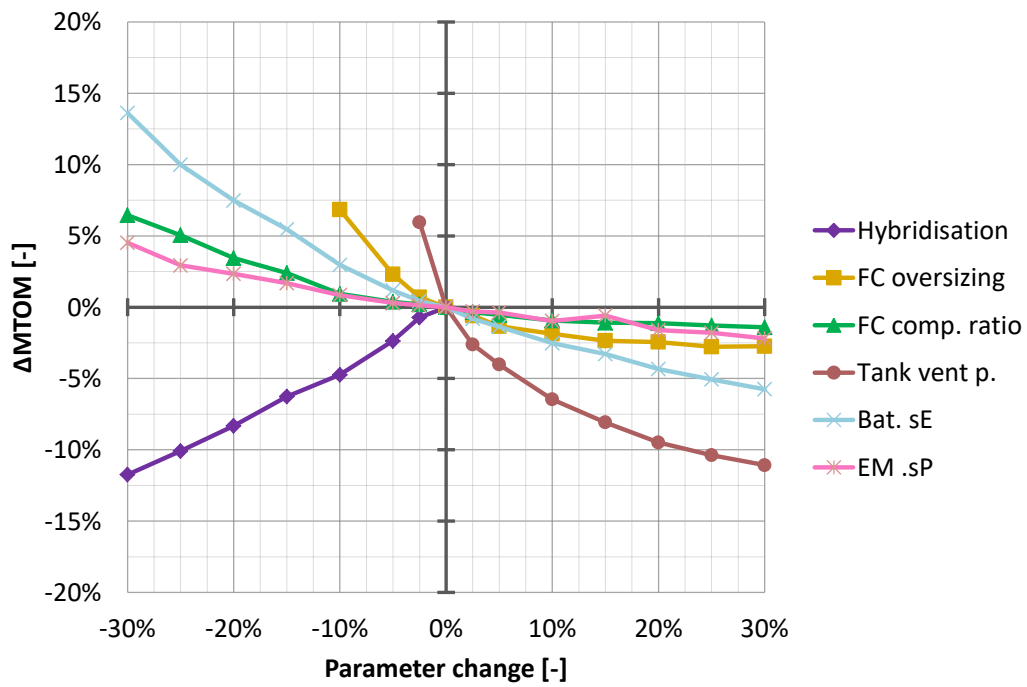


**Figure C.7:** Do 228-212 FC MTOM sensitivity to powertrain parameters
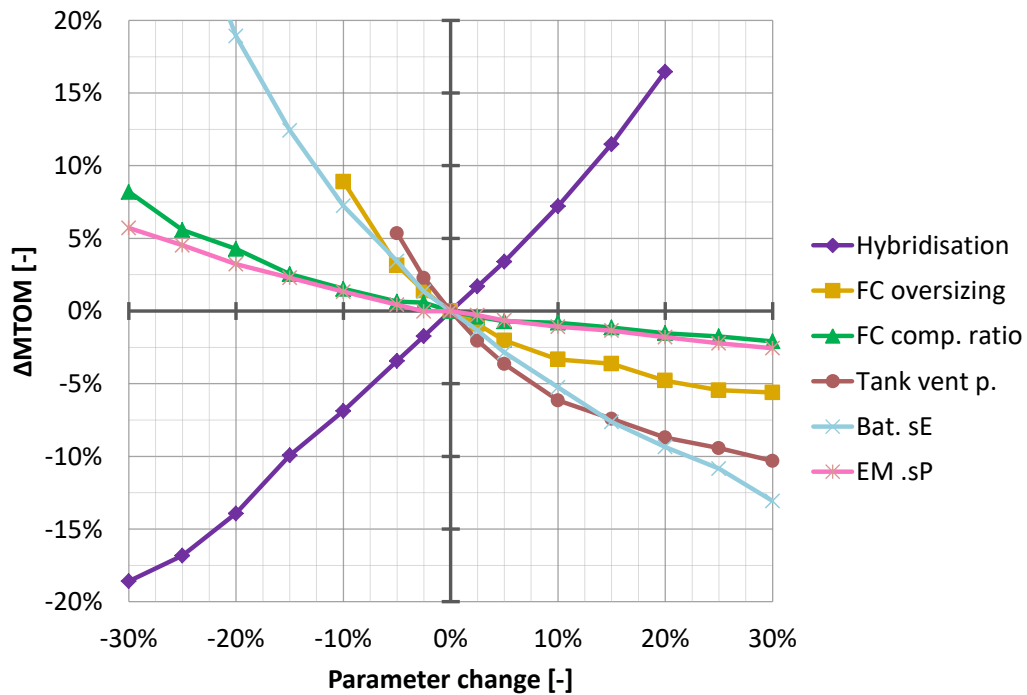


**Figure C.8:** Metro 23 FC MTOM sensitivity to powertrain parameters
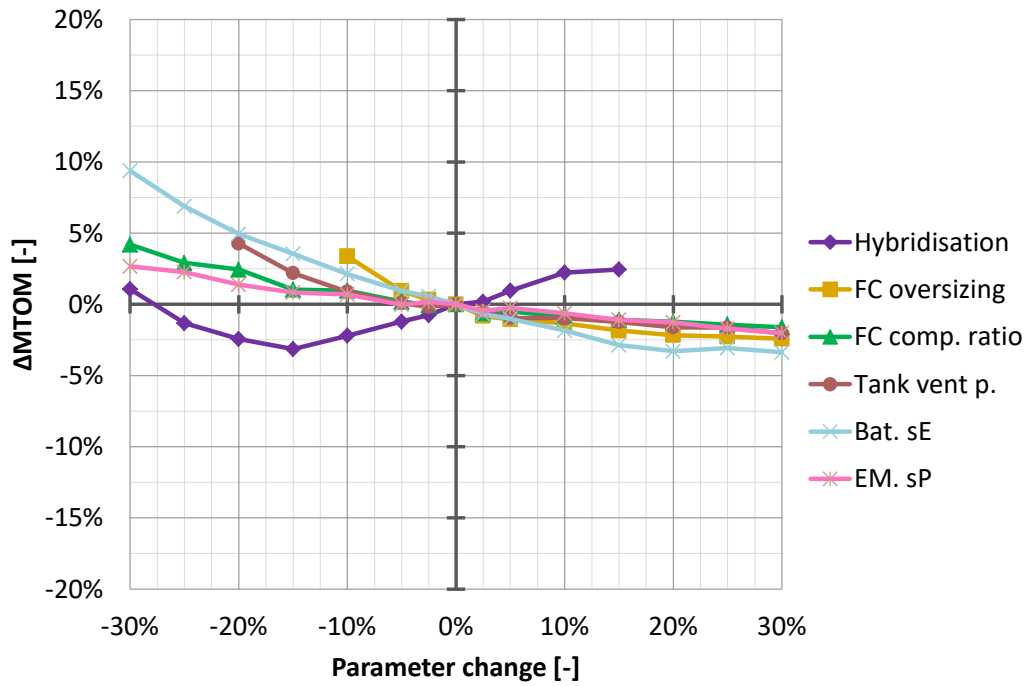
**Figure C.9:** EMB 110P2 FC MTOM sensitivity to powertrain parameters

## C.4.3. Mission Energy Sensitivity to Mission Parameters
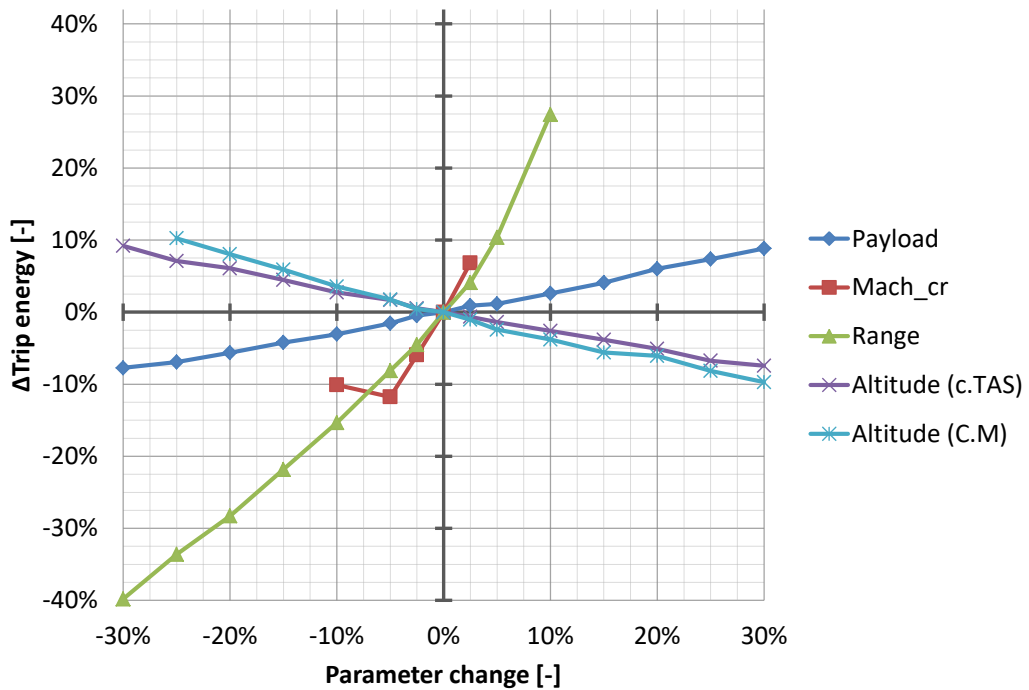


**Figure C.10:** Do 228-212 FC mission energy sensitivity to mission parameters
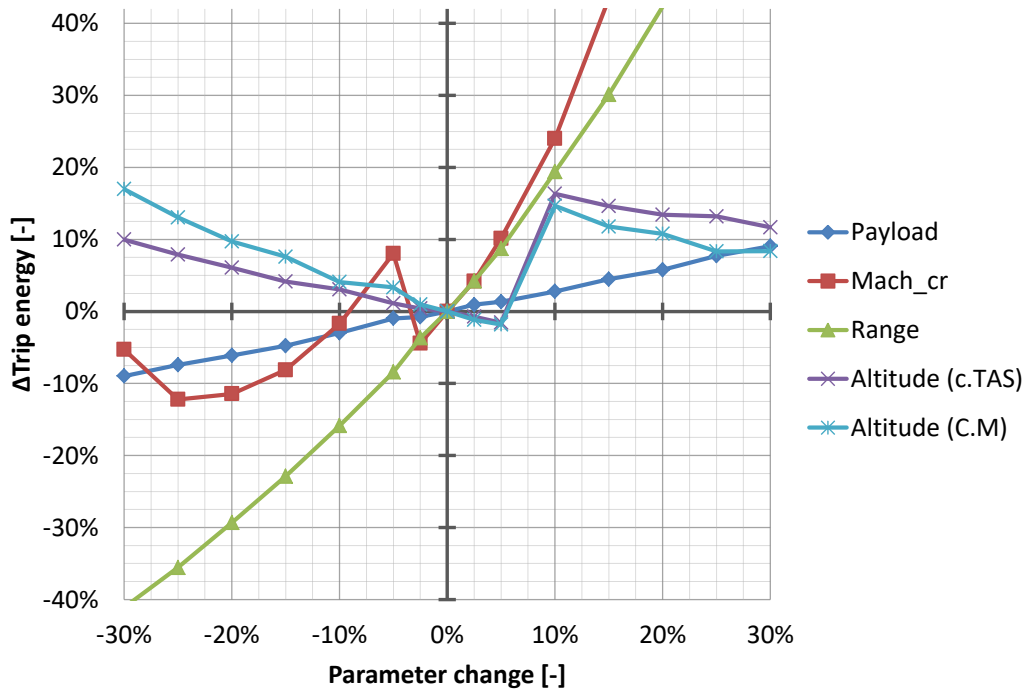
**Figure C.11:** Metro 23 FC mission energy sensitivity to mission parameters
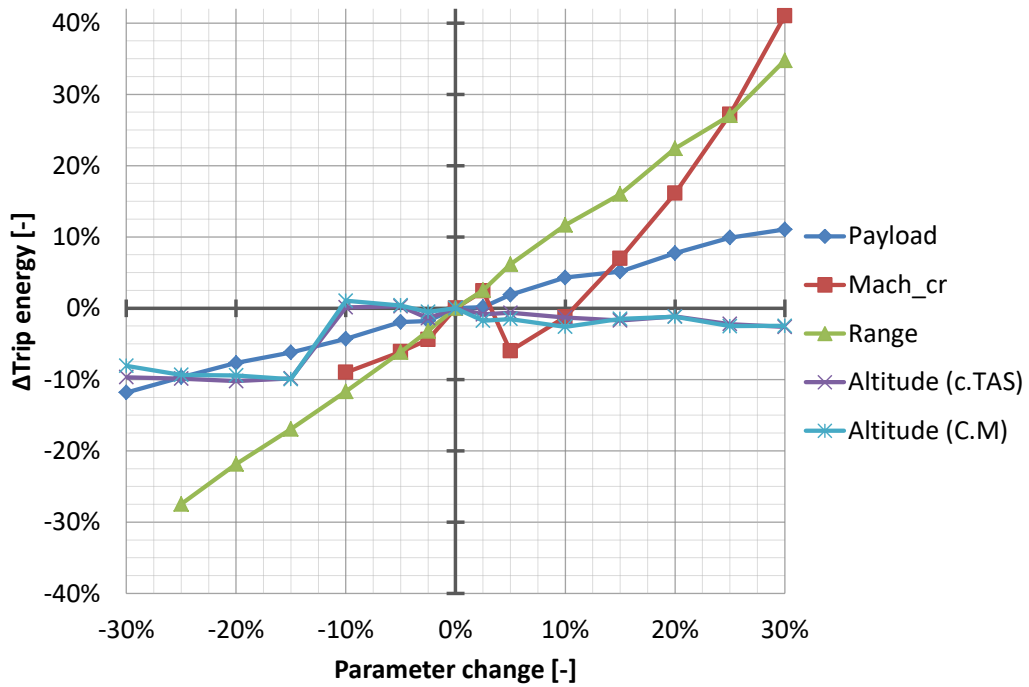


**Figure C.12:** EMB 110P2 FC mission energy sensitivity to mission parameters

## C.4.4. Mission Energy Sensitivity to Powertrain Parameters
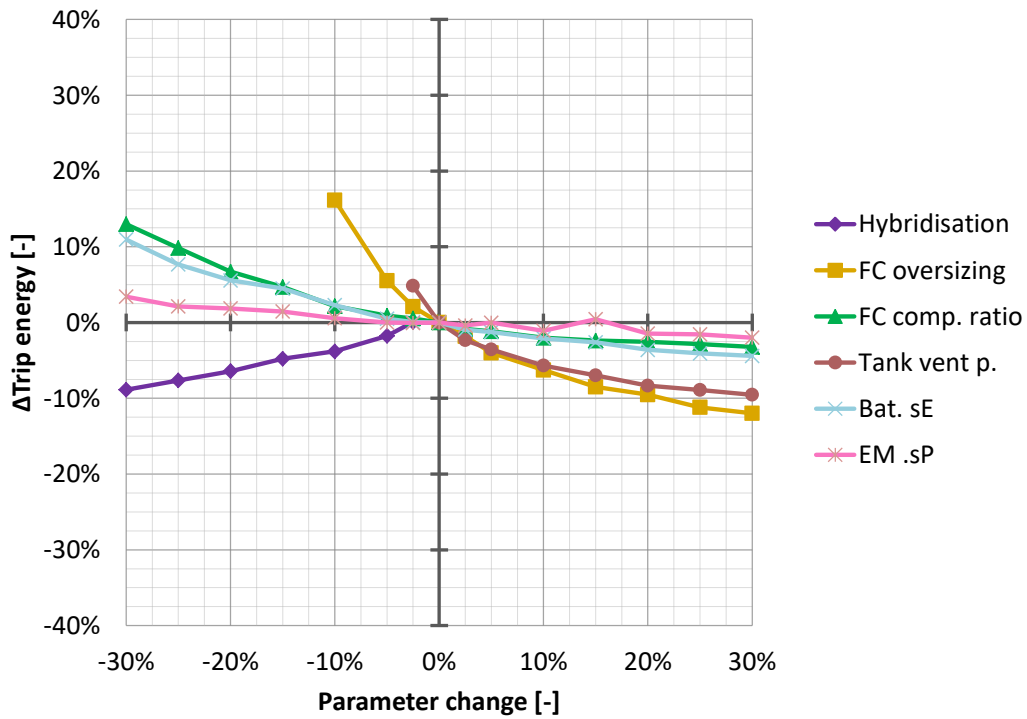


**Figure C.13:** Do 228-212 FC mission energy sensitivity to powertrain parameters
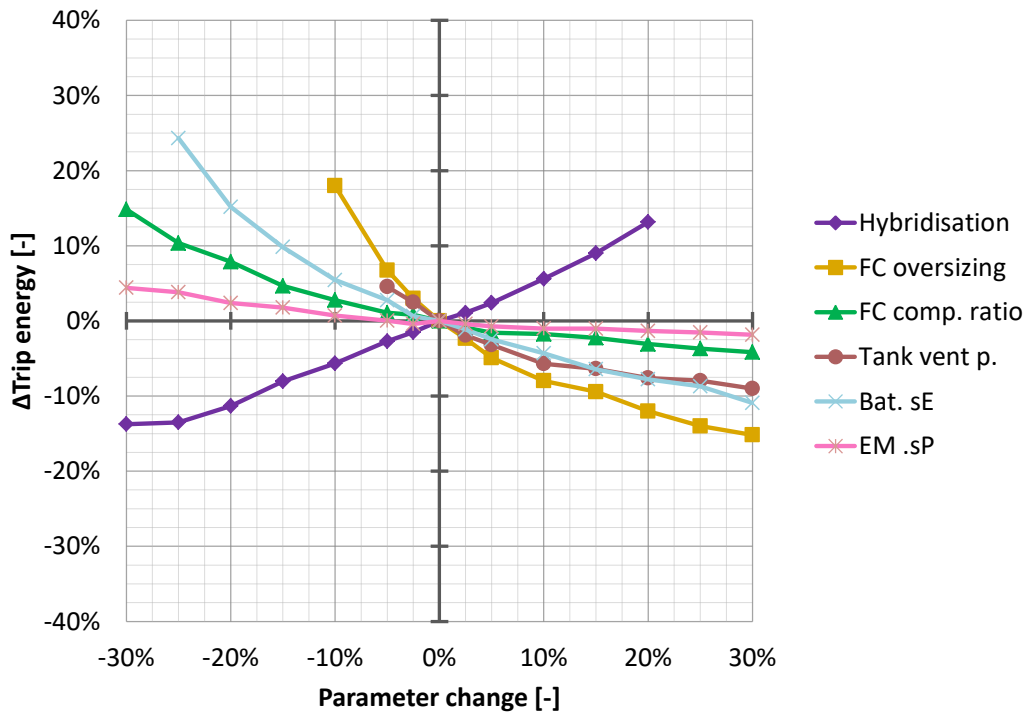


**Figure C.14:** Metro 23 FC mission energy sensitivity to powertrain parameters
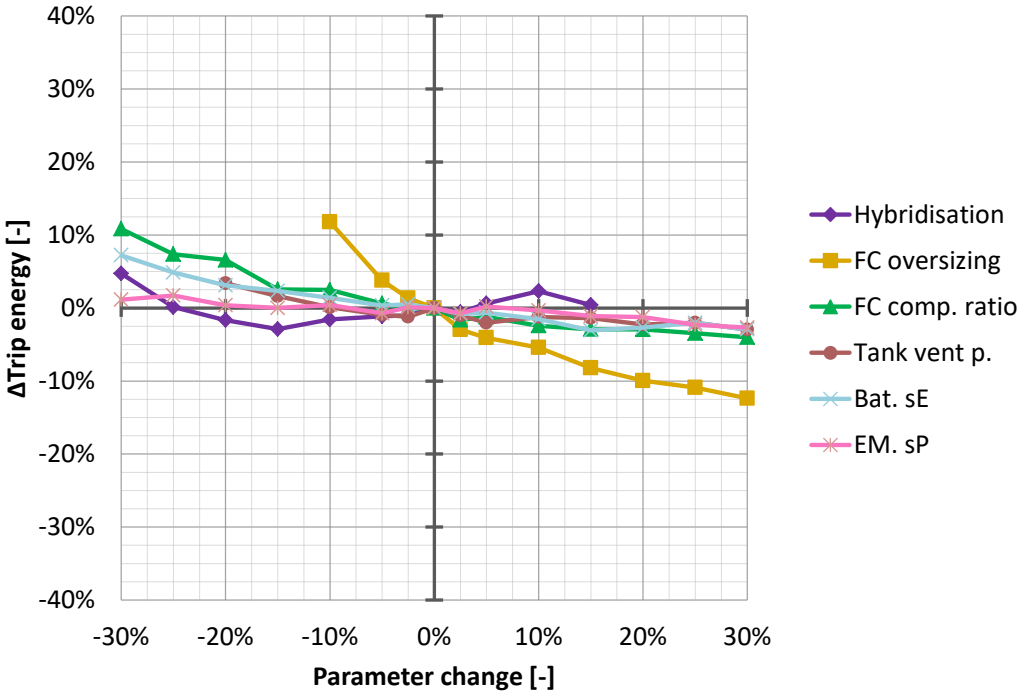
**Figure C.15:** EMB 110P2 FC mission energy sensitivity to powertrain parameters